Universitat Autònoma de Barcelona

Unravelling the positional behaviour of fossil hominoids: Morphofunctional and structural analysis of the primate hindlimb

Marta Pina Miguel

PhD Thesis

Doctorat en Biodiversitat

Unravelling the positional behaviour of fossil hominoids: Morphofunctional and structural analysis of the primate hindlimb

Marta Pina Miguel

2016

ICP
Institut Català de Paleontologia
Miquel Crusafont

UAB
Universitat Autònoma de Barcelona

Universitat Autònoma
de Barcelona

Doctorado en Biodiversitat
Facultad de Ciènces

Tesis doctoral

Unravelling the positional behaviour of fossil hominoids: Morphofunctional and structural analysis of the primate hindlimb

Marta Pina Miguel
2016

Memoria presentada por Marta Pina Miguel para optar al grado de Doctor por la Universitat Autònoma de Barcelona, programa de doctorado en Biodiversitat del Departamento de Biologia Animal, de Biologia Vegetal i d'Ecologia (Facultad de Ciències). Este trabajo ha sido dirigido por el Dr. Salvador Moyà Solà (Institut Català de Paleontologia Miquel Crusafont) y el Dr. Sergio Almécija Martínez (The George Washington Univertisy).

Director
Dr. Salvador Moyà Solà

Co-director
Dr. Sergio Almécija Martínez

A mis padres y hermana.
Y a todas aquelas personas que un
día decidieron perseguir un sueño

Contents

ACKNOWLEDGEMENTS [in Spanish]

Me enfrento a una hoja en blanco con el reto y la responsabilidad de mostrar mi agradecimiento a todas aquellas personas que han hecho posible esta tesis, directa o indirectamente, y espero saber hacerlo lo mejor posible. Lo hago en español para que este agradecimiento llegue a todas ellas. Sino lo consigo a través de estas líneas, espero haber sido capaz de expresarlo o demostrarlo de una manera u otra a lo largo de estos años, desde que pisé por primera vez un yacimiento con mi amiga María de Bellas Artes hasta hoy que escribo estas palabras.

Isaac Newton dijo una vez "*If I have seen further it is by standing on the shourlders of giants*" [Si he logrado ver más lejos, ha sido porque me he alzado sobre hombros de gigantes]. Yo no sería capaz de expresar mejor con palabras mi agradecimiento y admiración por los directores de esta tesis, el Dr. Salvador Moyà-Solà y el Dr. Sergio Almécija. Gracias a vuestra ayuda y consejos hoy tengo entre mis manos una tesis que casi me parecía imposible realizar, ¡gracias!. Me gustaría agradecerle a Salvador que contestara a ese primer email que le mandé y que tardé casi dos semanas en escribir. Agradecerle también que sin prácticamente conocerme pusiera en mis manos la responsabilidad de estudiar los fósiles que forman parte de este trabajo, por enseñarme que no hay mejor manera de lidiar con esta responsabilidad que desde la pasión, la pasión por la paleontología, y las ganas de aprender y descifrar el pasado. Debo agradecerle también que pensara en Sergio para codirigir esta tesis, sin duda mi futuro científico cambió en el momento que pronunció su nombre mientras conversábamos sobre el proyecto de la tesis sentados en el despacho de los antiguos módulos. A Sergio me gustaría agradecerle su gran exigencia y el continuo reto intelectual al que me ha hecho enfrentarme durante estos años. Aunque duro y difícil en algunos momentos, me atrevo a decir que ha valido la pena. Agradecerle también todo lo que se ha preocupado por mí y por mi carrera, así como porque las cosas salieran bien, por todos esos mails que ha mandado (los que sé y los que creo desconozco) para que consiguiera CTs, datos o lo que haya ido necesitando. Me tomo además la licencia de decir que para mí ha sido un placer poder crecer de manera paralela en nuestros recién estrenados papeles de director y doctoranda.

Quiero dar también las gracias a todos los investigadores con los que he compartido estos años y/o algunos trabajos, y que de alguna manera u otra me han dejado aprender de ellos y han compartido algo de su conocimiento conmigo, estar a su lado me ha permitido crecer científica y personalmente. Nombrar de manera especial al Dr. David M. Alba porque me gustaría agradecerle todos los consejos, charlas y discusiones científicas a lo largo de estos años (la mayoría de ellas con su café o su "piti" en la mano). Agradecerle también esos manuscritos corregidos "completamente en rojo", un reto, pero siempre un aprendizaje. Destacar igualmente mi agradecimiento al Dr. Daniel DeMiguel, por su paciencia, su ayuda incansable y por tener siempre una palabra amable y una respuesta para todas esas dudas y miedos científicos y personales. Pero gracias principalmente por haber sido siempre un gran amigo. Parte de los resultados expuestos en esta tesis forman parte de dos artículos ya publicados y otros manuscritos todavía en preparación. Por este motivo me gustaría darle las gracias al resto de coautores que no he nombrado hasta el momento: Dr. Josep Fortuny, por su ayuda durante mis primeros pasos (y no tan primeros...) en el mundo de la paleontología virtual; al Dr. Jordi Marcé-Nogué y Dr. Francesc Puigvert, por su paciencia y ayuda para sacar adelante el trabajo en algo tan nuevo para mí como eran los Elementos Finitos; al Dr. Matthew C. O'Neill, por su ayuda con las regresiones PGLs; a la Dra. Melissa Tallman, por su ayuda en el estudio de la tibia del "Hispano"; y al Dr. Christopher B. Ruff, por su ayuda en el estudio de las propiedades biomecánicas de los fémures. Gracias también al Dr. Isaac Casanovas-Vilar por todo lo que me ha contado sobre la geología y los yacimientos de esta fascinante cuenca (¡y por los mapas!); al Dr. Joan Madurell por esas charlas sobre los yacimientos cuaternarios, carnívoros y otros bichos varios; y a la Dra. Ashley Hammond por sus consejos y comentarios sobre algunas partes de esta tesis. Igualmente me gustaría agradecerle de manera muy especial a Marta Palmero todos esos consejos estéticos y de diseño a lo largo de estos años, así como su gran ayuda en la maquetación de este trabajo.

Darle también las gracias a los investigadores internacionales que amablemente se han prestados a revisar la tesis para que opte a la mención internacional: Dr. William I. Sellers y Dr. Christopher B. Ruff. Igualmente, recalcar mi agradecimiento a los miembros del tribunal de la defensa de este trabajo. Agradecerle también de manera especial toda la ayuda prestada con los temas relacionados con esta tesis o con la FPU a la coordinadora del doctorado, la Dra. Assumpció Malgossa.

Quisiera también dar las gracias a los investigadores que amablemente han compartido con nosotros datos, modelos 3D, imágenes o CTs para realizar los trabajos que conforman esta tesis: C. Owen Lovejoy, James C. Ohman, Michael D. Rose, Carol B. Ward, Christopher B. Ruff, Ashley Hammond, Pere Ibáñez, Masato Nakatsukasa, Daisuke Shimizu, Lorenzo Rook y Roberto Machiarelli. Gracias también a las empresas CESPA Gestión de Residuos y FOSSILIA Serveis Paleontològics i Geològic, S.L. por las fotografías del ACM que en algún momento de la tesis nos han cedido amablemente. Agradecer también a la empresa Transmitting Science S.L. y a Soledad de Esteban-Trivigno la organización de los cursos a los que he asistido y que han sido de gran ayuda en algunas partes de esta tesis.

Dar las gracias a todas aquellos centros e instituciones que me han permitido visitar y trabajar en sus colecciones o usar sus equipos:

- Institut Català de Paleontologia Miquel Crusafont (ICP, Sabadell).
- Hospital Universitari Mútua de Terrassa (Terrassa).
- Unitat de Antropologia (Dpto. de Biologia Animal, de Biologia Vegetal i d'Ecologia) de la Universitat Autònoma de Barcelona (UAB, Bellaterra).
- Universidad de Burgos (UBU, Brugos).
- American Museum of Natural History (AMNH, Nueva York): Mammalogy Collection y Microscopy and Imaging facilities.
- 'Abdus Salam' International Centre for Theoretical Physics (ICTP, Triestre). [*Multidisciplinary Laboratory of the International Centre for Theoretical Physics in the frame of the ICTP/Elettra EXACT Project, funded by the Regione Friuli-Venezia Giulia*].
- Royal Museum of Central Africa (RMCA, Tervuren).
- Stony Brook University (SBU, Stony Brook).
- Smithsonian National Museum of Natural History (USNM, Washington).
- Museum of Comparative Zoology (MCZ), PaleoLab, Peabody Museum of Archaeology and Ethnology (PMAE) y Center for Nanoscale Systems (CNS) pertenecientes a Harvard University (Cambridge). [*The CNS is a member of the National Nanotechnology Infrastructure Network (NNIN), which is supported by the National Science Foundation under NSF award no. ECS-0335765. CNS is part of Harvard University*].
- Naturischorisches Museum (NHMW, Viena) y MicroCT-Lab de la Universität Wien (UNIVIE, Viena);
- Museo Nacional de Ciencias Naturales-CSIC (MNCN, Madrid).

Igualmente, agradecer su ayuda y amabilidad a todos los conservadores, encargados o técnicos de colecciones de los museos e instituciones arriba enumerados, así como a los técnicos y encargados de los escáneres: Eileen Westwig, Ross McPhee, James O. Thostenson and Morgan Hill (AMNH); Clément Zanolli (UPST); Assumpció Malgossa, (UAB); Win Werdelen y Emmanuel Gilissen (RCMA); Judy Chupasko y Mark Omura (MCZ); David Pilbeam, Michele Morgan y Olivia Herschensohn (PaleoLab and PMAE); Fettah Kosar (CNS); Sergio Llácer (ICP); Matthew Tocheri (USNM); Ursula Göhlich (NHMW); Martin Dockner y Gerhard Weber (UNIVIE); Jorge Morales y Cristina Paradela (MNCN). Gracias a Paloma López Guerrero por su ayuda con las fotos de la rótula de *Epipliopithecus* y hacerme de guía por Viena. A Alexander Claxton por su ayuda durante mis primeros CTs en el CNS. Igualmente, darle las gracias a Remy Kusters por hacer que no me sintiera sola en Boston y abrirme las puertas de la Física Teórica. A todos quiero agradecerles que me hayan hecho mucho más fácil las estancias que he realizado y la

ayuda que desinteresadamente me han prestado. En especial, destacar la generosa acogida por todos los miembros del PaleoLab (David, Michele, Larry, John y Erik) durante mis dos estancias en Boston.

Gracias al resto de integrantes del Institut Català de Paleontologia Miquel Crusafont que no he nombrado hasta ahora, a los que están o un día estuvieron, por su cálida acogida cuando llegué, así como por hacer un poco más ameno el día a día que hemos compartido. Recalcar de manera muy especial a Nosky, por compartir todos estos años. También a Mireia y Laila, gracias rubias por esas risas que nos hemos echado en los desayunos y comidas. A Ale, por esos platos de pasta y por enseñarme a hacer pesto (¡con mortero!). Igualmente agradecerle a María, Gretell y Enric su ayuda con los temas administrativos, a Laura, Galindo y Marta su ayuda con el tema de las colecciones, a Pere su esfuerzo por acercar nuestro trabajo a la gente, a Torres su ayuda con los omnipresentes problemas informáticos, y a Pepi por mantener mi despacho siempre en orden.

Me gustaría darle las gracias a todas aquellas personas que me abrieron las puertas de la paleontología y la investigación, y con los que pude dar mis primeros pasos en el trabajo de campo, me he sentido siempre una privilegiada por compartir tiempo, conversaciones y fósiles con vosotros. Destacar a la Dra. Nieves López, Dr. Manuel J. Salesa, Dr. Manuel Hernández Fernández, Dra. Beatriz Azanza, Dra. Marian Álvarez y Dr. Israel M. Sánchez. Igualmente, me gustaría destacar de manera muy especial por sus palabras siempre amables, así como por su disponibilidad a responder cualquier pregunta o ayudar en cualquier cosa, al Dr. Jorge Morales y al Dr. Plinio Montoya.

Por su apoyo desde el primer día y porque me ayudan a mantener viva mi pasión por todo esto, mencionar especialmente a mis compañeros (¡y amigos!) de Bat-3 (¡takenaaa!): a Juan (siempre conmigo, aunque sea en la distancia), a Alberto (me encanta compartir camino paleontológico contigo… ¡lo conseguiremos!) y a Alex (Falconet, que poco tiempo estuviste en Barcelona…). Dar las gracias a los innumerables compañeros de excavación con los que he compartido horas de sol en Somosaguas, Batallones, Venta del Moro, Toril, Nombrevilla, Pinilla del Valle, Can Llobateres, La Valenciana y Castell de Barberà. De entre ellos me gustaría destacar a Marcos y Dani (MacLovin), y a los compañeros "internacionales", Alida, Anne-Claire y Dimitri.

Gracias a todas aquellas personas que sin tener nada que ver con la paleontología han hecho que todo esto valga la pena, entre ellos destacar a Silvia, Tamara, Mónica, Elena, Sara, Arancha, y Albert. No quiero dejar de mencionar y darle las gracias a Ana, que además de ayudarme a crecer como persona, hizo que nunca dejara atrás la curiosidad y siguiera creyendo en la inocencia intelectual (¡y por la paliza con el inglés!). Con especial cariño me gustaría agradecer a Juan y a David que me hayan acompañado en "el camino de la suavidad" porque el judo no terminó al dejar de entrenar, sigue conmigo en la manera de afrontar la vida, el esfuerzo, la lucha, la constancia, y la superación necesarias día a día.

Por último, quiero darle las gracias también a mi familia (primas, primos políticos, ti@s, cuñado, Bruno y Lola), también a Tere (¡y compañía!), porque habéis sido siempre un gran apoyo para mí. Mi agradecimiento más especial y sincero a mis padres, por darme siempre un suelo sólido donde pisar,

una mano a la que cogerme y un seguro donde apoyarme. Pero sobretodo les quiero dar las gracias por haberme proporcionado las herramientas para soñar y las alas para volar. A mi hermana, gracias por acompañarme siempre en este vuelo. A vosotros, porque mis éxitos no serían éxitos sin vosotros.

Finalmente, esta tesis no hubiera sido posible sin el apoyo económico e institucional recibido a través de las diferentes becas y proyectos que enumero a continuación:

- Ministerio de Educación, Cultura y Deporte de España: FPU AP2010-4579 y Estancias Breves FPU EST13/00930.
- Ministerio de Economía y Competitividad de España: CGL2008-00325/BTE, CGL2011-27343, CGL2011-28681 y CGL2014-54373-P.
- Generalitat de Catalunya: 2009 SGR 754 GRC y 2014 SGR 416 GRC.
- Collection Study Grant del AMNH.
- Synthesys-3 Project de la *European Community Research Infrastructure Action* (http://synthesys3.myspecies.info/) dentro del programa FP7: BE-TAF-3356 y AT-TAF-4689.
- Transmitting Science Grant - European Association of Vertebrate Paleontologists (EAVP).
- The Leakey Foundation Grant de la L.S.B. Leakey Foundation y el mecenas Mr Gordon Getty.

ABSTRACT

Living hominoids (apes and humans) are orthograde primates that rely on specialized modes of locomotion such as below-branch suspension, vertical climbing, and bipedalism. Identifying the functionally meaningful adaptations that characterize each locomotor type is therefore essential to make sound functional inferences about fossil species. Moreover, the hindlimb elements play an important role in primate locomotion, since they participate in body weight transmission, support and propulsion. Thus, this thesis focuses on the study of the (non-pedal) hindlimb remains of the Miocene great apes cf. *Dryopithecus fontani*, *Pierolapithecus catalaunicus*, *Hispanopithecus laietanus* and *Hispanopithecus crusafonti* from the Vallès-Penedès Basin (NE Iberian Peninsula), through morphometric and biomechanical analyses. These fossil apes are of utmost relevance to understand hominoid evolution because they constitute the largest currently available assemblage of fossil hominids (i.e., the great ape and human family) exhibiting the earliest unambiguous evidence of orthogrady. From an evolutionary viewpoint, these fossils represent a key moment for comprehending the origins of the orthograde behaviours. Hence, the aim of this thesis is to shed light on the positional behaviour of the Iberian fossil great apes and provide new insights on the evolutionary pathways of living hominoids locomotor modes. Results show that the hindlimb morphology of the Vallès-Penedès great apes is highly diverse. Each taxon combines a unique array of plesiomorphic ("monkey-like" or "stem hominoid-like") and derived (modern ape-like) traits, associated with either quadrupedalism or orthograde-like behaviours, respectively. Overall, these results support previous works suggesting that the Vallès-Penedès taxa would combine different degrees of above-branch quadrupedalism and orthograde-like behaviours (vertical climbing and/or below-branch suspension). These results also highlight the mosaic nature of the hominoid postcranium evolution and provide new morphological evidence of the incipient orthograde-related modes of locomotion that currently characterize this group of primates (including human bipedalism).

RESUMEN

Los hominoideos actuales (simios y humanos) son primates ortógrados con comportamientos locomotores especializados como la suspensión, la escalada vertical y el bipedismo. En este sentido, identificar aquellas adaptaciones relevantes desde un punto de vista funcional que caracterizan a cada tipo locomotor es esencial para poder hacer sólidas inferencias funcionales en los taxones fósiles. Asimismo, la pierna tiene un papel importante en la locomoción de los primates, ya que participa en la transmisión del peso corporal, y en tareas de soporte y propulsión. Por tanto, esta tesis se centra en el estudio de los restos de la extremidad posterior de los grandes simios antropomorfos cf. *Dryopithecus fontani*, *Pierolapithecus catalaunicus*, *Hispanopithecus laietanus* e *Hispanopithecus crusafonti* de la cuenca miocénica del Vallès-Penedès (NE Península Ibérica) mediante análisis morfométricos y biomecánicos. Además, los restos fósiles incluidos en esta tesis son de gran relevancia para comprender la evolución de los hominoideos, ya que constituyen actualmente el mayor conjunto disponible de homínidos fósiles (i.e., de la familia que incluye grandes simios antropomorfos y humanos) con evidencias inequívocas de ortogradía. Igualmente, desde un punto de vista evolutivo, estos taxones fósiles representan un momento clave para comprender el origen de los comportamientos ortógrados. Por tanto, el objetivo principal de esta tesis es arrojar luz en el comportamiento posicional de los taxones fósiles de grandes simios antropomorfos ibéricos, así como en los caminos evolutivos que condujeron a la locomoción observada en los hominoideos actuales. Los resultados muestran que la morfología de la pierna de los grandes simios antropomorfos del Vallès-Penedès es muy diversa. Además, cada taxón combina características plesiomórficas (similares a las de los monos u hominoideos basales) y derivadas (similares a las de los simios actuales), asociadas con cuadrupedismo y comportamientos ortógrados, respectivamente. En conjunto, estos resultados corroboran otros estudios previos en los que se sugiere que los taxones del Vallès-Penedès podrían combinar cuadrupedismo sobre las ramas con comportamientos ortógrados (escalada vertical y/o suspensión) en diferentes grados. Estos resultados ponen también de manifiesto la evolución en mosaico del esqueleto postcraneal de los hominoideos, y proporcionan nuevas evidencias morfológicas de los incipientes comportamientos ortógrados que más tarde caracterizarán a los miembros actuales de este grupo de primates (incluido el bipedismo de los humanos).

Science satisfies curiosity, gives you a new world view,
gives man the ability to do things, gives him power.

-- Richard Feynman --

Section I. INTRODUCTION

HOMINOID POSITIONAL BEHAVIOUR

The superfamily Hominoidea

Primates is an order of mammals that comprises a diverse set of species living worldwide, in highly different habitats and with notably different ecological behaviours and sizes (almost 300 species of primates are currently recognized; Fleagle 1980, 2013). A schematic representation of the living Primates classification is depicted in Figure 1. Together with platyrrhines (New World monkeys), catarrhines belong to the infraorder Simiiformes (=Anthropoidea) within the suborder Haplorrhini (dry-nosed primates; Table 1; Kay *et al.* 1997; Groves 2001; Chatterjee *et al.* 2009). Thus, hominoids are catarrhine primates, group that include Old World monkeys, apes and humans (Fleagle 2013).

The superfamily Hominoidea currently comprises two families (Hylobatidae and Hominidae), but the fossil record has yielded a number of hominoid fossil remains, which allows the identification of three additional families (Table 2). There exists a general consensus that Hylobatidae (the "lesser apes") and Hominidae ("great apes" and humans) are two monophyletic families that include the living genera *Symphalangus*, *Nomascus*, *Hoolock*, *Hylobates*, *Pongo*, *Gorilla*, *Pan*, and *Homo* (Table 2; Brandon-Jones *et al.* 2004; Chatterjee *et al.* 2009). The three last genera made up the subfamily Homininae (African apes + hominins), while orangutans are the only living members of the Ponginae (Fleagle 2013).

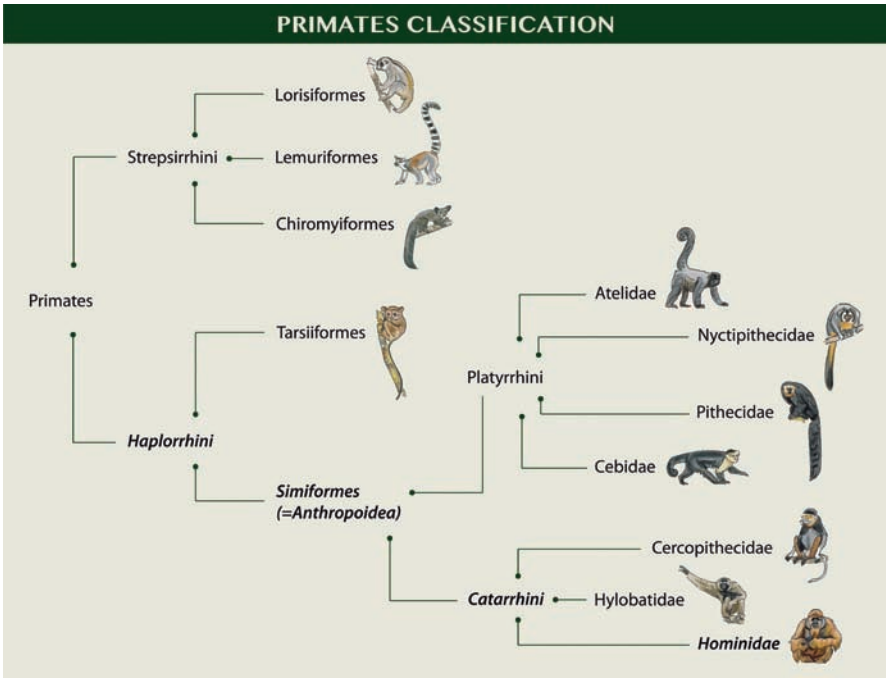

Figure 1 Main taxonomic groups of primates. Anthropoids are depicted in more detail, until a family level. Hominids belong to the parvorder Catarrhini within the infraorder Simiiformes or Anthropoidea and the suborder Haplorrhini. *[Art work by F. Desbordes]*

Table 1 Systematic classification of the living primates belonging to the infraorder Simiiformes or Anthropoidea. Classification based on Groves (2001) and Chatterjee *et al.* (2009).

SIMIIFORMES=ANTHROPOIDEA	
Parvorder PLATYRRHINI	Parvorder CATARRHINI
Fam. Atelidae	Superfam. CERCOPITHECOIDEA
Subfam. Atelinae	Fam. Cercopithecidae
Fam. Nyctipithecidae	Subfam. Cercopithecinae
Fam. Cebidae	Subfam. Colobinae
Subfam. Cebinae	Superfam. HOMINOIDEA
Subfam. Callitrichinae	Fam. Hylobatidae
Fam. Pithecidae	Fam. Hominidae
Subfam. Pithecinae	Subfam. Ponginae
Subfam. Callicebinae	Subfam. Homininae

Abbreviations: Superfam., superfamily; Fam., family; Subfam., subfamily.

Locomotion of the living hominoids

The positional behaviour profiles of living anthropoids, including hominoids, are greatly varied and they frequently combine several locomotor modes (with the exception of modern humans that are almost completely terrestrial bipeds; Fleagle 2013, though see Kraft *et al.* 2014; see also Appendix A). Although their positional behaviour repertoire is notably complex and diverse, living hominoids are altogether highly arboreal primates that favour climbing and/or suspensory behaviours, (Fleagle 1980, 2013; Isler 2005; Thorpe and Crompton 2006; Hunt 2016). When compared to other primates the combination of climbing and suspension is the common trait that characterizes the positional repertoires of apes, with the exception of gorillas (with a very low frequency of suspension; Hunt 1991a, 2016; Isler 2005). Nonetheless, hominoids also show some differences among their positional behaviour profiles mainly regarding locomotor types frequencies and kinematics (Isler 2005). Even intraspecific differences have even found during ontogeny (e.g., juvenile African apes and orangutans are more arboreal than adults; they climb more, with quicker cycles and lower duty factors; Doran 1992, 1997; Isler 2005).

Hylobatids and orangutans are the most arboreal hominoids, spending almost all their time on the trees (Hunt 1991a, 2016). Common chimpanzees (*Pan troglodytes*) spend around 50-60% of their daily activity in arboreal milieus, while mountain gorillas (*Gorilla beringei*) only occupy around 5% of their time on trees (arboreality in bonobos—*Pan paniscus*—would be intermediate between that of common chimpanzees and orangutans; Hunt 1991a, 2004). Nonetheless, the behaviours of great apes in an arboreal context would be apparently somewhat similar, that is, they all preferentially engage in vertical climbing and/or suspension for travelling on the trees (Hunt 2004; Fleagle 2013). Moreover, hylobatids and orangutans exhibit the highest levels of below-branch suspensory habits and the lowest degree of terrestrial quadrupedalism; whereas mountain gorillas represent the opposite pattern, since they are essentially terrestrial quadrupeds (Hunt 1991a; Gebo 1996). Chimpanzees would an intermediate pattern of arboreal *vs* terrestrial behaviours between Asian apes and gorillas (*ibid*).

More specifically, hylobatids are highly arboreal and versatile primates whose predominant locomotor type is brachiation (a special type of suspension in which the pendulous movement is faster, displaying a phase of free flight between handholds; Fleagle 1976; Gittins 1983; Hunt 1991a; Vereecke *et al*. 2006; Fig. 2g; Appendix A). Nonetheless, they are able to use a great variety of other locomotor types, such as leaping, bipedal walking, and climbing (Fleagle 1976, 1980; Gittins 1983; Vereecke *et al.* 2006). Although hylobatids can occasionally engage in quadrupedalism (0-4%), this behaviour is barely meaningful when compare with other primates (Fleagle 1980). Siamangs (*Symphalangus*) and gibbons (*Nomascus*, *Hoolock*, and *Hylobates*) tend to brachiate along large supports and climb among smaller ones. Bipedalism is commonly conducted along large horizontal branches (0-12%) and leaping is usually performed from large branches to smaller ones or lianas (0-24%; Fleagle 1976, 1980; Hunt 2004). Although all hylobatids prefer brachiation for travelling, the frequency they engage in this and other locomotor modes, as well as the support used during displacements, is different among the genera (Fleagle 1980; Hunt 2016). Thus, for example, the larger siamangs (around 11 kg) climb more than the smaller gibbons (6 kg on average; Fleagle 1976, 1980).

Table 2 Systematic classification of the superfamily Hominoidea including living and fossil taxa. Genera included in this work are highlighted in bold. Classification updated from Moyà-Solà *et al.* (2009a), Casanovas-Vilar *et al.* (2011) and Alba (2012).

SUPERFAMILY HOMINOIDEA

- Fam. *incertae sedis*
  - *Kamoyapithecus*†
- Fam. Proconsulidae†
  - Subfam. Proconsulinae†
    - *Proconsul*†
    - *Ekembo*†
    - *Ugandapithecus*†
  - Subfam. Nyanzapithecinae†
    - *Nyanzapithecus*†
    - *Mabokopithecus*†
    - *Rangwapithecus*†
    - *Turkanapithecus*†
    - *Xenopithecus*†
  - Subfam. *incertae sedis*
    - *Samburupithecus*†
- Fam. Afropithecidae†
  - Subfam. Afropithecinae†
    - *Afropithecus*†
    - *Heliopithecus*†
    - *Morotopithecus*†
  - Subfam. *incertae sedis*
    - *Otavipithecus*†
- Fam. Hylobatidae
  - *Hylobates*
  - *Nomascus*
  - *Hoolock*
  - *Symphalangus*
  - *Bunopithecus*†
- Fam. Hominidae
  - Subfam. *incertae sedis*
    - Trib. Oreopithecini†
      - *Oreopithecus*†
  - Subfam. Kenyapithecinae†
    - Trib. Equatorini†
      - *Equatorius*†
      - *Nacholapithecus*†
    - Trib. Kenyapithecini†
      - *Kenyapithecus*†
      - *Griphopithecus*†
  - Subfam. Dryopithecinae†
    - Trib. Dryopithecini†
      - ***Dryopithecus***†
      - ***Pierolapithecus***†
      - *Anoiapithecus*†
    - Trib. Hispanopithecini†
      - ***Hispanopithecus***†
    - Trib. Ouranopithecini†
      - *Ouranopithecus*†
    - Trib. *incertae sedis*
      - *?Udapnopithecus*†
  - Subfam. Ponginae
    - Trib. Sugrivapithecini†
      - *Sivapithecus*†
      - *Ankarapithecus*†
    - Trib. Lufengpithecus†
      - *Lufengpithecus*†
      - *Khorapithecus*†
    - Trib. Pongini
      - *Pongo*
      - *Indopithecus*†
      - *Gigantopithecus*†
  - Subfam. Homininae
    - Trib. *incertae sedis*
      - *Nakalipithecus*†
      - *Chorapithecus*†
      - *Sahelanthropus*†
    - Trib. Gorillini
      - *Gorilla*
    - Trib. Panini
      - *Pan*
    - Trib. Hominini
      - *Homo*
      - *Australopithecus*†
      - *Paranthropus*†
      - *Ardipithecus*†
      - *Orrorin*†

Abbreviations: Fam., family; Subfam., subfamily; Trib., tribe; †, extinct taxa.

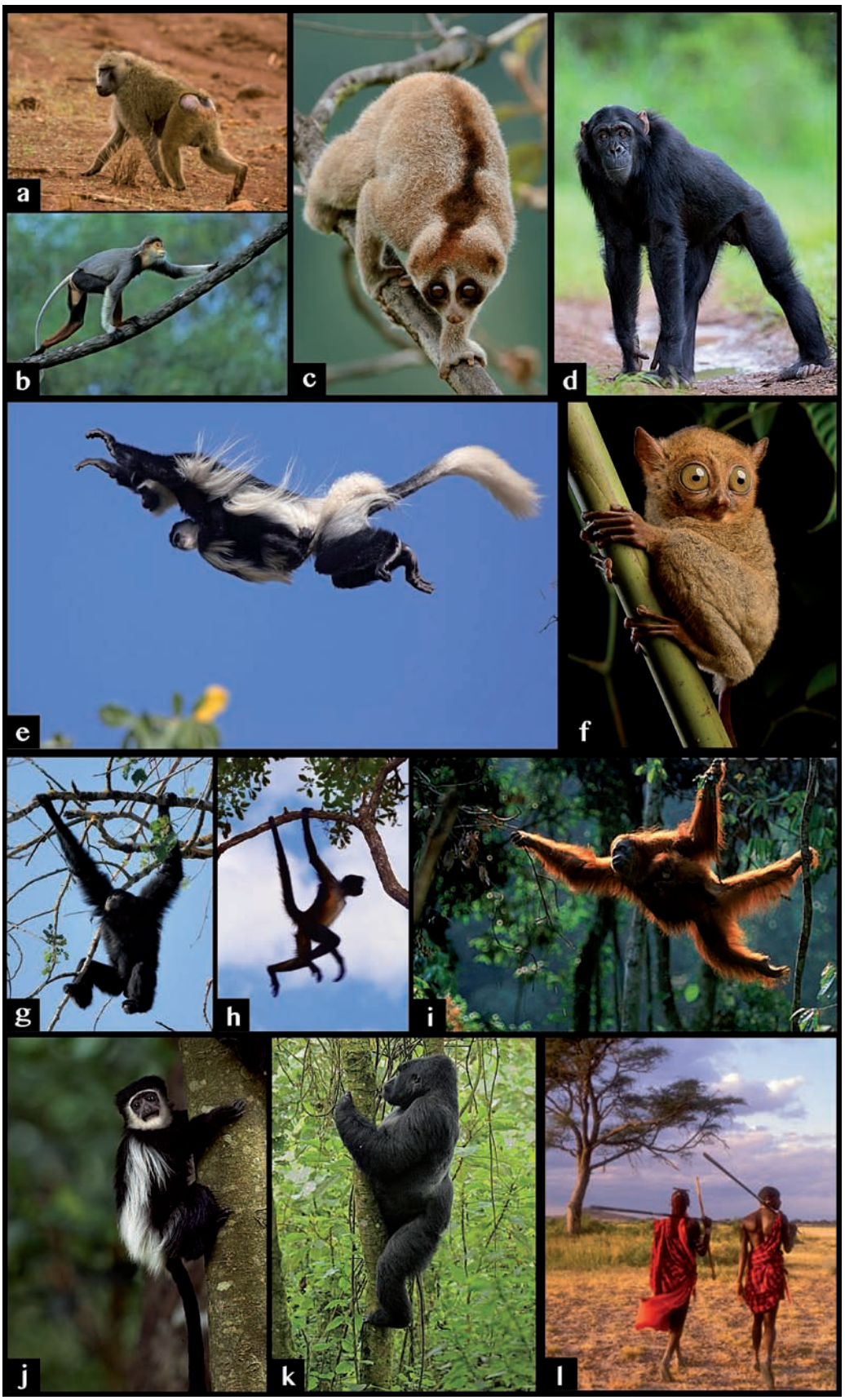

Figure 2 Locomotor modes. **a**, Terrestrial quadrupedalism (*Papio anubis*); **b**, arboreal quadrupedalism (*Pygathrix nemaeus*); **c**, slow climbing (*Nycticebus coucang*); **d**, knuckle-walking (*Pan paniscus*); **e**, leaping (*Colobus guereza*); **f**, vertical clinging and leaping (*Tarsius tarsier*); **g-h**, below-branch suspension (*Symphalangus syndactylus* and *Ateles geoffroyi*, respectively); **i**, clambering (*Pongo abelii*); **j-k**, vertical climbing (*Colobus guereza* and *Gorilla beringei*, respectively); and **l**, bipedalism (*Homo sapiens*).

Orangutans (genus *Pongo*) inhabit in the forests of Borneo (*P. pygmaeus*) and Sumatra (*P. abelii*). The latter species and the female Bornean orangutans are completely arboreal. However, males of *P. pygmaeus* usually go down to the ground (about 20% of their locomotion) to cross gaps of the canopy (Rodman 1979; Cant 1987; Povinelli and Cant 1995). These primates are the largest extant mammals that expend the most of their time on the trees (males reach up to 80 kg and females 40 kg; Cant 1987). A large body mass is a serious constrain to move in an arboreal milieu and, hence, orangutans locomotor repertoire is probably highly associated with its large size in an extent degree (related to spatial discontinuity in the canopy, and fragility and compliance of the arboreal supports; Cartmill 1985; Cant 1987, 1992). Orangutans mainly rely on suspension (more than 80%) and clambering, using orthograde positions and varied combinations of forelimb/hindlimb use (Sugardjito 1982; Sugardjito and van Hooff 1986; Cant 1987; Hunt 1991a; Fig. 2i). Otherwise, when they move quadrupedally (even below branches), they travel with a pronograde-like position, with the body as close to the substrate as the limbs permit (Cant 1987).

African apes comprise chimpanzees (*Pan troglodytes*), bonobos (*Pan paniscus*), and gorillas (Eastern gorillas: *Gorilla beringei*—mountain gorilla, *G. b. beringei*, and Grauer's gorilla, *G. b. graueri*—and Western gorillas: *Gorilla gorilla*; Caldecott and Miles 2005). Among hominoids, quadrupedal walking for travelling is only predominant within African apes (especially in bonobos and gorillas, constituting more than 60%), which travel by using their characteristic knuckle-walking mode, usually on the ground (Fig. 2d; Hunt 1991a, 2004, 2016; Doran 1993; Gebo 1996). This type of locomotion is the most common when chimpanzees move between feeding patches and even when travel with no recognizable purpose (more than 98.5% of their locomotor activity; Susman 1984; Hunt 1992; Gebo 1996). Even though, chimpanzees and bonobos also climb frequently (around 50.4% in bonobos; Hunt 1992, 2004, 2016). Gorillas do not engage regularly in arboreal travelling (especially the large males), but when they do, these animals usually move by means of climbing behaviours (a locomotor mode that can reach up to the 71% of the arboreal travelling; Fig. 2k; Remis 1995; Gebo 1996). Nevertheless, the primary locomotor type of gorillas is also quadrupedal walking (although lowland gorillas climb around 19.7% of their activity time; Hunt 2004).

Finally, modern humans are undoubtedly the top terrestrial bipeds and use both hindlimbs to travel while hands are free of locomotor tasks (Fig. 2l; Fleagle 2013). Nonetheless, humans are able to engage in some other locomotor modes, such as vertical climbing, which is practiced by some modern hunter-gatherers to obtain food (Kraft *et al.* 2014).

Postcranial anatomy of the Hominoidea

As seen in the previous section, living hominoids have very diverse and flexible positional behaviour repertoires, with each taxon combining several locomotor modes. Nonetheless, all hominoids (with only few exceptions) share an array of (functionally meaningful) morphological adaptations related to body organization for forelimb-dominated arboreal locomotion (Ward 2015; Hunt 2016).

Thus, a generalized increased body size in hominoids (relative to monkeys) might influence in somehow the appearance of suspensory behaviours (Preuschoft and Demes 1984; Fleagle 2013). Beyond a certain body mass, it is easier to move below the branches (suspension) than to struggle to stay balanced on top of them or even shift through more terrestrial habits (Cartmill 1985; Gebo 1996). Suspensory behaviours are also probably related to reaching supports in many directions (favouring eccentric positions of limbs and joints), and to negotiate terminal branches in arboreal milieus to harvest ripe fruit (Preuschoft and Demes 1984; Fleagle 2013; Ward 2015; Hunt 2016). This would also be the case of clambering that also permits crossing gaps between discontinuous arboreal supports (i.e., "bridging"; Appendix A) more safely than doing it by leaping (Cartmill 1985; Youlatos 1993). Furthermore, unlike suspension, clambering permits to feed on the slenderest branches by distributing the body weight over different limbs and supports that would otherwise break under the weight of the animal (Cartmill 1985; Cant 1987; Crompton *et al.* 2010).

Importantly, many of the features that characterize suspensory behaviours could also be considered as adaptations for vertical climbing and/or clambering, being difficult to discern whether they are adaptations for one or another locomotor mode (Gebo 1996; Crompon *et al.* 2010). Moreover, these three positional behaviours (suspension, vertical climbing and clambering) particularly distinguish the locomotor profiles of non-human hominoids, which use them in different frequencies (see above). For this reason, these three locomotor categories will be considered together as SVCC (suspension–vertical climbing–clambering), if not said otherwise (Table 3). Likewise, although non-human hominoids are the top suspensory primates, some platyrrhines (mainly *Ateles*, *Brachyteles* and in some lesser extent *Lagothrix*) also show morphological similarities with apes mainly related to arm-hanging and suspension (Cant 1987; Gebo 1996; Larson 1998a; Hirasaki *et al.* 2000; Cant *et al.* 2001, 2003; Arms *et al.* 2002; Youlatos 2002).

ANATOMICAL ADAPTATIONS		
	Monkey-like	**Ape-like**
Intermembral index	Low	High
Thorax	Narrow	Broad
Lumbar region	Long	Short
Tail	Present	Absent
Forelimb		
Scapular position	Lateral	Dorsal
Glenoid fossa *shape*	Elliptical	Ovoid
Humeral trochlea shape	Non-spool	Spool
Ulnar olecranon process	Long	Short
Ulna-triquetrum contact	Present	Absent
Phalanges	Short	Long
	Straight	Curved
Hindlimb		
Femoral head	Semi-spherical	Spherical
Patellar groove	Deep	Shallow
Femoral condyles	Symmetric	Asymmetric
Patellar apex	Present	Absent (except hylobatids)
Tibial articular surface shape	Squared	Rectangular

Table 3 Comparisson of some of the most representative features that differentiate monkeys and apes.

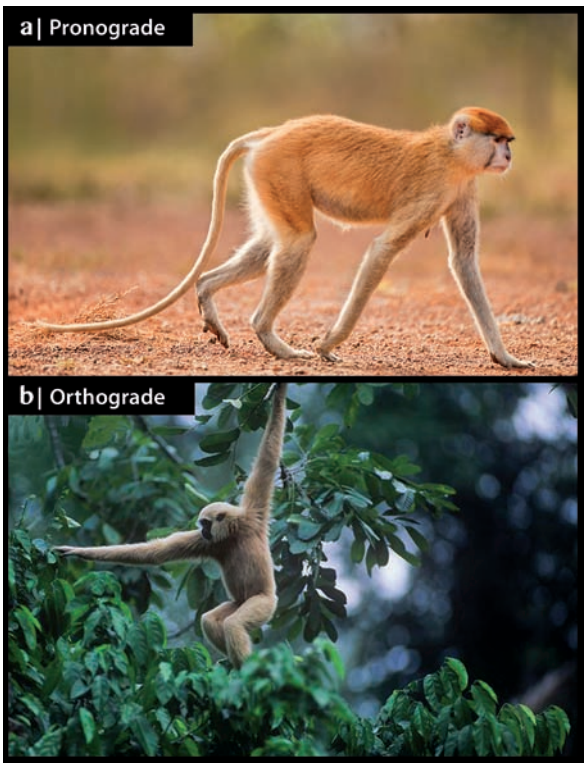

Figure 3 Primates are divided in **a**, pronograde (*Erythrocebus patas*) and **b**, orthograde (*Hylobates agilis*) based on their body plan. See text for further information.

Therefore, living primates can be distinguished in two separated groups depending on their body plan (a specific assemblage of morphological traits and skeletal organization share by the members of a group): *pronogrades* and *orthogrades* (Fig. 3; Stern 1975; Fleagle 2013). In a general sense, pronogrady is associated with any quadrupedal locomotion that takes place on a support(s) angled at less than 45º from the horizontal (including the ground), in which the hands and feet grip on most supports, but may be used in palmigrady/plantigrady or digitigrady on the largest supports. Displacement of the primates' trunk is roughly parallel to the support(s) on which they are moving. There are both arboreal and terrestrial pronograde primates, but they all preferentially move the limbs in the parasagittal plane (Fig. 3a; Madar *et al.* 2002; Fleagle 2013). Otherwise, orthogrady is normally associated with fore- and hindlimbs employed in tension, with joints characterized by high ranges of motion (Badoux 1974; Stern 1975; Madar *et al.* 2002; Cant *et al.* 2003). Thus, this type of body plan is related to forelimb-dominated behaviours such as vertical climbing and below-branch suspension, and hindlimb-dominated terrestrial bipedalism in the case of humans (Fig. 3b; Hunt *et al.* 1996; Hunt 2016). Probably, socioecological factors took an important role in acquisition of the "ape-like" traits (e.g., environment, food resources, predators, and social structure preferences; McGraw 1998; Fleagle 2013; Senut 2015; Hunt 2016). In this regard, such socioecological factors might be the reason for which some suspensory-related traits (mainly of the thorax, shoulder and elbow) that characterize living hominoids also evolved in other primate groups such as suspensory atelids (e.g., broad thorax, round humeral head, and oval glenoid fossa; see below; Erikson 1963; Larson 1998a; Hunt 2016). These similarities suggest that orthograde-like traits associated with suspensory behaviours and/or vertical climbing could evolve independently in several groups of primates (e.g., Erikson 1963; Larson 1998a; Young 2003; Almécija *et al.* 2007; Hunt 2016).

Hence, apart from the synapomorphies of the group concerning dental and cranial anatomy (see e.g., Fleagle 2013), hominoids are defined by possessing an orthograde body plan (Stern 1975; Martin 1990; Hunt 2016). Such body organization is characterized by a series of traits (see below; Table 3) mostly related to widen the range of motion of the joints and to reduce stresses derived of suspension and/or vertical climbing behaviours typical of living apes (and some atelids; Hunt 2016). Humans, although being orthograde primates and showing anatomical similarities with other non-human hominoids (e.g., broad and shallow thorax; see below), overall depart from the ape-like model due to their specialized terrestrial bipedalism (e.g., pelvis shape, lumbar lordosis, and non-opposable hallux; Schultz 1950, 1960, 1961; Martin 1990; Fleagle 2013).

Thus, orthograde primates usually display the following morphological features: short, wide and shallow thorax; large clavicles and scapulae placed dorsally (with the glenoid fossa facing laterally); expanded and dorsally rotated iliac blades; lumbar region short and stiff; lack of tail; and forelimbs longer than hindlimbs (Stern 1975; Cartmill and Milton 1977; Martin 1990; Cant *et al.* 2003; Fleagle 2013; Hunt 2016). Together with the previously mentioned orthograde-related anatomical traits, hominoids share (if not said otherwise below) a series of morphological adaptations associated with arm-hanging and SVCC (behaviours that distinguished apes from monkeys; see previous section; Isler 2005; Crompton *et al.* 2010; Crompton 2016; Hunt 2016). Thus, adaptation related to an orthograde body plan and/or key (functionally meaningful) morphological SVCC specializations that characterized apes (and also suspensory atelids in some cases) are summarized below (see also Table 3):

- *Mediolaterally wide and dorsoventrally shallow thorax, strongly curved ribs, and mediolaterally wide manubria:* all these features are related to orthogrady (Schultz 1960, 1961; Hunt 1991a, 1992, 2016; Fleagle 2013; Ward 2015). This complex of features is presumably associated with the reduction of cranio-caudal compressive and dorso-ventrally tensile forces in the rib cage during suspensory behaviours (Hunt 1991b, 2016). This is possible due to a more effective weight bearing and the counteraction of tensile forces generated by the conjunct of muscles and bone structures around the shoulder-thorax (Hunt 2016). Moreover, the shape of the thorax allows wider shoulder excursions, mainly in the coronal plane (Hunt 1991b, 2016). The hominoid trunk morphology results in a dorsally placed scapula (see below), more ventrally placed vertebral bodies and longer clavicles than in monkeys (Schultz 1950, 1961; Stern 1975; Fleagle 2013).

- *Dorsally placed scapula:* hominoids display in general a deep and narrow scapula that is situated dorsally relative to the thorax. The glenoid fossa is oval and faces cranially (Hunt 1991a, 1992; Rose 1993; Fleagle 2013; Ward 2015). A deep and narrow scapula increases the lever arm of the *serratus* and *trapezius* muscles for forelimb abduction, whereas favours low concentrations of stress at the thorax (Larson *et al.* 1991; Larson 2015; Hunt 2016). Moreover, the above-mentioned scapular shape allows the approximation of the bone to the mediolateral midline of the body, thus avoiding eccentric stresses at the thorax (Oxnard 1963; Hunt 1991a, 2016). However, hominoids that engage in SVCC in a lesser degree (gorillas and

humans) have broader scapulae, which do not approach to the midline as in the case of chimpanzees and hylobatids (Hunt 2016). Otherwise, the oval shape of the glenoid fossa allows for mobility of the humerus virtually in any direction, including complete abduction of the humerus for arm-hanging during suspension (Hunt 1991b, 2016).

- *Short and stiff lumbar region:* the number of lumbar vertebrae is variable among hominoids (3-4 in great apes, 4-5 in siamangs, 5-6 in gibbons, and 5 in humans), although is lower than in non-hominoid primates (cercopithecoids have long backs with 7 lumbar vertebrae; Schultz 1961; Fleagle 1978; Williams *et al*. 2016). Besides, these lumbar vertebrae display short and broad bodies, and have a ventral keel, as compared to pronograde monkeys (Schultz 1936, 1961). A reduced number of lumbar vertebrae closes the rib cage to the pelvis and, together with vertebral morphology, are associated with resistance to bending moments generated by ipsilateral movements during vertical climbing (Jungers 1984a; Hunt 1991a, 1992, 2016; Ward 1993, 2015; Fleagle 2013).

- *Long and broad ilium:* this iliac morphology has been related to either an allometric trait associated with maintaining of mechanical effectiveness of the glutei with increasing body size (needed to hindlimb extension during vertical climbing; Stern 1971); or, as in the previous case, to resist buckling forces generated from vertical climbing behaviours by reducing the bending moments (Hunt 2016). Nonetheless, these functional hypotheses still remain as tentative.

- *Tailless:* hominoids lack an external tail. The functional role of the tail absence has not been clarified yet. Nonetheless, some authors (Fleagle 2013; Hunt 2016) suggest that the hominoids tailless condition could be related to their large body size (allometric effect); whereas others proposed that, at some point, the balancing counteraction function of the tail during above-branch quadrupedalism was not needed anymore (probably also due to an increased body size and the shift towards suspensory behaviours in hominoids; Cartmill 1985; Cant 1987; Kelley 1997; Hunt 2016).

- *Long forelimbs (high intermembral index):* a good proxy of broad patterns of locomotion is the intermembral index: ratio of the forelimb length (humerus + radius) to hindlimb length (femur + tibia; Martin 1990). Species with high frequency of SVCC behaviours show high index values (100-150%; Napier and Walker 1967; Jungers 1984b, 1985; Martin 1990; Anemone 1993; Gebo and Chapman 1995). In other words, primates that rely on SVCC behaviours tend to have longer forelimbs relative to the hindlimbs than quadrupeds, leapers and bipeds (e.g., gibbons and siamangs show the highest values for this index, between 126-147%; Jungers 1984a,b, 1985; Hunt 1992; Isler 2005; Fleagle 2013). Modern humans (bipeds) are an exception among hominoids, since their hindlimbs are relatively much longer than their forelimbs compare to SVCC hominoids (72%; Jungers 1985; Martin 1990; Begun 2013; Fleagle 2013). Two functionally-related hypotheses have been proposed for the forelimb elongation in apes: favouring foraging efficiency (Tuttle 1969; Grand 1972) and increasing friction on the sole during climbing behaviours (e.g., Cartmill 1972; Jungers 1976; Sarmiento 1989; see also a review of both hypotheses in Hunt 2016). The former, together with a highly mobile forelimb and short hindlimbs (see below), is related to the capacity of covering a

larger area in which food items can be foraged, thus improving feeding efficiency by reducing movement between feeding points (Tuttle 1969; Grand 1972; Jungers 1984a). Likewise, the larger the forelimb, the further the distance achieving to obtain food from the most terminal branches while maintaining the body in a stable support (Tuttle 1969). Otherwise, longer forelimbs would allow primates to move along large-diameter supports (those not accessible by grasping with the feet) by increasing friction between the vertical support and the feet (Cartmill 1972; Jungers 1976; Fleagle 2013).

- *Mobile shoulder:* the proximal hominoid humerus usually shows a globular head with distally displaced tubercles and a narrow bicipital groove (Rose 1988; Gebo 1996; Fleagle 2013). Moreover, the shoulder joint faces cranially due to the dorsal position of the scapula (see above; Fleagle 2013). Overall, all these adaptations physically favour forelimb mobility at the shoulder joint in any direction, but mainly the craniodorsal movement, thus facilitating arm-raising (especially in hylobatids, which have the most dorsally placed scapula relative to the other non-hylobatid hominoids; Chan 2008; Hunt 2016). Moreover, all hominoids show a relatively high humeral torsion (head facing more medially), a trait derived from the dorsal position of the scapula and usually related to suspensory habits (allowing higher shoulder mobility; Napier and Davis 1959; Campbell 1966; Larson 1996). In this regard, African apes show the highest humeral torsion among hominoids probably due to their quadrupedal habits (Larson 1988, 1996). In addition, the globular and large head of the humerus reduces stress concentrations, spreading it over a greater area (Kimura *et al*. 1979; Hunt 2016). Likewise, the scapula usually shows a long acromion, a distally place deltoid crest, and an elongated coracoid process (Tuttle 1975; Harrison 1987). The morphology of the acromion and the deltoid crest are associated with the moment arm increasing of the deltoid muscle and the forelimb itself, also favouring the arm-raising. Finally, the elongation of the coracoid process enhances the *biceps* muscle lever arm, which improves a powerful flexion of the elbow (Hunt 2016).

- *Stable extended elbow:* hominoids display an array of characteristic traits at the elbow. The distal humerus shows a large and medially faced medial epicondyle, a spool-shaped trochlea, a steep zona conoidea, a globular capitulum, and a deep olecranon fossa. The ulna displays a short olecranon and a large coronoid process, whereas the radius has a symmetrical radial head. Both ulna and radius are generally long, slender and bowed (Tuttle 1975; Rose 1988, 1993; Gebo 1996; Fleagle 2013; Hunt 2016). Overall, these features allow full extension of the elbow and favour stabilization of the joint at this position and during pronation/supination of the forearm (Rose 1988; Hunt 2016). On the one hand, the shape of the humeral trochlea (spool-like), the angle formed by this trochlea and the capitulum (steep), and the radial head (round and bevelled) prevent for the dislocation of the ulna and radius (*ibid*). Otherwise, the globular morphology of the humeral capitulum allows for larger excursions of the forearm during pronation-supination (Rose 1988). These movements are also enhanced by the increasing of the moment arm of the pronators muscles due to the bowed morphology of the forearm bones (Hunt 2016). Regarding the ulna, the short olecranon process and its articular surface morphology (posteriorly covering the olecranon trochlea of the humerus) allow the full extension of the elbow like a hinge joint and assume the

most of the weight loading during arm-hanging. Finally, the coronoid process of the ulna usually extends anteriorly, increasing the moment arm of the *brachialis* muscle in full-extended positions of the elbow. This fact favours the flexion of that joint from extended positions (Fleagle 2013; Hunt 2016).

- *Wrist morphology:* the wrist plays an important role during climbing and suspension by increasing mobility and grasping capabilities. Thus, the ulna lacks its contact with the carpal bones and the pisiform is placed more distally than in monkeys. This morphology increases ulnar deviation and rotational capabilities, mainly related to pronation/supination (Lewis 1969, 1989; Tuttle 1969; Sarmiento 1988; Fleagle 2013; Hunt 2016). Hunt (1991b) also suggested that the combination of reduced ulno-carpal contact and long fingers (see below) would decrease the stress at the wrist during arm-hanging due to a lower deviation of the ulna.

- *Long and curved phalanges:* this morphology is typical of Asian apes and chimpanzees. Among these groups, hylobatids have the longest phalanges and chimpanzees the shortest, being orangutans intermediate between these two taxa. Regarding the curvature, orangutans show the most curved phalanges whereas chimpanzees display the least curved phalanges among the three (*Pan*, *Pongo* and hylobatids). Otherwise, gorillas and humans show shorter and more robust phalanges (Lewis 1969, 1989; Tuttle 1969; Susman 1979; Sarmiento 1988; Stern *et al.* 1995; Fleagle 2013; Almécija *et al.* 2015a; Hunt 2016). Furthermore, the overall proportions of the hand (phalanges + metacarpals) result in high relative hand lengths in hominoids, higher in specialized suspensory apes (mainly orangutans) than in those that perform a more generalized positional behaviour (e.g., gorillas; Moyà-Solà *et al.* 2005a). Furthermore, living apes can be also distinguished by their extrinsic hand proportions, with hylobatids having elongated digits and thumb, chimpanzees and orangutans displaying elongated digits relative to the thumb, and gorillas (as humans) showing more plesiomorphic proportions (long thumb relative to the digits; Almécija *et al.* 2015a). Despite these differences, the long and curved phalangeal shape reduces stresses derived of arm-hanging a circular support and allow for a more effective circumduction of the supports (Cartmill and Milton 1977; Preuschoft and Demes 1984; Hunt 1991b, 2016; Preuschoft *et al.* 1993). Moreover, phalanges also display robust flexor sheath ridges where the flexor tendons attach. This morphology prevents for bow stringing during suspension (Tuttle 1969; Hunt 2016).

- *Hindlimb:* the hominoid femur displays a spherical head fully covered by articular surface, a high neck-shaft angle, and short biomechanical neck length; a broad distal femur, and shallow condyles and patellar groove (Lovejoy *et al.* 1973; Rose 1983; Lovejoy 1988, 2005, 2007; Aiello and Dean 1990; Stern and Susman 1991; Fleagle 2013). The tibia has a mediolaterally wide distal articular surface, and a relatively thick medial malleolus; whereas the fibula is robust and its distal articular surface is obliquely faced (Rose *et al.* 1996; Marchi 2007; DeSilva 2008; DeSilva *et al.* 2010). Altogether, these traits are related to enhance hindlimb joint mobility, favouring non-stereotyped positions, mainly related to abduction and lateral rotation of the hip, and dorsiflexion and inversion of the ankle (see Chapter 1 for detailed information on the functional meaning of these features; Lovejoy *et al.* 1973, 2002; Aiello and Dean 1990; Rose *et al.* 1996;

DeSilva *et al.* 2010). Moreover, the fibular robusticity and the morphology of its distal articular surface are associated with the important role of the hominoid fibula in weight bearing (Marchi 2007).

- *Feet:* as in the case of hands, feet of suspensory primates have in general long and curved fingers for enhancing gripping abilities, mainly during vertical climbing along low-diameter supports. Moreover, the talus has a shallow trochlea and the calcaneus is short to favour eccentric, non-stereotyped movements of the ankle (Schultz 1936, 1963; Tuttle 1970; Rose 1993).

As shown above, hominoids have in common an important array of morphological features related to SVCC behaviours. However, due to their specialized locomotor modes, African apes and humans departs from the common pattern, showing a differential morphology in some cases. Thus, African apes (gorillas and common chimpanzees) are the unique primates that engage in knuckle-walking (Tuttle 1967; Doran 1996; Richmond *et al.* 2001; Fleagle 2013). The majority of differences related to the rest of SVCC primates are found at the wrist and hand. They are usually associated with the way of loading weight along the forelimbs (e.g., increasing of articular surfaces of the wrist, and further reduced ulnar styloid process; Tuttle 1967, 1969; Sarmiento 1988; Hunt 1991a, 1992; Kivell *et al.* 2009). Another adaptation commonly associated with this locomotor type is the presence of strong dorsal ridges on the distal metacarpals (this trait has been also found in large terrestrial digitigrade monkeys, although less marked). This morphology provides further stabilization of the joints during hyperextended positions of the proximal phalanges (Tuttle 1969; Jenkins and Fleagle 1975; Hunt 2016).

Finally, the acquisition of bipedalism in modern humans implied the reorganization of critical portions of the postcranial (and cranial) skeleton (Ward 2015). Nonetheless, similarities linking the anatomy of apes and humans' forelimb and foot have been also found and well documented (Morton 1926; Fleagle *et al.* 1981; Lewis 1989). The pelvic and hindlimb anatomy is unique in modern humans (Zuckerman *et al.* 1973; Fleagle *et al.* 1981). Stern (1971) proposed that, despite being humans and apes closer relatives, the howling monkey (*Alouatta*) would have the hip and hindlimb musculature that more easily transformed into a human-like anatomy. Hence, as in leapers, the forelimbs in humans do not take an important role in locomotion and the main anatomical changes are associated with the thorax and hindlimbs (Lovejoy 2005, 2007; Fleagle 2013). Among the most diagnostic changes, the vertebral column integrates two curvatures at the thoracic (kyphosis) and lumbar (lordosis) levels; spines of the cervical vertebrae were reduced; the foramen magnum moved to a basal position in the skull; the pelvis was shortened and the iliac blade is broad (implying a reorganization of the glutei muscles complex); the femora is long and the femoral head is very large; in the posterior side of the neck, the femur exhibits the *obturator externus* groove; the knee joint acquired a position *in valgus* and then the femur has a high bicondylar angle; the femur also displays an anteriorly projected lateral lip of the patellar groove; finally, the opposability of the hallux was lost and the phalanges were extremely shortened; the feet also show a marked plantar arch unique among primates (Lovejoy *et al.* 1973, 2002; Aiello and Dean 1990; Martin 1990; Lovejoy 2005, 2007; Fleagle

2013). The most of the changes have been associated with prevent mediolateral excursions of the centre of mass and prevent body from gravity, provide propulsive force and weight-bearing exclusively with the hindlimbs, and reduce locomotor energy cost (Badoux 1974; Alexander 1984; Eng and Winter 1995; Presuchoft 2004; Brujin *et al.* 2008; Herr and Popovic 2008; Pontzer *et al.* 2009).

Evolutionary history of hominoids

Hominoids diverged from cercopithecoids (Old World monkeys) in the late Oligocene, back to ca. 25 million of years ago, Ma (Springer *et al.* 2012; Harrison 2013). Within the Hominoidea, authors have estimated a pattern of divergence as follows: Hylobatydae (*Symphalangus* > *Nomascus* > *Hoolock* > *Hylobates*) > *Pongo* > *Gorilla* > *Pan* > *Homo*; branching off at around 17 Ma (Hylobatidae-Hominidae), ~15 Ma (Ponginae-Hominidae), ~8.0 Ma (*Gorilla-Pan+Homo*), and ~6.7 Ma (*Pan-Homo*; Springer *et al.* 2012). The hominoid fossil record backs up to ~25.2 Ma (late Oligocene) and is represented by a fragmentary jaw with teeth from the Nsungwe 2B locality (Tanzania) attributed to the genus *Rukwapithecus* (Stevens *et al.* 2013). At around this time (25 Ma), there are other fossil remains, a partial mandible and some isolated teeth, that probably belonged to the Hominoidea. These remains were assigned to the genus *Kamoyapithecus*, although its taxonomic attribution to this group is still uncertain (Leakey *et al.* 1995; Begun 2013). Likewise, the hominoid-like fossil remains found at Meswa Bridge (Kenya), dated in ca. 23.5 Ma, have been also tentatively attributed to the taxon *Proconsul* (Andrews *et al.* 1981; Pickford and Andrews 1981; Finarelli and Clyde 2004; McNulty *et al.* 2015). Proconsuloids were probably the precursors of modern hominoids during the early Miocene (23-16 Ma), being considered stem members of the group (e.g., Begun *et al.* 1997; although see Harrison and Rook 1997 and Harrison 2010a for a different interpretation; Table 2). Its diversity decreased with the environmental changes happening at that time in Africa, allowing other early hominoids to become more diversified between 17-14 Ma (e.g., *Equatorius*, *Kenyapithecus*, *Nacholapithecus*; Harrison 2010b). The Middle Miocene Climatic Optimum (16-15 Ma) allowed the widespread of hominoids from Africa through Eurasia, becoming highly diverse between 13-9 Ma especially in western and central Europe (e.g., presence of *Griphopithecus*, *Kenyapithecus*, *Dryopithecus*, *Pierolapithecus*, *Anoiapithecus*, and *Hispanopithecus*; Moyà-Solà and Köhler 1996; Moyà-Solà *et al.* 2004, 2009a,b; Kelley *et al.* 2008; Harrison 2010a,b; Alba 2012; Begun *et al.* 2012; Begun 2015) and Asia (e.g., radiation of *Sivapithecus*, *Lufengpithecus* and *Ankarapithecus*; Pilbeam *et al.* 1980; Kelley and Pilbeam 1986; Begun and Güleç 1998; Kelley 2002; Harrison 2010b; Begun 2013, 2015). Phylogenetic relations of these taxa are still under debate and many problems in interpreting hominoid evolution remain due in part to the mixture of primitive-derived features found in these fossil taxa (see below). Notwithstanding, most authors agree that *Sivapithecus* belongs to the Ponginae, whereas the taxonomic affinities of the European fossil hominoids (the "dryopithecins") are more controversial. Some authors proposed that these taxa relate to hominines (e.g., Begun *et al.* 1997; Begun 2009); but others considered them as stem hominids or even stem pongines (Moyà-Solà and Köhler 1996; Alba 2012; Pérez de los Ríos *et al.* 2012; Alba

et al. 2015; and references therein).

At around 9.6 Ma, an extinction is detected for some mammalian taxa in Europe, including primates (traditionally known as the Vallesian Crisis; Casanovas-Vilar *et al.* 2015). At this point only *Oreopithecus*, in its Tuscano-Sardinian island refuge, and the dry-open woodlands-specialists *Ouranopithecus* and *Udabnopithecus* survived during the late Miocene of Europe (until ca. 6 Ma; de Bonis and Koufos 1997; Begun 2013). By 5 Ma, hominoids had become extinct from Eurasia, with the exception of *Gigantopithecus* (which survived until ca. 0.3 Ma) and the currently living taxa, orangutans and hylobatids (Harrison 2010b; Begun 2015).

Africa has a scarce fossil record of late Miocene hominoids (between 13-7 Ma). However, new discoveries are shedding light to this period and to the evolution of the younger ancestral hominids and hominins, as well as their phylogenetic relationships with the living taxa (e.g., *Nakalipithecus*, *Samburupithecus* and *Chororapithecus*; Ishida and Pickford 1997; Kunimatsu *et al.* 2007; Suwa *et al.* 2007; Harrison 2010b; Begun 2013; Katoh *et al.* 2016). More recently, during the last part of the late Miocene and the beginning of the Pliocene, Africa has yielded the possible earliest hominins (i.e., the human clade), including the genera *Sahelanthropus*, *Orrorin*, and *Ardipithecus* (White *et al.* 1994, 2009; Senut *et al.* 2001; Brunet *et al.* 2002). At about 4 Ma-onwards, the fossil record of the closer humans relatives is more abundant and diverse (especially in East Africa), and has generated a great amount of information about our most recent past by the study of *Australopithecus*, *Paranthropus* and early *Homo* species (e.g., see extensive recent reviews in Reed *et al.* 2013 and Henke and Tattersal 2015).

Locomotion of fossil hominoids

Shape results from a compromise between the interaction of different selective pressures emanating from the environment, substrate, size and mechanical factors efficiency and, consequently, specific adaptations to different locomotor modes can be some times identified in the morphology preserved in the hard tissues of the postcranial skeleton. Furthermore, a high frequency of a specific positional behaviour (and its associated muscular loads) probably favour the reinforcement of the locomotor apparatus against specific mechanical stress and injuries related to that locomotor mode, as well as encouragement against fatigue and energy lost (Cant 1992; Hunt 1992). This fact could also result in specific recognizable adaptations within a species when it is compared with others that show similar locomotor profiles (Hunt 1992). These assumptions support the notion that morphological resemblances indicate also functional similarities (e.g., Pilbeam and Simons 1971; Rose 1983, 1993). Thus, recognizing the adaptive traits in extant primates is essential to do locomotor inferences in fossil taxa. Nonetheless, it is also important take into account that most (if not all) of the primate extinct taxa do not show a complete set of exact resemblances with any living primate (e.g., Anemone 1993; Rose 1993; Moyà-Solà *et al.* 2004; Almécija *et al.* 2007; Senut 2015). Hence, the sometimes-elusive relation between form-function and the lack of extant

morphological analogues make difficult to reconstructing the locomotor behaviour of fossil primates.

Currently, the Hominoidea superfamily is represented only by few taxa (see above), a scarce representation of the diversity for this group in the past, especially during the Miocene (Table 2; Harrison 2010b; Alba 2012; Begun 2013). Thus, the Miocene was probably the "golden age" of hominoids, due to the high diversity that they reached in relation to taxonomy, biogeographic ranges, sizes, diets, and positional behaviours (e.g., Begun 2013; Fleagle 2013). Some –but not all– of the key traits defining crown hominids such as large brains, long life histories, those related to an orthograde body plan, and other diagnostic morphological features of their cranium (all considered synapomorphies of the group) are first observed in the middle and early late Miocene of Eurasia (Moyà-Solà and Köhler 1996; Begun 2002, 2009, 2013; Moyà-Solà *et al.* 2004, 2009a,b; Harrison 2010b; Begun *et al.* 2012). These traits could be considered incipient innovations that foreshadowed the suite of features and positional behaviours that currently characterize living hominoids (Rose 1993; Richmond and Jungers 2008; Begun 2013; Senut 2015). Thus, given the scarce diversity of living hominoid species, the study of Miocene apes—and especially those from the Vallès-Penedès Basin, which represent the earliest evidence of unambiguous orthograde-related features (Moyà-Solà and Köhler 1996; Moyà-Solà *et al.* 2004) —becomes essential to understand the evolutionary history of the group, giving also a deep time perspective on their morphological adaptations (Rose 1993; Senut 2015; Ward 2015).

Miocene hominoids have been characterized by a high diversity within their positional behaviours (Begun *et al.* 1997; Moyà-Solà *et al.* 2004; Almécija *et al.* 2007; Nakatsukasa and Kunimatsu 2009; Alba 2012; Ward 2015). Nonetheless, these taxa do not fit neither in the evolutionary model predicted based only with living hominoids nor within any living species positional repertoire currently known. Even though, there is a general agreement that these forms were arboreal hominoids with some extent of (mostly above-branch) quadrupedal locomotion, combined with some other locomotor modes, including orthograde behaviours, such as climbing and/or suspension, in some degree (see details on specific taxa below; Martin 1990; Rose 1993; Almécija *et al.* 2007, 2009; Senut 2015). Some of the Miocene hominoids, for which hindlimb remains are available, included in this work are: *Morotopithecus*, *Proconsul*, *Ekembo*, *Equatorius*, *Nacholapithecus*, *Sivapithecus*, *Oreopithecus*, and *Orrorin* (see Section III for the specific sample used). In spite of being a putative stem catarrhine, *Epipliopithecus* is also included in this thesis due to the available number and quality of its hindlimb remains. An overview of these taxa and their inferred positional behaviour repertoires are accounted below.

Morotopithecus bishopi

Morotopithecus bishopi remains have been found at the Moroto I and II localities (Uganda), dated at around 20.6 Ma (Gebo *et al.* 1997; MacLatchy *et al.* 2000; MacLatchy 2004; see Pickford *et al.* 1999 for a younger date estimation, 17-15 Ma, based on faunal comparisons).

This taxon is similar to other early Miocene hominoids in its cranium and teeth, but its postcranium displays more derived traits, showing some orthograde-related features (estimated body mass of 35-40 kg; Gebo *et al.* 1997; Ruff 2003; Begun 2013; Ward 2015). Only a glenoid fossa, few vertebrae and partial femora are known for *Morotopithecus* (Fig. 4a; Walker and Rose 1968; Gebo *et al.* 1997; MacLatchy *et al.* 2000, 2015; Nakatsukasa 2008). This postcranial evidence suggests that this taxon would be the first representative of orthogrady in the fossil record, being even more derived postcranially than other younger Miocene hominoids (e.g., *Ekembo* or *Kenyapithecus*; see below; Gebo *et al.* 1997; MacLatchy *et al.* 2000; MacLatchy 2004; Young and MacLatchy 2004). Authors proposed that *Morotopithecus* would be an arboreal primate that engaged in quadrupedal behaviours, but that also displayed forelimb-dominated habits, such as vertical and cautious climbing, clambering, below-branch suspension and arm-hanging (Gebo *et al.* 1997; MacLatchy *et al.* 2000, 2015; MacLatchy 2004).

Proconsul major and *Ekembo* spp.

Proconsul (*sensu lato*, that is, including the recently erected genus *Ekembo*; see below) is probably the best known Miocene hominoid due to the numerous fossils recovered from virtually any anatomical region (cranial, dentognathic and postcranial remains; e.g., Le Gros Clark and Leakey 1951; Napier and

Figure 4 Some of the most representative postcranial remains of Miocene hominoids included in this work. **a**, *Morotopithecus bishopi* partial femur (MUZM80; anterior view); **b**, *Proconsul major* proximal femur (NAP IX 49'99; anterior view); **c**, *Proconsul major* distal tibia (NAP I'58; anterior view); **d**, *Ekembo nyanzae* partial femur (KNM-MW13142A; anterior view); **e**, *Ekembo nyanzae* patellae (KNM-RU18384, top; KNM-RU17382, bottom; posterior view); **f**, *Sivapithecus indicus* distal tibia (YGSP1656; anterior view); **g**, *Nacholaptihecus kerioi* partial femur (KNM-BG35250A; anterior view); **h**, *Nacholapithecus kerioi* distal tibia (KNM-BG35250H; anterior view); **i**, *Nacholapithecus kerioi* patella (KNM-BG15535; posterior view); **j**, *Epipliopithecus vindobonensis* femur (NHMW1970/1397/0023; anterior view); **k**, *Epipliopithecus vindobonensis* tibia (NHMW1970/1398/0003; anterior view); **l**, *Epipliopithecus vindobonensis* patella (NHMW1970/1397/0025; posterior view); **m**, *Orrorin tugenensis* partial femur (BAR1002'00; anterior view). Scale bar = 10 mm. Images from (a,b,d) Senut (2015), (c) Rafferty *et al.* (1995), (e) Ward *et al.* (1995), (f) DeSilva *et al.* (2010), (g-i) Ishida *et al.* (2004), (j-l) this work, and (m) Pickford *et al.* (2002).

Davis 1959; Walker and Pickford 1983; Walker *et al.* 1985, 1993; Walker and Teaford 1988; Ward *et al.* 1993; Walker 1997; Gommery *et al.* 1998, 2002; Senut *et al.* 2000). Fossil material assigned to *Proconsul s.l.* is abundant and diverse, resulting in a controversial taxonomy recently revisited by McNulty and colleagues (2015). They proposed splitting *Proconsul* into two genera *Proconsul* (including *P. africanus*, *P. major*, and *P. meswae* from the Tinderet and Ugandan localities) and *Ekembo* (including *E. heseloni* and *E. nyanzae* from the Kisingiri localities). This work follows this new taxonomic approach and considers fossils from the Kisingiri localities within the new taxon *Ekembo* (*E. nyanzae* and *E. heseloni*.) and Ugandan remains (except those of Moroto) within the genus *Proconsul* (*P. major*). However, other authors (Senut *et al.* 2000; Gommery *et al.* 2002; Senut 2015) consider that *Proconsul major* would be a different genus, *Ugandapithecus*. They also include some of the specimens from Moroto (e.g., the palate of the holotype specimen) within *Ugandapithecus* (Senut *et al.* 2000). Nonetheless, Moroto specimens are sustained within the genus *Morotopithecus* in this work following those of Gebo *et al.* (1997), MacLatchy (2000), and McNulty *et al.* (2015).

Overall, and despite taxonomic disagreements, *Proconsul* and *Ekembo* material has been dated between 20-17.8 Ma, early Miocene (see specific estimations for every species / fossil remains included in this work in Section III; Harrison 1982; Ward *et al.* 1993, 1995; Rafferty *et al.* 1995; DeSilva 2008). There exists material that would extent the upper and lower range of appearance of *Proconsul-Ekembo*, although taxonomic attributions are still tentative (remains from Meswa Bridge, 23.5 Ma, and Ngorora Formation at Tugen Hills, 12.5 Ma; Pickford and Andrews 1981; Hill and Ward 1988; Hill *et al.* 2002). *Proconsul major* material dates from 20-19 Ma and is represented by a scapular fragment, a distal humerus, a proximal radius, several partial femora, a distal tibia, and several tarsals (Fig. 4b; Rafferty *et al.* 1995; Gommery *et al.* 1998, 2002; Senut *et al.* 2000; MacLatchy and DeSilva 2009; Senut 2015). In the case of *Proconsul*, the morphology of its fore- and hindlimb remains stresses more ape-like affinities than in *Ekembo* (see below; Rafferty *et al.* 1995; MacLatchy and DeSilva 2009; Senut 2015). The overall morphology of the large-bodied (60-90 kg; Gommery *et al.* 1998; MacLatchy and DeSilva 2009) *Proconsul* suggests that this taxon, apart from those associated with above-branch quadrupedalism, could already have some orthograde-related adaptations for (likely slow) climbing behaviours that well fit with the forested and humid environments inferred for Napak (Uganda; Gommery *et al.* 2002; Senut 2015).

Ekembo material has been dated between 19.7-17.8 Ma, early Miocene (Harrison 1982; Ward *et al.* 1993, 1995; Rafferty *et al.* 1995; DeSilva 2008). Postcranial remains of this taxon show an exclusive mixture of monkey- and ape-like traits and show little interspecific morphological variation despite differences in size (10-20 kg for *E. heseloni* and 20-50 kg for *E. nyanzae*; Ruff *et al.* 1989; Rafferty *et al.* 1995; Ward 1998). The postcranial remains of *Ekembo* are represented by several partial skeletons, as well as a number of isolated remains (Fig. 4c,d,e; Walker and Pickford 1983; Beard *et al.* 1986; Rose 1988, 1993; Walker and Teaford 1988; Ward *et al.* 1991, 1993; Begun *et al.* 1993; Walker *et al.* 1993; Ward 1993, 1997, 1998; Walker 1997; Harrison 2002, 2010a; Nakatsukasa *et al.* 2004a; among others). These remains evidence that this

taxon would probably be a generalized pronograde primate that relied on above-branch quadrupedalism, although showing joint morphologies that allow more versatile movements (Harrison 2010a; Senut 2015; Ward 2015).

Equatorius africanus

This gnus comprises a single species, *Equatorius africanus* (formerly *Kenyapithecus africanus*), whose fossil remains have been recovered from several contemporary sites in the Maboko Formation and Kipsaramon (Tugen Hills), Kenya (Benefit and McCrossin 1993; Ward *et al.* 1999; Kelley *et al.* 2002). Fossil localities at these formations have been dated at around 16-15 Ma (Ward *et al.* 1999; Kelley *et al.* 2002).

Together with several isolated fragments, the partial skeleton of this taxon found at Kipsaramon resembles that of *Ekembo* in several traits and a body mass of about 27 kg has been estimated (range between 17.3-36.3 kg including the sample of Maboko; McCrossin 1994a, 1997; McCrossin and Benefit 1997; McCrossin *et al.* 1998; Ward *et al.* 1999; Sherwood *et al.* 2002). Its general morphology suggests that *Equatorius* probably was a generalized pronograde quadruped, although showing some ape-like affinities related to orthograde habits, which might probably engage in frequent semiterrestrial behaviours (McCrossin 1997; McCrossin and Benefit 1997; Ward 1997; McCrossin *et al.* 1998; Sherwood *et al.* 2002; Patel *et al.* 2009; Ward 2015).

Nacholapithecus kerioi

Nacholapithecus kerioi species was erected by Ishida *et al.* (1999) based on the material from Nachola that was originally attributed to *Kenyapithecus africanus* (Nakatsukasa *et al.* 1998) and posteriorly transferred to *Equatorius africanus* (Ward *et al.* 1999). Then, the material assigned to *N. kerioi* was found within the Aka Aitheputh Formation (Samburu Hills, Kenya) in Nachola, and is dated in ca. 15 Ma (Nakatsukasa *et al.* 1998; Ishida *et al.* 1999; Nakatsukasa and Kunimatsu 2009).

Apart from a number of isolated fossil remains attributed to this species (most of them described by Rose *et al.* 1996), it was recovered a partial skeleton and other isolated bony specimens that provide a highly complete view on its postcranial morphology (Fig. 4g-i; Rose *et al.* 1996; Nakatsukasa *et al.* 1998, 2003a,b, 2007a,b, 2012; Takano *et al.* 2003; Ishida *et al.* 2004; Nakano *et al.* 2004; Senut *et al.* 2004; Nakatsukasa 2008; Nakatsukasa and Kunimatsu 2009; Kikuchi *et al.* 2015; Ogihara *et al.* 2016). A body mass of 20-23 kg has been estimated for *Nacholapithecus* (Rose *et al.* 1996; Ishida *et al.* 2004; Nakatsukasa and Kunimatsu 2009). The overall body plan of *Nacholapithecus* is similar to that of *Ekembo* (e.g., narrow thorax and lumbar vertebrae morphology), although the former exhibits more derived features (e.g., longer pedal digits, longer clavicle, a clear ball-and-socket morphology at the distal humerus, and higher neck-shaft angle; Nakatsukasa *et al.* 1998, 2004b, 2007a; Ishida *et al.* 2004; Senut *et al.* 2004). These derived (towards living hominoids) features provide insights into the positional behaviour of *Nacholapithecus*, which would

include the one of the earliest evidence of forelimb-dominated behaviours with enhancement of vertical climbing capabilities (no specific adaptations for suspension have been found). Nonetheless, this taxon would also retain several traits related to arboreal quadrupedalism (Nakatsukasa and Kunimatsu 2009; Nakatsukasa *et al.* 2012; Begun 2013).

Epipliopithecus vindobonensis

Epipliopithecus vindobonensis is one of the best well-known Miocene putative stem catarrhines due to the abundant postcranial remains from several individuals (Fig. 4j-l; Zapfe 1958, 1960). Two partial skeletons and some other isolated bones of additional individuals were found at the Neudorf a.d. March (Devínská Nová Ves) locality in Slovakia and dated in the early middle Miocene (Zapfe 1958, 1960).

The anatomy of this taxon was deeply described in a monograph by Zapfe (1960) and refined by subsequent authors (e.g., Fleagle 1983; Rose 1988, 1993, 1994; Rein *et al.* 2011; Harrison 2013; Arias-Martorell *et al.* 2015). *Epipliopithecus* was a medium-sized primate (around 7 kg; Fleagle 2013), whose positional behaviour has been the focus of an intense debate along the years because it resembles suspensory platyrrhines, quadruped cercopithecids and, in somehow, specialized hylobatids. Nonetheless, the positional behaviour repertoire inferred for *Epipliopithecus* would include generalized arboreal quadrupedalism (or even terrestrial), with some degree of agile above-branch quadrupedalism, combined with climbing, and probably hindlimb and forelimb suspension and leaping in some extent (Zapfe 1958, 1960; Fleagle 1983; Rose 1983, 1989, 1994; Rein *et al.* 2011; Harrison 2013; Arias-Martorell *et al.* 2015). Thus, *Epipliopithecus* positional behaviour may likely be similar to that observed in extant *Ateles* and/or *Lagothrix*, which combine a pronograde body plan with orthograde-related behaviours, such as suspension (Fleagle 1983; Rose 1983; Arias-Martorell *et al.* 2015).

***Sivapithecus* spp.**

Sivapithecus remains have been recovered from more than 100 localities in the Siwalik molasse of India, Nepal and Pakistan. Stratigraphy of this complex has been deeply studied, throwing a range of appearance for *Sivapithecus* from 12.7 Ma to ca. 8.5 Ma (Johnson *et al.* 1983; Kelley and Pilbeam 1986; Kappelman *et al.* 1991; Barry *et al.* 2002; Kelley 2005; Morgan *et al.* 2015).

Sivapithecus is a well-known taxon regarding dental and mandibular remains. Likewise, postcranial remains of several anatomical regions have been also recovered (e.g., pelvis, humerus, femur, tibia, hand and feet; Fig. 4f; Pilbeam *et al.* 1980, 1990; Raza *et al.* 1983; Rose 1986, 1993; Spoor *et al.* 1991; Richmond and Whalen 2001; Madar *et al.* 2002; DeSilva *et al.* 2010; Begun and Kivell 2011; Morgan *et al.* 2015). The combination of a mosaic postcranial morphology with orang-like cranial affinities led to mixed inferences about its phylogenetic relations, as well as its positional behaviour. This currently unknown mixture of features observed in this taxon was referred by Pilbeam and Young (2001) as the "*Sivapithecus* dilemma".

Postcranial remains of *Sivapithecus* have been assigned to three different species: *S. indicus* (12.7-11.4 Ma), *S. sivalensis* (11-8.5 Ma), and *S. parvada* (10.1 Ma; Kelley 2005). Although they diverge on body size (estimated on about 69 kg for *S. parvada* and around 50 kg for *S. indicus*; Kelley 1988), no substantial morphological differences among them have been found (DeSilva *et al.* 2010; Morgan *et al.* 2015). Therefore, although facial features more resemble living orangutans, postcranial morphology of *Sivapithecus* throws a mixed framework of its locomotor repertoire (Pilbeam *et al.* 1980; Pilbeam and Young 2001; Morgan *et al.* 2015). This evidence suggests pronograde quadrupedal habits with slow-motion and deliberate above-branch arborealism (probably with hand/feet grasping capabilities), combined with some degree of orthograde behaviours (most likely vertical climbing; Spoor *et al.* 1991; Madar *et al.* 2002; Begun 2013; Morgan *et al.* 2015; Ward 2015). Besides, this taxon might also rely on some terrestrial behaviours (Madar *et al.* 2002; Begun 2013; Ward 2015). Some authors have even proposed that *Sivapithecus* developed some knuckle-walking adaptations in parallel with living African apes (Begun and Kivell 2011).

Oreopithecus bambolii

Oreopithecus bambolii is the unique species erected for this genus (Gervais 1872), and it has been found in several localities of the late Miocene of Italy: five localities at the Maremma Valley (Tuscany), Serrazzano, and Sardinia (Azzaroli *et al.* 1986; Harrison and Rook 1997; Rook *et al.* 2000). A specific horizon of Baccinello (Maremma Valley) has been dated in ca. 7.55 Ma (Rook *et al.* 1996, 2000). Only Baccinello has been dated by palaeomagnetism, but both Serrazzano and Sardinia correlate with the Baccinello horizon and their biocronology also situate these localities within the Turolian-Ventian (MN12-13, 8.5-6.5 Ma; Azzaroli *et al.* 1986; Agustí *et al.* 2001; Begun 2013).

An amount of fossil remains have been found of this taxon, but its phylogenetic relationships and morphological affinities have generated a number of articles and even though they already remain unclear (see a revision in Begun 2002, 2013). Among the *Oreopithecus* remains, there is a nearly complete skeleton, crushed during fossilization (Schultz 1960; Straus 1963; Hürzeler 1968; Harrison 1986; Rose 1993), which allows for a body weight estimation of around 32 kg (Stern and Jungers 1985; Jungers 1987, 1990a). The study of *Oreopithecus* postcranial remains has yielded a considerable number of articles (Schultz 1960; Hürzeler 1968; Harrison 1986, 1991a; Jungers 1987; Sarmiento 1987; Ruff 1988; Rose 1993; Ward *et al.* 1995; Harrison and Rook 1997; Köhler and Moyà-Solà 1997; Moyà-Solà *et al.* 1999, 2005b; Rook *et al.* 1999; Susman 2004, 2005; Begun 2013; Russo and Shapiro 2013; Almécija *et al.* 2014; Ward 2015). From these works is derived that *Oreopithecus* most probably had an orthograde body plan and was clearly adapted for below-branch suspensory and climbing behaviours (Jungers 1990a; Susman 2004; although see Moyà-Solà *et al.* 1999 and Rook *et al.* 1999 for an alternative hypothesis for *O. bambolli* positional behaviour, which would include an important component of bipedalism, as well as pad-to-pad precision gripping capabilities).

Orrorin tugenensis

Orrorin tugenensis is a 6 million-year-old fossil hominoid species erected from remains recovered in several localities of the Lukeino Formation (Tugen Hills, Kenya; Senut *et al.* 2001). Among these remains, there are teeth, mandible fragments, three partial femora, a partial humerus, and two phalanges (Fig. 4m; Senut *et al.* 2001; Pickford *et al.* 2002; Galik *et al.* 2004; Gommery and Senut 2006; Nakatsukasa *et al.* 2007c; Richmond and Jungers 2008; Almécija *et al.* 2010, 2013; Kuperavage *et al.* 2010; Bleuze 2012; Senut 2015). Nakatsukasa *et al.* (2007c) estimated a body mass of around 35-50 kg for this taxon (based on the femur BAR1002'00 attributed to a young adult). Altogether, the external morphology of this Miocene basal hominin would be intermediate between older Miocene apes and early hominins (australopiths), probably sharing hip gait biomechanics with the latter (Richmond and Jungers 2008; Almécija *et al.* 2013). Features of the humerus and the juvenile manual proximal phalanx have been linked with climbing behaviours, whereas the pollical distal phalanx inform us of the presence of human-like precision grasping capabilities in *Orrorin*. The femora shows a combination of derived (hominin-like) adaptations (e.g., hyperextension of the hip joint), probably related to habitual bipedal habits (Senut *et al.* 2001; Pickford *et al.* 2002; Richmond and Jungers 2008; Senut 2015) superimposed in a plesiomorphic (Miocene ape-like) morphology (Almécija *et al.* 2010, 2013).

THE GREAT APES OF THE VALLÈS-PENEDÈS BASIN: STATE-OF-THE-ART

The Vallès-Penedès Basin (NE, Iberian Peninsula; see Section III) has yielded a surprisingly rich and diverse number of Miocene primates (from the late Aragonian to the late Vallesian; Casanovas-Vilar *et al.* 2011, 2015), including pliopithecoids (which are stem catarrhines preceding the monkey-ape divergence; Begun 2002) and hominoids (see a review in Marigó *et al.* 2014). Among the former group, three genera have been identified: one pliopithecine, *Pliopithecus* (Abocador de Can Mata Series, ACM; Alba *et al.* 2010a); and two crouzelines, *Barberapithecus* (Castell de Barberà; Alba and Moyà-Solà 2012) and *Egarapithecus* (Torrent de Febulines; Moyà-Solà *et al.* 2001). However, the fossil hominoids recovered along the localities of the Vallès-Penedès Basin deserve special attention because the Miocene is a key moment for the evolution of the Hominoidea, as well as for the origin of the orthograde behaviours. Among the Vallès-Penedès hominoid findings there are the first unambiguous evidence of orthogrady (*Pierolapithecus*) and suspensory behaviours (*Hispanopithecus*) in the fossil record (see below). Hence, a variety of fossil remains have been found within the ACM localities. These remains have been attributed to the recently erected stem hominoid *Pliobates* (Alba *et al.* 2015), and to three additional genera of fossil great apes: *Pierolapithecus* (Moyà-Solà *et al.* 2004), *Dryopithecus* (Moyà-Solà *et al.* 2009a), and *Anoiapithecus* (Moyà-Solà *et al.* 2009b). Moreover, two other species of the genus *Hispanopithecus* have been identified in the Vallès-Penedès Basin: *H. laietanus* (Villalta Comella and Crusafont Pairó 1944) and *H. crusafonti* (Begun 1992a).

Fortunately, except in the case of *Anoiapithecus*, postcranial remains have been recovered in association with the rest of hominoid taxa, including two partial skeletons (*Pierolapithecus* and *Hispanopithecus*), which allow doing more complete locomotor inferences about their positional preferences.

As has been evidenced in previous sections, Miocene hominoids positional repertoires are unlike those of any living primate and they more resemble each other than any extant species, thus being "Miocene ape-like" (e.g., Rose 1983; Almécija *et al.* 2009, 2013; Ward 2015). Miocene great apes from the Vallès-Penedès also follow this trend. Overall, the Spanish fossil hominoids *Pierolapithecus*, *Dryopithecus* and *Hispanopithecus* exhibit a mixture of plesiomorphic (monkey- or stem hominoid-like) and derived (ape-like) traits within their postcranial anatomy (an even within every single fossil bone). This fact outlines the uniqueness of these taxa and the lack of extant positional repertoire analogues among living forms. Furthermore, these evidences advocate for a mosaic-fashion origin and evolution of the hominoid postcranium and the orthograde-like behaviours observed in extant hominoids. Thus, hominoids probably abandoned progressively (in frequency) the arboreal quadrupedalism in favour of suspensory behaviours that became more habitual and more adaptively significant with time (Rose 1983, 1993; Rae 1999; Almécija *et al.* 2007, 2009; Alba 2012, Alba *et al.* 2012a; Ward 2015;). Therefore, the mosaic nature of the hominoid postcranium during the Miocene, together with the difficulty of interpreting the functional signal of plesiomorphic traits (e.g., Latimer 1991; Lauder 1996; Ward 2002), stress in turn the difficulty of reconstructing the functional morphology of these fossil taxa.

Pierolapithecus catalaunicus

Moyà-Solà and colleagues formally erected the species *Pierolapithecus catalaunicus* in 2004 on the basis of a partial skeleton including a large part of the splachnocranium, IPS21350, found few years before in the Barranc de Can Vila 1 locality (within the Abocador de Can Mata Series, ACM, Hostalets de Pierola; Fig. 5; Moyà-Solà *et al.* 2004). This new fossil hominoid was dated in ca. 11.9 Ma (late Aragonian, middle Miocene; Moyà-Solà *et al.* 2009a; Casanovas-Vilar *et al.* 2011).

The facial morphology of *Pierolapithecus* shows some similarities with that of great apes, although it already retains a primitive more prognathous sagittal profile (Moyà-Solà *et al.* 2004; Alba 2012). Together with the ape-like characteristics of its postcranial skeleton (see below), Moyà-Solà and co-authors (2004, 2005a) stated that *Pierolapithecus* might be a stem hominid (early member of the great apes and human clade). Otherwise, Begun and Ward (2005) and Begun (2009) proposed that this taxon would be a stem hominin. A more recent study on the internal morphology of the face has related *Pierolapithecus* more closely to pongines (e.g., lack of a true frontal sinus; Pérez de los Ríos *et al.* 2012; see also Alba 2012). Despite these phylogenetic discrepancies and on the light of new taxa descriptions (Moyà-Solà *et al.* 2009a,b), *Pierolapithecus* has been included within the subfamily Dryopithecinae (Casanovas-Vilar *et al.* 2011; Alba 2012). Dryopithecines, although generally accepted as crown hominids, it is still unclear where within the Hominidae this subfamily belongs (Alba 2012).

The more than 80 bones recovered of the IPS21350 *Pierolapithecus* skeleton allow the assemblage of a largely complete view for its body plan and positional behaviour. Thus, a body mass of about 30-35 kg has been estimated for this individual, as well as hard-object feeding dietary preferences based on a relatively thick enamel thickness and dental microwear analysis (Moyà-Solà *et al.* 2004; Alba *et al.* 2010b; DeMiguel *et al.* 2014).

The degree and type of rib curvature, a long clavicle, and the lumbar vertebral morphology (lacking a ventral keel, neural process caudally oriented, and transverse processes inserted in the pedicle-body junction, among other features) suggest that *Pierolapithecus* would have an orthograde body plan with a broad and shallow thorax (Moyà-Solà *et al.* 2004; Susanna *et al.* 2010a,b). Although very fragmentary, the pelvic remains of *Pierolapithecus* show primitive features (e.g., concave gluteal surface) combined with others more derived (e.g., somewhat iliac flaring), outlining incipient orthograde-like affinities in this anatomical region (Hammond *et al.* 2013).

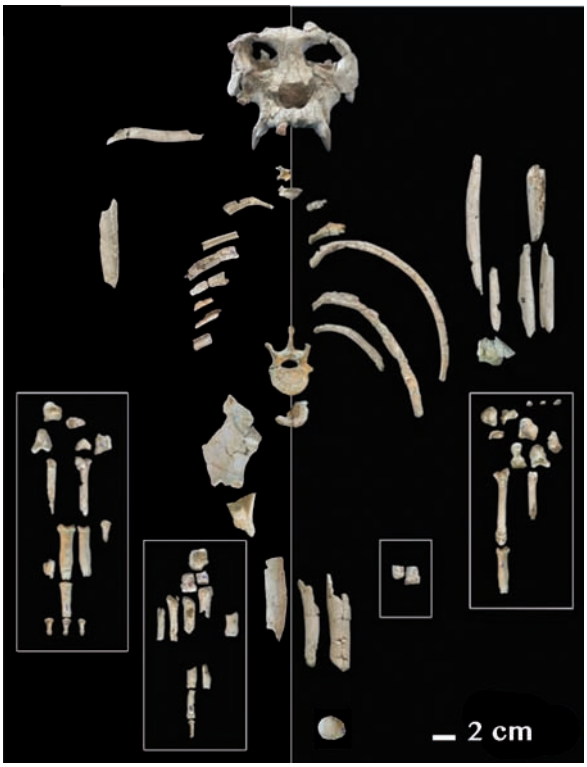

Figure 5 Partial skeleton of *Pierolapithecus catalaunicus* found in Barranc de Can Vila 1 (IPS21350). Modified from Moyà-Solà *et al.* (2004).

Within the wrist bones of *Pierolapithecus*, the most characteristics traits are the unfused os centrale (thus lacking this important African ape-human clade sinapomorphy) and the lack of contact between the ulna and the triquetrum (a hominid synapomorphy; Moyà-Solà *et al.* 2004). Contrary, the fingers of this taxon exhibit a more primitive morphology, with short metacarpals and phalanges (Moyà-Solà *et al.* 2004, 2005a). In addition, the phalanges show a series of traits related to powerful-grasping palmigrady with assistance of the pollex/hallux, such as a proximodorsally tilted proximal articular facet that besides is wide and flat, and a large and widely separated plantar tubercles surrounding a deep central depression (Moyà-Solà *et al.* 2004; Almécija *et al.* 2009). The presence of palmigrady-related features in *Pierolapithecus* are symplesiomorphies shared with earlier Miocene apes such as *Ekembo.* These hand features are commonly associated with the tail loss and the necessity of supplying the lack of a balancing system that aid on avoiding toppling from the branches (Cartmill 1985; Kelley 1997; Almécija *et al.* 2009). Furthermore, phalanges are not markedly curved as in suspensory primates (Moyà-Solà *et al.* 2004, 2005a; Alba *et al.* 2010c; contra Deane and Begun 2008, 2010).

The only complete non-pedal hindlimb remain preserved in the *Pierolapithecus* skeleton is a left patella (Moyà-Solà *et al.* 2004). An in-depth analysis of this fossil bone is presented in this work, but its general morphology clearly resemble those of great apes and is associated with versatility of the knee joint.

Altogether, the morphological traits of the *Pierolapithecus* postcranium suggest that above-branch quadrupedalism still remained an important component of its positional behaviour in combination with novel orthograde related positional behaviours, a currently unseen combination (Moyà-Solà *et al.* 2004; Almécija *et al.* 2009). Therefore, *Pierolapithecus* might display some degree of modern ape-like behaviours, such as vertical climbing (Moyà-Solà *et al.* 2004). However, this taxon lacked specific adaptations for below-branch suspension on the basis of phalangeal curvature and elongation, its monkey-like metacarpophalangeal joint morphology, and the lack of clear suspensory affinities in other anatomical regions. Nonetheless, this locomotor mode cannot be completely ruled out (Moyà-Solà *et al.* 2004, 2005a; Almécija *et al.* 2009; Alba *et al.* 2010c; although Begun and Ward 2005 and Deane and Begun 2008, 2010 account for a significant degree of below-branch suspension in the locomotor repertoire of *Pierolapithecus*).

Dryopithecus fontani

This species have been recovered from the fossil localities of St. Gaudens (type locality; France; Lartet 1856; Begun 1994), St. Stephen (Austria; Andrews *et al.* 1996) and, probably, the Abocador de Can Mata Series and Castell de Barberà (Vallès-Penedès Basin, Spain; Moyà-Solà *et al.* 1990, 2009a; Alba *et al.* 2011a; Almécija *et al.* 2012). The presence of only lower teeth and a juvenile humerus in the type locality of the species *Dryopithecus fontani* (St. Gaudens) hinders the possibility of unambiguously attributing upper teeth or other cranial and postcranial elements to this taxon (see a more extensive discussion on this topic in Moyà-Solà *et al.* 2009a). Hence, postcranial remains from Castell de Barberà have been either tentatively attributed to *D. fontani* (humerus; Alba *et al.* 2011a) or just assigned to a large-bodied hominoid (phalanges; Almécija *et al.* 2012). Hitherto, the only large hominoid identified, although tentatively based on the humeral size and age at this locality is *D. fontani* and, for this reason, phalanges described by Almécija and colleagues (2012) are considered in this section.

All the localities with noted presence of *Dryopithecus* have been dated within the middle Miocene

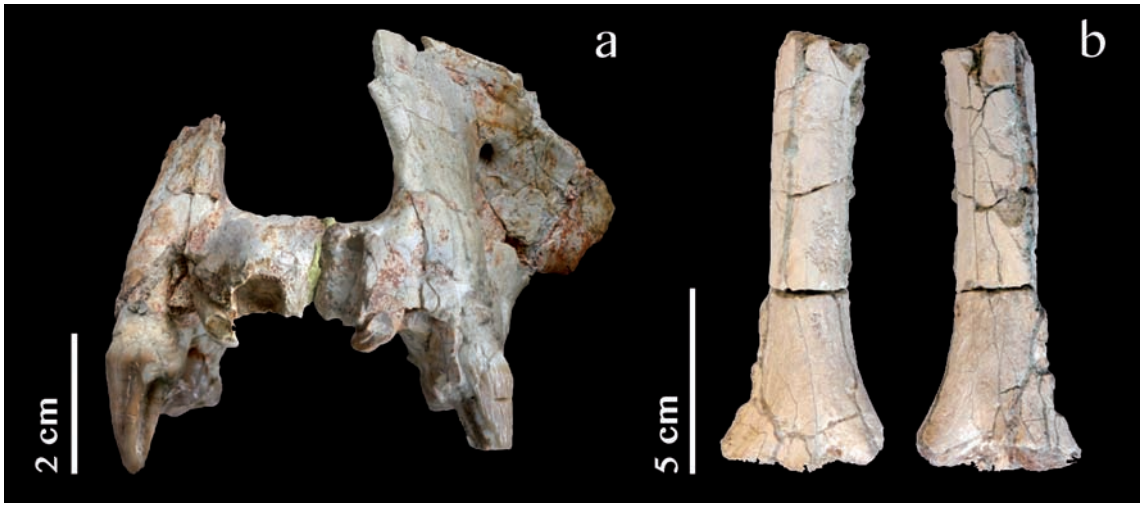

Figure 6 a, Palate of *Dryopithecus fontani* (IPS35026; frontal view) and **b**, partial humerus tentatively assigned to this taxon (IPS4334; left, anterior view; right, posterior view). Modified from Moyà-Solà *et al.* (2009a) and Alba *et al.* (2011a).

(MN7-8; Andrews *et al.* 1996; Moyà-Solà *et al.* 2009a), although the age of St. Gaudens is not accurately known (see Begun 1992b). A body mass of around 46-55 kg has been estimated for this taxon on the basis of the humeral shaft (Alba *et al.* 2011a) and between 40.1-49.5 kg based on the femora head (Moyà-Solà *et al.* 2009a). As most of the Miocene hominoids, *Dryopithecus* lacks clear extant dietary analogues, showing a mixed soft/hard-fruit feeder pattern, although with closer affinities with hard-object feeders (DeMiguel *et al.* 2014). Besides, contrary to *Pierolapithecus* (see above), *Dryopithecus* has a relatively thin enamel thickness that suggests differences on dietary preferences related to *Pierolapithecus* (Alba *et al.* 2010b).

Apart from isolated teeth and mandibular fragments, *Dryopithecus* remains from the Vallès-Penedès Basin include a maxillar and, probably, a partial humeral shaft, several phalanges, and a partial femur (Moyà-Solà *et al.* 1990, 2009a; Alba *et al.* 2011a; Almécija *et al.* 2012). Although preliminary described by Moyà-Solà and co-authors (2009a), the partial femur is deeply studied and analysed in this work.

The lower face unearthed in the fossil locality ACM/C3-Ae, together with other dentognathic remains, evidences the morphological differences between the middle and late Miocene fossil hominoids recovered in Catalonia, as well as the taxonomic diversity within the fossil primates found in the ACM (Fig. 6; Moyà-Solà *et al.* 2009a). Thus, *Dryopithecus* facial morphology shows a combination of primitive (e.g., the maxillary sinus does not penetrate into the zygomatic root) and derived (great ape-like) features (e.g., vertical nasomaxillary suture; Moyà-Solà *et al.* 2009a). Moreover, shape analysis accommodates the *Dryopithecus* lower face close to that of gorillas, suggesting that it might be a stem member of the Homininae (Moyà-Solà *et al.* 2009a).

Concerning the forelimb of this taxon, two humeri are known up to date, one from St. Gaudens (likely belonging to a juvenile; Depéret 1887; Pilbeam and Simons 1971; see also Begun 1992b) and probably a partial distal shaft from Castell de Barberà (Alba *et al.* 2011a). The general appearance of the humeri is hominoid-like (e.g., rounded cross-section and deep olecranon and coronoid fossae; Pilbeam and Simons 1971; Begun 1992b; Alba *et al.* 2011a). Nonetheless, this morphology cannot be directly linked with suspensory behaviours because they also characterize above-branch quadrupedalism (Begun 1992b; Rose 1994; Alba *et al.* 2011a). Manual remains from Castell de Barberà include a complete proximal phalanx and a partial distal phalanx whose overall morphology is similar to that of other Miocene apes (relatively long, proximal phalanx with a high degree of curvature, and marked insertions for the flexor muscles, among others; Almécija *et al.* 2012). Thus, phalangeal morphology claims for grasping capabilities due to the association of pollex's traits with enhancement of flexion (Almécija *et al.* 2012). Preliminary description of the femur also highlighted the mixture of primitive and derived features within this Miocene hominoid fossil bone (Moyà-Solà *et al.* 2009a).

Thereby, overall postcranial morphology of *Dryopithecus* advocates for a positional repertoire with an important component of above-branch quadrupedalism combined with climbing behaviours. Suspension could integrate *Dryopithecus* positional set in some degree, although less than in the younger taxon *Hispanopithecus* (see below; Begun 1992b; Alba *et al.* 2011a).

Hispanopithecus crusafonti

This species was erected in 1992 after a reviewing of the sample of Miocene hominoid remains from Spain by Begun (1992a; but see Harrison 1991b and Ribot *et al.* 1996 for a different taxonomic interpretation). In addition, the partial mandible from Teuleria del Firal (Seu d'Urgell Basin, Spain) traditionally attributed to *Dryopithecus fontani* (Vidal 1913; Woodward 1914), has been recently included in the hypodigm of *H. crusafonti* (Casanovas-Vilar *et al.* 2011; Alba 2012; Alba *et al.* 2012b; Marigó *et al.* 2014). Begun (1992a; see also Begun 1989, 2002 and a revision in Alba *et al.* 2012b) found that the teeth from the fossil locality of Can Poncic (Sant Quirze, Vallès-Penedès Basin) were different from those of *Hispanopithecus laietanus* on the basis of morphological traits and size (e.g., mesiodistally elongated upper premolars and absence of molar cingula; Fig. 7). The teeth shape and dental microwear analysis suggest that *H. crusafonti* might have soft/hard-fruit feeder affinities, although feeding predominantly on hard-fruits (but also on leaves in some degree), with different anterior dental processing strategies compared with living great apes (Puech *et al.* 1989; Begun 1992a; DeMiguel *et al.* 2014).

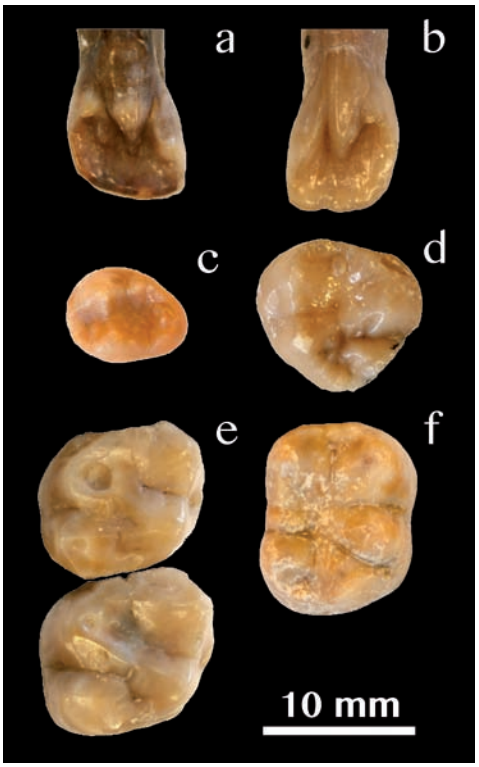

Figure 7 Some dental remains attributed to *Hispanopithecus crusafonti*. **a**, IPS1808: left I^1 (lingual view); **b**, IPS1807: right I^1 (lingual view); **c**, IPS1811: right P_4 (occlusal view); **d**, IPS1812: right M^3 (occlusal view); **e**, IPS1798 (holotype; occlusal view): left M^1-M^2 series (occlusal view); **f**, IPS1816: right M_2 (occlusal view). From Alba *et al.* (2012a,b).

Only the small sample of teeth (including the maxillary fragment that compounds the holotype) attributed to this species has been described and studied (Crusafont Pairó and Hürzeler 1969; Crusafont-Pairó and Golpe-Posse 1973; Begun 1992a; Alba *et al.* 2012b,in prep). Nonetheless, few postcranial remains were found in this locality that are already unpublished: a femoral shaft fragment (this study), one hamate (Almécija *et al.* in prep a) and several partial metatarsals (Almécija *et al.* in prep b). Description of the partial femoral shaft is included in this work. Consequently, the positional behaviour of this fossil species remains still unknown.

Hispanopithecus laietanus

Hispanopithecus laietanus is a fossil hominoid recovered from several late Miocene (MN9-MN10) localities within the Vallès-Penedès Basin (La Tarumba 1, type locality; Can Llobateres 1 and 2, Polinyà 2, Can Feu, EDAR6 and 7; Villalta Comella and Crusafont Pairó 1944; Begun *et al.* 1990; Golpe Posse 1993; Moyà-Solà and Köhler 1993, 1995, 1996; Köhler *et al.* 2001; Almécija *et al.* 2007; Alba *et al.* 2012a,b; Tallman *et al.* 2013; Susanna *et al.* 2014). After being firstly attributed to this genus by Villalta Comella and Crusafont Pairó (1944), fossil remains of this taxon were relocated into the genus *Dryopithecus* (Begun *et*

al. 1990; Moyà-Solà *et al.* 1990; Harrison 1991b; Andrews *et al.* 1996; among others). On the light of the new discoveries of Spanish fossil hominoids, Moyà-Solà and colleagues (2009a) resurrected the genus *Hispanopithecus* to designate the late Miocene species of dryopithecins (see also Casanovas-Vilar *et al.* 2011). Teeth and postcranial morphology of *H. laietanus* accommodates this taxon as an extinct member of the Hominidae (Alba 2012).

Hispanopithecus laietanus postcranium is mostly known from the partial skeleton recovered at Can Llobateres 2 (Fig. 8; Moyà-Solà and Köhler 1996) and the partial upper skeleton from Can Feu (Alba *et al.* 2012a). The former comprises several elements of the hindlimb (femora and tibia) that are further studied and analysed in this work. Moreover, an estimated body mass of 34-43 kg and 39-40 kg has been inferred for this taxon based on femoral and vertebral measurements, respectively (Moyà-Solà and Köhler 1996; Moyà-Solà *et al.* 2009a; Susanna *et al.* 2014). A range of 22-25 kg was calculated for the Can Feu partial skeleton, which presumably belongs to a female on the basis of its third lower premolar (see discussion in Alba *et al.* 2012a). Besides, although not falling within any specific dietary category, among Spanish Miocene hominoids, *Hispanopithecus* is the taxon that more clearly shows a dietary preference for soft-fruits (DeMiguel *et al.* 2014).

Vertebrae morphology (e.g., dorsally-situated costal foveae in the thoracic vertebrae, no ventral keel, and transverse processes originating from a the pedicle in lumbar vertebrae) indicates the presence of an orthograde body plan with hominoid-like wide and shallow thorax and a somewhat short and stiff lumbar region, (Moyà-Solà and Köhler 1996; Köhler *et al.* 2001; Susanna *et al.* 2014). In this regard, the morphology of the scapula (acromion process longer and more compressed than in monkeys), and first rib (e.g., craniocaudally compression) from the Can Feu partial skeleton also support these inferences (Alba *et al.* 2012a).

The humerus of *H. laietanus* is straight and displays a slightly convex deltoid plane; whereas the radius is markedly curved. These features, together with those of the ulna (see below), indicate that the forelimb was probably able of broad movements, including abduction, flexion and pronation, which are frequently associated with climbing and suspensory behaviours (Moyà-Solà and Köhler 1996). Likewise, the elbow of *H. laietanus* would also favour wide ranges of movement (mainly regarding pronation-supination), as well as stabilization of the joint during flexion-extension as can be inferred from the proximal ulnar morphology (e.g., reduced olecranon process; Alba *et al.* 2012a). Nonetheless, other ulnar

Figure 8 Partial skeleton of *Hispanopithecus laietanus* found in Can Llobateres 2 (IPS18800). Modified from Moyà-Solà and Köhler (1996).

features are more related to quadrupedal behaviours, such as the posteromedially tilted olecranon process (Alba *et al.* 2012a).

Manual phalanges of *H. laietanus* are long and highly curved, highlighting the use of the hand in suspensory behaviours. Contrary, some other traits in the proximal phalanges (i.e., dorsal extension of the articular surface) and metacarpal proportions and morphology (short length and stoutness) are more closely related to above-branch palmigrade quadrupedalism (Moyà-Solà and Köhler 1996; Almécija *et al.* 2007; Alba *et al.* 2010c; see Begun *et al.* 2012 for a different interpretation). Moreover, powerful grasping capabilities are inferred from the marked insertions for the flexors on the phalangeal shafts and the large pits for the collateral ligaments (Almécija *et al.* 2007).

Previous works focusing on the femora outlined the hominoid-like morphology of these fossil bones (e.g., large femoral head relative to the neck and high neck-shaft angle), which are usually related to abduction capabilities of the hip joint (Moyà-Solà and Köhler 1996; MacLatchy *et al.* 2001; Köhler *et al.* 2002). The *Hispanopithecus* tibia, as other anatomical regions, exhibits a combination of monkey- (e.g., articular surface with median keel) and ape-like (e.g., metaphysis anteroposterior compression) morphological features. The latter traits (ape-like) are associated with vertical climbing behaviours, while the former (monkey-like) with quadrupedalism (Tallman *et al.* 2013).

Morphological evidence for *H. laietanus* reveals that it might retain some features related to above-branch palmigrady, which are uniquely coupled with others unambiguously associated with below-branch suspensory behaviours, as well as other orthograde-like locomotor types such as vertical climbing (Almécija *et al.* 2007; Alba *et al.* 2012a). Moreover, the high intermembral index estimated for this primate also indicates clear adaptations for suspensory behaviours (Moyà-Solà and Köhler 1996). Therefore, postcranial remains attributed to *Hispanopithecus laietanus* evidence that this taxon is one of the oldest orthograde hominoids with the undoubted below-branch suspensory adaptations, although also retaining features functionally related to above-branch palmigrady with powerful grasping capabilities (Moyà-Solà and Köhler 1996; Almécija *et al.* 2007; Alba *et al.* 2012a; Tallman *et al.* 2013).

Knowledge and understanding. Hard work and persistance.
-- Jane Goodall --

Section II. OBJECTIVES

The fossil great apes of the Vallès-Penedès Basin are key to better comprehend the origin and evolution of the Hominoidea (especially the Hominidae). Nonetheless, the mosaic nature of their postcranium and the still elusive functional interpretation of plesiomorphic traits make difficult to reconstruct their positional behaviours. For these reasons, this thesis focuses on the study of the hindlimb (excluding the feet), which is functionally relevant because it participates in weight loading, support and propulsion during locomotion. Additionally, the study of the Vallès-Penedès hindlimb remains is addressed from different methodological approaches (further information is provided in the following section) emphasizing morphological features with a clear functional link to biomechanics.

Therefore, works included in this thesis are primarily devoted, in a broad sense, to shed light on the origin and evolution of the positional behaviours of the Miocene great apes found in the Vallès-Penedès Basin: *Pierolapithecus catalaunicus*, *Dryopithecus fontani* and *Hispanopithecus laietanus*. Individual studies on the femora, tibia and patella are performed to solve specific questions related to functional morphology and mechanics of the hindlimb bones. Specific objectives are listed below:

1. Description and morphometric study of the partial femora of cf. *D. fontani* and *Hispanopithecus* spp. (Chapter 1).
2. Analysis and quantification of the cortical bone distribution at the femoral neck of cf. *D. fontani* and *H. laietanus* (Chapter 2).
3. Analysis of the structural properties of the femoral shaft of cf. *D. fontani* and *H. laietanus* (Chapter 3).
4. Description and morphometric study of the distal tibia of *H. laietanus* (Chapter 4).
5. Description and morphometric study of the patella of *P. catalaunicus* (Chapter 5).
6. Analysis of the biomechanical response of the *P. catalaunicus* patella during knee flexion (Chapter 6).
7. Comparison of fossil taxa results with extant primate species with known locomotor patterns.

Altogether, this work will contribute to increase our knowledge on the ape hindlimb bones' shape and mechanics, and complete the positional behaviour profiles of the Iberian Miocene great apes, which were previously inferred on the basis of other anatomical regions.

Always do what you are afraid to do.
-- R. Waldo Emerson --

Section III. MATERIAL & METHODS

HINDLIMB FOSSIL REMAINS OF THE VALLÈS-PENEDÈS HOMINOIDS

This work focuses on the study of the fossil hindlimb (non-pedal) remains of the Vallès-Penedès great apes. They include femoral, tibial and patellar elements. These fossils have been attributed to four different taxa: *Pierolapithecus catalaunicus*, cf. *Dryopithecus fontani*, *Hispanopithecus crusafonti* and *Hispanopithecus laietanus*. All specimens are curated by the Institut Català de Paleontologia Miquel Crusafont (ICP, Universitat Autònoma de Barcelona, Spain; collection acronym IPS, 'Institut de Paleontologia de Sabadell'). Details of the specimens and its preservation are reported below:

***Pierolapithecus catalaunicus* Moyà-Solà *et al.*, 2004**

- IPS21350.37. Complete left patella that belongs to the type skeleton of *Pierolapithecus catalaunicus* (IPS21350; Fig. 9a) found in the Barranc de Can Vila 1 (BCV1) locality (within the Abocador de Can Mata local stratigraphic series, ACM). It was firstly referred by Moyà-Solà *et al.* (2004: fig. 1). The *Pierolapithecus* patella displays a very minor damage on its proximal and medial portions, and some slight abrasion on the distal end. However, its shape and size are completely conserved.

- IPS21350.81 and **IPS21350.85.** Long bone cortical fragments (Fig. 9b). Both fragments were assigned to the femoral diaphyses of the *Pierolapithecus catalaunicus* partial skeleton found in BCV1 by Moyà-Solà *et al.* (2004: fig. 1). They consist of several reconstructed cortical bone fragments. IPS21350.81 is slightly eroded at the borders, whereas de cortical thickness edges of IPS21350.85 are better preserved.

cf. *Dryopithecus fontani* Lartet, 1856

- IPS41724. Partial (proximal) right femur (Fig. 9c). First described by Moyà-Solà *et al.* (2009a: fig. 11), who tentatively attributed it to cf. *Dryopithecus fontani* on the basis of its geographical proximity to the partial face IPS35026 attributed to this taxon, and its large body mass (see further explanation in Chapter 1 and Alba 2012: fig. 6C). IPS41724 is a well-preserved femur that conserves almost the proximal half of the bone and that was found in the ACM/C3-Az locality. This partial femur shows some erosion at the most proximal part of the greater trochanter and two natural transverse fractures at the base of the femoral head and the proximal shaft (below the lesser trochanter). In addition, IPS41724 displays several proximodistal cracks along the diaphysis and one at the anterior half of the greater trochanter. Furthermore, small transverse cracks are shown at the distal portion of the preserved shaft. The bone

consists of almost the 50% of the total femoral length (estimated in around 31 cm on the basis of its femoral head superoinferior height; see Chapter 3).

***Hispanopithecus crusafonti* (Begun, 1992a)**

- IPS11426. Diaphyseal fragment of a left femur from the locality of Can Poncic (CP). This specimen remains unpublished, but it is here provisionally attributed to *Hispanopithecus crusafonti* (see Chapter 1 for further explanation on the taxonomic attribution; Fig. 9d). IPS11426 is formed by two diaphyseal fragments that are continuous with one another, which are well preserved, and presumably corresponds to the distal half of the shaft, just above the distal epiphysis. With a total length of ca. 12.2 cm, this femoral shaft appears more slender and smaller than other Vallès-Penedès hominoids femora (IPS41724 and IPS18800), thus probably belonging to either a juvenile individual or an adult female. Although none of these two possibilities can be discounted, the fact that the cortical bone tissue appears completely formed supports the latter possibility.

***Hispanopithecus laietanus* Villalta Comella and Crusafont Pairó, 1944**

- IPS18800. Right and left proximal femora (Fig. 9f,g) and left distal tibia (Fig. 9e) from the partial skeleton of *Hispanopithecus laietanus* (IPS18800) recovered at the late Miocene locality of Can Llobateres 2 (CLL2). Femora have previously described by Moyà-Solà and Köhler (1996: fig. 1), MacLatchy *et al.* (2001), Köhler *et al.* (2002: fig. 1; see also Alba 2012: fig. 6B and D). Both femora lack the distal end. The right femur preserves the entire proximal half (up to ca. 70% of bone length; see Chapter 3). It displays some erosion at the anterior side of the femoral head and the greater trochanter is slightly damaged at the anterior and lateral sides. In turn, the left femur preserves until ca. 87% of bone length (almost only lacking the distal epiphysis and the most distal part of the shaft; see also Chapter 3). The left femur further shows a damaged femoral neck and lacks the proximal-most part of the greater trochanter.

The distal tibia was included in the holotype description of Moyà-Solà and Köhler (1996: fig. 1; see also Alba 2012: fig. 6B) and it has been analysed and described in-depth by Tallman *et al.* (2013: fig. 1). It represents ca. 30% of total bone length (judging on the basis of 23.6 cm of total tibial length, estimated by Moyà-Solà and Köhler 1996 based on femoral length). Although the distal portion of the shaft is partly damaged, the epiphysis is well preserved.

Computed tomography scans of the Vallès-Penedès hominoids

IPS41724 and IPS18800 (both femora and tibia) have been scanned through computed tomography (CT) in order to study their internal structure. Thus, fossil remains were CT-scanned in several institutions: the Human Evolution Lab (LEH) at the Universidad de Burgos (UBU, Burgos); Microscopy and Imaging Facility (MIF) at the American Museum of Natural History (AMNH, New York); the Multidisciplinary

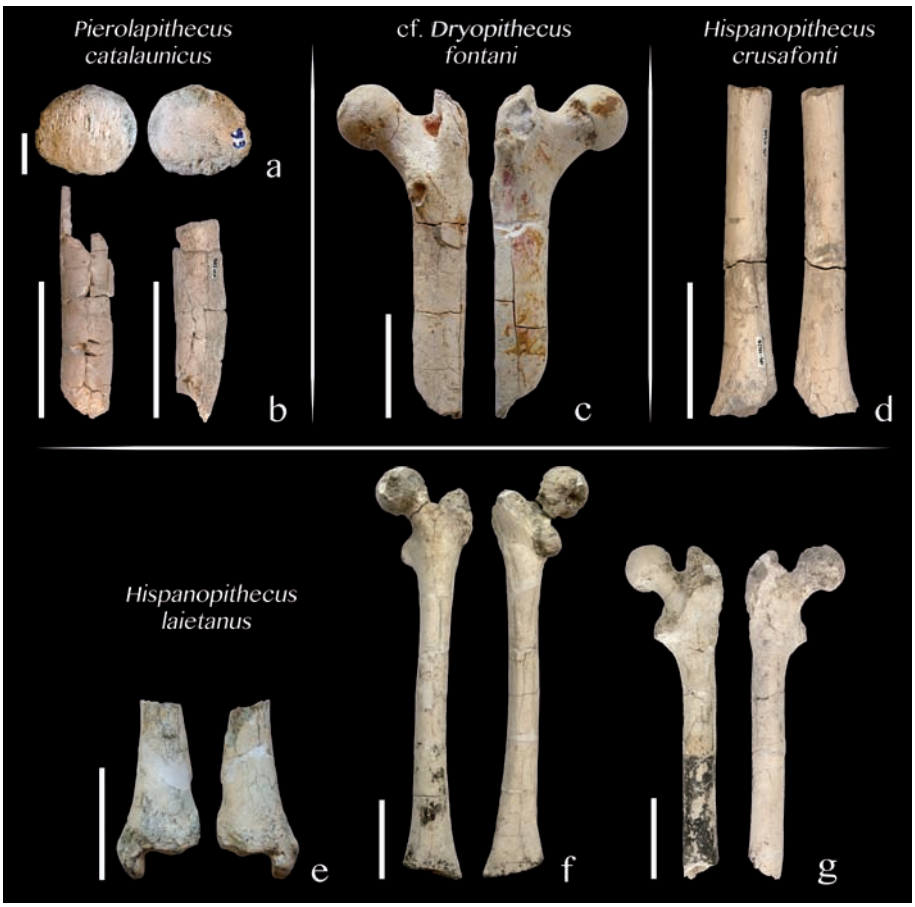

Figure 9 Glimpse to the non-pedal hindlimb fossil remains of the Vallès-Penedès hominoids (see following chapters for detailed images of every anatomical view). **a**, IPS21350.37 (anterior view, left; posterior view, right); **b**, IPS21350.85 (left) and IPS21350.81 (right; external views); **c**, IPS41724 (posterior view, left; anterior view, right); **d**, IPS11426 (posterior view, left; anterior view, right); **e-g,** IPS18800 (e and g, posterior view, left; anterior view, right; f, posterior view, right; anterior view, left). Scale bar = 50 mm (patella scale bar = 10 mm).

Laboratory of the International Centre for Theoretical Physics (ICTP, Trieste); the Museo Nacional de Ciencias Naturales-CSIC (MNCN, Madrid); and the Virtual Lab at the Institut Català de Paleontologia Miquel Crusafont (ICP, Sabadell). See Chapters 2 and 3 for details on CT-settings used in every scan.

COMPARATIVE SAMPLE

Hindlimb fossil remains have been compared with a sample of extant and extinct primates. Living taxa sample covers all the major taxonomic groups of anthropoids, including cebids, atelids, cercopithecoids (cercopithecines and colobines), hylobatids, and hominids (gorillas, chimpanzees, orangutans, and modern humans). A general summary of the specimens included in the studies is listed in Table 4 (specific samples used in every study are specify in their correspondent chapter). Morphometric data was collected at the American Museum of Natural History (AMNH, New York), Royal Museum of Central Africa (RMCA, Tervuren) and Museum of Comparative Zoology and Peabody Museum of Archaeology and Ethnology at Harvard University (MCZ and PBMA, Cambridge).

Fossil specimens used for comparisons range from the early to the late Miocene and spread geographically from Africa to Eurasia (see Section I). Table 5 shows taxa and fossil bones included in the sample. As in the case of living primates, specific specimens used in every study will be detail in its correspondent chapter.

AREA OF STUDY: THE VALLÈS-PENEDÈS BASIN

Geological remarks and fossil localities

The Vallès-Penedès Basin is a small half-graben situated in the NE of the Iberian Peninsula and bounded by the Pre-littoral and Littoral ranges (Fig. 10). The basin is about 100 km long, 12-14 km wide and has an NNE-SSW orientation (Moyà-Solà *et al*. 2009a; Casanovas-Vilar *et al*. 2015). The Vallès-Penedès Basin is filled by Neogene sediments, ranging from the early Miocene (Ramblian-early Burdigalian, ca. 19.6 Million years ago, Ma) to the Late Miocene (Turolian-Tortonian, 7.4/6.8 Ma; Casanovas-Vilar *et al*. 2015).

Table 4 Species of living primates included in this work. Sample used in every study is specified in its correspondent chapter.

LIVING PRIMATES			
Catarrhines			**Platyrrhines**
Hominidae	**Cercopithecoidea**		**Atelidae**
Hominins	Cercopithecines	Colobines	Atelines
Homo	*Papio*	*Nasalis*	*Alouatta*
H. sapiens	*Pp. anubis*	*N. larvatus*	*A. caraya*
Gorilla	*Pp. cynocephalus*	*Colobus*	*A. seniculus*
G. beringei beringei	*Pp. doguera*	*Co. badius*	*A. fusca*
G. beringei graueri	*Pp. hamadryas*	*Co. guereza*	*A. palliata*
G. gorilla gorilla	*Pp. ursinus*	*Co. polykomos*	*A. seniculus*
Pan	*Mandrillus*	*Lophocebus*	*Ateles*
P. paniscus	*M. sphinx*	*L. albigena*	*At. belzebuth*
P. troglodytes schweinfurthii	*M. leucophaeus*	*L. aterrimus*	*At. fusciceps*
P. troglodytes troglodytes	*Macaca*	*L. galeritus*	*At. geoffroyi*
P. troglodytes verus	*Ma. cyclopsis*	*Presbytis*	*At. paniscus*
	Ma. fascicularis	*Pr. aygula*	
Pongins	*Ma. fuscata*	*Pr. cristata*	**Cebidae**
Pongo	*Ma. mulatta*	*Pr. frontatis*	Cebines
Po. abelii	*Ma. nemestrina*	*Pr. johni*	*Cebus*
Po. pygmaeus	*Cercopithecus*	*Pr. melalophos*	*Ce. apella*
	C. aethiops	*Pr. obscurus*	
Hylobatidae	*C. albogularis*	*Pr. rubicunda*	
Symphalangus	*C. ascanius*	*Trachypithecus*	
S. syndactylus	*C. diana*	*T. cristatus*	
Hylobates	*C. dogguetti*		
Hy. funerus	*C. l'hoesti*		
Hy. lar	*C. mitis*		
	C. mona		
	Chlorocebus		
	Ch. cynosuros		
	Ch. pygerythrus		
	Ch. tantalus		

Authors divided the Miocene record of the Vallès-Penedès Basin in four lithostratigraphical units based on biostratigraphy and magnetostratigraphy (Casanovas-Vilar *et al.* 2015 and references therein): the Basal Breccia Unit (the oldest records dates from the Ramblian, MN3, and the Aragonian, MN4, in the Vallès and Penedès sectors, respectively); the Lower Continental Units (Ramblian-early Aragonian, MN3-MN4); the Marine and Transitional Units (Burdigalian-Serravalian, MN3-MN7+8); and the Upper Continental Units (Serravalian-onwards; Fig. 10). During this last unit, alluvial fan sediments dominated sedimentation, mainly between the middle Aragonian and the middle Turolian, and the most of the mammal sites of the Basin are located in distal to terminal, mudstone-dominated facies. Specifically, the Abocador de Can Mata local stratigraphic series fossil sites are found within the inter-fan zones of two major coalescing alluvial fan systems (Moya-Solà *et al.* 2009a); whereas the Can Llobateres site is located in a distal-interchannel alluvial plain (Alba *et al.* 2012b). The depositional environment of Can Poncic has been less studied, but Begun (1992a) claimed that it would be similar to that of Can Llobateres, consisting of a channel and floodplain or a delta. Finally, during the Early Pliocene and posteriorly during the Pleistocene-Holocene, the older sediments were covered by the younger, unconformably overlying the Neogene series (Casanovas-Vilar *et al.* 2015).

Table 5 Fossil remains included in this work. Fossil sample used in every study are specified in their correspondent chapter.

FOSSIL REMAINS					
Taxa	**Specimen**	**Element**	**Locality**	**Age**	**Bone descriptions**
Morotopithecus					
M. bishopi	MUZM80	Femora	Moroto, Uganda	20.6 Ma, early Miocene	MacLatchy *et al.* 2000
Dendropithecus/Proconsul					
D. africanus	KNM-LG583	Tibia	Legetet, Kenya	19.5 Ma, early Miocene	Harrison 1982
Proconsul					
P. major	NAP IX 46'99	Femur	Napak, Uganda	19 Ma, early Miocene	Gommery *et al.* 2002
P. major	NAP I'58	Tibia	Napak, Uganda	19.5 Ma, early Miocene	Harrison 1982
Ekembo					
E. nyanzae	KNM-RU1939	Tibia	Napak, Uganda	19 Ma, early Miocene	Rafferty *et al.* 1995
E. nyanzae	KNM-RU17382	Patella	R106 (Rusinga Island), Kenya	18 Ma, early Miocene	Ward *et al.* 1995
E. nyanzae	KNM-RU18384	Patella	R106 (Rusinga Island), Kenya	18 Ma, early Miocene	Ward *et al.* 1995
E. nyanzae	KNM-MW13142A	Femur	Mfangano Island, Kenya	17.9 Ma, early Miocene	Ward *et al.* 1993
E. nyanzae	KNM-RU5527	Femur	R106 (Rusinga Island), Kenya	18 Ma, early Miocene	Ruff *et al.* 1989
E. heseloni	KPS PT 1-4	Patellae	R5 (Rusinga Island), Kenya	18 Ma, early Miocene	Ward *et al.* 1995
E. heseloni	KNM-RU3589	Tibia	Kaswanga, Kenya	17.8 Ma, early Miocene	DeSilva 2008
Equatorius					
Eq. africanus	BMNH M16331	Femur	Maboko, Kenya	15 Ma, middle Miocene	McCrossin 1994a
Eq. africanus	KNM-MB24738	Patella	Maboko, Kenya	15 Ma, middle Miocene	McCrossin 1994a
Nacholapithecus					
N. kerioi	KNM-BG35250A	Femur	Nachola, Kenya	15 Ma, middle Miocene	Nakatsukasa *et al.* 1998
N. kerioi	KNM-BG35250Z	Patella	Nachola, Kenya	15 Ma, middle Miocene	Ishida *et al.* 2004
N. kerioi	KNM-BG15535	Patella	Baragoi, Kenya	15 Ma, middle Miocene	Rose *et al.* 1996
Epipliopithecus					
Ep. vindobonensis	Individual II	Patella	Devinska Nova Ves, Slovakia	15.3 Ma, middle Miocene	Zapfe 1960
Sivapithecus					
S. indicus	YGSP1656	Tibia	Y076 (Siwaliks), Pakistan	11.4 Ma, late Miocene	DeSilva *et al.* 2010
Oreopithecus					
O. bambolii	BAC122	Patella	Monte Bamboli, Italy	9 Ma, late Miocene	Schultz 1960
Orrorin					
Or. tugenensis	BAR1002'00	Femur	Kapsomin, Kenya	5.8 Ma, late Miocene	Senut *et al.* 2001

As mentioned in previous sections, the hindlimb fossil remains of the Vallès-Penedès hominoids were recovered in the fossil sites of Abocador de Can Mata local stratigraphic series (ACM), Can Poncic (CP) and Can Llobateres 2 (CLL2). ACM (Els Hostalets de Pierola) comprises more than 200 mammal sites whose dates range from ca. 12.5 to 10.6 Ma (MN6, late Aragonian; Casanovas-Vilar *et al.* 2011, 2015). The fossil remains included in this work were recovered specifically from the localities of Barranc de Can Vila 1 (BCV1) and ACM/C3-Az (Moyà-Solà *et al.* 2004, 2009a). Can Poncic (Sabadell) is the type locality of the species *Hispanopithecus crusafonti* and is dated in 10.4-10.0 Ma (MN9, early Vallesian; Casanovas-Vilar *et al.*

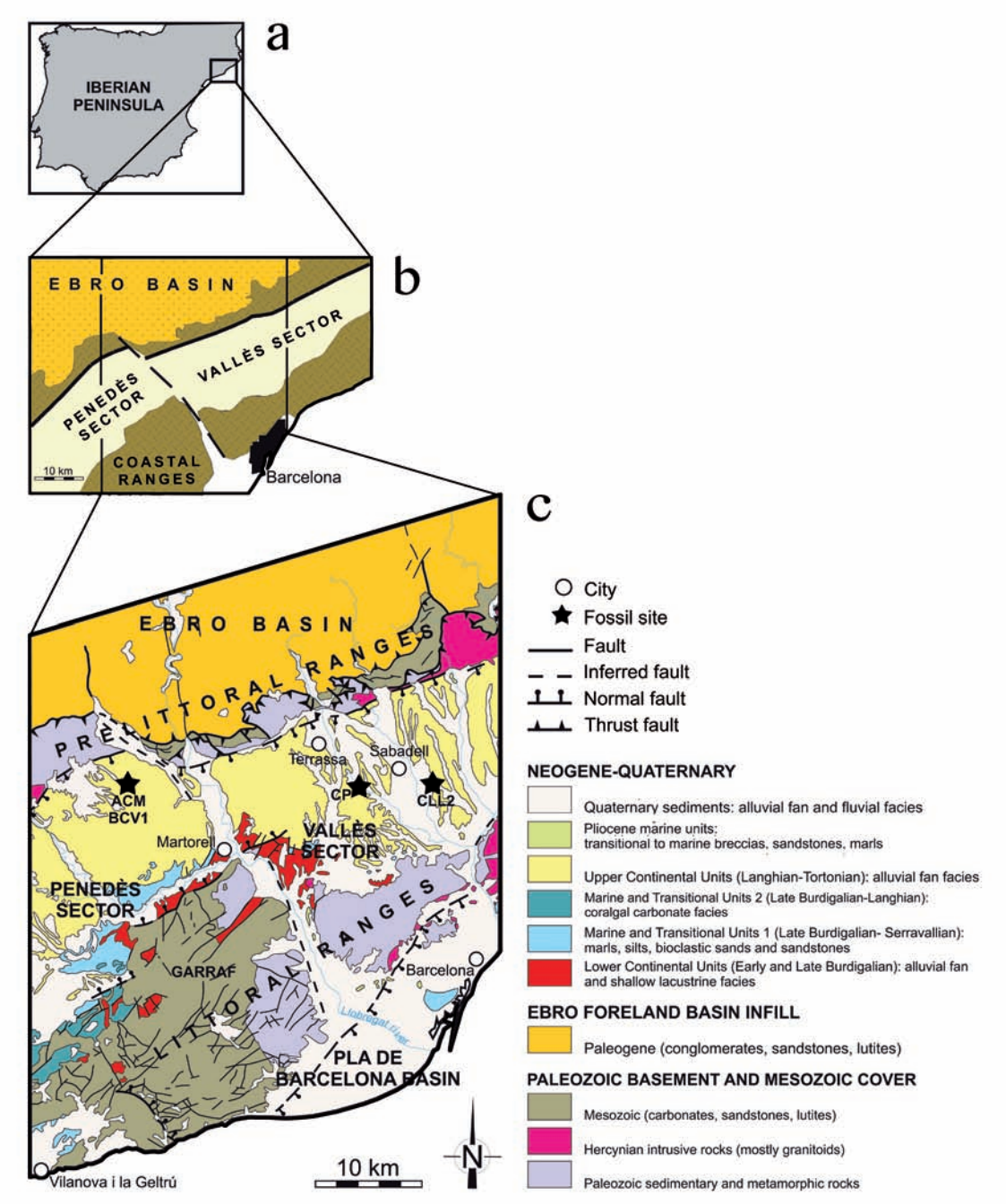

Figure 10 **a**, Geographic map showing the situation of the Vallès-Penedès Basin in the Iberian Peninsula. **b**, Schematic geological map illustrating the structure of the Vallès-Penedès Basin, which is formed by two sectors (Penedès and Vallès) surrounded by the coastal ranges. **c**, Geological map zooming up the area where the fossil localities related to this work are situated. ACM, Abocador de Can Mata Stratigraphic Series; BCV1, Barranc de Can Vila 1; CP, Can Poncic; CLL2, Can Llobateres 2. Modified from maps kindly provided by I. Casanovas-Vilar.

2011, 2015; Alba 2012). Finally, the Late Miocene site of Can Llobateres (Sabadell) comprises two different fossil points: CLL1 and CLL2. The former has been dated in ca. 9.72 Ma (MN9, early Vallesian) and the latter in ca. 9.64 Ma (MN10, late Vallesian; Casanovas-Vilar *et al.* 2011; Alba *et al.* 2012b).

Faunal context and paleoenvironmental reconstruction

The oldest locality included in this work, ACM, belongs to the late Aragonian. During this period, cricetids such as *Hispanomys*, *Democricetodon* and *Megacricetodon* dominate the rodent assemblages (Casanovas-Vilar *et al.* 2015). Likewise, there existed a certain dominance of forest-dwelling genera of glirids, as well as eomyids, flying squirrels, and diverse eulipotyphla taxa, including talpids, dimylids, heterosoricids, erinaceids and soricids (Casanovas-Vilar and Agustí 2007; Furió *et al.* 2011, 2015; Casanovas-Vilar *et al.* 2015). Moreover, the record of large mammals is highly relevant, with the registration of several genera of proboscideans, chalicotheres, rhinocerotids, suoids, cervids, mustelids, hyaenids, felids, and false sabertooths, among others. The most common taxa in ACM are the suid *Listriodon*, the rhino *Alicornops*, and the moschid *Micromeryx*. An important characteristic of the ACM is the large diversity of primates recovered, since it includes four different genera of hominoids (*Dryopithecus*, *Anoiapithecus*, *Pierolapithecus* and *Pliobates*) and one genus of pliopithecoids (*Pliopithecus*; Alba *et al.* 2010a, 2015). The presence of the tragulid *Dorcatherium* (dweller of wet and densely-forested habitats), the bovid *Miotragocerus*, and beavers are a proxy indicator of the existence of humid conditions and water streams, at least during certain time intervals (Casanovas-Vilar *et al.* 2008a; Alba *et al.* 2011b). On the basis of the genera *Micromeryx* (Moschidae) and *Euprox* (Cervidae), a relatively closed and humid forest habitat has been inferred (Casanovas-Vilar *et al.* 2008a,b;

Figure 11 Reconstruction of the paleoenvironment that probably surrounded the fossil locality of Hostalets, showing the humid and warm-temperate forest inferred for this area during the middle Miocene. Oscar Sanisidro / Institut Català de Paleontologia Miquel Crusafont (ICP).

DeMiguel *et al.* 2011). This fact is confirmed by the presence of several genera of Suidae and other taxa, such as arboreal micromammals (dormices and flying squirrels) or the equid *Anchiterium*. The latter is a browser species (those feeding mainly on soft and ligneous foods) that inhabited generally tropical and warm-temperate forest environments (Casanovas-Vilar *et al.* 2008a; Rotger *et al.* 2011). Considering these facts, ACM localities were probably formed in a humid and warm-temperate forested area during the Middle Miocene (Casanovas-Vilar *et al.* 2008a, 2015; Alba *et al.* 2009, 2011b). Furthermore, this hypothesis is supported by the identified primate taxa, mainly hominoids. This group is typically related to closed and humid forested environments, with dense and continuous canopy necessary for its arboreal locomotor adaptations (Moyà-Solà *et al.* 2004; Casanovas-Vilar *et al.* 2008a; DeMiguel *et al.* 2011). Therefore, authors proposed that the ACM environment was a warm to tropical, relatively humid, dense evergreen forest (Fig. 11; Casanovas-Vilar *et al.* 2008a, 2015).

The site of CLL2, where the *Hispanopithecus laietanus* remains included in this work were found, belongs to the late Vallesian (Casanovas-Vilar *et al.* 2011). The Vallesian is characterized by the presence of the first hipparionins (the genus *Hippotherium*) that coexisted with the forest faunas of the Middle Miocene, such as rhinos, cervids, suoids, and chalicotheres (Casanovas-Vilar *et al.* 2015). Among the micromammals, the genus *Rotundomys* is the most abundant component and the number of taxa with forest affinities decreases. At the same time, the register of eastern immigrants increases, including new suids, equids, bovids, hyaenids, or ursids, among others. As in the case of ACM, both hominoids (*Hispanopithecus*) and pliopithecoids (*Egarapithecus*) are recovered from this period (Moyà-Solà and Köhler 1996; Moyà-Solà *et al.* 2001; Alba *et al.* 2012a,b). The presence of some glirids, flying squirrels, chalicotheres and hominoid primates supports the presence of subtropical to warm-temperate humid forest environments (Casanovas-Vilar and Agustí 2007; DeMiguel *et al.* 2011; Casanovas-Vilar *et al.* 2015). Lithological and sedimentological features in CLL1 indicate sedimentation in a poorly drained area, with development of ponds and shallow small lakes (Alba *et al.* 2012b). Flora recovered from this site supports both faunal and geological evidences, showing a zonal vegetation consisted of a warm-temperate mixed forest defined by evergreen laurels, leguminous trees and shrubs, and the absence of deciduous elements. Moreover, the subtropical taxa would have been mostly restricted to the humid areas in the lowlands (Sanz de Siria Catalán, 1993, 1994; Marmi *et al.* 2012).

Finally, CP has been dated as slightly older than CLL (10.4-10.0 Ma) and its somewhat more primitive fauna, although still very similar to that of CLL, corroborates this estimation and suggests the presence of a humid and forested environment (Crusafont-Pairó and Golpe-Posse 1973; Begun 1992a; Casanovas-Vilar *et al.* 2011; Alba 2012).

METHODOLOGY: GENERALITIES AND PRINCIPLES

Since the beginning of the morphofunctional studies on fossil remains (see Bock and Wahlert 1965 for a classical discussion regarding living forms), palaeontologists deeply understood the complexity of the form-function relationships (e.g., skeletal design, animal behaviour, evolutionary history), to adequately infer how fossil taxa moved. Partitioning of this pairing by studying the morphology and functionality separately has allowed a somewhat better understanding of each of the components and their association, although in most instances in a largely theoretical framework (e.g., Preuschoft 1970; Richmond and Jungers 2008; Ruff and Higgins 2013). However, disentangling the role of each of these two factors and determining the influence of their mechanical environment, as well as the phylogenetic and developmental control of bone morphology, is still one of the main sources of conflict in palaeontology (e.g., see Skinner *et al.* 2015a,b and Almécija *et al.* 2015b for a recent discussion). In this context, unravelling the postcranial adaptations and locomotor evolution of hominoids (through the study of the ape fossil record) has been one of the main aims of paleoanthropologists during the last decades (e.g., Stern 1971, 1975; Pilbeam *et al.* 1980; Rose 1983; Walker and Pickford 1983; Stern and Susman 1991; Begun 1992b; Ward *et al.* 1993; Moyà-Solà and Köhler 1996; Rook *et al.* 1996; Ward 1997, 2015; Rae 1999; Pilbeam and Young 2001; Pickford *et al.* 2002; Ishida *et al.* 2004; Moyà-Solà *et al.* 2004; Susman 2004; Begun *et al.* 2012; Nakatsukasa *et al.* 2012), since this is also of utmost relevance to assess the "starting point" from which hominin bipedalism evolved (Almécija *et al.* 2013). Likewise, it is also highly relevant to address this problem from different perspectives to achieve a more complete and diverse approaches to the question. Thus, integrating different methodologies and disciplines is currently essential in the study of fossil remains. Hence, this work combines several techniques, from the most classical (e.g., study of bone shape through linear measurements) to others with younger trajectories in the field of Palaeontology (e.g., Finite Element Analysis). Principles and basics of these methodologies are explained below.

Traditional and 3D geometric morphometrics

This section includes two different morphometric techniques to quantify bone external shape variation and its covariation with other variables: the traditional collection of linear measurements and the more innovative approach of 3D Geometric Morphometrics (3DGM). The former simply consists of taking interpoint distances (e.g., maximum lengths, widths, diameters) or angles with the aid of a digital calliper or other tools (e.g., goniometer). For this work, the selected measurements taken on femora, tibiae, and patellae of the previously mentioned sample of extant and fossil primates are illustrated in Figure 12 and listed in Table 6. Application of this technique has traditionally related to the study of allometry (changes in shape as a function of size; e.g., Sprent 1972) and size correction (to enable the study of shape differences among samples of organisms adjusted to a common size; e.g., Jungers *et al.* 1995) among other approaches. Normally, multivariate analyses were the statistical tool to solve these problems (Dryden and

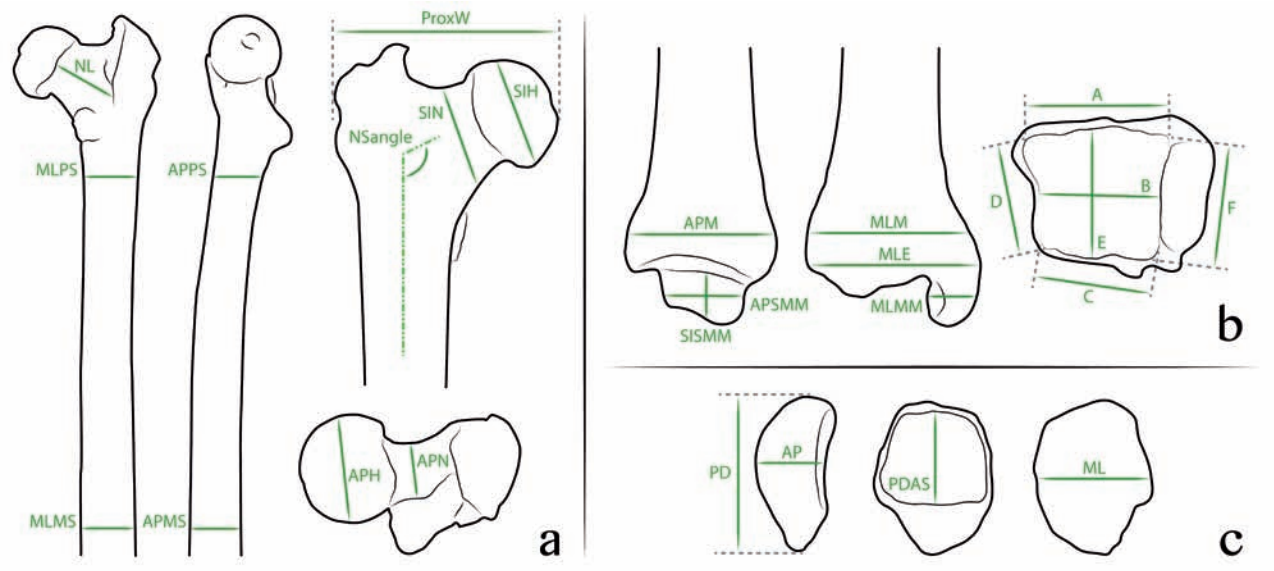

Figure 12 Graphical explanation of linear measurements used along the text. Measures taken on **a**, proximal femur; **b**, distal tibia; and **c**, patella. See abbreviation definitions in Table 6. Further information about measurements can be found in Ward *et al.* (1995), Bacon (2001), DeSilva *et al.* (2010), and Tallman *et al.* (2013).

Mardia 1998; Adams *et al.* 2004). The results are mostly expressed numerically and graphically in terms of linear combinations of the measured variables (Rohlf and Marcus 1993).

Nonetheless, the aforementioned technique is limited in somehow, since it is not possible to recover the shape of complex geometries (e.g., those of many bones). This limitation favoured the appearance of the "new morphometrics", basically based on 3DGM. The latter also focuses on the retention of geometric information of external bones' morphology through a coordinates-based system. The basis of the method consists of selecting a set of anatomically homologous points or *landmarks* (biologically meaningful or homologous among individuals), in two (2D) or three-dimensions (3D), which capture the shape variation amongst specimens (see an example in Figure 13; see Bookstein 1991 and Dryden and Mardia 1998 for a deep and extensive explanation of the method). The shape coordinates of these landmarks are digitized and then subjected to a series of analyses.

Although the study of quantitative data based on sets of morphological variables started at the end of the nineteenth century (see Bumpus 1898), in the late 1980s and early 1990s, a new way of morphological quantification strengthened. Exploration of methods that emphasize the capture of shape geometry and preserve this information throughout the analysis finally led to the called "geometric morphometrics" (GM) technique (Rohlf and Marcus 1993; Adams *et al.* 2004). Since the first works

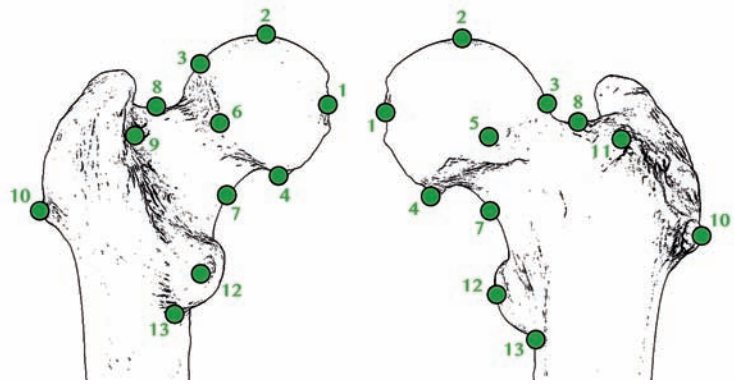

Figure 13 Example of landmarks (close green circles 1-13) used for studying shape variation in the proximal primate femur. Modified from Almécija *et al.* (2013).

of Kendall (1984, 1985), this emergence occurred parallel to the development of statistical methods that allowed the analysis of the morphological information captured (Adams *et al.* 2004).

The *Landmark-based GM method* consists of the collection of points (configuration) related to a previously defined coordinate axes (Bookstein 1991; Dryden and Mardia 1998). The set of points constitutes a configuration matrix *X* of Cartesian coordinates that is defined as *k* x *m* (*k* landmarks in *m* dimensions; Dryden and Mardia 1998). The numerical value of these points will reflect the unique location and orientation of each specimen with respect to the coordinate axes (specimen's size is also recorded; Adams *et al.* 2004; Slice 2007). Therefore, in order to analyse specimens' coordinates, *Generalised Procrustes Analysis* (GPA; a type of Superimposition method based on minimizing the total sum of square distances between configurations) is the approximation most widely used (nonetheless, there exist others like the Euclidean Distance Matrix Analysis, EDMA, or the Finite Element Scaling Analysis, FESA; Rohlf and Marcus

Table 6 Abbreviations of the external linear measurement used in the text. See Figure 12 for an illustrated explanation of the measurements.

LINEAR MEASUREMENTS	
Abbreviations	**Definition**
Proximal femur	
ProxW	Proximal epiphysis width
APH	Femoral head anteroposterior length
SIH	Femoral head superoinferior height
APN	Femoral neck anteroposterior length
SIN	Femoral neck superoinferior height
NL	Femoral neck length
NSangle	Femoral neck-shaft angle
APMS	Midshaft anteroposterior length
MLMS	Midshaft mediolateral length
APPS	Proximal shaft anteroposterior length
MLPS	Proximal shaft mediolateral length
Distal tibia	
APM	Anteroposterior metaphysis length
MLM	Mediolateral metaphysis length
MLE	Anterior mediolateral maximum breadth of the epiphysis
MLMM	Medial malleolus mediolateral length
APSMM	Anteroposterior length of the articular surface of the medial malleolus
SISMM	Superoinferior length of the articular surface of the medial malleolus
A	Mediolateral anterior breadth of the distal trochlear surface
B	Mediolateral midline breadth of the distal trochlear surface
C	Mediolateral posterior breadth of the distal trochlear surface
D	Anteroposterior medial length of the distal trochlear surface
E	Anteroposterior midline length of the distal trochlear surface
F	Anteroposterior lateral length of the distal trochlear surface
Patella	
PD	Total proximodistal height
PDAS	Proximodistal height of the articular surface
AP	Anteroposterior thickness
ML	Mediolateral breadth

1993; Adams *et al.* 2004). This method allows analysing the structure of shape variability in a sample by investigating it in a linearized space about the average shape (a tangent space). Standard multivariate techniques in tangent space are good approximations to non-Euclidean shape methods such as those of 3DGM (Dryden and Mardia 1998). Thus, the GPA method superimposes sets of landmark coordinates (configurations) for pair of specimens by translating the centroid of each landmark configuration to the origin. Posteriorly, configurations are scaled to a common unit size usually by dividing by the *centroid size* (the squared root of the sum of squared distances of the landmarks in a configuration to their average location; Adams *et al.* 2004; Slice 2007). Finally, configurations are rotated to minimize the squared, summed distances (squared Procrustes distance) between corresponding landmarks and iteratively computed mean shape (or consensus) configurations (Dryden and Mardia 1998; Slice 2007). After superimposition, pure shape differences can be described by the differences in coordinates of corresponding landmarks between objects since differences in orientation, position and size have been removed (Adams *et al.* 2004; Lawing and Polly 2010).

Summarizing, this method brings the landmark configurations of all specimens into a common coordinate system in which differences in landmark coordinate values reflect differences in shape configurations (Slice 2007).

After superimposition, the final result is the transformation of landmarks into Procrustes shape coordinates, which are variables that describe the variation in the original shapes in a curved space related to Kendall's shape space. GPA residuals can be statistically analysed with standard multivariate procedures (e.g., principal component analysis). The coordinates are typically oriented orthogonally into a linear tangent space yielding Kendall's tangent space coordinates (Lawing and Polly 2010; Adams *et al.* 2004, 2013). Finally, shape change vectors of each principal component can be visualized through *thin-plate splines* (Dryden and Mardia 1998; Adams *et al.* 2004).

Nonetheless, the landmark-based GM method has an important limitation. There are some cases where landmarks are not able to cover the total shape of the structure, that is, relevant differences in the morphology can be located also between landmarks (Adams *et al.* 2004). In these cases, a set of *semilandmarks* (defined on the basis of the "true" landmarks) can be slid along an outline curve or surface until they match as well as possible the positions of the corresponding points along an outline in a reference specimen. Then, the semilandmarks are constrained to retain their relative position on the outline curve (2D) or surface (3D; Dryden and Mardia 1998; Adams *et al.* 2004; Slice 2007). This has been called the *Sliding semilandmark method* (Bookstein 1997). Once the optimally adjusted positions of the landmarks and semilandmarks are determined, they can all be treated in the same way for statistical analyses (Adams *et al.* 2004).

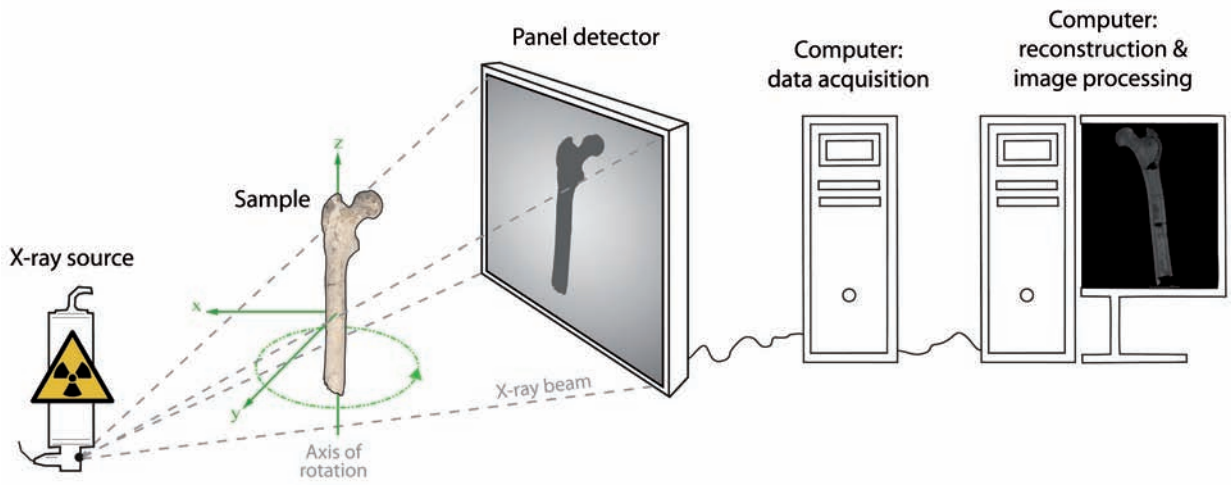

Figure 14 Basic geometry of a computer tomography (CT) scanner. The X-ray source throws a beam of X-rays that collides with the sample and crosses it. The sample is rotating in the z axis usually placed over a turn platform. X-rays that cross the sample arrive to the panel detector, which is composed by smaller detector units. Every unit receives different amounts of electrons depending on the attenuation coefficients of the sample. This information is sent to a computer for data acquisition. Normally, another computer is in network for reconstruction of the CT-scan and image processing.

Computed tomography

Computed tomography (CT) is a powerful technique of visualization that relies on imaging of serial parallel planes (two-dimensional images called *tomographs*) through a three-dimensional object or structure, allowing the study of its internal structure (mainly), but also of its external morphology (Kak and Slaney 1988; Sutton 2008; Mallison *et al.* 2009). The stack of tomograms (tomographic dataset) obtained is image scaled, resolution and slice spacing are constant, and they can be reconstructed as 3D volumes, in which pixels (2D) are voxels (i.e., volume elements, 3D; Sutton 2008; Hsieh 2009).

There are several types of tomography including physical-optical, optical and scanning (Sutton 2008). The latter is the most widely used since it is non-invasive (i.e., the object does not suffer any damage in the process of obtaining the serial images), accurate high-resolution final images can be obtained, and it can be applied almost to any object of study. The use of tomographic techniques in palaeontology started at the beginning of the 20th century with the classical studies of Sollas (1903), Sollas and Sollas (1913) and Stensiö (1927), who used physical-optical tomography (see further explanation in Sutton 2008). Otherwise, in 1906, Gorganovic-Kramberger used for the first time x-rays to study Neanderthal remains from Croatia (Gorganovic-Kramberger 1906). Since then, especially from the 1980s onwards with the development of medical applications, tomography was widely spread and tens of articles have been published hitherto covering a broad range of taxonomic groups using all types of tomographic techniques (e.g., Muir-Wood 1934; Ager 1965; Spoor *et al.* 1993; Sutton *et al.* 2001; Tafforeau *et al.* 2006; Tuniz *et al.* 2013), becoming an important analytical tool to explore external shape and internal design of fossil remains.

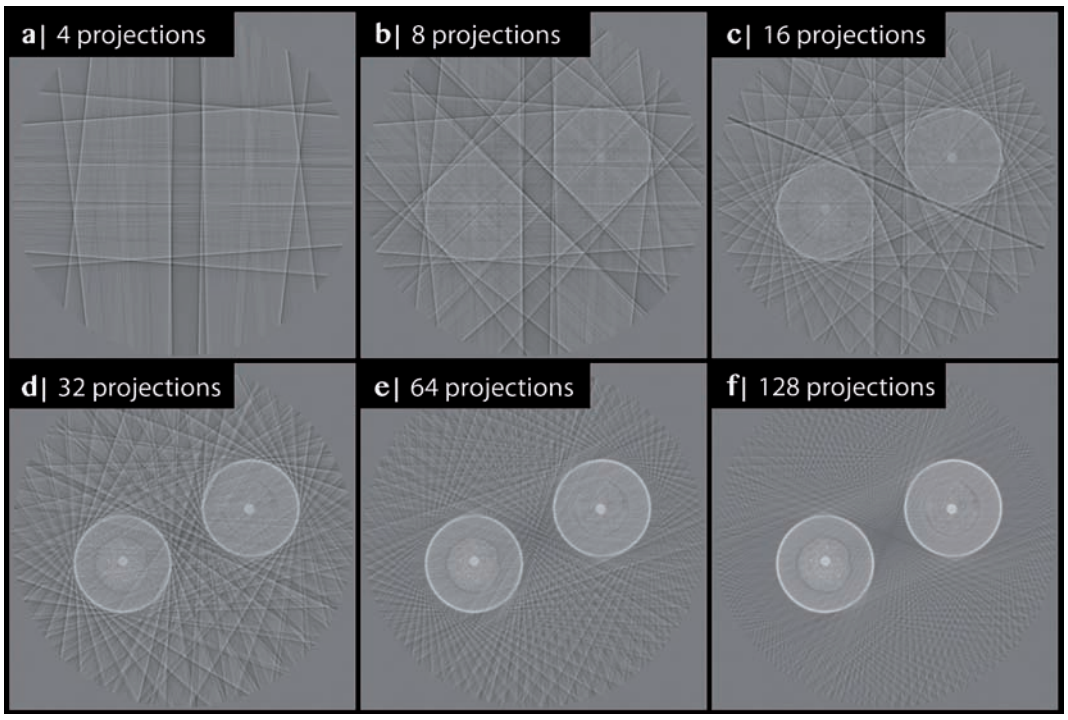

Figure 15 Computed tomography (CT) slices of two E90 batteries in an increasing sequence of projections: **a,** 4 projections; **b,** 8 projections; **c,** 16 projections; **d,** 32 projections; **e,** 64 projections; and **f,** 128 projections. Each projection of the batteries is back-projected (or superimposed) from the sample and when they are summed together result in the reconstruction of the original object (and in its volume in the last instance). For a good quality CT-reconstruction the displacement between projections must be no more than that of the voxel size, usually resulting in images from more than 1000 projections.

Thus, most of the latest works used scanning tomographic techniques, specifically X-ray CT or microCT. This type of CT-technique produces images that represent x-ray linear attenuation coefficient maps of the scanned object, which depend mainly (but no exclusively) on the density of the different materials of the sample (see below for further explanation; Kak and Slaney 1988; Hsieh 2009).

The first X-ray CT-scanner was performed by Hounsfield and it was implemented with some of the reconstruction algorithms discovered by Cormack (Kak and Slaney 1988). An illustrated scheme of X-ray microCT-scanner basic geometry and operation can be seen in Figure 14. The sample is positioned in a platform that usually rotates in an axis (in medical CT-scanners the source of X-rays and/or the detector rotate instead of the sample, that is, the patient). Then, a source of X-rays throws beams onto the sample and a detector collects the electrons that have crossed the sample (Kak and Slaney 1988; Sutton 2008). Image reconstruction is derived computationally from the data obtained usually by using the known as filtered back-projection algorithm (see formulation in Hsieh 2009 and an illustrated explanation in Fig.15).

Isotropic data (volume elements or voxels with pixel size identical to slice thickness) is usually the final result of an X-ray microCT (Spoor *et al*. 2000a; Hsieh 2009). Practically, this data are images that have been reconstructed from their different projections (rotation angles). The formulation for reconstructing an object from multiple projections was demonstrated in 1917 by Radon, who showed than an object can be replicated from an infinite set of its projections through mathematical equations (Hsieh 2009; Cierniak

2011). Therefore, it can be said that projections are a set of measurements of the integrated values of some parameters of the sample (line integrals of the attenuation coefficient, μ, in the case of X-ray CT). Hence, solving these equations (integrals) through specific algorithms will allow the reconstruction of the original object. In the case of X-ray CT, the physical phenomenon that generates line integrals is the attenuation of the x-rays as they propagate through the sample. Hence, projection data is the results of the interactions between the radiation used for imaging the sample (x-rays) and the materials of which the object is composed (Claussen and Lochner 1985; Kak and Slaney 1988). Thus, the sample is modelled as a three-dimensional distribution of the x-ray attenuation constant and a line integral represents the total attenuation suffered by the beam of x-rays that has crossed through the sample in a straight line (calculated as the logarithm of the ratio of monochromatic x-rays photons that enter the object to those that leave).

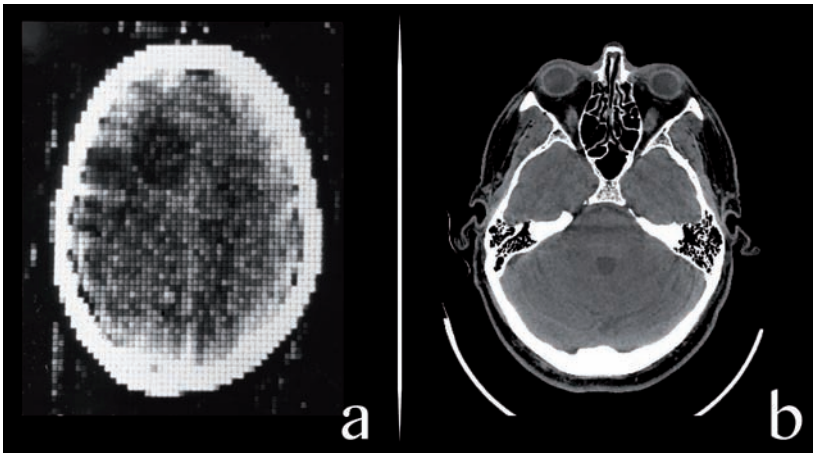

Figure 16 Differences on final resolution between two medical computed tomography (CT)-scans. Axial section of a human head from **a,** one of the first CT-scanners used and **b,** a more modern CT-device. In the former case, pixel size is larger and spatial resolution lower than in b. Modified from Hsieh (2009).

Thus, the x-ray beam is attenuated according to known physical laws by interaction with electrons at every point along its path within a sample. Therefore, the attenuation coefficient is determined by a series of interrelationships (e.g., photoelectric absorption and Compton effect) and is a function of the chemical composition of the sample, density, x-ray filtration, and voltage of the system (Claussen and Lochner 1985). Attenuation in a given medium can be described with the following equation:

$$I=I_0 e^{-\mu L}$$

where I is the resulting intensity, I_0 is the initial intensity of the x-ray beam, μ is the linear attenuation coefficient of the material (that is a function of the incident x-ray photon energy), and L the thickness of the material (Claussen and Lochner 1985; Hsieh 2009). This equation is often called the Beer-Lambert law (Hsieh 2009). Consequently, an increase in thickness or in linear attenuation coefficient fallouts in a reduction of the resulting radiation intensity I. When the sample is not homogeneous and/or is composed by different materials, then the μL product is the sum of all the different material-types (Hsieh 2009):

$$I=I_0 e^{-\Sigma \mu i L i}$$

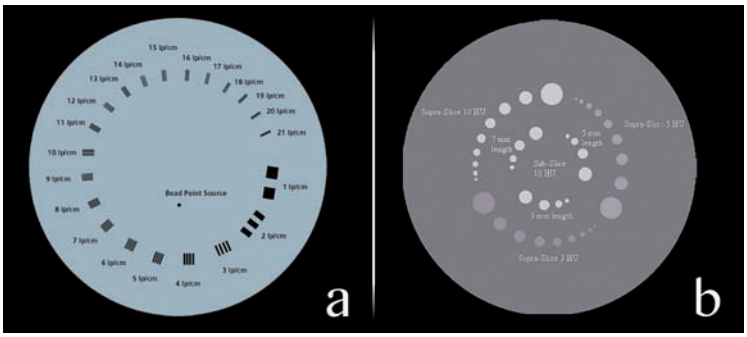

Figure 17 Phantoms used to measure the **a,** spatial and **b,** contrast resolutions of a computed tomography scanner. Spatial resolution is related to the ability of resolving closely placed objects whose density is significantly different from the background; whereas contrast resolution is the ability to differentiate a low-contrast object from its background.

The extensive mathematical formulation of this technique that follows this "starting-point" can be found in Hsieh 2009 and Cierniak 2011. Notwithstanding, in summary, projections are formed by combining a set of line integrals that lead to calculate the average linear attenuation coefficient for each volume element (voxel) of a sample (Kak and Slaney 1988).

The resolution (voxel count) of a tomographic dataset from an axial scan is directly proportional to detector resolution, but the range of absolute voxel sizes a scanner can achieve also depends on the physical configuration and precision of the device (e.g., dimensions of the scan window), and varies from millimeters to less than 1 μm in the case of microCT-scanners (Fig. 16; Rayfield 2007; Sutton 2008). However, not only the CT-scanner characteristics influence the final resolution, it is also highly dependent on the size of the sample and the contrast between bone and matrix, especially in the case of paleontological samples (Rayfield 2007). Several types of resolution can be distinguished. In a general way, "resolution" alone usually referred to *spatial resolution*, which is the ability to resolve closely placed objects whose density is significantly different from the background (Fig. 17a). Spatial resolution is influenced by the detector size, focal spot size, system geometry, sample size, data sampling rate, and reconstruction algorithms (Spoor *et al.* 2000b; Hsieh 2009). Otherwise, the *contrast resolution* of a CT-scanner is the ability to differentiate a low-contrast object from its background, that is, to detect small differences of attenuation coefficient between different materials. In other words, it is typically defined as the smallest object that can be visualized at a given contrast level and a given x-ray dose (Fig. 17b; Spoor *et al.* 2000a,b; Hsieh 2009). It is measured in percentage units, since it is defined as the ratio between the smallest detectable difference of attenuation coefficient (on the Hounsfield scale; see below) and the average value within an object of a given size, for a specific radiation dose (Cierniak 2011). Therefore, the visibility of an object depends on its size, but also on its contrast (intensity difference) with the background (Spoor *et al.* 2000a,b; Hsieh 2009).

In practice, the result of an X-ray CT-scan is a set of tomographs, images that are digital matrices of pixels (Ohman *et al.* 1997; Hsieh 2009). These tomographs are grey-scale images, where every pixel has a grey-value depending on their obtained linear attenuation coefficient (largely the result of material density; Hsieh 2009). These values are expressed in grey-scale units named Hounsfield Units (HU) or CT numbers that are defined as follows (μ is the linear attenuation coefficient; Hounsfield 1973, 1976; Claussen and Lochner 1985; Hsieh 2009):

$$CT\ number = \frac{\mu - \mu_{water}}{\mu_{water}} x1000$$

The Hounsfield scale ranges from black that is the lowest density, typically air (-1,000 HU), to water (0 HU), and white that is the highest density, usually fossilized bone in paleontological samples (~3,000 HU; Spoor *et al.* 1993; Ohman *et al.* 1997; Mafart *et al.* 2004). Hence, HU increase with increasing linear attenuation coefficient. However, the human eye cannot discriminate such amount of density levels. Thus, for displaying in a computer monitor, HU scale is converted into a 256 levels within the grey-scale (Spoor *et al.* 2000a,b; Hsieh 2009). Posteriorly, in order to measure a particular structure, the sample needs the establishment of a threshold value (i.e., grey-scale value) to distinguish the material of interest from those that surround it. However, determining the proper threshold is not a trivial task, since boundaries are not usually well-defined (Spoor *et al.* 1993; Coleman and Colbert 2007). Nonetheless, several methodologies have been developed to define the boundaries between adjacent materials and specialized softwares even have automatic or semi-automatic threshold options (Spoor *et al.* 1993; Coleman and Colbert 2007; Sutton 2008).

Finally, the stack of images can be assembled into 3D volumetric data for different purposes of study with the aid of specialized softwares packages that allow rendering (surface/volume imaging), segmentation (isolation of a material and/or specific structure), and measuring (lengths, areas and volumes), among other functions.

Methodological validation: Data comparability from different CT-scanners

Quality of the final results of a CT-scan is highly dependent on the CT-device and its geometry (range of applicable magnification and detector size and resolution, among others), as well as on several modifiable parameters (e.g., energy of the electron beam, current, projections, exposition time, number of frames, etc.; see above). Therefore, images extracted from different CT-scanners exhibit different spatial resolution (voxel size) and apparently different distribution of pixels ranging in the spectrum of grey-scale values. As a result, depending on the CT-device, the final reconstruction of the scanned structures could be different.

Moreover, once these images are obtained, measurements of the cortical bone thickness or any other variable require to clearly distinguishing the boundaries between the structure/material of interest and their surrounding areas. As seen earlier, this fact could become an issue since boundaries (determined by a grey-scale value) between two adjacent materials are generally not clearly defined (transitions between grey-values are progressive instead of abrupt). Hence, previously to take measurements, there is the need to apply a threshold for acquiring the grey-value which represents the limit between the materials (in the case of paleontological samples, fossilized bone and air/matrix; Coleman and Colbert 2007). Thus, boundaries between materials are better defined in an image obtained from a microCT-scanner (final voxel sizes can arise less than 1 **µ**m) than those taken from a medicalCT-scanner (with minimum pixel sizes around the 0.1 mm; see below for example the models used in this validation study). Such differences might apparently limit comparison between data collected from images with different resolution.

Acquiring a large and diverse sample of primate bones for comparative purposes is essential to obtain rigorous results. The problem is that a unique museum primate collection does not usually have such broad samples, either because the species diversity is low or the number of specimens per species is scarce. Moreover, in most instances, collections do not have an associated computed tomography facility

CT-SETTINGS		
Settings	**medicalCT**	**microCT**
Voltage (kV)	120	165
Current (mA)	250	165
Exposure time (ms)	1825	333
Magnification	-	2.156
Filter	-	0.1 mm Cu
Voxel size (mm)	-	0.093
Interslice (mm)	0.625	-

Table 7 Settings used to perform the computed tomography (CT) scanners of the gorilla femur in a medicalCT (SBU) and a microCT-scanner (AMNH).

where CT-scanning the bones. For this reason, the use of several CT-devices is almost unavoidable in order to get a consistent sample of CT-scans. This fact conducts to the obtaining of a sample that somehow could combine CT-scans from several microCT-scanners, from microCT and medicalCT-scanners, etc. Thus, despite the continuing and rapid expansion of CT-methodologies and their utility, especially in biological studies, and almost a compulsory combination of CT-scans from different institutions and devices to compile a large database, no study has comprehensively assessed the comparability of images extracted from different scans. Therefore, it emerges the question if measurements of the same element taken on CT-images extracted from different CT-devices are comparable or not. For this reason, this section does not focus on testing threshold issues (fairly checked elsewhere; see Hara *et al.* 2002 and Coleman and Colbert 2007), but in checking for the comparable character of measurements obtained from CT-scans performed in different CT-scanners.

CORTICAL THICKNESSES				
Measure no.	**SMSUP**	**AMSUP**	**SBINF**	**ABINF**
1	1.598	1.465	2.899	2.746
2	1.598	1.465	2.885	2.73
3	1.612	1.544	2.838	2.775
4	1.714	1.463	2.746	2.841
5	1.549	1.508	2.823	2.746
6	1.497	1.59	2.841	2.802
7	1.661	1.55	2.894	2.775
8	1.453	1.683	2.784	2.847
9	1.601	1.548	2.779	2.821
10	1.497	1.544	2.823	2.775
11	1.392	1.555	2.88	2.831
12	1.489	1.672	2.855	2.903
13	1.661	1.593	2.775	2.775
14	1.489	1.544	2.818	2.791
15	1.497	1.675	2.841	2.858

Table 8 Thickness measurements (in mm) taken in the superior region of the midneck (SMSUP and AMSUP) and inferior region of the base-of-neck sections (SBINF and ABINF) in a medical (SMSUP and SBINF) and micro computed tomography-scanenr (AMSUP and ABINF). See text for abbreviations.

Thus, a pilot study has been conducted in order to comprehensively assessed the comparability of images extracted from different CT-scanners, and ensure their use in comparative studies, by scanning the right femur (AMNH201460) of the species *Gorilla gorilla gorilla* in two different CT-devices: (1) the medicalCT of the Stony Brook University hospital (SBU, New York), and (2) the microCT of the Microscopy and Imaging facilities of the American Museum of Natural History (AMNH, New York). Although both scanners were designed by the same company, General Electrics (GE), they have different specific characteristics. Thus, the medicalCT is a GE Lightspeed VCT 64-slice high image resolution system with a MX 240 8.0 MHU tube and 64 x 912 ceramic detectors. Its slice thickness acquisition ranges between 0.625-10 mm, its voltage and current between 80-140 kV and 10-800 mA, respectively. It has a HiLight/Lumex solid-state detector with 888 detectors/row. Otherwise, the microCT-scanner is a GE phoenix v|tome|x s240 system. It counts with two x-rays tubes: a nano-focus high resolution x-ray tube and a micro-focus high energy x-ray tube. For this study, the femur was scanned with the nano-focus tube that produces x-rays until 180 kV of power and 833 mA of current. It has a DXR250RT real time detector, composed by a 1024x1024 pixel array at 200 μm pixel pitch that can raise a minimum voxel size of less than 1 micron. The system allows a geometrical magnification of 1.3x to 160x at 800 mm focus detector distance.

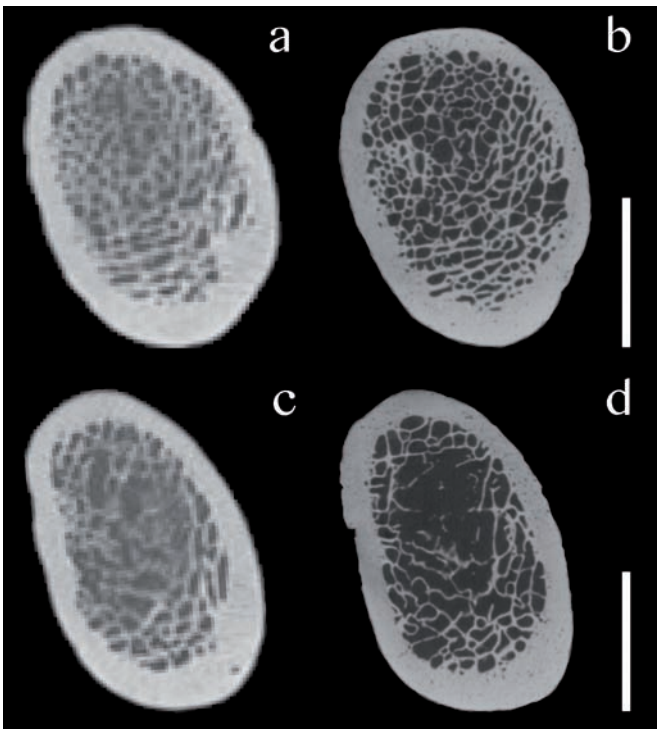

Figure 18 Computer tomography (CT)-sagittal images of the **a-b,** midneck and **c-d,** base-of-neck of a gorilla femur. Images arising from a medical (a, c) and a micro (b, d) CT-scanner. Scale bar = 10 mm; up, superior; right, posterior.

The femur was scanned transversely in both cases, that is, perpendicular to its proximodistal main axis. Settings used to scan the femur and interslice/voxel size obtained for both scans are shown in Table 7. Image stack was exported as DICOM files from the medicalCT and as *.tiff files from the microCT. 3D volumetric reconstruction and visualization of the scans and acquisition of CT-sections were conducted

Table 9 Descriptive statistics of the four variables used in this study (in mm). *Abbreviations:* SD, standard deviation; see text for variables abbreviations.

DESCRIPTIVE STATISTICS				
	SMSUP	**AMSUP**	**SBINF**	**ABINF**
Mean	1.554	1.560	2.832	2.801
SD	0.090	0.073	0.047	0.048
Variance	0.008	0.005	0.002	0.002
Minimum	1.392	1.463	2.746	2.730
Maximum	1.714	1.683	2.899	2.903

with the software *VGS-Avizo* 7.0. Images were obtained at the base-of-neck and midneck of the femur as explained in Ruff and Higgins (2013). In order to perform the statistical analyses, superior (SUP) and inferior (INF) cortical thicknesses were measured in the midneck and base-of-neck sections, respectively, following the procedure of Ruff and Higgins (2013; Fig. 18). The interface between cortical bone and air was determined by a semi-automatic thresholding with the software *VGS-Avizo* 7.0 and, when needed, by calculating the mean of the threshold value between the minimum values of cortical and air materials at both sides of the boundary (see Spoor *et al.* 1993 for further information). Measure acquisition was repeated 15 times for each of the CT-images (Table 8), resulting in four different variables: SMSUP, superior cortical thickness taken from medicalCT-images; AMSUP, superior cortical thickness taken from microCT-images; SBINF, inferior cortical thickness taken from medicalCT-images; and ABINF, inferior cortical thickness taken from microCT-images. Pairwise independence of the groups of measurements was checked with the chi-squared test (SMSUP *vs* AMSUP and SBINF *vs* ABINF). Variable distributions were tested for normality through the Shapiro-Wilk test. Finally, a *t*-test analysis was applied for checking whether there exist mean differences between the groups of measurements taken from a medical- or a microCT-scanner in both SUP and INF thicknesses separately. As measurements sample is under 20 values and, in some cases, chi-squared approximation may lead to incorrect results, and additional *t*-test was performed to prove mean differences assuming not independency of the variables. Analyses were conducted using the R statistical package (R Core Team 2015).

Descriptive statistics obtained for every of the four variables are depicted in Table 9. When independence of the pairwise variables is tested, no-relation between them is obtained: SMSUP *vs* AMSUP chi-squared = 116.67, df = 99, p-value = 0.1085; and SBINF *vs* ABINF chi-squared = 129.38, df = 120, p-value = 0.2634. Likewise, all the four variables are normally distributed (p-value > 0.05 in all instances; SMSUP W = 0.955, AMSUP W = 0.897, SBINF W = 0.954, ABINF W = 0.957). Finally, when *t*-test is applied for testing mean differences between the pairwise variables, results do not show such differences between taken linear measurements in either medical- or microCT-scanners (SMSUP *vs* AMSUP: t = -0.203, p = 0.840; SBINF *vs* ABINF: t = 1.792, p = 0.084). When non-independence of the variables is assumed for conducting the *t*-test, non-differences between the pairwise variables are even statistically greater than in the first case (SMSUP *vs* AMSUP: t = 1.792, p = 0.138; SBINF *vs* ABINF: t = -0.165, p = 0.871).

Therefore, the results strongly indicate that visual differences due to different resolution/voxel size of the scans performed in different CT-machines with different settings are not statistically significant when linear measurements are compared between them. In any case, microCT-scanners tend to generate better, in terms of spatial resolution and definition of the materials boundaries, final images of the object/specimen of study, with voxel sizes that can raise even a hundred times lesser in size compared to a medicalCT. Thus, a microCT-scanner reconstructs images that better approximates to reality and, thereby, collecting data on higher-resolution images will result in more accurate data when measurements involve very thin or micro-size elements (e.g. trabecular bone). However, as shown from these results, resolution

seems not to deeply influence the determination of the cortical bone boundaries in a cross-section image, maintaining the overall morphology of the cortical bone edges and its endosteal-periosteal thicknesses in a large species like *Gorilla*. Therefore, these results open then the possibility of comparing data collected from CT-scan conducted in different devices and/or with different applied settings (e.g., voltage and amperage) and, thus, the possibility of compiling larger and more complete and diverse CT-databases of bones with comparative purposes.

Although this pilot study is limited to one specimen that belongs to the largest primates species, the gorilla, it already demonstrates the possibility of comparing images extracted from different CT-scanners (mainly medical- *vs* microCT-scanners). Nonetheless, a larger sample size and, specially, the inclusion of smaller species in the comparisons are needed to more accurately assessing the comparability of data extracted from different CT-devices.

Finite element analysis (FEA)

Finite Element Analysis (FEA) is a procedure of general discretization of complex continuous systems (problems) through their subdivision in a limited (finite) number of well-defined components that approach in the limit the true continuum solution (Zienkiewicz *et al.* 2005). In other words, this method allows estimating how an object with a complex or irregular geometrical shape (e.g., bones) behaves when it is subjected to external loads by subdividing it in simple geometric entities that are individually analysed (Morgan and Bouxsein 2005; Engel *et al.* 2011).

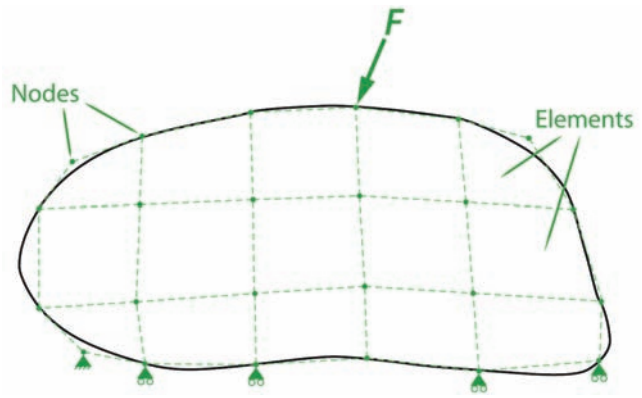

Figure 19 Schematic representation of a finite element problem. A complex geometry (black line) is discretized in a collection of elements (light green dashed line) linked by nodes (green closed circles). Forces (F) and boundary conditions (green closed triangles) applied are also illustrated. Modified from Morgan and Bouxsein (2005).

Although the division in portions to solve a continuum problem started in the 1940s (Hrenikoff 1941; McHenry 1943; Southwell 1946; Zienkiewicz 2004), the term "finite element" was firstly used by Clough (1960, 2004) in an engineering context, implying the direct use of a standard methodology applicable to discrete systems by showing that by minimizing the total potential energy, the approximate solution would converge to the exact mathematical solution as the size of the elements decreased (Zienkiewicz 2004; Zienkiewicz *et al.* 2005). From the early 1960s onwards, the method was fully recognized and generalized not only in solid and fluid mechanics (engineering), but also in other areas of study, such as Medicine (mainly orthopaedics; e.g., Skinner *et al.* 1994), Biomechanics (Rafferty *et al.* 2003), Sports (Dabnichki and Avital 2006), Palaeontology (Rayfield *et al.* 2001), Zoology (Thomason 1991), etc.

Conceptually, the finite element approach to solid or structural mechanical problems begins by representing the object as a collection of a finite number of simple geometric elements, each of which is defined by a small number of reference points, or nodes (Fig. 19; Morgan and Bouxsein 2005). The deformation of each element, which occurs in response to the applied loads, is represented by simple yet versatile functions, shape or basis functions, in which the only unknowns are the displacements of the nodes. Therefore, once the nodal displacements are computed, the strain distribution throughout each element, and consequently the entire object, can be obtained (Morgan and Bouxsein 2005; Zienkiewicz *et al.* 2005). In order to solve the unknowns (displacements), boundary conditions (which are the applied loads and constraining anchors) and material properties for each element have to be implemented in the model to define the physical behaviour of the original problem (Morgan and Bouxsein 2005; Engel *et al.* 2011). Among the material properties, the Young's modulus (elasticity) and the Poisson's ratio (the change in width after a given change in length) have to be always defined (others like the shear modulus, density of the material, and bone mineral fraction should be also included depending on the question to solve; Rayfield 2007). Therefore, the approximated solution of the problem yields the set of nodal displacements that satisfies the mechanical equilibrium given the geometry of the object, the boundary conditions, and the material properties. The nodal displacements and material properties are then used to compute the stress distribution throughout the entire object (Morgan and Bouxsein 2005).

In order to mathematically solve the continuum problem aforementioned, this problem is recognized as a structural system that can be transformed to equations. An element is associated with *n* nodes (e.g., a tetrahedral element can be defined to have four nodes on each of its corners or ten if nodes on the connecting lines are added), and forces acting at these nodes are uniquely defined by their displacements, the distributed loading acting on the element, and its initial strain (Zienkiewicz *et al.* 2005; Engel *et al.* 2011). The last may be due to temperature, shrinkage, or simply an initial "lack of fit" (Zienkiewicz *et al.* 2005). A typical mathematical approach to solve continuum problems is the *Matrix analysis* or S*tiffness method*, in which the displacements given to the ends (nodes) of an element are related to the forces acting at these ends (Zienkiewicz 2004). Then, assuming that the sum of the forces contributed by each element to a node must equal the force that is externally applied to that node and that the element properties (forces and displacements) follow a simple linear relationship (stiffness), a sequence of linear equations can be assemblage in which the nodal displacements are the unknowns and the applied nodal forces are known quantities (Zienkiewicz *et al.* 2005). This assertion is algebraically translated as follows:

$$\begin{bmatrix} K_{11} & K_{12} & \cdots & K_{1n} \\ K_{21} & K_{22} & \cdots & K_{2n} \\ \vdots & \vdots & \ddots & \vdots \\ K_{n1} & K_{n2} & \cdots & K_{nn} \end{bmatrix} \begin{Bmatrix} u_1 \\ u_2 \\ \vdots \\ u_n \end{Bmatrix} = \begin{Bmatrix} f_1 \\ f_2 \\ \vdots \\ f_n \end{Bmatrix}$$

in which u_i and f_j indicate the deflection at the i^{th} node and the force at the j^{th} node. The K_{ij} coefficient is known as the stiffness matrix, with the *ij* component being physically the influence of the j^{th} displacement on the i^{th} force. In other words, the global stiffness matrix is the sum up of every element stiffness matrices

and represents the resistance of the element to change when subjected to external influences (Zienkiewicz *et al.* 2005; Engel *et al.* 2011). Assuming that the model follows the Hooke's law and the force-loaded material returns completely to its initial shape after it is unloaded (that is, the problem has a linear elastic behaviour), the matrix equations can be abbreviated as:

$$K_{ij}u_j = f_i \text{ or } Ku = f$$

Thus, this equation represents the nodal displacements (u_j) of the body when an external force (f_i) is applied (Engel *et al.* 2011). Moreover, to obtain a solution of a structural system, two conditions have to be satisfied: displacement compatibility and equilibrium of the problem. Any system of nodal displacements u_j in which all elements participate automatically covers the first condition. As the conditions of overall equilibrium have already been satisfied within an element, all that is necessary is to establish equilibrium conditions at the nodes (or assembly points) of the structure, that is, the sum of all the forces exerted at the nodes has to be zero (Zienkiewicz 2004). The resulting equations will contain the displacements as unknowns, and once these have been solved the structural problem is determined. The internal forces in elements, or the stresses, can easily be found by using the characteristics established *a priori* for each element (Zienkiewicz *et al.* 2005).

Additionally, the system of equations performed anteriorly can be solved by substituting with zero the first and last pairs of prescribed displacements and thus reducing the number of unknown displacements components. Without substitution of a minimum number of prescribed displacements to prevent rigid body movements of the structure, it is impossible to solve the equations of the system. Mathematically, the prescription of appropriate displacements after the assembly stage will permit a unique solution to be obtained by deleting appropriate rows and columns of the various matrices (Zienkiewicz *et al.* 2005). Such mathematical changes are known as *boundary conditions*, and once these are integrated in the system it can be solved for the unknown nodal displacements and the internal forces in each element can be also obtained (Zienkiewicz *et al.* 2005).

The mathematical formulation and numerical development of the method is out of the scope of this work, but an expanded and in-depth explanation of the algebraic solution of FEA can be found in Zienkiewicz *et al.* (2005) and references therein.

In practice (such as in the case of bones or fossil remains), a typical procedure to solve continuum problems follows three steps: (1) pre-processing, (2) analysis and (3) post-processing. The former (1) consists of representing the real geometry by the construction of a mesh (model) and dividing it in a number of discrete subregions (elements) that connect at discrete points (nodes; Morgan and Bouxsein 2005; Rayfield 2007). Moreover, boundary conditions have to be included in the model, that is, certain nodes will have fixed displacements (physical constrains) and others will have prescribed loads. Likewise, material properties (Young's modulus and Poisson's ratio suffice for an elastic material) of the elements have to be added in the finite element (FE) model at this point (Engel *et al.* 2011). During the analysis phase (2), the mathematical equations proposed for the system will be solved, computing and assembling

the element arrays, and finally calculating nodal displacements, strain and stress during the loading interval (Rayfield 2007; Kupczik 2008). The last step, the post-processing (3), comprises the interpretation and evaluation of the results, many times represented as scaled colour maps of the stress/strain and/or displacement levels along the structure in order to assist in visualization of these results (Rayfield 2007; Kupczik 2008).

As commented in step 3, FEA is a technique that reconstructs stress, strain, and displacements in structures and those are commonly the engineering parameters of interest to study in vertebrate functional morphology and vertebrate palaeontology (Rayfield 2007; Kupczik 2008). Thus, a force applied in a structure generates *stress* within this structure (σ), as well as deformation or *strain* (ε). The orientation, distribution, and magnitude of the stress and strain are dependent on the applied load, the material properties (Young's modulus, E, and Poisson's ratio, ν), and the structural organization of the geometry (Rayfield 2007). It is important to take into account that under normal loading conditions, a linear elastic isotropic behavior is usually assumed for bones. Thereby, in this type of mechanical models, stress and strain change proportionally through the Hooke's law (Rayfield 2007; Korhonen and Saarakkala 2011):

$$\sigma = E\varepsilon$$

One of the most common types of stress analysed in studies that include bones and/or fossil specimens is the *von Mises stress*. It is a function of the principal stress (σ_1, σ_2, σ_3) and measures how stress distorts a material. Von Mises stress is a good estimator of failure in a ductile material, since failure would happen when von Mises stress equals the yield strength of the material in uniaxial tension (Rayfield 2007; Gröning *et al.* 2013). Moreover, this type of stress is an appropriate metric for comparing the strength of models of bones (Dumont *et al.* 2009), being for this reason one of the most widely used to show loading results in paleontological studies.

Somewhere, something incredible is waiting to be known.
-- Carl Sagan --

Section IV. THE FEMORA

Chapter 1
External morphology of the femur

DESCRIPTIONS

IPS21350.81 & IPS21350.85.- Diaphyseal fragments

IPS21350.81 and IPS21350.85 are two long bone shaft portions (Fig. 20), each one constituted by several fragments of cortical bone. They most likely belong to the femur of the same *Pierolapithecus catalaunicus* skeleton (Moyà-Solà *et al.* 2004), based on their possible diameter. IPS21350.81 is slightly eroded at the borders and a cortical thickness of around 4.3 mm is measured (around the midpoint of the longest axis). On the other hand, cortical thickness edges of IPS21350.85 are better preserved, being 4.4 mm and 4.3 mm in the left and right sides respectively if observed the cortical fragment in interior view (see Fig. 20d). In addition, IPS21350.81 displays a mild rough line that probably corresponds to the medial/lateral line of the posterior side of the femoral shaft (Fig. 20a). Apart from this line, the fragments do not show any other informative feature that allows accurately distinguishing the bone side or the bone to which they belonged.

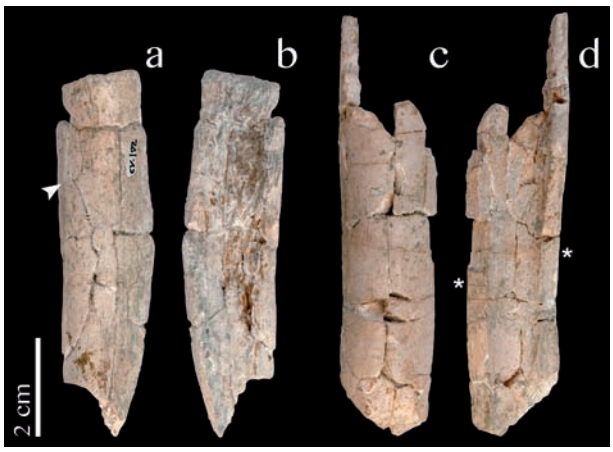

Figure 20 Diaphyseal cortical fragments of long bones (probably femur) of *Pierolapithecus catalaunicus* (IPS21350, holotype) from ACM/BCV1. **a–b**, IPS21350.81, in **a**, external; and **b**, internal views. **c–d**, IPS21350.85, in **c**, external; and **d**, internal views. The black arrowhead in (a) shows one of the possible posterior lines (spiral or lateral) of the femur. Asterisks in (d) indicate the locations where the cortical thicknesses were measured.

IPS41724.- Right partial proximal femur

IPS41724 is a well-preserved right partial femur tentatively attributed to cf. *Dryopithecus fontani* (Fig. 21; Table 10; Moyà-Solà *et al.* 2009a). The IPS41724 femur is robust in appearance, with a spherical femoral head that is small relative to the neck (see following sections and Almécija *et al.* 2013: fig. 6). Its articular surface extends only very slightly onto the femoral neck on the posterior side, but is mediolaterally broad on its anterior side (Fig. 21; Table 10). The *fovea capitis* is large and relatively shallow, and is located at

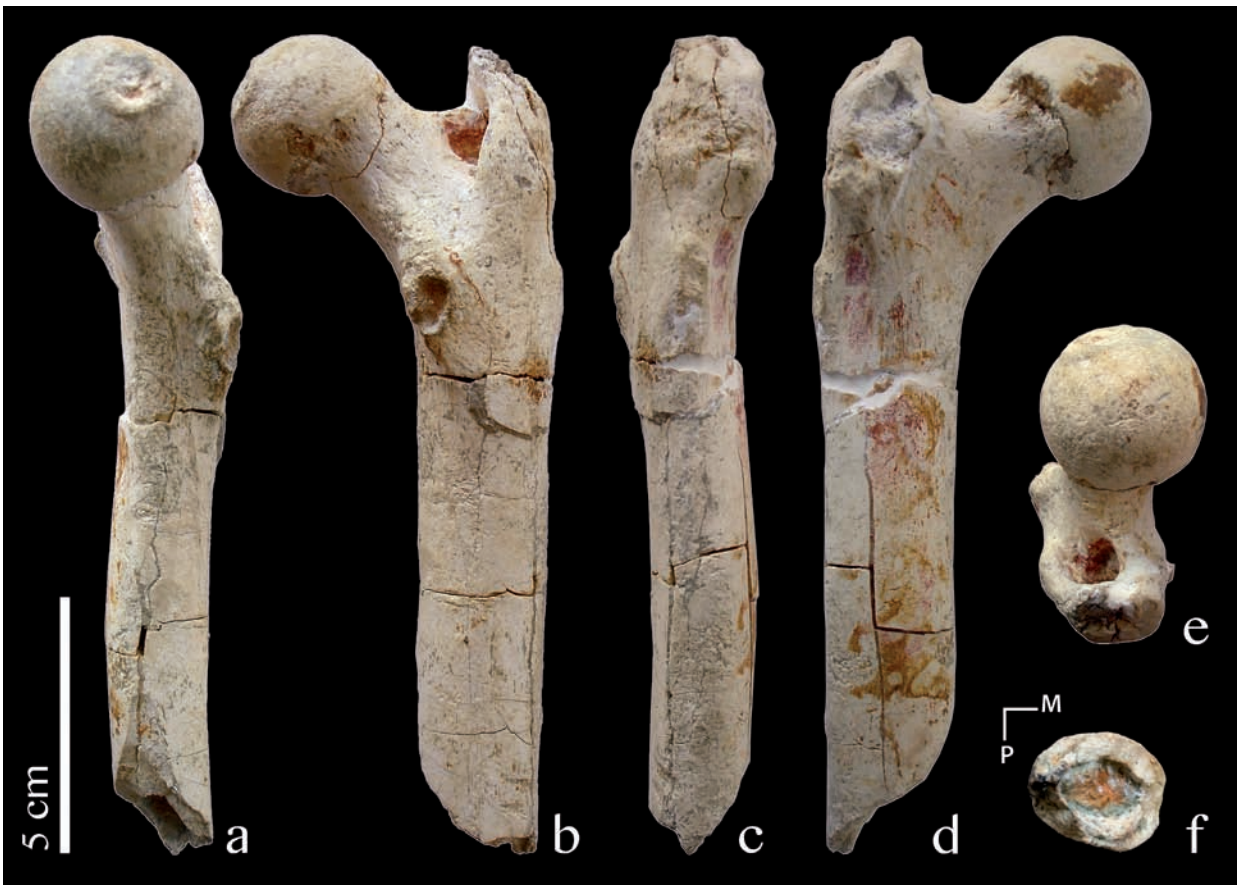

Figure 21 Right proximal femur cf. *Dryopithecus fontani* (IPS41724) from ACM/C3-Az, in **a**, medial; **b**, posterior, **c**, lateral; **d**, anterior; **e**, proximal; and **f**, distal views. *Abbreviations:* M, medial; P, posterior.

the superoposterior quadrant of the femoral head. The proximal portion of the bone (the femoral head and neck) shows a slight anteversion in medial view, although the head itself is slightly tilted posteriorly relative to the neck (Fig. 21a). The latter is robust and anteroposteriorly flattened, displaying an elliptical cross-section (SIN/APN = 1.48; for abbreviation definitions see Table 6 and Fig. 12). IPS41724 displays a long biomechanical neck length relative to its proximal femur size, and the angle between the neck and the diaphysis is rather relatively high (Tables 10 and 11). An *obturator externus* groove is not evident on the posterior surface of the neck. The greater trochanter is superoinferiorly short and anteroposteriorly narrow, and displays a slight lateral flare, being situated somewhat below the femoral head. The femoral notch (between the head and the greater trochanter) is deep and broad. IPS41724 also has a moderately deep and broad trochanteric fossa. The trochanteric crest is slightly prominent, although the quadrate tubercle is clearly marked. Despite some erosion of the greater trochanter, there is a large square area

Table 10 External measurements of the femur remains of Vallès-Penedès hominoids. For measurement abbreviations and units see Table 7.

VALLÈS-PENEDÈS FEMORA MEASUREMENTS												
Catalogue no.	**Taxon**	**ProxW**	**APH**	**SIH**	**APN**	**SIN**	**NL**	**NSangle**	**APMS**	**MLMS**	**APPS**	**MLPS**
IPS18800 (right)	*H. laietanus*	58.0	29.6	26.6	12.9	17.9	17.4	130.1	20.5	22.3	20.1	21.6
IPS18800 (left)	*H. laietanus*	—	—	31.5 [a]	—	—	—	140.4 [a]	19.9	19.3	20.0	22.1
IPS41724	cf. *D. fontani*	63.0	31.0	30.7	16.4	24.3	23.3	124.0	20.9	27.0	20.6	27.0

[a] Estimated values (due to the damage in the femoral head and neck).

for the attachment of the *gluteus medius* and *piriformis* muscles. Along the anterior side of the femur, IPS41724 displays a prominent well-marked surface that spreads medially and through the lateral side of the greater trochanter, where probably attached the *gluteus minimus* muscle. The lesser trochanter is well developed. It is placed in the posterior side of the femur (not visible in anterior view; see Fig. 21d) and faces posteriorly. The surface for the insertion of the *illiopsoas* muscle is deep and extends over almost the whole surface of the lesser trochanter. In anterior view, the intertrochanteric line is slightly prominent, running from the femoral tubercle to the inferomedial side of the femoral neck. The proximal portion of the shaft is anteroposteriorly flattened (APPS/MLPS = 0.76), and the lateral and medial lines on the posterior side of the shaft, defining the insertion of the *vastus lateralis* and *vastus medialis* muscles, respectively, do not meet to form a *linea aspera* (i.e., the posterior side of the shaft is flat). Moreover, a well-developed gluteal tuberosity is present on the lateral side of the proximal shaft, to which the ascending tendon of the *gluteus maximus* attaches in living primates. A smooth and shallow hypotrochanteric fossa is placed on the

Table 11 Descriptive statistics for femoral neck-shaft angle (NSangle, in degrees) in a sample of extant primates (total sample size, N = 359 individuals), and measurements of this variable in fossil taxa. *Abbreviations:* M, males; F, females; U, unknown sex; N, sample size; SD, standard deviation; CI, confidence interval.

FEMORAL NECK-SHAFT ANGLE										
Group	**M**	**F**	**U**	**N**	**Mean**	**SD**	**CI 95%**		**Range**	
Gorilla beringei beringei	4	4		8	121.09	5.25	116.71	125.48	113.94	129.04
Gorilla beringei graueri	13	8		21	117.04	4.21	115.12	118.95	107.75	122.61
Gorilla gorilla gorilla	13	13		26	121.95	3.98	120.35	123.56	113.31	127.82
Pan paniscus	9	11		20	122.77	5.31	120.29	125.25	114.23	130.85
Pan troglodytes schweinfurthii	16	8	2	26	123.00	5.11	120.94	125.07	114.27	132.69
Pongo pygmaeus	5	5	3	13	134.93	5.81	131.24	138.62	127.29	145.07
Hylobates lar	13	13		26	123.95	5.16	121.87	126.04	115.43	134.82
Papionins [a]	15	7	8	30	111.57	5.98	109.34	113.80	97.84	119.31
Macaca fascicularis	13	13		26	110.53	4.67	108.64	112.41	101.93	120.16
Cercopithecus mitis	8	5	1	14	112.11	4.89	109.29	114.94	104.15	123.18
Nasalis larvatus	13	12		25	111.55	4.71	109.61	113.50	101.33	120.52
Colobus sp.	14	12	1	27	112.94	6.24	110.47	115.41	97.86	126.27
Presbytis sp.	17	16		33	113.23	4.23	111.73	114.73	103.77	122.19
Atelids [a]	12	16	10	38	124.45	6.20	122.42	126.49	111.03	134.48
Cebus apella	14	12		26	121.16	5.40	119.03	123.30	111.99	133.20
Ekembo nyanzae (KNM-MW13142A)				1	115.35					
Ekembo nyanzae (KNM-RU5527)*				1	128.71					
Morotopithecus bishopi (MUZM80)*				1	114.23					
Nacholapithecus kerioi (KNM-BG35250A)				1	126.10					
Orrorin tugenensis (BAR1200'00)				1	115.95					
cf. *Dryopithecus fontani* (IPS41724)				**1**	**124.01**					
***Hispanopithecus laietanus* (IPS18800, right)**				**1**	**130.07**					
***Hispanopithecus laietanus* (IPS18800, left)**				**1**	**140.41**					

* Measurements of KNM-RU5527 and MUZM80 are approximated due to the incomplete nature of their femoral head and femoral shaft, respectively. Measurements for KNM-RU5527 were taken from photos kindly provided by Christopher B. Ruff.

[a] The composition of papionins and atelids is specified in Table 12.

anterior side of the proximal portion of the shaft. Although incomplete, the shaft is slightly bent anteriorly and displays some degree of anteroposterior compression, exhibiting an elliptical cross-section (APMS/MLMS = 0.77; see Chapter 3 for further information on the cross-sectional structural properties).

IPS11426.- Partial diaphysis femur

IPS11426 is a partial left femur from CP composed of two well-preserved diaphyseal fragments that are continuous with one another (Fig. 22), and which have not been previously described. On its proximal half, diaphyseal cross-section is approximately round (with its anteroposterior and mediolateral diameters being about equal, AP/ML = 0.98; see Fig. 22), whereas toward its distal portion the shaft becomes anteroposteriorly flattened (mediolaterally broader than anteroposteriorly thick; AP/ML = 0.79; see Fig. 22). At the proximal (broken) end, cortical bone thickness is approximately uniform (anterior = 17.4 mm; medial = 21.5 mm; posterior = 21.6 mm; lateral = 21.3 mm). All these features are not very diagnostic, but more closely resemble the condition of the *Hispanopithecus laietanus* femora from CLL2 (IPS18800, see below) than that of cf. *Dryopithecus fontani* from ACM (IPS41724, see above), since both IPS11426 and IPS18800 display a similar diaphyseal geometry (essentially rounded and more anteroposteriorly flattened through the distal region), and a homogeneous distribution of the cortical bone. Given that CP is the type locality of *Hispanopithecus crusafonti* and that no more hominoid species have been described in this fossil site, this femoral shaft, like the hamate and several partial metatarsals recovered from the same locality (Almécija *et al.* in prep.a), is attributed to this taxon, in spite of the fact that it was originally described only based on dental remains (Begun 1992a; see also Alba *et al.* in prep).

Figure 22 Partial left femoral diaphysis of *Hispanopithecus crusafonti* (IPS11426) from Can Poncic (CP), in **a**, medial; **b**, posterior; **c**, lateral; **d**, anterior; **e**, proximal; and **f**, distal views. *Abbreviations:* M, medial; L, lateral; P, posterior. Asterisks indicate the locations where the shaft diameters were measured.

IPS18800.- Right & left partial proximal femora

The partial skeleton of *Hispanopithecus laietanus* (IPS18800) from CLL2 preserves both femora (Figs. 23 and 24; Table 10; Moyà-Solà and Köhler 1996). They are slender than that of cf. *D. fontani* and the diaphysis is slightly anteriorly concave. The femoral head is spherical and large in comparison to the femoral neck (see following sections and Almécija *et al.* 2013: fig. 6), and its articular surface hardly extends posteriorly onto the neck. The femoral head of the left femur is larger and the neck-shaft angle

Figure 23 Left femur of *Hispanopithecus laietanus* (IPS18800), in **a**, medial; **b**, posterior; **c**, lateral; **d**, anterior; **e**, proximal; and **f**, distal views. In (e), the head and diaphysis of the femur are separated for better visualization. *Abbreviations:* L, lateral; M, medial; P, posterior.

higher than those of the right femur (see absolute values in Table 10). Since these femora belong to a single individual, two possible explanations emerged for these discrepancies (see also the "Comparisons" section). Firstly, such differences might be due to normal lateral asymmetries within an individual and/or intraspecific variability. On the other hand, differences might be consequence of some taphonomic factor during fossilization (e.g., water exposure, since the left femoral head seems to be inflated). Any of the two possibilities remains feasible and further analyses are needed to favour one of the two hypotheses. The *fovea capitis* is well marked, somewhat large and deep, being situated on the superoposterior aspect of the head. The biomechanical length of the femoral neck and the femoral neck-shaft angle are high (particularly in the left specimen; Table 11; see below). The cross-sectional geometry of the femoral neck is slightly elliptical (SIN/APN = 1.39) and, internally, the distribution of the cortical bone is homogeneous (see Chapter 2). Both femora lack a discernible *obturator externus* groove. The greater trochanter is superoinferiorly long and anteroposteriorly wide, being located inferiorly to the femoral head, so that the femoral notch is deep and narrow. Although the greater trochanter of the right femur is slightly damaged (and missing from the left femur), a small insertion for the *gluteus minimus* muscle can be observed on its lateral side. The trochanteric fossa is deep and wide, and the two femora display a shallow depression from the trochanteric fossa to the lesser trochanter. The latter is well developed and medially oriented. The two femora display a gluteal ridge, instead of a tuberosity, and two mild *spiral* and *pectineal* lines are present on the posterior aspect of the diaphysis. The cross-section at the proximal shaft and the midshaft is subcircular (APPS/MLPS = 0.92 and APMS/MLMS = 0.97; see Chapter 3 for further information on cross-section geometry).

Figure 24 Right femora of *Hispanopithecus laietanus* (IPS18800) in **a**, medial; **b**, posterior; **c**, lateral; **d**, anterior; **e**, proximal; and **f**, distal views. *Abbreviations:* M, medial; P, posterior.

COMPARATIVE SAMPLE, MEASUREMENTS AND STATISTICAL ANALYSES

The hindlimb remains of the Vallès-Penedès hominoids are compared with a sample of extant and extinct primates, including platyrrhines, cercopithecoids and apes. The composition of the extant primate comparative sample is summarized in Table 12. Other fossil specimens included in this study are listed in Table 13.

External bone measurements used in this work are defined in Table 6 and illustrated in Figure 12a. Measurements of the proximal femur were taken to the nearest 0.1 mm with digital callipers in extant primates and the original Vallès-Penedès fossils, and from the literature for the comparative fossil sample (Table 13).

Several indices based on some of the linear measurements were also calculated, given their previously stated functional relevance. Thus, SIH/SIN has been related to hip range of motion, since a large femoral head relative to neck size seems to favour wide excursions of the joint, especially abduction movements (Ruff 1988). SIH/MLPS and SIN/MLPS, in turn, have been associated with robusticity of the proximal femur and the amount of body weight transferred through this bone (Napier 1964; Walker 1973; Ruff 1988).

The NSangle was measured with the software *Fiji* (Schindelin *et al.* 2012) from photographs with the femora in anterior view for the extant and fossil sample listed in Table 11. The BMNL of the femur was measured from the most lateral point of the greater trochanter to the most proximal point of the femoral head and then depicted as an index relative to the proximal femur size (see Almécija *et al.* 2013 for further explanation).

Values for the aforementioned indices of the Vallès-Penedès hominoids were visually compared with those for the extant and fossil comparative sample using boxplots, whereas statistical differences between taxonomic groups were tested via analysis of variance (ANOVA) and post hoc Tukey's pairwise comparisons. The latter method was used due to the unequal nature of the groups' sample sizes within the whole sample of extant anthropoids (Tables 11 and 12; Kramer 1956; Sokal and Rohlf 1995). To

Table 12 Femoral comparative sample of extant primates.

EXTANT PRIMATES FEMORA SAMPLE				
Taxon	**Males**	**Females**	**Unknown**	**N**
Gorilla beringei beringei	5	5		**10**
Gorilla beringei graueri	13	8		**21**
Gorilla gorilla gorilla	18	13		**31**
Pan paniscus	9	11		**20**
Pan troglodytes schweinfurthii	17	8		**25**
Pan troglodytes troglodytes	14	14		**28**
Pongo pygmaeus	5	4	3	**12**
Hylobates lar	13	13		**26**
Papionins[a]	31	11	11	**53**
Macaca fascicularis	15	15		**30**
Cercopithecus sp.	30	19		**49**
Chlorocebus sp.	8	6	2	**16**
Nasalis larvatus	13	12		**25**
Colobus sp.	15	13		**28**
Presbytis sp.	14	20		**34**
Atelids[b]	21	27	1	**49**
Cebus apella	20	13		**33**
			Total N	**490**

Abbreviation: N, sample size.

[a] Papionins include *Papio hamadryas* sspp., *Mandrillus sphinx*, *Mandrillus leucophaeus* and *Lophocebus* sp.

[b] Atelids include *Alouatta caraya*, *Alouatta seniculus*, *Alouatta fusca*, *Alouatta palliata*, *Alouatta seniculus*, *Ateles belzebuth*, *Ateles fusciceps*, *Ateles geoffroyi*, and *Ateles paniscus*.

facilitate comparisons, monkey genera were grouped into subfamily (cercopithecines and colobines) or family (atelids) groups in subsequent analyses after testing the absence of statistical differences between the included genera by means of ANOVAs ($p > 0.05$ in all instances). Thus, cercopithecines include *Papio*, *Mandrillus*, *Macaca*, *Cercopithecus*, *Lophocebus*, and *Chlorocebus*; colobines include *Nasalis*, *Colobus*, and *Presbytis*; and atelids include *Alouatta* and *Ateles*. Statistical analyses were performed using the statistical package *SPSS* v15.0.

COMPARISONS

The external morphology of the hominoid partial femora from ACM (IPS41724) and CLL2 (IPS18800), attributed respectively to cf. *Dryopithecus fontani* and *Hispanopithecus laietanus*, is notably different (Table 14; see also Figs. 25 and 26).

Femoral head relative size.- This variable is quantified by means of the SIH/SIN index. Results obtained clearly depart the most suspensory taxa (*Pongo* and *Hylobates*) from quadruped cercopithecoid species (Fig. 27a; Table 15). Platyrrhines (specially the suspensory atelids) and African apes show an intermediate position between the former two groups (Asian apes and cercopithecoids). Among these "intermediate" forms, *Cebus* and *G. b. beringei* display closer index values to cercopithecoids than the rest of taxa (Fig. 27a; Table 15). When compared with extant primates, the femur of cf. *D. fontani* clearly falls in the range of cercopithecoids, having the lowest index among fossil apes (Fig. 27a). Moreover, the femoral head is larger relative to the neck in IPS18800 than in IPS41724 (Fig. 27a; see also Almécija *et al.* 2013: fig. 6). The remaining Miocene apes display intermediate values between cf. *D. fontani* and *H. laietanus*. Thus, *Morotopithecus bishopi* (MUZM80) and *Proconsul major* (NAP IX'46'99) show low SIH/SIN indices. Contrarily, *Nacholapithecus kerioi* (KNM-BG35250A; although anteroposteriorly crushed, this specimen maintains the original shape for reliable measurements of the superoinferior length of both femoral head and neck), *Equatorius africanus* (BMNH M16331) and *Ekembo nyanzae* (KNM-MW13142A) have higher values than *M. bishopi* and *P. major*. The SIH/SIN values for all these fossil specimens mainly

Table 13 Measurements of the femur in the comparative sample of fossil primates. See Table 6 for measurement abbreviations. and units.

FOSSIL PRIMATE FEMORA						
Catalog No.	**Taxon**	**Element**	**SIH**	**SIN**	**MLPS**	**Measurements source**
NAP IX 46'99	*Proconsul major*	Femur	29.7	22.4		Gommery *et al.* 1998, 2002
KNM-MW 13142A	*Ekembo nyanzae*	Femur	28.5	20.1	23.6	Ruff *et al.* 1989, Ward *et al.* 1993
MUZM 80	*Morotopithecus bishopi*	Femur	25.9	20.1	23.4	Gebo *et al.* 1997, MacLatchy *et al.* 2000
MUZM 80	*Morotopithecus bishopi*	Femur	25.8		25.7	Gebo *et al.* 1997, MacLatchy *et al.* 2000
KNM-BG 35250A	*Nacholapithecus kerioi*	Femur	22.1	16.2		Ishida *et al.* 2004
BMNH M 16331	*Equatorius africanus*	Femur	22.5	16.4	20.5	McCrossin 1994a
BAR 1002'00	*Orrorin tugenensis*	Femur	32.1	22.5	25.5	Senut *et al.* 2001, Pickford *et al.* 2002

overlap the ranges of African apes (especially gorillas), platyrrhines (mainly *Cebus*) and the upper range of cercopithecoids, as it is also true for the early hominin *Orrorin tugenensis* (BAR1002'00). *Hispanopithecus laietanus* displays the highest SIH/SIN index of the fossil hominoids inspected, falling within the interquartile range of chimpanzees and atelids, and the lower ranges of Asian apes. Conversely, cf. *D. fontani* overlaps with the interquartile ranges of cercopithecines and colobines (Fig. 27a).

Femoral head shape.- Both cf. *D. fontani* and *H. laietanus* display a spherical femoral head that is similar to that of apes and atelids, against that of cercopithecoids, which exhibit a more hemispherical head. The articular surface in cf. *D. fontani* covers almost the entire head and is laterally expanded in the anterior side. This expansion results in a high femoral head depth (as measure by Ruff 2002), which is a typical trait of living great apes.

Femoral head position relative to the greater trochanter.- Moreover, the femoral head of *H. laietanus* projects more proximally than its greater trochanter; while in cf. *D. fontani* the greater trochanter projects slightly above the femoral head. The former condition is typical of the more suspensory taxa, such as *Pongo* and atelids to a lesser extent, whereas the condition of cf. *D. fontani* is more similar to that of African apes (more stricter quadrupeds, such as cercopithecoids, show a stronger proximal projection of the greater trochanter relative to the femoral head; Lovejoy *et al.* 2002; Harmon 2007).

Fovea capitis.- As most of primates (except orangutans), cf. *D. fontani* and *H. laietanus* display a well-marked *fovea capitis* (deeper in the latter) placed at the superoposterior quadrant of the head in medial view. Regarding the presence of the *fovea*, both taxa of the Vallès-Penedès resemble other Miocene apes and extant non-orangutan catarrhines. However, cf. *D. fontani* and *H. laietanus* femora depart from cercopithecoids in the *fovea* position on the head, since the latter group display the *fovea capitis* in a more inferior (and sometimes anterior) position (Jenkins and Camazine 1977; Ward *et al.* 1993).

Neck-shaft angle.- Differences in the femoral NSangle are depicted in Figure 27b (see also Figs. 25 and 26, and Tables 11 and 16). Three patterns are observed in extant catarrhines: cercopithecoids show the lowest NSangle values, orangutans the highest, and the group of African apes-gibbons-platyrrhines display intermediate values between the two former (cercopithecoids and orangutans; Fig. 27b). Nonetheless, ranges of intraspecific variability in living species are somewhat wide, especially those of monkeys. Thus, the ranges of cercopithecoids even overlap with that of gibbons, whereas platyrrhines overlap with those that show the most extreme values for the index, represented by cercopithecoids (the lowest) and orangutans (the highest). African apes display narrower ranges than the remaining taxa, although also overlap with cercopithecoids and orangutans (except in the case of lowland gorillas, which only overlap with anthropoid monkeys; Fig. 27b). For this variable, the femur of cf. *D. fontani* overlaps with the interquartile range of atelids, hylobatids, and African apes (except *Gorilla gorilla gorilla*). The femora of *H. laietanus* show the highest neck-shaft angle among fossil hominoids, mainly overlapping with orangutans and, to a lesser extent, gibbons, chimpanzees and platyrrhines. The left femur falls in the upper range of orangutans, showing a much higher NSangle value than the remaining fossil taxa,

Table 14 Main morphological differences and similarities between the femora of Vallès-Penedès great apes (see also Fig. 26). Only the right femur of *H. laietanus* is considered for morphological comparisons (see text for further explanation).

FEMORA COMPARISONS		
Head	**IPS18800 (*H. laietanus*)**	**IPS41724 (cf. *D. fontani*)**
Size (relative to the neck)	Very large	Small
Shape	Spherical	Spherical
Articular surface	Slight postereomedial extension onto the neck	Slight postereomedial extension onto the neck
Direction in proximal view	Anterior	Anterior
Fovea capitis	Deep, large and posteroproximally oriented	Modelartely developed and posteromedially oriented
Neck	**IPS18800**	**IPS41724**
Biomechanical neck length	Short	Long
Shape	Circular cross-section and proximodistally constricted	Elliptical cross-section and proximodistally long
Neck-shaft angle	Wide	Intermediate
Obturator externus groove	Absent	Absent
Greater trochanter	**IPS18800**	**IPS41724**
Position	Well inferior to the head	Slightly inferior to the head
Proportions	Long and wide	Short and narrow
Lateral flare	Strongly marked	Marked
Trochanteric fossa	Deep	Deep
Lesser trochanter	**IPS18800**	**IPS41724**
Size	Well developed and proximodistally long	Moderately developed and proximodistally long
Orientation	Posteromedial	Posterior
Intertrochanteric crest	Moderately developed	Moderately developed
Intertrochanteric line	Absent	Absent
Shaft	**IPS18800**	**IPS41724**
Cross-sectional geometry	Anteriorly convex and posteriorly flat	Anteroposteriorly flattened
Linea aspera	Absent	Absent
Gluteal tuberosity	Slightly developed, but with a well developed gluteal line	Well developed

including the right femur of the same individual. As previously mentioned, this might be due to either intra-individual asymmetries, intraspecific variability, or some distortion of the left femur associated with taphonomic processes. Although the two former possibilities remain unexplored (intra-individual asymmetries and intraspecific variability), the fact that the left femur has an apparently inflated head and a more proximally faced head-neck complex (Fig. 23) outcomes in a broad variability between the *H. laietanus* femora (Fig. 27b; see also Chapter 3 for side differential results on mechanical properties). Such morphological peculiarities on the left femur, not shown at the right specimen, make results for the right femur more representative *a priori*. Thus, the right femur of *H. laietanus* still displays an angle value that falls within the interquartile range of orangutans and which is higher than that displayed by the remaining fossil taxa. The latter are more comparable in this regard to hylobatids and chimpanzees (*N. kerioi*), and also to cercopithecoids and some gorillas (*M. bishopi*, *Or. tugenensis*, and KNM-MW13142A, *E. nyanzae*; Fig. 27b). The KNM-RU5527 femur (*E. nyanzae*) also shows a high angle, approaching the index value displayed by the right femur of *H. laietanus* and even overlapping with the lower range of orangutans.

The biomechanical neck length.- Modern humans show the longest BMNL relative to proximal femoral size (as approximated by its centroid size) among extant catarrhines (Fig. 28), . Nonetheless, its range clearly overlaps with the rest of taxa (especially *Callicebus*, *Aotus* and *Alouatta*). Chimpanzees, gorillas and macaques show the shortest relative BMNL, although their index ranges overlap with those

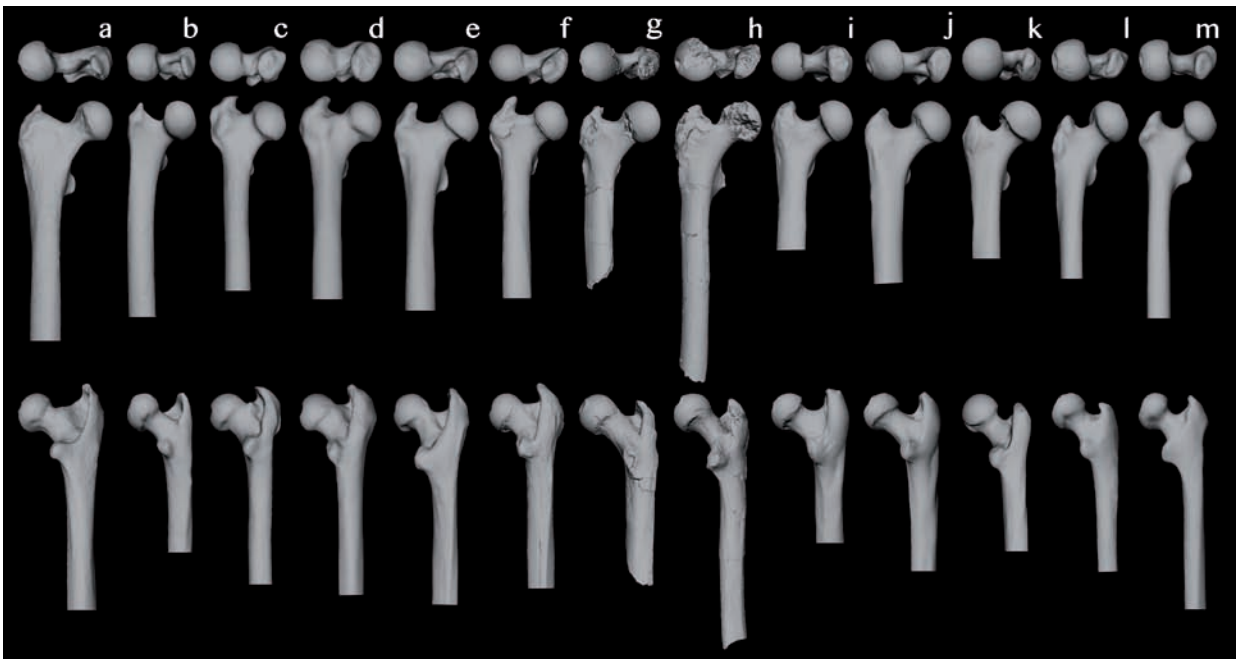

Figure 25 Digital renderings of 3D models of the proximal femora of Vallès-Penedès great apes compared with those of a selected extant primate sample: **a**, *Cebus apella*; **b**, *Ateles fusciceps*; **c**, *Colobus guereza*; **d**, *Nasalis larvatus*; **e**, *Macaca fascicularis*; **f**, *Papio anubis*; **g**, cf. *Dryopithecus fontani* (IPS41724); **h**, *Hispanopithecus laietanus* (IPS18800, right); **i**, *Gorilla gorilla*; **j**) *Pan troglodytes*; **k**, *Pongo pygmaeus*; **l**, *Symphalangus syndactylus*; **m**, *Hylobates lar*. For comparative purposes, all models are depicted as if from the right side and were scaled to the same femoral head superoinferior length. Only the proximal half of the femur is shown, in proximal (top), anterior (middle) and posterior (bottom) views.

of the other taxa (Fig. 28). The relative BMNL of cf. *D. fontani* is higher than that of *H. laietanus* (Fig. 28). Nonetheless, the relative BMNL of cf. *D. fontani* and *H. laietanus* is comparable to that of humans in both cases. Their relative BMNL values also overlap with non-*Ateles* platyrrhines and *Macaca*. In the case of *H. laietanus*, its relative BMNL is also comparable to that of *Mandrillus* and hylobatids. Similarly, *Eq. africanus* displays a value of relative BMNL intermediate between the two Vallès-Penedès hominoids, while *E. nyanzae* shows the highest value among middle Miocene apes. Both *Eq. africanus* and *E. nyanzae* also overlap with the range of values of modern humans and some platyrrhines (e.g., *Aotus* and *Alouatta*; Fig. 28). The latter shows the highest values among middle Miocene apes. Finally, *Or. tugenensis* displays an even higher relative BMNL than *E. nyanzae* and does not overlap with any of the living primates included in the sample.

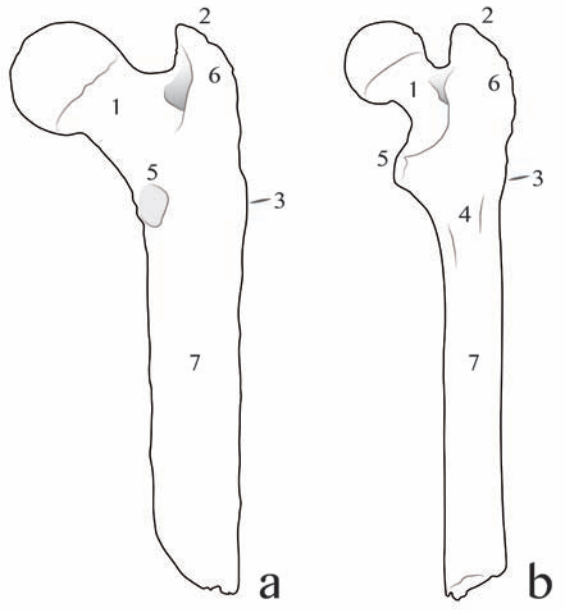

Figure 26 Schematic line drawing in posterior view of the femora of Vallès-Penedès great apes, illustrating their main morphological differences (see also Table 14): **a**, cf. *Dryopithecus fontani* (IPS41724); **b**, *Hispanopithecus laietanus* (IPS18800, right). Legend: 1, biomechanical neck length and neck-shaft angle; 2, position of the greater trochanter relative to the head; 3, gluteal tuberosity; 4, spiral and pectineal lines; 5, lesser trochanter; 6, insertions for the gluteal muscles; 7, diaphyseal cross-sectional geometry.

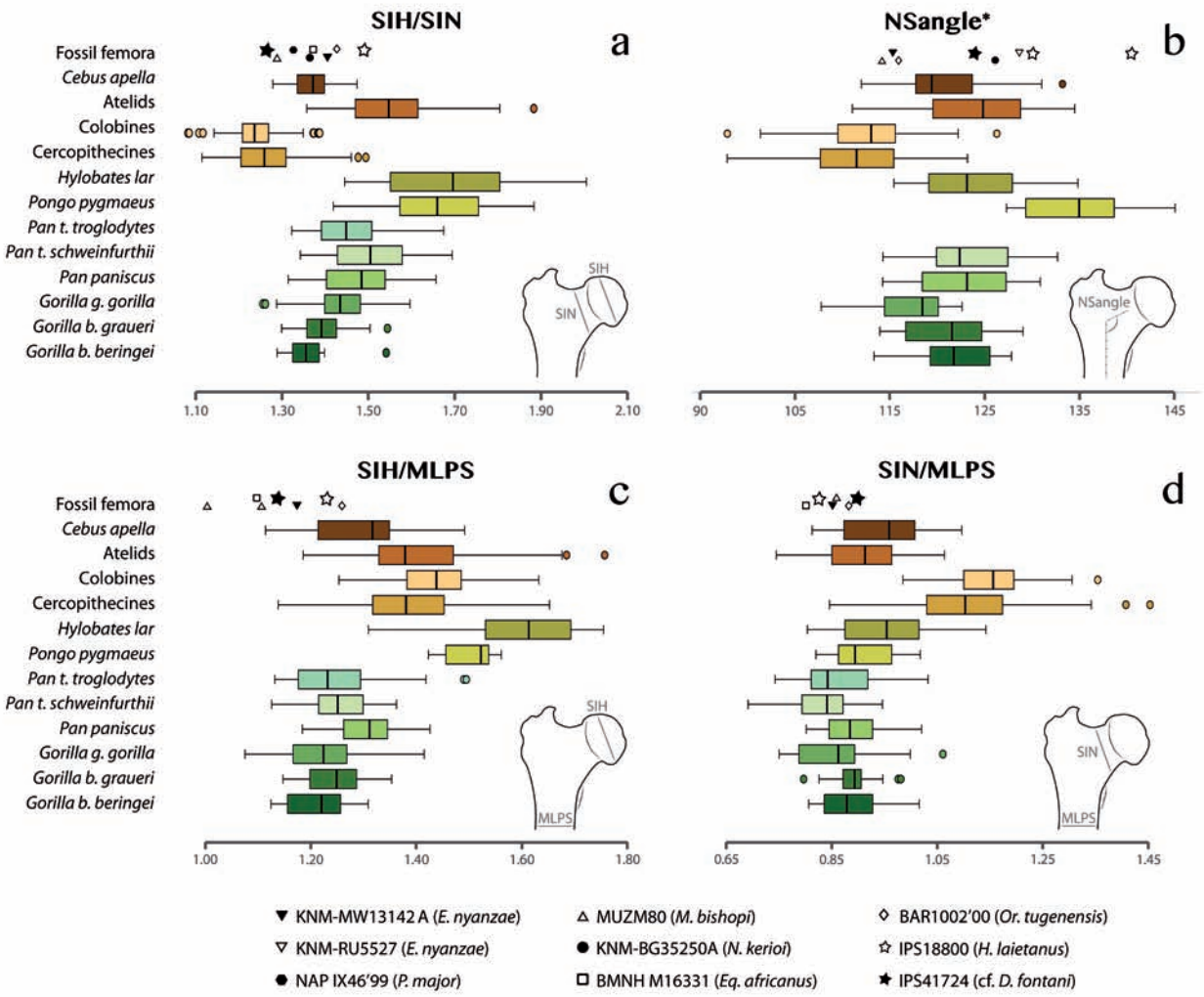

Figure 27 Boxplot showing variation in fossil hominoids compared to a sample of extant primates in **a**, the index of superoinferior femoral head length and the superoinferior femoral neck length (SIH/SIN); in **b**, femoral neck-shaft angle (NSangle, in degrees); **c**, superoinferior femoral head length (SIH) and **d**, superoinferior femoral neck length (SIN) relative to the mediolateral length of the proximal shaft (SIH/MLPS and SIN/MLPS, respectively) .Vertical lines represent the median, boxes the interquartile range (between the 25th and the 75th percentiles), whiskers the extreme values, and circles the outliers. No statistical differences among the genera of the following groups were found: cercopithecines (*Papio*, *Mandrillus*, *Macaca*, *Cercopithecus*, *Lophocebus*, and *Chlorocebus*), colobines (*Nasalis*, *Colobus*, and *Presbytis*), and atelids (*Alouatta* and *Ateles*). *, see the different sample size for NSangle in Table 11.

Proximal femur robusticity.- Figure 27c,d depicts the relationship between both SIH and SIN relative to MLPS, which is indicative of the robusticity of the proximal femoral epiphysis as compared to the proximal portion of the shaft (Napier 1964; Walker 1973). Relative to the femoral head (Fig. 27c), African apes show the highest relative robusticity (lowest values of the index), although their ranges overlap with *Cebus* values and also with cercopithecines in the case of bonobos (Table 15). Asian apes display the lowest relative robusticity of the proximal femur among extant catarrhines, whereas cercopithecoids and atelids exhibit an intermediate position between the orangutans-gibbons group and the African apes-*Cebus* group (Fig. 27c; Table 15). In the case of the Vallès-Penedès femora, cf. *D. fontani* shows a relatively higher proximal femur robusticity relative to the femoral head than *H. laietanus* (Fig. 27c). Concerning the rest of fossil femora, the left *M. bishopi* femur shows the lowest index value among Miocene taxa. Nonetheless,

POST HOC PAIRWISE COMPARISONS

	G. b. beringei	*G. b. graueri*	*G. g. gorilla*	*P. paniscus*	*P. t. schweinfurthii*	*P. troglodytes*	*Po. pygmaeus*	*H. lar*	Cercopithecines	Colobines	Atelids
SIH/SIN											
G. b. graueri	NS										
G. g. gorilla	NS	NS									
P. paniscus	*	NS	NS								
P. t. schweinfurthii	**	**	NS	NS							
P. troglodytes	NS	NS	NS	NS	NS						
Po. pygmaeus	**	**	**	**	**	**					
H. lar	**	**	**	**	**	**	NS				
Cercopithecines	*	**	**	**	**	**	**	**			
Colobines	**	**	**	**	**	**	**	**	NS		
Atelids	**	**	**	NS	NS	**	**	**	**	**	
C. apella	NS	NS	NS	**	**	**	**	**	**	**	**
SIH/MLPS											
G. b. graueri	NS										
G. g. gorilla	NS	NS									
P. paniscus	NS	NS	NS								
P. t. schweinfurthii	NS	NS	NS	NS							
P. troglodytes	NS	NS	NS	NS	NS						
Po. pygmaeus	**	**	**	**	**	**					
H. lar	**	**	**	**	**	**	NS				
Cercopithecines	**	**	**	*	**	**	**	**			
Colobines	**	**	**	**	**	**	NS	**	NS		
Atelines	**	**	**	**	**	**	NS	**	NS	NS	
C. apella	NS	NS	NS	NS	NS	NS	**	**	**	**	**
SIN/MLPS											
G. b. graueri	NS										
G. g. gorilla	NS	NS									
P. paniscus	NS	NS	NS								
P. t. schweinfurthii	NS	NS	NS	NS							
P. troglodytes	NS	NS	NS	NS	NS						
Po. pygmaeus	NS	NS	NS	NS	NS	NS					
H. lar	NS	NS	**	NS	**	**	NS				
Cercopithecines	**	**	**	**	**	**	**	**			
Colobines	**	**	**	**	**	**	**	**	**		
Atelines	NS	NS	NS	NS	*	NS	NS	NS	**	**	
C. apella	NS	NS	**	NS	**	*	NS	NS	**	**	NS

Table 15 Significance of post hoc pairwise comparisons (Tukey) for the size of the femoral head relative to the neck (SIH/SIN), and the proximal femur robusticity based on both the size of the head relative to the proximal shaft (SIH/MLPS) and the size of the neck relative to the proximal shaft (SIN/MLPS) among extant primates. *Abbreviations:* NS, not significant; *, $p<0.05$; **, $p<0.01$.

the value of the right femur is more similar to those of other Miocene apes, such as *Eq. africanus* and cf. *D. fontani*. Femoral robusticity related to the head in *H. laietanus* is close to that of *Or. tugenensis*, which displays the relatively larger femoral head within the fossil sample. Comparing with living taxa, cf. *D. fontani* falls within the lower values of the ranges of *Cebus* and African apes, in which the femoral head roughly equals the width of the proximal portion of the shaft. *Hispanopithecus laietanus* displays a lower proximal femoral robusticity regarding the head, clearly overlapping with the interquartile range of *Cebus* and African apes, but also with the lower ranges of cercopithecines and atelids.

Otherwise, when the robusticity of the proximal femur is measured related to the neck (SIN/MLPS; Fig. 27d), differences among extant taxa are less clear. Nonetheless, cercopithecoids depart from the rest of primates by showing larger femoral necks relative to the proximal portion of the shaft, that is, higher

POST HOC PAIRWISE COMPARISONS

	G. b. beringei	*G. b. graueri*	*G. g. gorilla*	*P. paniscus*	*P. troglodytes*	*Po. pygmaeus*	*H. lar*	Cercopithecines	Colobines	Atelids
Nsangle										
G. b. graueri	NS									
G. g. gorilla	NS	NS								
P. paniscus	NS	NS	*							
P. troglodytes	NS	NS	**	NS						
Po. pygmaeus	**	**	**	**	**					
H. lar	NS	NS	**	NS	NS	**				
Cercopithecines	**	**	**	**	**	**	**			
Colobines	**	**	*	**	**	**	**	NS		
Atelids	NS	NS	**	NS	NS	**	NS	**	**	
C. apella	NS	NS	NS	NS	NS	**	NS	**	**	NS

Table 16 Significance of post hoc pairwise comparisons (Tukey) for the size of the relative thickness of the femoral neck-shaft angle (NSangle) among extant primates. *Abbreviations:* NS, not significant; *, p<0.05; **, p<0.01.

relative robusticity of the proximal femur (Fig. 27d; Table 15). In this case, SIN/MLPS index ranges obtained for platyrrhines and apes are similar and highly overlap among them (Table 15). Contrary to the results obtained for the SIH/MLPS index, cf. *D. fontani* shows a higher value of SIN/MLPS (i.e., more robust proximal femur on the neck basis) than *H. laietanus* (Fig. 27d). Moreover, not great differences are shown among fossil apes for this index, showing cf. *D. fontani* the highest proximal femur robusticity relative to the neck and *Eq. africanus* the lowest. Overall, fossil femora overlap with the ranges of non-cercopithecoid taxa (Fig. 27d).

Importantly, due to the wide ranges displayed by extant primates for these two indices, and the small sample sizes available for fossil taxa, it is difficult to discern whether differences among cf. *D. fontani* and *H. laietanus* might have a clear functional meaning or might relate to a high intraspecific variation as shown in living catarrhines.

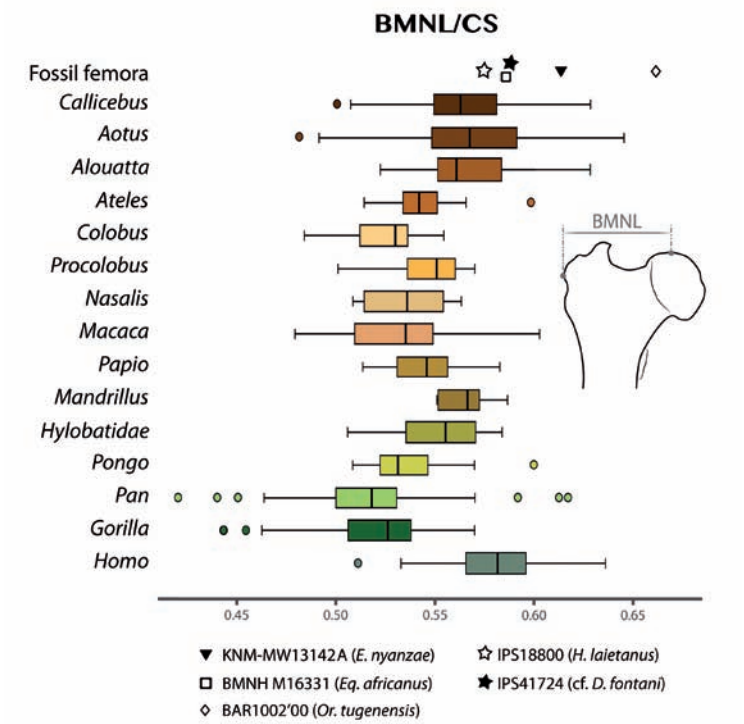

Figure 28 Boxplot showing variation in biomechanical neck length (BMNL) relative to the proximal femur size (represented by its centroid size, CS; see Almécija *et al.* 2013 for further explanation on calculation of CS). Vertical lines represent the median, boxes the interquartile range (between the 25th and the 75th percentiles), whiskers the extreme values, and circles the outliers. Modified from Almécija *et al.* (2013).

Greater trochanter.- The general shape of the greater trochanter in both cf. *D. fontani* and *H. laietanus*, being proximodistally short and anteroposteriorly wide, resembles that of hylobatids and platyrrhines more than that displayed by cercopithecoids (Fig. 25). The most proximal part of the greater trochanter, where the *piriformis* and *gluteus medius* muscles attach, faces laterally in *H. laietanus* (as in extant apes and platyrrhines) but more proximally in cf. *D. fontani* (as in cercopithecoids; Fig. 25). The lateral flare of the greater trochanter is more marked in *H. laietanus* (similar to the condition of atelids and gibbons) than in cf. *D. fontani* (similar to that in great apes, especially gorillas; Fig. 25). In fossil Miocene apes, the greater trochanter is in general similar to that of cercopithecoids (i.e., proximodistally long and anteroposteriorly wide; Fig. 25). Thus, the greater trochanters of both *Ekembo* spp. and *N. kerioi* display a morphology closer to that of quadrupeds, by displaying a larger proximal projection (even above the head in *Ekembo* spp.) and a more marked lateral flare than both cf. *D. fontani* and *H. laietanus*. The greater trochanter of *M. bishopi* and *P. major* is more similar to that of *H. laietanus*, with the most proximal part facing laterally (Fig. 25).

Gluteal tuberosity.- The gluteal tuberosity can be clearly observed on the lateral side of the proximal portion of the shaft in cf. *D. fontani*, as in other fossil apes and even early hominins (Lovejoy *et al.* 2002; Almécija *et al*. 2013). However, *H. laietanus* displays a less developed gluteal tuberosity that is represented by a gluteal ridge. This condition is similar to that of platyrrhines, but mainly gibbons (Fig. 25).

Diaphyseal cross-sectional geometry.- Cf. *D. fontani* and *H. laietanus* also show some differences concerning the cross-sectional geometry of the proximal shaft. The former displays an elliptical shape (mediolaterally expanded), whereas *H. laietanus* exhibits an almost circular geometry. The proximal shaft shape of cf. *Dryopithecus fontani* (APPS/MLPS = 0.76) resembles that of *Or. tugenensis* (APPS/MLPS = 0.73; Senut *et al.* 2001), and is slightly more anteroposteriorly flattened than in *E. nyanzae* (APPS/MLPS = 0.80; Ward *et al.* 1993) and *Eq. africanus* (APPS/MLPS = 0.81; McCrossin 1994a). *Hispanopithecus laietanus* clearly departs from this pattern (APPS/MLPS = 0.92). This taxon shows a similar condition of hylobatids and monkeys; whereas cf. *D. fontani* farther resembles the more mediolaterally-expanded pattern displayed by living great apes (Ward *et al.* 1993).

Chapter 2
Femoral neck cortical bone distribution

The femoral neck transmits body weight and supports the loadings coming from the muscles of the hip joint complex (e.g., Lovejoy *et al.* 1973; Ruff 1995, 1998). Depending on the type of locomotion, the loading patterns are different among primates and the organization of the internal structure of the femoral neck responds to these differences in locomotor demands (e.g., Rafferty 1998; Demes *et al.* 2000; Ruff 2002; Scherf 2008). In mechanical terms, quadrupeds and bipeds share an important compressive component that runs from the femoral head to the inferior edge of the femoral neck, and the tensile areas are situated in the superior part of the femoral neck and the greater trochanter (Fig. 29a; Lovejoy *et al.* 2002; Scherf 2008). These loads results in a distribution of the femoral neck cortical bone (FNCB) markedly thinner superiorly than inferiorly (Lovejoy 1988; Rafferty 1998; Demes *et al.* 2000). Moreover, humans exhibit a strong association of trabeculae, known as the arcuate system, that counteracts the compressive stresses (Frankel 1960; Scherf 2008). Contrarily, compression and tension are more uniformly distributed in the femoral neck of apes and this is reflected in similar thicknesses at the superior and inferior edges of the femoral neck (Fig. 29b; Lovejoy 1988; Lovejoy *et al.* 2002; Scherf 2008).

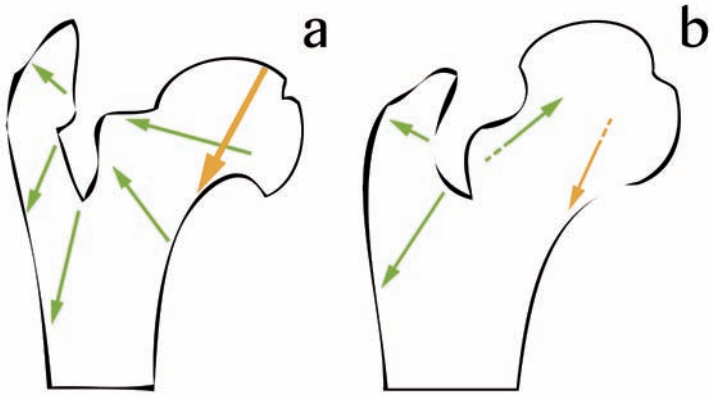

Figure 29 Midcoronal schematic section of the femur of **a**, a pronograde quadruped, and **b**, an orthograde suspensory primate. Main compressive (orange) and tensile (green) loads along the proximal femur are illustrated. The thicker arrow thickness in (a) represents the higher compressive component at the quadruped femur relative to the tensile component (stereotyped loading pattern). Contrary, the femur of the orthograde suspensory primate (b) displays the compressive and tensile components more evenly distributed (non-stereotyped loading pattern; see text for further explanations). Modified from Scherf (2008).

Therefore, the distribution of the FNCB is related to the main direction of the stresses experienced by the proximal portion of the femur (e.g., Aiello and Dean 1990; Rafferty 1998; Lovejoy *et al.* 2002; Pickford *et al.* 2002). In fact, this feature is also ecophenotypic (which includes influence by function and adaptive requirements as well) to some degree, as suggested by comparisons between wild and captive chimpanzees, and between young and adult chimpanzees (Matsumura *et al.* 2010a; Claxton 2015). As such, this feature has been related to specific locomotor adaptations in primates (e.g., Rafferty 1998; Demes *et al.* 2000) and is very promising for making paleobiological inferences on the

positional behaviour of fossil primates. Indeed, the FNCB distribution has been traditionally used for inferring bipedalism in early hominins (e.g., Lovejoy 1988, 2005; Ohman *et al.* 1997; Lovejoy *et al.* 2002; Galik *et al.* 2004; Ruff and Higgins 2013). However, the diagnostic value of this feature in fossil apes remains completely unexplored. Nonetheless, some authors have stressed that non-human hominoids display a more homogeneous distribution of cortical bone at the mid-point of the femoral neck than humans and most monkeys (except *Ateles* and *Alouatta*; Ohman *et al.* 1997; Rafferty 1998). This fact presumably reflects the less stereotyped loading patterns at the hip joint of apes and atelids (Ohman *et al.* 1997; Raffery 1998; Ruff and Higgins 2013). Hence, FNCB thickness appears more useful for distinguishing taxa with some suspensory and/or vertical-climbing component within their locomotor repertoire than for specifically distinguishing bipeds, since the latter largely overlap with the more generalized quadrupedal taxa. Recently, Ruff and Higgins (2013) demonstrated that differences on FNCB distribution among living hominoids at the base of the femoral neck were even greater than at the midneck. Unfortunately, the sample analysed in their study did not incorporate non-hominoid primates, thus limiting the possibility of further inspecting the potential similarities between bipedalism and quadrupedalism biomechanical requirements at both femoral neck locations. To build in the pioneering work of Ruff and Higgins, in this chapter, the FNCB distribution at the mid- and base-of-neck sections of the partial femora of the Vallès-Penedès great apes is compared to the available sample provided by these and other authors (see below) to provide insights into the loading patterns at the hip joint on these fossil taxa .

COMPARATIVE SAMPLE, MEASUREMENTS AND METHODS

The taxonomic composition of the extant primate comparative sample employed in this chapter is reported in Table 17. Superior (SUP) and inferior (INF) cortical thicknesses mean values for these taxa (see Table 17), with separate sexes in the case of anthropoids, were taken from the literature (Rafferty 1998; Demes *et al.* 2000; Matsumura *et al.* 2010a,b) or computed from unpublished individual measurements kindly provided by O. Lovejoy. Mean values of body mass (BM), employed to evaluate size-related

Table 17 [*next page*] Mean sex/species values of midneck superior cortical thickness (SUP, in mm), inferior cortical thickness (INF, in mm) and body mass (BM, in kg), as well as SUP/INF ratios, allometric residuals of SUP *vs* INF (RES) and allometric residuals of SUP *vs* BM (RESBM), in extant primates and Vallès-Penedès great apes (in bold type). In the case of fossil taxa, both the estimated BM and its confidence intervals (see Moyà-Solà *et al.* 2009a) were employed to compute RESBM (confidence interval values reported within parentheses). Residuals were computed on the basis of non-hominoid regressions reported in Table 19. Locomotor subgroups employed in ANOVA comparisons (Table 20) are also reported. *, tentative (see text for further explanation). *Abbreviations:* N, sample size used to derive the mean values; M, male; F, female; LG, locomotor groups; VCL, vertical clinging and leaping; Q, generalized quadrupedism; SC, slow quadrumanous climbing; SUS, arboreal locomotion with significant suspensory component; KW, orthograde semi-terrestrial locomotion, combining knuckle-walking with vertical climbing and suspension to some degree; BIP, terrestrial bipedalism. Letters after taxon names indicate the sources for the SUP, INF and BM mean data: a, Smith and Jungers (1997); b, Rafferty (1998); c, Lovejoy (pers. comm.); d, Matsumura *et al.* (2010a); e, BM estimate from Moyà-Solà *et al.* (2009a), SUP and INF measured in this work.

EXTANT PRIMATE SAMPLE									
Taxon	**N**	**SEX**	**LG**	**BM**	**SUP**	**INF**	**SUP/INF**	**RES**	**RESBM**
Indri indri [a]	15	M/F	VCL	6.33	0.95	1.74	0.55	0.15	0.36
Propithecus diadema [a]	10	M/F	VCL	6.10	1.09	1.61	0.68	0.37	0.51
Propithecus verreauxi [a]	14	M/F	VCL	6.10	0.57	1.22	0.47	0.00	-0.14
Avahi laniger [a]	11	M/F	VCL	1.17	0.58	0.93	0.62	0.29	0.37
Lepilemur leucopus [a]	18	M/F	VCL	0.60	0.45	0.87	0.52	0.11	0.31
Hapalemur griseus [a]	3	M/F	VCL	0.83	0.37	0.86	0.43	-0.08	0.02
Lemur catta [a]	19	M/F	Q	2.21	0.55	1.09	0.50	0.08	0.13
Eulemur fulvus [a]	10	M/F	Q	2.20	0.49	0.97	0.51	0.08	0.01
Varecia variegata [a]	11	M/F	Q	3.53	0.59	1.19	0.50	0.06	0.06
Cheirogaelus major [a]	1	M/F	Q	0.40	0.32	0.65	0.49	0.06	0.09
Cheirogaelus medius [a]	4	M/F	Q	0.23	0.15	0.47	0.32	-0.37	-0.50
Microcebus murinus [a]	7	M/F	Q	0.09	0.11	0.37	0.30	-0.44	-0.53
Mirza coquereli [a]	1	M/F	Q	0.32	0.26	0.67	0.39	-0.18	-0.05
Phaner furcifer [a]	1	M/F	Q	0.46	0.33	0.62	0.53	0.14	0.08
Daubentonia madagascariensis [a]	2	M/F	Q	2.55	0.49	1.44	0.34	-0.32	-0.03
Galago moholi [a]	5	M/F	VCL	0.18	0.19	0.40	0.48	0.03	-0.19
Galago senegalensis [a]	6	M/F	VCL	0.25	0.26	0.43	0.60	0.27	0.02
Otolemus crassicaudatus [a]	3	M/F	Q	1.15	0.28	0.73	0.38	-0.19	-0.36
Euoticus elegantulus [a]	17	M/F	VCL	0.28	0.35	0.66	0.53	0.13	0.29
Galago alleni [a]	2	M/F	VCL	0.27	0.34	0.57	0.60	0.25	0.27
Galago demidovii [a]	5	M/F	Q	0.06	0.24	0.36	0.67	0.37	0.37
Nycticebus coucang [a]	8	M/F	SC	0.86	0.27	0.88	0.31	-0.42	-0.31
Loris tardigradus [a]	7	M/F	SC	0.23	0.31	0.56	0.55	0.18	0.22
Perodicticus potto [a]	1	M/F	SC	1.04	0.35	1.00	0.35	-0.29	-0.10
Ateles fusciceps [b]	4	M	SUS	8.30	1.28	1.40	0.91	0.67	0.58
Ateles fusciceps [b]	5	F	SUS	9.10	1.30	1.52	0.86	0.60	0.57
Ateles paniscus [b]	3	M/F	SUS	9.00	1.30	1.90	0.68	0.37	0.57
Alouatta seniculus [b]	7	M	SUS	7.50	1.10	1.74	0.63	0.30	0.46
Alouatta seniculus [b]	7	F	SUS	5.80	0.74	1.43	0.52	0.10	0.14
Macaca fascicularis [b]	10	M	Q	4.90	0.47	1.35	0.35	-0.30	-0.27
Macaca fascicularis [b]	9	F	Q	3.30	0.47	1.03	0.46	-0.02	-0.15
Macaca nemestrina [b]	5	M/F	Q	6.90	0.55	1.24	0.44	-0.05	-0.21
Papio/Mandrillus [b]	4	M	Q	27.30	0.90	2.30	0.39	-0.19	-0.13
Lophocebus albigena [b]	5	M	Q	9.00	0.70	1.86	0.38	-0.22	-0.05
Lophocebus albigena [b]	5	F	Q	6.40	0.42	1.52	0.28	-0.53	-0.46
Colobus guereza [b]	8	M	Q	9.30	0.88	1.83	0.48	0.02	0.17
Colobus guereza [b]	9	F	Q	7.90	0.62	1.58	0.39	-0.18	-0.13
Trachypithecus cristatus [b]	5	M	Q	7.00	0.48	1.40	0.34	-0.31	-0.35
Trachypithecus cristatus [b]	5	F	Q	5.80	0.42	0.96	0.44	-0.06	-0.43
Presbytis rubicunda [b]	5	M	Q	6.10	0.40	1.04	0.38	-0.19	-0.49
Presbytis rubicunda [b]	5	F	Q	6.10	0.56	1.26	0.44	-0.05	-0.16
Nasalis larvatus [b]	5	M	Q	21.10	0.66	1.60	0.41	-0.13	-0.36
Nasalis larvatus [b]	5	F	Q	10.50	0.66	1.58	0.42	-0.12	-0.15
Hylobates lar [b]	5	M	SUS	5.90	0.82	1.50	0.55	0.15	0.23
Hylobates lar [b]	5	F	SUS	5.40	0.86	1.30	0.66	0.35	0.31
Hylobates syndactylus [b]	3	M	SUS	11.30	1.23	1.37	0.90	0.65	0.45
Hylobates syndactylus [b]	4	F	SUS	11.30	0.90	1.40	0.64	0.32	0.13
Pongo pygmaeus [b]	9	M	SUS	36.10	2.71	2.74	0.99	0.74	0.89
Pongo pygmaeus [b]	11	F	SUS	81.30	2.14	2.47	0.87	0.61	0.41
Gorilla gorilla [a,c]	5	M	KW	169.37	5.19	6.21	0.84	0.56	1.08
Gorilla gorilla [a,c]	5	F	KW	80.00	4.49	4.93	0.91	0.65	1.16
Pan paniscus [a,c]	9	M/F	KW	39.10	2.13	2.61	0.82	0.55	0.62
Pan troglodytes [b,d]	16	M	KW	46.40	2.10	2.61	0.80	0.53	0.56
Pan troglodytes [b,d]	16	F	KW	37.15	2.20	2.75	0.80	0.53	0.67
Homo sapiens [b]	5	M	BIP	57.60	1.67	3.31	0.50	0.06	0.27
Homo sapiens [b]	5	F	BIP	52.80	1.12	3.88	0.29	-0.50	-0.11
cf. *Dryopithecus fontani* [e]	**1**	**M**	**--**	**44.4 (40.1-49.5)**	**2.40***	**5.42**	**0.44**	**-0.07**	**0.71 (0.68-0.74)**
Hispanopithecus laietanus [e]	**1**	**M**	**--**	**38.6 (34.3-43.1)**	**2.51**	**2.46**	**1.02**	**0.77**	**0.79 (0.83-0.76)**

scaling effects, were also taken from the literature (Smith and Jungers 1997; Rafferty 1998; Demes *et al.* 2000). To carry out statistical comparisons, sex-means of extant primates were grouped into locomotor groups based on the most frequent locomotor mode performed during travelling (see Table 17 for further details; Hunt 2004, 2016; Fleagle 2013). In addition, for both the mid- and base-of-neck sections, the SUP/INF ratio obtained for the Vallès-Penedès great apes were also compared with a more specific sample of extant hominoids (data from Ruff and Higgins 2013).

The partial femur IPS41724 (cf. *Dryopithecus fontani*) and the right femur of the IPS18800 partial skeleton (*Hispanopithecus laietanus*) are included in the analyses of this chapter. The left specimen of the latter taxon is damaged at the femoral neck and, consequently, the FNCB cannot be inspected.

A BM estimate of 44.4 kg and 38.6 kg, computed from femoral head measurements, was taken from the literature for IPS41724 and IPS18800, respectively (Moyà-Solà *et al.* 2009a: table 7). Statistical analyses relying on BM were repeated for these fossils using the 50% confidence interval for their predicted BM (IPS41724 = 40.1-49.5 kg, and IPS18800 = 34.3-43.1 kg; Moyà-Solà *et al.* 2009a) to test that results were not an artefact of uncertainties in body size estimation.

Computed tomography scans and cortical thicknesses measurements

FNCB thicknesses in the Vallès-Penedès hominoids were computed using high-resolution computed tomography (CT). IPS18800 was scanned using an Yxlon Compact CT-scanner at the Universidad de Burgos (Spain), whereas IPS41724 was scanned several times at different locations with different CT-devices (see further explanation below). Applied CT-settings and parameters obtained for each CT-scan are listed in Table 18. CT-scans were processed using the software *VSG-Avizo* v 7.0.

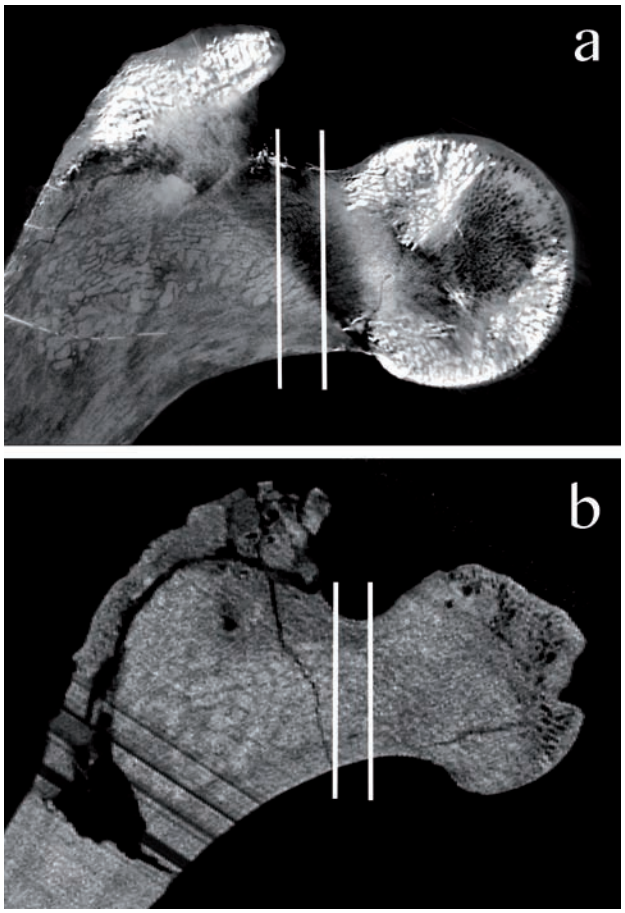

Figure 30 Midcoronal computed tomography section showing the location of the base-of-neck (left vertical white line) and midneck (right vertical white line) slices used for measuring the cortical bone thicknesses at the superior and inferior cortices in **a**, IPS41724 (cf. *Dryopithecus fontani*), and **b**, IPS18800 (*Hispanopithecus laietanus*).

Two slices were selected at the femoral neck in the two fossil taxa, orthogonally to its main neck axis (sagittal plane), following Ruff and Higgins (2013). One of the sections was placed at the base of the neck, just medial to the intertrochanteric line, and the other in the mid-point of the femoral

Table 18 Computed tomography (CT) settings and parameters obtained from scanning the fossil femora of the Vallès-Penedès.

CT-SETTINGS								
Specimen	**Institution**	**CT-scanner model**	**CT-scanner type**	**No. slices**	**Pixel size (mm)**	**Interslice (mm)**	**Voltage (kV)**	**Current (mA)**
IPS18800, right	UBU	YXLON Compact	Industrial-CT	1612	0.04	0.30	180	3.20
IPS41724 (scan 1)	UBU	YXLON Compact	Industrial-CT	546	0.04	0.30	200	3.20
IPS41724 (scan 2)	AMNH	GE phoenix v | tome | x s240	Micro-CT	1600	0.07	0.07	185	1.80
IPS41724 (scan 3)	ICTP	Elettra	Micro-CT	4800	0.03	0.03	150	2.00
IPS41724 (scan 4)	ICP	YXLON Y.TU450.D09	Industrial-CT	451*	0.27	0.20	300	2.30

*, Only the most proximal part of this specimen was scanned at the ICP, removing part of the diaphysis and also the femoral head (see text for further explanation). *Abbreviations:* UBU, Universidad de Burgos (Spain); AMNH, American Museum of Natural History (USA); ICTP, 'Abdus Salam' International Centre for Theoretical Physics (Italy); ICP, Institut Català de Paleontologia Miquel Crusafont (Spain).

neck between the base-of-neck section and the most lateral edge of the femoral head (Fig. 30). Slices were imported into *Fiji* 1.50e (Schindelin *et al.* 2012) to threshold them using different densities. This process was made with the help of the image histogram, which allowed distinguishing changes in the grey scale of densities by means of changes in the Hounsfield units (Hounsfield 1973, 1976; Ohman *et al.* 1997). Subsequently, thicknesses of the SUP and INF cortices were measured (in mm) along the greatest superoinferior height of the femoral neck (following Ruff and Higgins 2013).

Statistical analyses

The relationship between SUP and INF, considered to be functionally related to positional behaviour (see above; e.g., Rafferty 1998), can be measured by a simple dimensionless shape index, computed as the SUP/INF ratio. However, in order to make reliable paleobiological inferences on positional behaviour, it is essential to ensure that differences between the various taxa are not merely attributable to size-related effects (i.e., allometry). Hence, allometric techniques were used as a criterion of subtraction for the midneck section (see reviews in Gould 1966; Klingenberg 1998) and complement the results provided by the shape ratios. Mean values for the various taxa were therefore log-transformed (by means of natural logarithms, ln), and analysed through both ordinary least-squares (OLS) and reduced major axis (RMA) regression methods. Although the use of OLS in allometry has been discouraged by some authors (Hofman 1988; Martin and Barbour 1989; Aiello 1992), this method is only clearly favoured when the primary interest of the study is the slope of the best-fit line (Smith 1994; Warton *et al.* 2006). The use of OLS can be appropriate when making predictions or computing residuals (Smith 1994, 2009).

Regressions were computed for the whole primate sample (including humans), as well as for apes (non-human hominoids) separately from strepsirrhines and anthropoid monkeys, since apes stood out as outliers compared to the rest of primates. Fossil taxa were excluded from the computation of the allometric regressions. Allometric residuals of SUP *vs* INF (RES) were computed as metrics of intrinsic relative cortical thickness, whereas allometric residuals of SUP *vs* BM (RESBM) were employed as metrics of superior cortical thickness relative to body size. Given that apes are outliers compared to most other primates, in order to compute the allometric residuals, the non-hominoid regression is used as the baseline.

Size-scaling effects concerning the SUP/INF index were further evaluated by investigating the allometric relationship between this index and BM. The existence of scaling differences and allometric grade shifts (elevation differences) between apes and non-hominoid primates were evaluated by using analysis of covariance (ANCOVA). First, the equality of slopes was tested between the various groups, and when no statistical differences were found, equality of intercepts was then checked (elevation; e.g., McDonald 2008). The significance of differences in mean values for indices and residuals between extant locomotor subgroups was tested by means of analysis of variance (ANOVA) and post hoc pairwise comparisons (Bonferroni method). Given the fact that a single specimen is available for fossil taxa, comparisons with extant subgroups mainly relied on boxplots, 95% confidence intervals (CI) for the mean, and maximum-minimum ranges. Statistical computations were made by using *SPSS* v 15.0.

RESULT S

Femoral neck cortical thicknesses of the Vallès-Penedès great apes

IPS18800 (*Hispanopithecus laietanus*) has a homogeneous distribution of cortical thickness around the femoral neck, displaying very similar values for both midneck (SUP = 2.934 mm and INF = 2.725 mm) and base-of-neck sections (SUP = 3.960 mm and INF = 3.158 mm), so that the SUP/INF ratio is close to 1 in all instances (1.077 and 1.254, respectively; Table 17; Fig. 31). In the case of IPS41724 (cf. *Dryopithecus fontani*), however, exploring its FNCB distribution is tougher due to the strong mineralization found at its femoral head and its greater trochanter (Fig. 32), which results in low quality CT-images with extremely bright areas (which is known as "bulb effect"). Moreover, the interaction of these two bright points creates an area of shadow just in the superior half of the femoral neck, where SUP should be measured (Fig. 32). To obtain reliable measurements of this variable in IPS41724, this fossil was scanned several times. This approach allowed obtain increasing resolution, although the definition of the cortical bone boundaries were still relatively low (see Table 18). In a final instance, the partial femur was scanned after

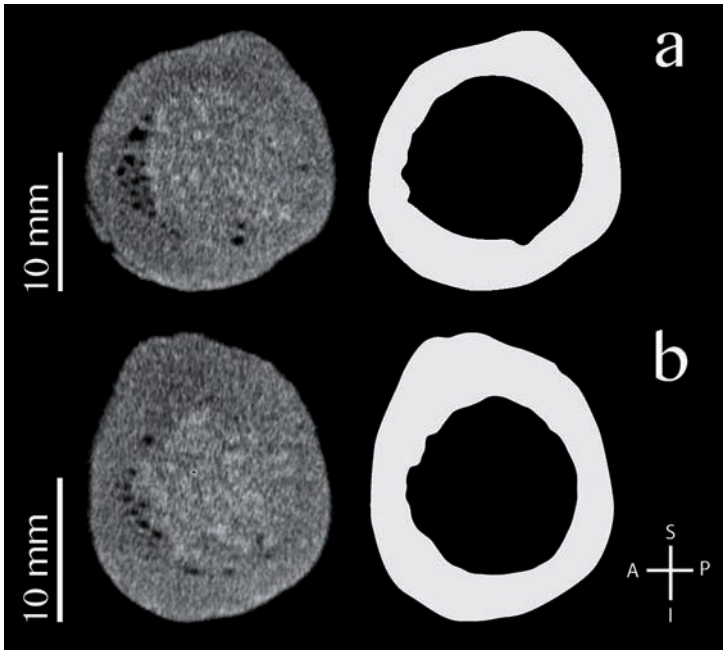

Figure 31 Original sagittal computed tomography sections (left) and isolated cortical bone cortices (right) at **a**, the midneck and **b**, the base of the neck of IPS18800 (*Hispanopithecus laietanus*). S, superior; P, posterior; I, inferior; A, anterior.

physically removing one of the focuses of brightness, the femoral head, along a natural break situated around the base of its head. Moreover, the most distal part of the preserved shaft was also removed by separating it through another natural break (just below the lesser trochanter; Fig. 21). CT-images acquired from this scan had less resolution, but slightly better cortical bone boundaries definition (Fig. 33). Therefore, cortical bone thicknesses of IPS41724 were measured combining the images of the four CT-scans (Fig. 34). Thus, the inferior cortical thickness was reliably measured in any of the performed CT-scans at both midneck (INF = 5.422 mm) and the base of the neck (INF = 4.836 mm). Likewise, it can be observed that inferior thickness progressively decreases towards the anterior and posterior edges, becoming thinner superiorly. Then, cf. *D. fontani* clearly displays an asymmetric FNCB distribution with more elliptical cross-section geometry than in *H. laietanus* (Fig. 34). Although absolute values for IPS41724 SUP cortices are tentative due to the low quality of the CT-images, a superior cortical thickness of 2.40 mm for the midneck section and 2.16 mm for the base-of-neck section were estimated. Hence, such exploratory measurements result in SUP/INF indices of around 0.4 (even if measurements are taken at the most superior part of the posterior edge, where the boundary of the cortical bone is still clear in both sections; Fig. 34).

Figure 32 X-rays image of the IPS41724 (cf. *Dryopithecus fontani*) partial femur. Black arrowheads point the densest (black) regions found at the femoral head and greater trochanter of the femur. These regions are associated with high mineralization that results in extremely bright (white) areas in the final computed tomography images (see Figure 33).

Relative femoral neck cortical thickness

The obtained results show that the relationship between ln SUP and ln INF is statistically significant ($p<0.001$, $r = 0.920$) among extant primates, which is slightly positively allometric, irrespective of the regression technique applied (Fig. 35a; Table 19). However, when allometric regressions are computed separately for apes and non-hominoid primates (strepsirrhines + anthropoid monkeys), an isometric relationship cannot be discounted for either of these groups (Table 19), based on both OLS and RMA confidence intervals for the slope. This suggests that the slope slightly above 1 for primates as a whole might stem from allometric grade shifts between primate subgroups. These allometric grade shifts are further suggested by a visual inspection of Figure 35a, with apes displaying a trend towards a relatively

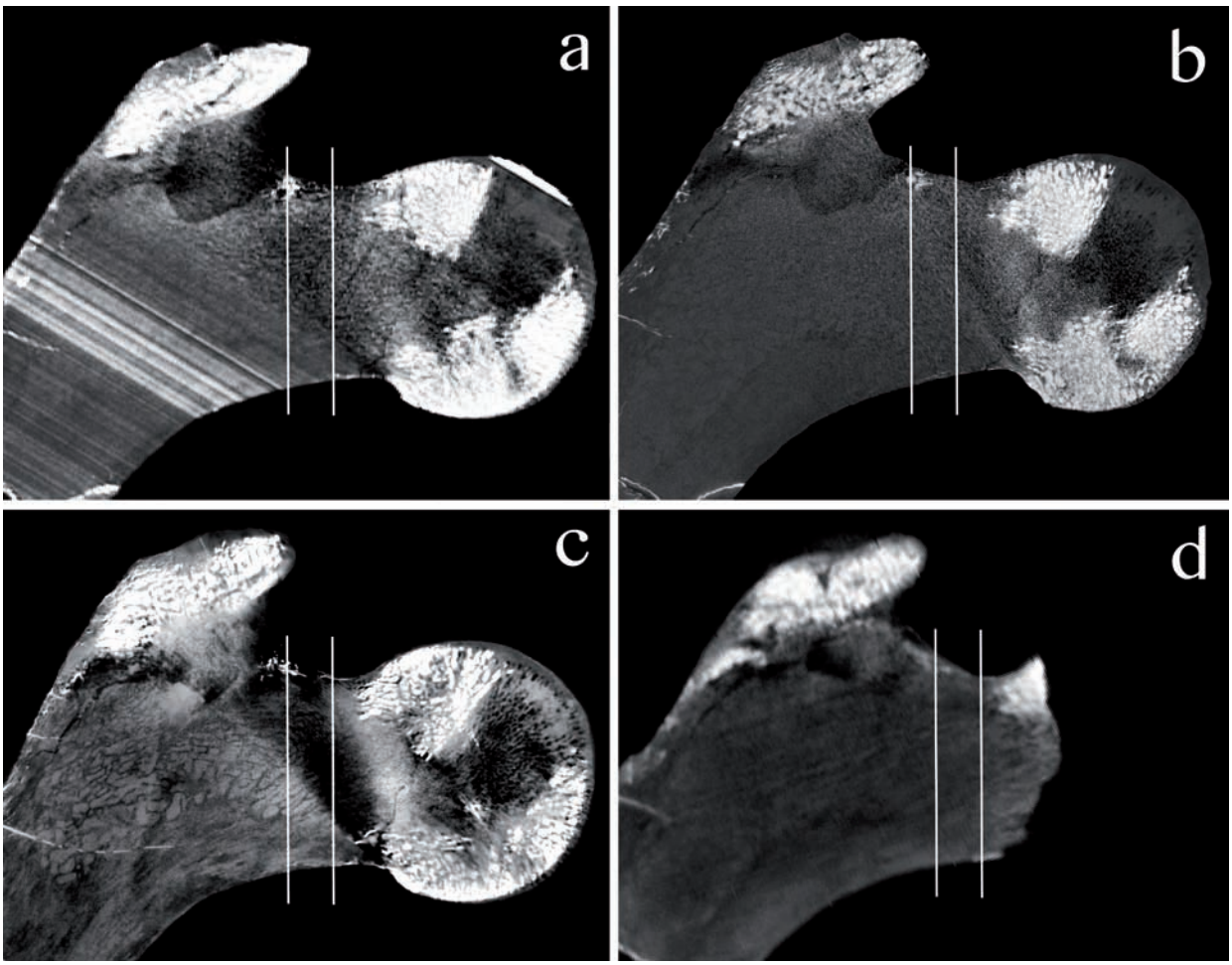

Figure 33 Midcoronal computed tomography (CT) sections of the IPS41724 (cf. *Dryopithecus fontani*) proximal femur obtained at **a**, the industrial CT-scanner of the Universidad de Burgos (Spain); **b**, the microCT-scanner of the American Museum of Natural History (USA); **c**, the microCT-scanner of the 'Abdus Salam' International Centre for Theoretical Physics (Italy); and **d**, Institut Català de Paleontologia Miquel Crusafont (Spain). See Table 18 for the CT-settings applied in every scan. As remarked in Figure 32, the densest areas observed in the IPS41724 femur result in bright regions (white) that in this specimen are mainly located at the femoral head and the greater trochanter. Interaction of the electrons reflected from these areas results in a region of shadow that crosses from the inferior most medial part of the femoral neck to its superior edge. Hence, in sagittal CT-images (see Figure 34), the final resolution of the most superior part of the neck is low (see text for further explanation).

Vertical white lines point the location of the selected slices for this study: midneck (left) and base of the neck (right).

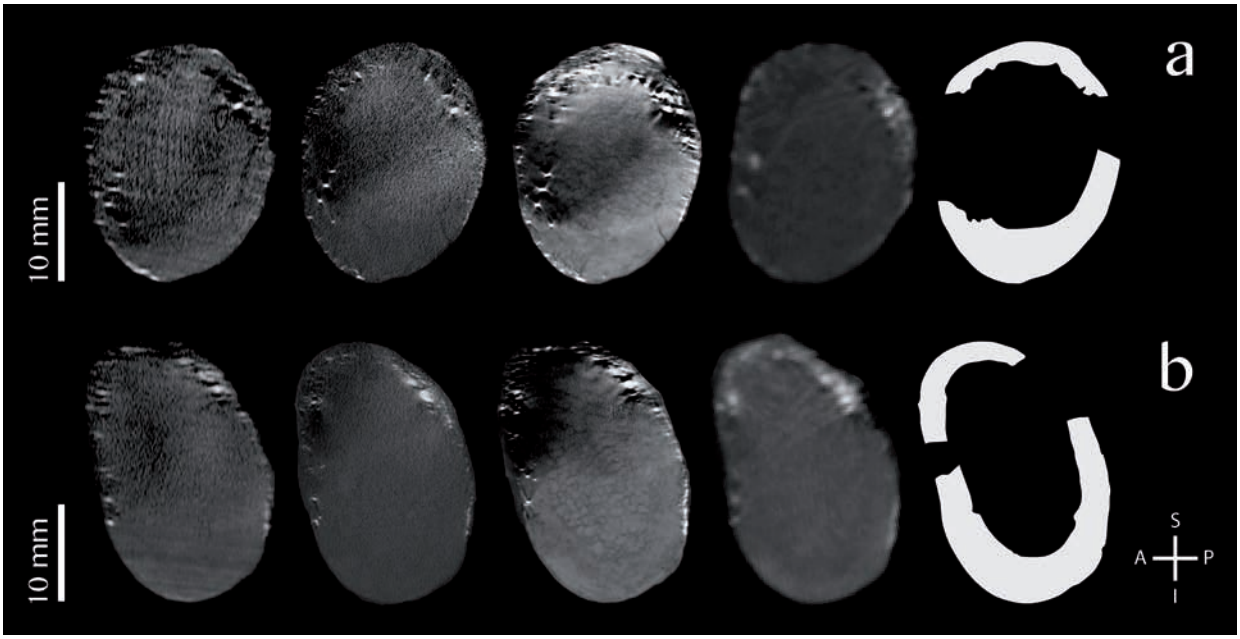

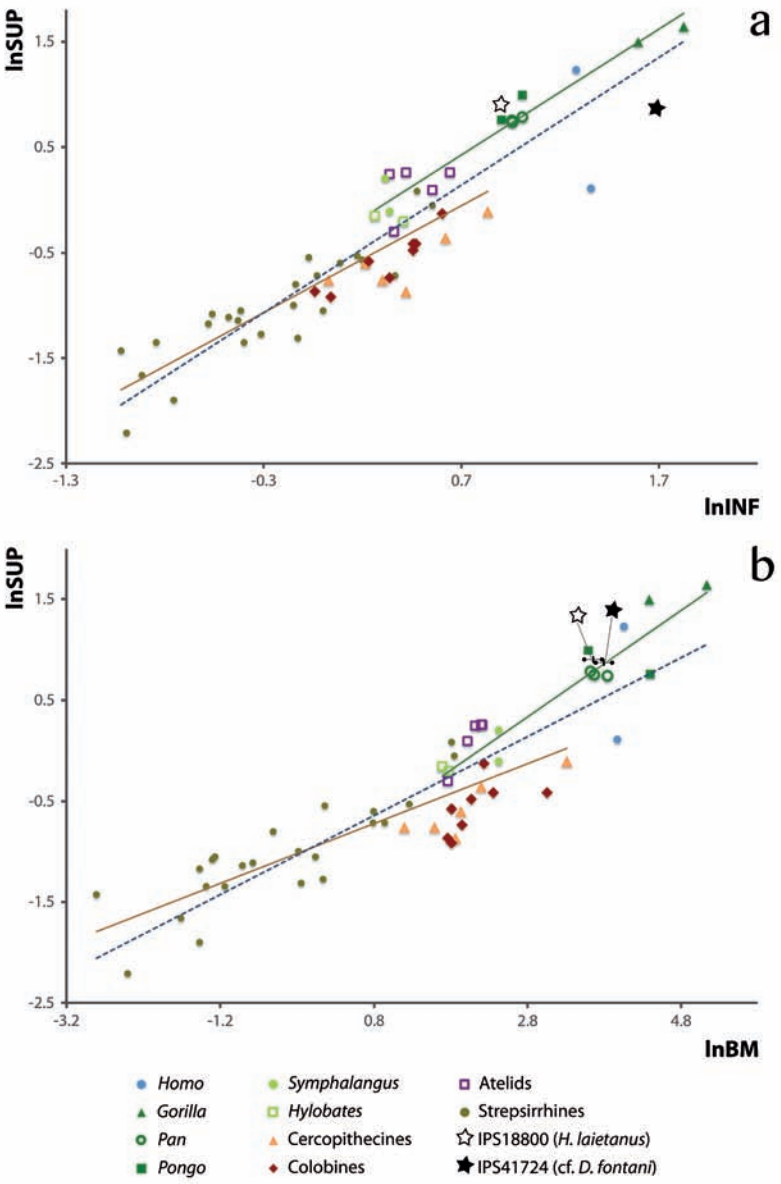

Figure 35 Bivariate allometric (least squares) plots depicting intrinsic proportions of femoral neck cortical thickness and proportions of superior cortical thickness relative to body size, in extant primates and the Vallès-Penedès great apes. **a**, Superior (SUP) *vs* inferior (INF) cortical thickness; **b**, SUP *vs* body mass (BM). Dark blue dashed line corresponds to all extant primates; given that apes appear as outliers compared to other primates, separate regressions were also computed for apes (non-human hominoids; green continuous line) and non-hominoid primates (strepsirrhines and monkeys; continuous brown line). The points depicted correspond to sex/species means reported in Table 17. In **b**, cf. *Dryopithecus fontani* and *Hispanopithecus laietanus* are represented by three points (estimated BM, black line, and its 50% confidence intervals, black closed points; Moyà-Solà *et al.* 2009a). See allometric regression coefficients in Table 19.

thicker SUP compared to INF than non-hominoid primates, once size-scaling effects are taken into account. This relationship is confirmed by ANCOVA results: whereas the slope between these primate subgroups (reported in Table 19) is not statistically different ($F = 0.079$, $p = 0.924$), the elevation of the regression lines shows significant differences ($F = 68.355$; $p<0.001$). When SUP (Fig. 35b) and INF are regressed separately against BM (Table 19), both independent variables show a similar allometric regression relative to body size among extant primates. When geometric scaling is taken into account, the confidence interval

Figure 34 [*previous page*] Original sagittal computed tomography (CT) sections (four left) and isolated cortical bone cortices (right) at **a**, the midneck and **b**, the base of the neck of IPS41724 (cf. *Dryopithecus fontani*). CT-sections were extracted from scanners performed at (left to right) the Universidad de Burgos (Spain), the American Museum of Natural History (USA), the 'Abdus Salam' International Centre for Theoretical Physics (Italy), and the Institut Català de Paleontologia Miquel Crusafont (Spain). S, superior; P, posterior; I, inferior; A, anterior.

Table 19 Allometric regression equations derived for intrinsic proportions and proportions relative to body mass of the femoral neck cortical thickness in extant primates. Regressions were derived using the least-square method (OLS), but reduced major axis (RMA) slopes also reported within parentheses.

ALLOMETRIC REGRESSION EQUATIONS										
ln SUP vs. ln INF										
Taxa	**N**	**r**	**SEE**	**p**	**Slope**	**95% CI**		**Intercept**	**95% CI**	
Extant primates	56	0.920	0.32	p<0.001	1.180 (1.312)	1.042 (1.164)	1.317 (1.463)	-0.71	-0.80	-0.62
Strepsirrhines+monkeys	43	0.878	0.27	p<0.001	1.013 (1.153)	0.839 (0.959)	1.187 (1.351)	-0.76	-0.85	-0.68
Apes	11	0.973	0.15	p<0.001	1.193 (1.225)	0.981 (0.924)	1.404 (1.422)	-0.41	-0.62	-0.20
ln SUP vs. ln BM										
Taxa	**N**	**r**	**SEE**	**p**	**Slope**	**95% CI**		**Intercept**	**95% CI**	
Extant primates	56	0.894	0.362	p<0.001	0.382 (0.438)	0.329 (0.383)	0.434 (0.495)	-0.955	-1.075	-0.835
Strepsirrhines+monkeys	43	0.831	0.319	p<0.001	0.297 (0.357)	0.234 (0.288)	0.360 (0.424)	-0.959	-1.067	-0.85
Apes	11	0.943	0.223	p<0.001	0.529 (0.561)	0.387 (0.434)	0.670 (0.677)	-1.143	-1.642	-0.645
ln INF vs. ln BM										
Taxa	**N**	**r**	**SEE**	**p**	**Slope**	**95% CI**		**Intercept**	**95% CI**	
Extant primates	56	0.961	0.174	p<0.001	0.320 (0.334)	0.295 (0.307)	0.345 (0.363)	-0.203	-0.261	-0.146
Strepsirrhines+monkeys	43	0.953	0.151	p<0.001	0.295 (0.310)	0.265 (0.285)	0.325 (0.335)	-0.195	-0.246	-0.143
Apes	11	0.921	0.213	p<0.001	0.421 (0.458)	0.287 (0.328)	0.556 (0.607)	-0.544	-1.019	-0.069
ln (SUP/INF) vs. ln BM										
Taxa	**N**	**r**	**SEE**	**p**	**Slope**	**95% CI**		**Intercept**	**95% CI**	
Extant primates	56	0.348	0.316	p<0.05	0.062 (0.183)	0.016 (0.147)	0.107 (0.213)	-0.752	-0.856	-0.647
Strepsirrhines+monkeys	43	0.01	0.274	0.947	0.002 (0.171)	-0.052 (0.120)	0.056 (0.538)	-0.764	-0.857	-0.671
Apes	11	0.688	0.135	p<0.05	0.107 (0.156)	0.022 (0.081)	0.192 (0.230)	-0.599	-0.9	-0.299

Abbreviations: N, sample size; r, correlation coefficient; SEE, standard error of estimate; p, significance, CI, confidence interval.

for the slope does not permit to exclude isometric scaling (i.e., based on an allometric expectation of 1/3) regarding the relationship of INF *vs* BM. In the case of SUP *vs* BM, the RMA slope for all primates is slightly higher than 1/3, apparently resulting from the positively allometric relationship displayed by apes, since the remaining primates show an isometric relationship in this regard. These allometric relationships, coupled with the isometry observed between SUP and INF (when allometric grade shifts are taken into account), explains why there is not a significant relationship between the SUP/INF ratio and BM among non-hominoid (Table 19).

Overall, the results reported above suggest that the SUP/INF ratio is a reliable (size-unrelated) metric for assessing the distribution of cortical thickness in the femoral neck. Not surprisingly, hence, when the various primate locomotor groups are compared, the results are very similar irrespective of whether indices or intrinsic residuals are employed (Fig. 36a,b; Table 20). Specialized suspensory taxa (atelids, hylobatids and orangutans) and knuckle-walking taxa (African apes; which frequently incorporate suspension and vertical climbing mainly during feeding behaviours) display on average a slightly thicker superior cortical thickness relative to the inferior one, whereas bipedal taxa (i.e., humans) display just the opposite condition (although with a substantial overlap with generalized quadrupedal and slow-climbing taxa), with the superior thickness notably thinner than the inferior cortical cortex. ANOVA results confirm that there are significant differences between the several groups, regarding both indices

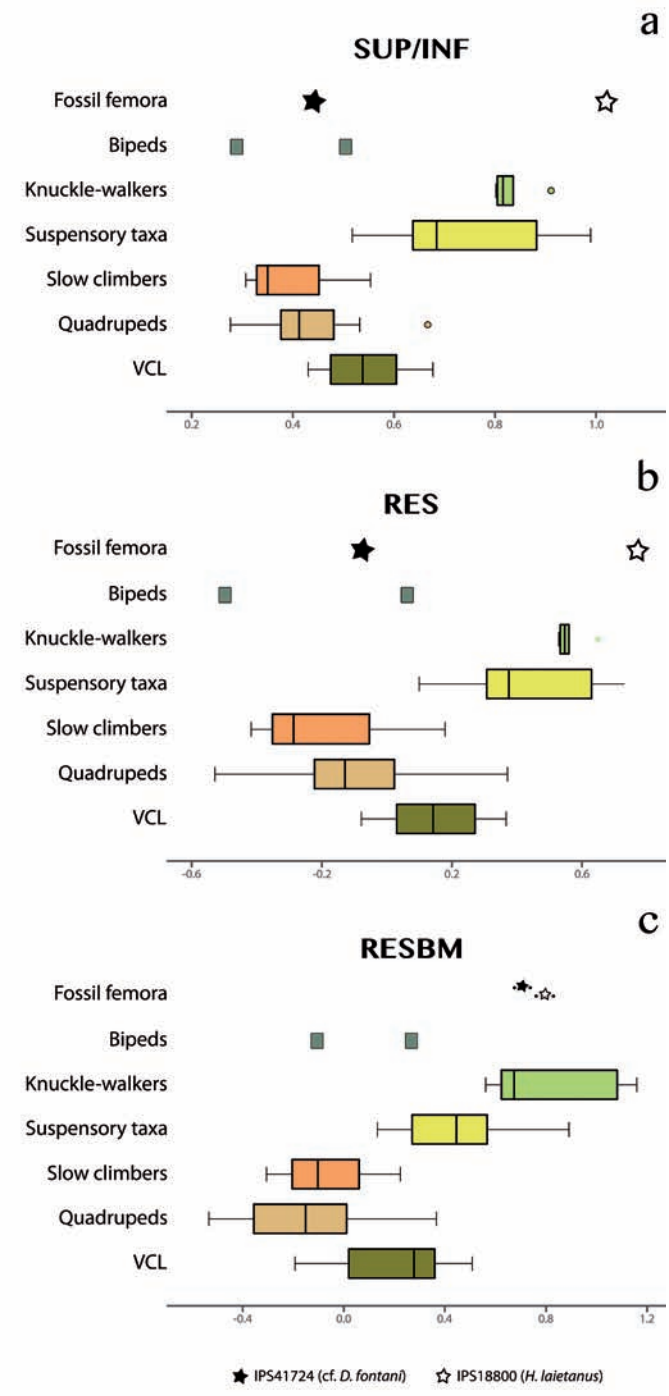

Figure 36 Boxplots comparing proportions of femoral neck cortical thickness in extant non-human primates (grouped according the locomotor groups reported in Table 17), humans (male and female means) and the Vallès-Penedès great apes. **a**, Indices between superior and inferior cortical thickness (SUP/INF). **b**, Allometric residuals of SUP *vs* INF. (RES). **c**, Allometric residuals of SUP *vs* BM (RESBM), in the case of IPS41724 (cf. *Dryopithecus fontani*) and IPS18800 (*Hispanopithecus laietanus*) depicting the ±50% uncertainty range of BM estimates (black circles). These boxplots are based on species means (with separate sexes for anthropoids), reported in Table 17 (see also descriptive statistics for ratios and residuals in Table 20). Vertical lines represent the median, boxes the interquartile range (between the 25th and the 75th percentiles), whiskers the extreme values, circles the outliers and asterisks the extreme outliers. VCL, vertical clingers and leapers.

(F= 24.238, p<0.001) and residuals (F = 20.205, p<0.001). Post hoc comparisons further show that knuckle-walking and specialized suspensory taxa significantly differ from the remaining locomotor groups at least at p<0.05 (p<0.001 in most instances), by displaying relatively thicker superior cortical cortex (Table 21). Irrespective of the metric employed, differences between knuckle-walking and suspensory taxa are not significant, although in all instances knuckle-walkers are on the upper range of specialized suspensory taxa (Fig. 36), by tending to display a relatively thicker superior thickness relative to the inferior one (see values for each genus in Table 17). *Hispanopithecus laietanus* (RES = 0.771, SUP/INF = 1.020) shows an even more extreme condition than both specialized suspensory (mean RES = 0.441, mean SUP/INF = 0.746) and knuckle-walking (mean RES = 0.563, mean SUP/INF = 0.834) taxa (Tables 17 and

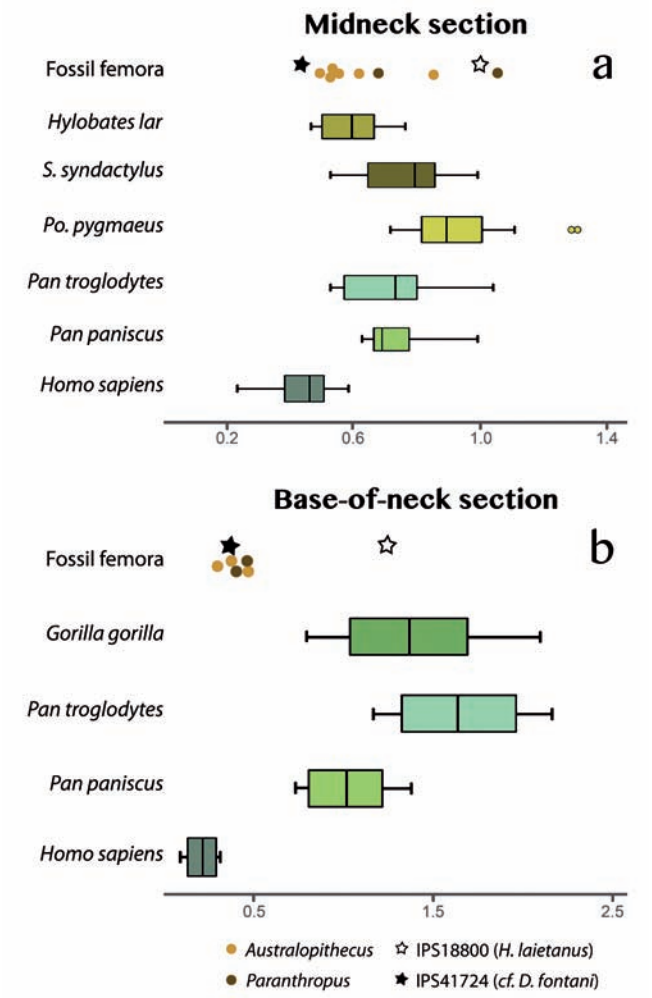

Figure 37 Boxplots comparing proportions of femoral neck cortical thickness in a selected sample of hominoids and the Vallès-Penedès great apes (data from Ruff and Higgins 2013). Indices between superior and inferior cortical thickness (SUP/INF) at **a**, the midneck, and **b**, the base of the neck. Vertical lines represent the median, boxes the interquartile range (between the 25th and the 75th percentiles), whiskers the extreme values, and green circles the outliers.

20). Contrarily, results for cf. *D. fontani* (RES = -0.074, SUP/INF = 0.443) fall in the range of generalized quadrupeds, also overlapping with bipeds (mean RES = -0.219) for cortical thickness proportions, and with slow-climbers for the SUP/INF index (mean SUP/INF = 0.403; Tables 17 and 20). Similar results are obtained for proportions relative to body size (Fig. 36c; Table 17), with significant differences among the several groups ($F = 19.209$, $p<0.001$), mostly between knuckle-walkers and specialized suspensory taxa on the one hand, and the remaining locomotor groups on the other, at $p<0.001$ (Table 21). Bipeds occupy a more intermediate condition (Fig. 36c), showing significant differences compared to knuckle-walkers ($p<0.05$) but not to specialized suspensory taxa. *Hispanopithecus laietanus* (RESBM = 0.950) and cf. *D. fontani* (RESBM = 0.708) most closely resembles knuckle-walkers (mean RESBM = 0.820), but the former further falls within the range of suspensory taxa (mean RESBM = 0.430; Table 20). Uncertainties in BM estimation of fossil specimen do not affect such conclusions.

Additionally, when FNCB distribution is also inspected at the midneck and the base of the neck for a more specific sample of extant apes and early hominins (SUP/INF ratio; Fig. 37), previous results for cf. *D. fontani* and *H. laietanus* are corroborated. The SUP/INF ratio of *H. laietanus* at the midneck overlaps with those of orangutans and chimpanzees, and with the uppermost ranges of bonobos and siamangs (Fig.

Table 20 Descriptive statistics for the several metrics of proportions of femoral neck cortical thickness employed in this work (see Table 17). Due to the uncertainties of body size estimation for cf. *D. fontani* and *H. laietanus*, RESBM for minimum and maximum body mass are given within parentheses.

DESCRIPTIVE STATISTICS							
SUP/INF							
Locomotor group	**N**	**Mean**	**SD**	**95% CI**		**Range**	
Bipedalism	2	0.395	0.148	-0.939	1.729	0.290	0.500
Knuckle-walking	5	0.834	0.046	0.777	0.891	0.800	0.910
Suspension	11	0.746	0.163	0.637	0.856	0.520	0.990
Quadrupedalism	25	0.421	0.086	0.386	0.457	0.280	0.670
Slow-climbing	3	0.403	0.129	0.084	0.723	0.310	0.550
Vertical-clingers-and-leapers	10	0.548	0.077	0.493	0.603	0.430	0.680
cf. *Dryopithecus fontani*	**1**	**0.443**					
Hispanopithecus laietanus	**1**	**1.020**					
RES							
Locomotor group	**N**	**Mean**	**SD**	**95% CI**		**Range**	
Bipedalism	2	-0.219	0.398	-3.791	3.352	-0.501	0.062
Knuckle-walking	5	0.563	0.049	0.502	0.624	0.528	0.649
Suspension	11	0.441	0.221	0.293	0.590	0.099	0.739
Quadrupedalism	25	-0.122	0.200	-0.204	-0.039	-0.529	0.371
Slow-climbing	3	-0.175	0.313	-0.954	0.604	-0.417	0.179
Vertical-clingers-and-leapers	10	0.152	0.143	0.050	0.255	-0.079	0.367
cf. *Dryopithecus fontani*	**1**	**-0.074**					
Hispanopithecus laietanus	**1**	**0.771**					
RESBM							
Locomotor group	**N**	**Mean**	**SD**	**95% CI**		**Range**	
Bipedalism	2	0.078	0.266	-2.315	2.472	-0.110	0.267
Knuckle-walking	5	0.820	0.279	0.474	1.166	0.561	1.160
Suspension	11	0.430	0.224	0.279	0.580	0.133	0.891
Quadrupedalism	25	-0.157	0.239	-0.256	-0.059	-0.534	0.367
Slow-climbing	3	-0.062	0.267	-0.725	0.602	-0.306	0.224
Vertical-clingers-and-leapers	10	0.181	0.237	0.012	0.350	-0.193	0.508
cf. *Dryopithecus fontani*	**1**	**0.708 (0.676-0.738)**					
Hispanopithecus laietanus	**1**	**0.794 (0.829-0.762)**					

Abbreviations: N, sample size; SD, standard deviation; CI, confidence interval.

37a). Conversely, cf. *D. fontani* ratio falls in the range of modern humans and behind the apes and early hominins. At the base of the neck section, differences between these two taxa are even greater (Fig. 37b), since *H. laietanus'* ratio clearly overlaps with the ranges of African apes, whereas the ratio of cf. *D. fontani* is close to the upper range of modern humans and similar to the values of early hominins.

POST HOC PAIRWISE COMPARISONS	VLC	Quadrupeds	Slow-climbers	Suspensory taxa	Knuckle-walkers
SUP/INF					
Quadrupeds	*				
Slow-climbers	NS	NS			
Suspensory taxa	**	**	**		
Knuckle-walkers	**	**	**	NS	
Bipeds	NS	NS	NS	**	**
RES					
Quadrupeds	**				
Slow-climbers	NS	NS			
Suspensory taxa	*	**	**		
Knuckle-walkers	**	**	**	NS	
Bipeds	NS	NS	NS	**	**
RESBM					
Quadrupeds	**				
Slow-climbers	NS	NS			
Suspensory taxa	NS	**	*		
Knuckle-walkers	**	**	**	NS	
Bipeds	NS	NS	NS	NS	**

Table 21 Significance of Bonferroni post hoc pairwise comparisons among locomotor groups of extant primates for the superior cortical thickness relative to the inferior cortices (SUP/INF), allometric residuals of SUP *vs* INF (RES), and allometric residuals of SUP *vs* body mass (RESBM). *Abbreviations:* NS, not significant; *, $p<0.05$; **, $p<0.01$.

Chapter 3
Cross-sectional structural properties of the shaft

As transmitters of body weight and muscle loadings (mainly bending and torsional loads) during active movement and support, mechanical properties of the hindlimb long bone diaphyses have constituted a good proxy for locomotor behaviour differentiation among living primates (Schaffler *et al.* 1985; Ruff 2002). Although further research is still needed in order to accurately relate bone structure and loading patterns, several authors have demonstrated that long bones show some degree of developmental and mechanical loadings plasticity (e.g., Ruff 1988; Trinkaus *et al.* 1994). Therefore, depending on the different mechanical and loading environments consequence of limb specialization (e.g., in load magnitude, frequency or variability), previous authors have stated that the dynamic relationship between bones and their structure tend to minimize bending and torsional stresses in primate long bones, economizing the amount of material used (Schaffler *et al.* 1985; Demes *et al.* 2001; Carlson 2005). Thus, the internal architecture of long bones seem to reflect, at least in part, the loading patterns supported during life and, consequently, the study of the mechanical properties of these bones become essential for a fully understanding of their functionality (Lovejoy *et al.* 1976). The mechanical differences on primate long bones (i.e., bone tissue distribution and orientation) can be inspected by the analysis of their cross-sectional geometry properties when they are consider under the engineering beam theory (e.g. Lovejoy *et al.* 1976; Burr *et al.* 1981; Ruff and Hayes 1983; Demes *et al.* 1991; Ruff and Runestad 1992; Ruff *et al.* 1999, 2015; Ruff 2002; Carlson 2005; Yamanaka *et al.* 2005). Therefore primates, depending on their primary (most frequent) positional behaviour, exhibit different mechanical parameters (strength and rigidity), such as cortical area (CA), second moments of area (I), section moduli (Z) and polar moments of area (J), when diaphyseal sections are analysed (Schaffler *et al.* 1985; Daegling 2002; Ruff 2002). CA measures resistance to axial compressive loads and is proportional to tensile strength, that is, the higher the CA the larger the capability to resist proximodistally-stereotyped loads of the bone (Burr *et al.* 1981; Ruff 1987; Hill and Durband 2014). I quantifies the maximum (Imax), minimum (Imin), anteroposterior (Ix), and mediolateral (Iy) beam strength and rigidity under bending loadings (Ruff and Hayes 1983; Hill and Durband 2014). I is defined by both the cross-section and the squared distance of each unit area from the neutral axis of the section in the plane of the bending load. Thus, the principal axes of a section define the directions of greatest and least bending rigidity (Ruff and Hayes 1983). Z is proportional to bending strength of the diaphysis and is used in calculating the maximum stress occurring in the outermost fiber of the cross section in the plane of bending (Ruff and Hayes 1983; Ruff 1995, 2002; Heinrich and Biknevicius

1998; Jungers *et al.* 1998; Ruff *et al.* 1999). Finally, J measures the torsional rigidity of the diaphysis and is used as an index of average bending strength (Ruff 1987; Daegling 2002; Shaw and Ryan 2012; Hill and Durband 2014). It is important take into account at this point that rigidity measures the internal resistance of a structure to an external applied mechanical loading; whereas strength measures the maximum stress (force/unit area) sustained by a structure prior to failure (Reilly and Burstein 1974; Ruff and Hayes 1983). Therefore, I, Z and J reflect the distribution of bone area about the cross-section centroid and, hence, these structural parameters are indicative of bone "shape" (in biomechanical regards) and stress directionality preferences through the bone. Thus, in general, I, Z and J derived from long bones diaphyseal cross-sections tend to be in accordance with the loading regimes suffered by the bones, which are ultimately determined by the positional repertoire of the species and the way the body weight is transmitted (Ruff and Hayes 1983; Demes *et al.* 1991; Heinrich and Biknevicius 1998).

Therefore, taxa performing forelimb-dominated suspensory behaviours show lower strength and bending peaks at the hindlimb, whereas those primates that usually rely on quadrupedalism tend to show higher loadings and strength at these bones (Ruff and Runestad 1992; Ruff *et al.* 1999; Ruff 2002). For example, within cercopithecoids, the more arboreal colobines display lower bending stress and axial loads than the more terrestrial cercopithecines (which overall show stronger bones) due to the higher compliance of branches and trees compared to the ground (Jungers *et al.* 1998).

Thus, the disparity of loading regimes derived from differential substrate and limbs use in extant primates is reflected in somehow in their geometrical properties of the hindlimb long bones, thus allowing previous authors to make locomotor inferences on extinct primate species, including fossil hominins (e.g., Ruff *et al.* 1999, 2015; Puymerail *et al.* 2012; Ruff 2002; Hill and Durban 2014). Thus, this chapter focuses on exploring the structural diaphyseal properties of the partial femora of the Vallès-Penedès attributed to the Miocene great apes cf. *Dryopithecus fontani* and *Hispanopithecus laietanus*. The goal of this chapter is thus giving a novel and broader biomechanical viewpoint to the study of the positional behaviour of these fossil taxa.

COMPARATIVE SAMPLE, MEASUREMENTS AND METHODS

Femoral shaft structural properties of the Vallès-Penedès great apes are compared with the sample of extant catarrhines used by Ruff (2002: table 1; data available at the website http://www.hopkinsmedicine.org/fae/cbr.htm). Additionally, a sample of modern humans kindly provided by C. Ruff has been also included in the sample of living primates (Table 22).

Moreover, the fossil sample included in this chapter consists of the partial proximal femur IPS41724 (cf. *Dryopithecus fontani*), and both femora of the partial skeleton IPS18800 (*Hispanopithecus laietanus*). Moreover, structural properties of KNM-MW13142A (*Ekembo nyanzae*) and MUZM80 (*Morotopithecus*

bishopi) were taken from Ruff (2002) and included in the analyses in order to compare these Miocene primates with those of the Vallès-Penedès Basin.

Total femoral length estimation

Total femoral length (TFL) is necessary to locate the cross-sections of interest through percentages of bone *length'* (length parallel to the longitudinal axis from the average distal projection of the condyles to the superior surface of the neck at its deepest point; Ruff 2002). Thus, TFL of the Vallès-Penedès femora was estimated through the superoinferior diameter of the femoral head (FHSI) using the allometric regression published by Köhler *et al.* (2002: table 3, equation 1), which is based on a sample of extant anthropoids.

Diaphyseal cross-sections location

Following Ruff (2002), length' in fossil femora was estimated by subtracting the length of the greater trochanter proximal projection from the TFL. Then, the 50% and 80% cross-sections used for the biomechanical analyses (measured from the distal end) were located at the 50% and 20% percentages of bone length from the most-proximal point of the femoral length', respectively. Although location of the selected cross-sections in fragmentary fossils could not be entirely accurate because of their incomplete nature, some authors have already demonstrated that the inaccuracy in the femoral midshaft location does not affect significantly the cross-sectional parameters (tested for cortical area, CA; polar moments of area, J; and biomechanical "shape", Imax/Imin, in a sample of human, chimpanzee and gorilla femora; Sládek *et al.* 2010; Mongle *et al.* 2015). Thus, no significant differences in the values of these three structural parameters have been found between 35% and 65% of bone length' (see specific variations for bones/taxa in Mongle *et al.* 2015). Following our estimation of cf. *D. fontani* TFL, location of its midshaft point would span from around 47.3%-52.7% of bone length' and that of *H. laietanus* from 47.1%-52.9% of bone length'. This variation is in all cases within the ranges of error estimated for the different structural parameters by Mongle *et al.* (2015). Furthermore, in the case that TFL cannot be estimated, the cross-section at 80% of bone length' could be selected 10 mm below the lesser trochanter, throwing similar results for cross-sectional geometry properties than sections with more accurate location along the bone length' (Ruff and Hayes 1983; Ruff *et al.* 1999). Thus, despite the fragmentary nature

EXTANT PRIMATE SAMPLE

Taxon	N
Homo	**100**
Gorilla	**20**
Pan	**23**
Pongo	**20**
Symphalangus	**8**
Hylobates	**10**
Papio	**20**
Macaca	**29**
Nasalis	**11**
Colobus	**18**
Trachypithecus	**10**
Presbytis	**10**
Total N	**279**

Table 22 Comparative sample of extant primates. Data for modern humans was kindly provided by Christopher B. Ruff. N, sample size.

of the Vallès-Penedès hominoid femora, diaphyseal cross-sectional properties can be reliably estimated for these fossil taxa.

Computed tomography and cross-section mechanical parameters

In order to obtain the structural parameters of the femoral shafts at 50% and 80% percentages of bone length', IPS41724 and IPS18800 (left and right) were scanned by high-resolution X-ray computed tomography (CT) techniques. The IPS41724 CT-scan used in this chapter was that performed at the microCT-scanner of the ICTP (see Chapter 2 and Table 18; Tuniz *et al.* 2013). The parameters used were 150 kV, 200 μA and 2400 projections, resulting in 4034 slices and a voxel size of 37.88 μm. IPS18800 femora were CT-scanned at the UBU (see also Chapter 2 and Table 18). Both femora were scanned at 180 kV, 320 μA and 720 projections. 815 slices, a pixel size of 0.040 mm and an inter-slice of 0.30 mm were obtained for the left femur; and 680 slices, a pixel size of 0.049 mm and an inter-slice of 0.30 mm for the right femur. In order to obtain the cross-sections of the femoral shafts, CT-image stacks were processed using *VSG-Avizo* 7.0. Cortical bone was inspected in this software by using semi-automatic thresholding techniques. Cortical bone boundaries were posteriorly drawn by using *Adobe Illustrator* CS5.1, following the periosteal and endosteal contours (see Figs. 38 and 39). Small damages at the fossil external edges where filled following the closest borders of the immediately proximal and/or distal sections following comparable analyses (see e.g., Ruff and Higgins 2013; Figs. 38a,c and 39b,c). In the case of IPS41724, the 50% section displays a larger broken area in the medial side (Fig. 38a), which, due to its femoral shaft is highly straight and important

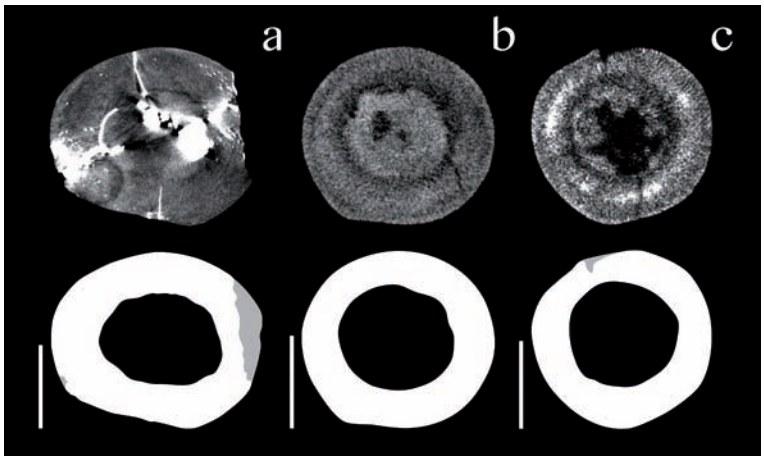

Figure 38 Computed tomography images of the femoral shaft cross-sections (top) and cortical thickness (bottom) located at 50% of the femoral length' of **a**, IPS41724; **b**, IPS18800 right; and **c**, IPS18800 left femora. Dark gray represents the reconstructed cortical areas. Anterior is top, medial to the right. Scale bar = 10 mm.

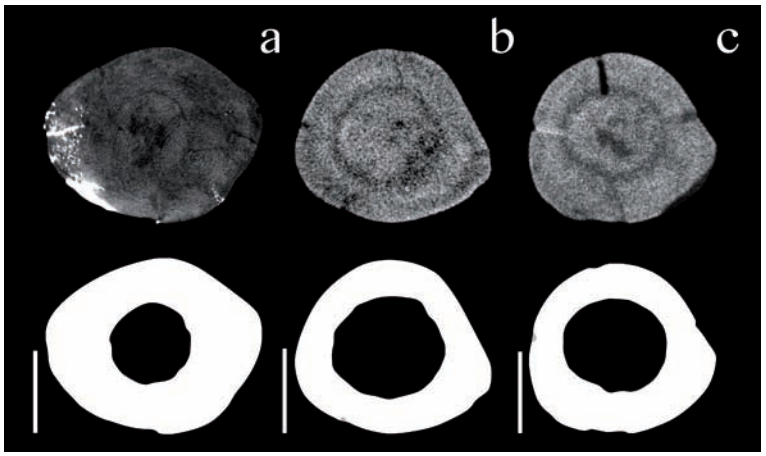

Figure 39 Computed tomography images of the femoral shaft cross-sections (top) and cortical thickness (bottom) located at 80% of the femoral length' of **a**, IPS41724 (see also Fig. 40); **b**, IPS18800 right; and **c**, IPS18800 left femora. Dark gray represents the reconstructed cortical areas. Anterior is top, medial to the right. Scale bar = 10 mm.

changes in cross-sectional geometry were not noticed, was reconstructed comparing the selected slice with more complete cross-sections located immediately above. Cortical bone boundaries of the IPS41724 80% cross-section CT-image was compared directly with the fossil specimen, which displays a natural break at an approximated location (below the lesser trochanter) and that was physically separated for this study (Fig. 40; see also Fig. 21). Then, final cortical bone images were imported to *Fiji* 1.50e (Schindelin *et al.* 2012) to obtain the structural properties of the femoral shaft cross-sections using the *BoneJ* plugin (Doube *et al.* 2010).

Statistical analyses

Relationships between the femoral head surface area (FHSA; formula as reported in Ruff 2002: appendix table 1) and the section modulus around the anteroposterior axis (Zx) of the 50% and 80% sections were inspected by means of allometric regressions in order to account for size-related shape changes (i.e., allometric effects). Allometric regression by means of the ordinary least-square (OLS) method of log-transformed (natural logarithms, ln) data were performed on the sample, with Zx (at both 50% and 80%) as the independent variable and FHSA as the dependent variable.

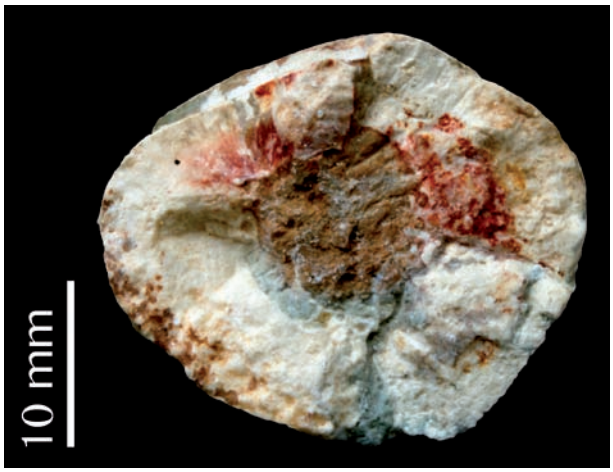

Figure 40 Proximal shaft cross-section of IPS41724. Proximal femur and shaft of IPS41724 were separated through a natural break in order to directly inspect the cortical bone boundaries and distribution at this section (close to the 80% of the femoral length'). Anterior is top, medial to the right.

Posteriorly, comparisons of the perpendicular distance of the n (X,Y) points (n being the individuals of the sample) in a log-log space to an arbitrary baseline (whose slope is the theoretical isometric value) were performed as the ln ratios between FHSA / $Zx^{2/3}$ (denominator corrected for differences in measurements units). This procedure allows the inspection of differences among taxonomic groups. Values of the ratios are depicted in boxplots for the whole sample of living and extinct primates (see Ruff 2002 for an in-depth explanation of the benefices of using this method). Analysis of variance (ANOVA) and post-hoc pairwise comparisons (Tukey method) were performed to evaluate mean differences between generic taxa. Moreover, scaling differences and allometric grade shifts between below-branch suspensory (BBS) and 'quadrupedal' taxa (Q) are inspected by means of analyses of covariance (ANCOVA). The former group includes taxa that habitually employ the hindlimb in tension (mainly during below-branch suspension), that is, orangutans and hylobatids. Otherwise, Q includes pronograde cercopithecoids and African ape knuckle-walkers, which are taxa that mainly use the hindlimb in compression during locomotion (see Stern 1975). Furthermore, homogeneity of slopes and intercepts among the living genera of each locomotor group (BBS and Q) are also explored by ANCOVA. Statistical analyses were made using the software *SPSS* v 15.0.

Table 23 Cross-sectional structural properties at the 50% and 80% sections of bone length' of the Vallès-Penedès great ape femora.

CROSS-SECTIONAL MECHANICAL PROPERTIES														
Specimen	**Taxon**	**Section**	**TA**	**CA**	**%CA**	**Ix**	**Iy**	**Ix/Iy**	**J**	**Zx**	**Zy**	**Zp**	**Imax**	**Imin**
IPS18800, right	*H. laietanus*	50%	308.70	204.56	66.26	7441.96	6421.67	1.16	13863.63	715.77	656.66	1040.49	7471.13	6392.50
		80%	364.73	236.55	64.86	9669.67	9165.12	1.06	18834.79	820.86	832.79	1529.47	10479.21	8355.57
IPS18800, left	*H. laietanus*	50%	325.94	207.02	63.52	7474.87	7166.38	1.04	14641.26	708.02	696.18	1369.86	7569.39	7071.87
		80%	365.45	253.60	69.39	10579.58	9046.79	1.17	19626.37	885.26	807.02	1639.91	10584.47	9041.90
IPS41724	cf. *D. fontani*	50%	444.64	312.18	70.21	17898.35	11912.13	1.50	29810.49	1364.83	1076.22	2225.98	17914.04	11896.44
		80%	425.28	345.50	81.24	17170.48	10873.41	1.58	28043.89	1288.29	1010.02	2086.57	17170.96	10872.93

Abbreviations: TA, total cross-section area (mm^2); CA, cortical area (mm^2); %CA, relative cortical area (%CA=(CA/TA)*100); Ix and Iy, second moments of area about anteroposterior and mediolateral axes, respectively (mm^4); Ix/Iy, biomechanical cross-sectional "shape"; J, polar second moment of area (mm^4); Zx and Zy, section moduli around the anteroposterior and mediolateral axes, respectively (mm^3); Zp, polar section modulus (mm^3); Imax and Imin, maximum and minimum second moments of area (mm^4).

RESULTS

Total femoral length

TFL estimated for IPS41724 (FHSI = 30.7 mm) is 31.0 ± 0.1 cm; whereas the mean TFL estimated for the right (FHSI = 26.6 mm) and left (FHSI = 31.5 mm) IPS18800 femora is 29.7 ± 0.1 cm (slightly longer than the TFL of 27.4 cm reported by Moyà-Solà and Köhler 1996).

Cross-sectional mechanical properties of the femoral diaphyses

Principal mechanical cross-sectional properties at both 50% and 80% sections of the femoral shaft are given in Table 23. Femoral diaphyseal cross-sections in cf. *D. fontani* show an elliptical biomechanical "shape" (mediolaterally expanded; Figs. 38 and 39), with an Ix/Iy ratio around 1.5 (Table 23). Contrarily, *H. laietanus* sections display a more circular biomechanical "shape", showing an Ix/Iy ratio closer to 1. Overall, cross-sectional structural parameters estimated for *H. laietanus* femora are lower than those of cf. *D. fontani*.

Table 24 Linear allometric regression equations derived for anteroposterior section moduli (Zx) of 50% and 80% sections related to the articular surface of the femoral head (FSHA) of a sample of extant anthropoids.

ALLOMETRIC REGRESSION EQUATIONS											
Group	**Section**	**N**	**r**	**SEE**	**p**	**Slope**	**95% CI**		**Intercept**	**95% CI**	
Extant sample	50%	279	0.979	0.25	<0.001	1.29	1.26	1.32	-3.31	-3.55	-3.08
	80%	279	0.981	0.24	<0.001	1.31	1.28	1.34	-3.46	-3.69	-3.24
BBS	50%	38	0.991	0.14	<0.001	1.29	1.23	1.35	-3.69	-4.12	-3.26
	80%	38	0.989	0.16	<0.001	1.37	1.30	1.44	-4.19	-4.71	-3.68
Q	50%	141	0.989	0.19	<0.001	1.38	1.35	1.41	-3.82	-4.06	-3.59
	80%	141	0.988	0.20	<0.001	1.42	1.38	1.45	-4.07	-4.32	-3.82

Abbreviations: N, sample size; r, correlation coefficient; SEE, standard error of estimate; p, significance; CI, confidence interval; BBS, below-branch suspensory taxa; Q, "quadruped" taxa.

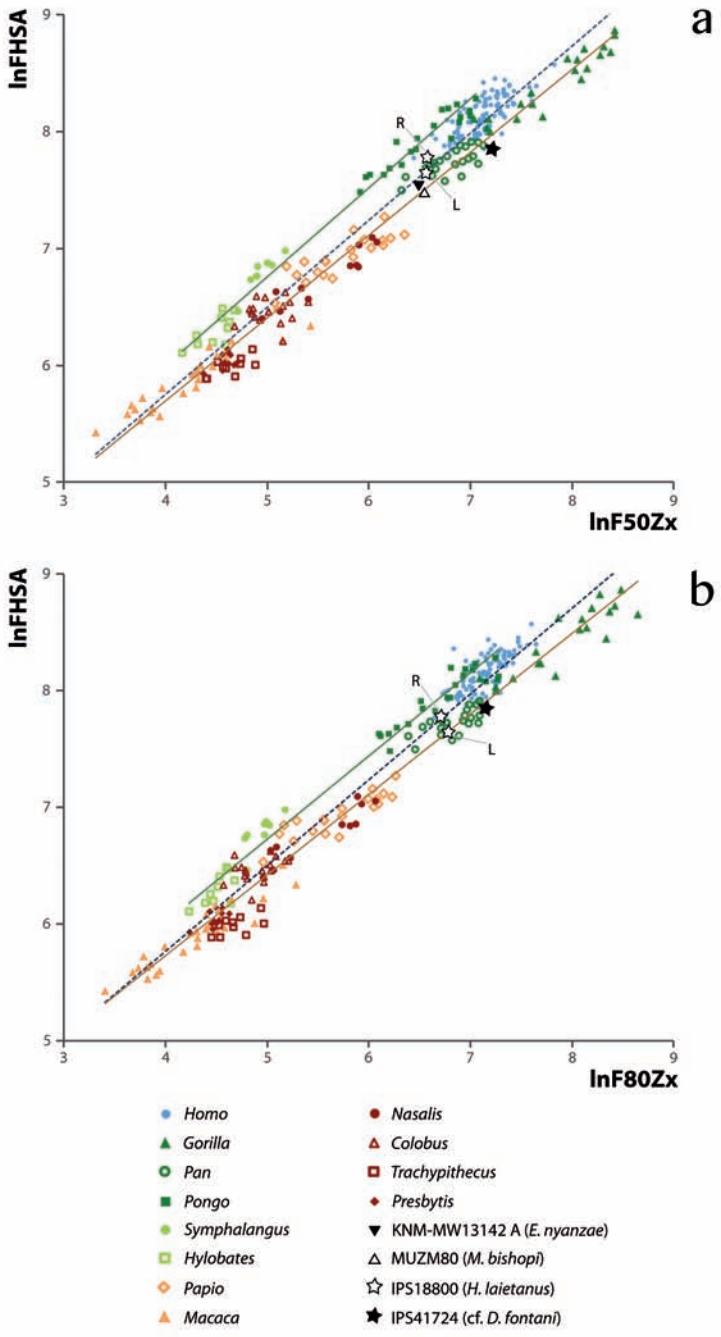

Figure 41 Bivariate allometric plots regressing the anteroposterior section modulus (Zx) of **a**, 50% and **b**, 80% sections against the articular surface of the femoral head (FHSA) for a sample of extant anthropoids and Miocene fossil specimens (including KNM-MW13142A, *Ekembo nyanzae;* MUZM80, *Morotopithecus bishopi*; IPS41724, cf. *Dryopithecus fontani*; and IPS18800, *Hispanopithecus laietanus*). Dashed dark blue line depicts all extant sample linear trend. Moreover, separate regressions were computed for below-branch suspensory (BBS) taxa (continuous green line) and "quadruped" (Q) taxa (continuous brown line). Colours correspond to major taxonomic groups: light blue, humans; green, apes; orange, cercopithecines; red, colobines. R, right; L, left.

When section modulus in the anteroposterior axis (Zx) is related to the articular surface of the femoral head (FSHA) in both 50% and 80% sections (Fig. 41; Table 24), extant primates exhibit a slight negative allometry (based on an isometric expectation of 1.5). These results are similar when BBS and Q taxa are regressed separately, being the BBS group (that includes orangutans and hylobatids) upshifted relative to both the general baseline for the whole sample and the Q baseline (Fig. 41). As visually observed in Figure 40, ANCOVA analysis confirms the allometric shift displayed in the anteroposterior strength values between BBS and Q groups for both sections, showing statistical differences in their intercept values (50%: $F = 616.382$, $p<0.01$; 80%: $F = 641.778$, $p<0.01$), instead of differences on their slopes. However, when intragroup differences are inspected for both BBS and Q by ANCOVAs (Table 25), results outline that these two groups were not completely consistent. For example, among BBS, there is observed an

ANCOVA ANALYSES											
lnFHSA vs lnF50Zx	**Loc**	**r2**		**F**	**p**	**lnFHSA vs lnF80Zx**	**Loc**	**r2**		**F**	**p**
Pongo-Hylobates	BBS	0.987	Slope	2.419	0.132	*Pongo-Hylobates*	BBS	0.987	Slope	4.857	0.037
			Intercept	7.513	0.011				Intercept	7.730	0.064
Pongo-Symphalangus	BBS	0.982	Slope	3.709	0.066	*Pongo-Symphalangus*	BBS	0.979	Slope	4.571	0.043
			Intercept	7.042	0.014				Intercept	3.447	0.076
Hylobates-Symphalangus	BBS	0.884	Slope	0.029	0.867	*Hylobates-Symphalangus*	BBS	0.872	Slope	0.006	0.949
			Intercept	0.725	0.409				Intercept	0.059	0.812
Gorilla-Pan	Q	0.943	Slope	0.037	0.848	*Gorilla-Pan*	Q	0.923	Slope	0.006	0.941
			Intercept	13.512	0.001				Intercept	8.793	0.005
Gorilla-Papio	Q	0.977	Slope	0.834	0.367	*Gorilla-Paio*	Q	0.973	Slope	2.624	0.114
			Intercept	33.204	<0.001				Intercept	29.734	<0.001
Gorilla-Macaca	Q	0.992	Slope	1.388	0.245	*Gorilla-Macaca*	Q	0.991	Slope	0.598	0.443
			Intercept	67.994	<0.001				Intercept	44.883	<0.001
Gorilla-Nasalis	Q	0.985	Slope	0.249	0.622	*Gorilla-Nasalis*	Q	0.976	Slope	0.461	0.503
			Intercept	37.685	<0.001				Intercept	21.494	<0.001
Gorilla-Colobus	Q	0.987	Slope	8.152	0.007	*Gorilla-Colobus*	Q	0.985	Slope	2.776	0.105
			Intercept	0.383	0.540				Intercept	1.389	0.247
Gorilla-Trachypithecus	Q	0.992	Slope	0.001	0.976	*Gorilla-Trachypithecus*	Q	0.986	Slope	0.088	0.769
			Intercept	5.925	0.022				Intercept	1.974	0.172
Gorilla-Presbytis	Q	0.993	Slope	1.582	0.220	*Gorilla-Presbytis*	Q	0.989	Slope	0.213	0.648
			Intercept	1.018	0.322				Intercept	1.250	0.274
Pan-Papio	Q	0.922	Slope	0.570	0.455	*Pan-Papio*	Q	0.937	Slope	1.810	0.186
			Intercept	12.727	0.001				Intercept	17.286	<0.001
Pan-Macaca	Q	0.985	Slope	0.648	0.425	*Pan-Macaca*	Q	0.987	Slope	0.330	0.568
			Intercept	16.471	<0.001				Intercept	16.374	<0.001
Pan-Nasalis	Q	0.947	Slope	0.253	0.619	*Pan-Nasalis*	Q	0.956	Slope	0.443	0.511
			Intercept	13.912	0.001				Intercept	14.719	0.001
Pan-Colobus	Q	0.967	Slope	4.951	0.032	*Pan-Colobus*	Q	0.977	Slope	2.663	0.111
			Intercept	0.124	0.727				Intercept	1.185	0.283
Pan-Trachypithecus	Q	0.980	Slope	0.004	0.950	*Pan-Trachypithecus*	Q	0.981	Slope	0.104	0.749
			Intercept	4.079	0.053				Intercept	2.627	0.116
Pan-Presbytis	Q	0.983	Slope	1.155	0.291	*Pan-Presbytis*	Q	0.987	Slope	0.320	0.576
			Intercept	0.639	0.431				Intercept	1.919	0.177
Papio-Macaca	Q	0.956	Slope	0.018	0.894	*Papio-Macaca*	Q	0.958	Slope	1.882	0.177
			Intercept	47.706	<0.001				Intercept	60.329	<0.001
Papio-Nasalis	Q	0.800	Slope	0.150	0.701	*Papio-Nasalis*	Q	0.820	Slope	0.747	0.395
			Intercept	27.470	<0.001				Intercept	35.428	<0.001
Papio-Colobus	Q	0.840	Slope	8.026	0.008	*Papio-Colobus*	Q	0.881	Slope	7.126	0.012
			Intercept	0.933	0.341				Intercept	5.108	0.030
Papio-Trachypithecus	Q	0.922	Slope	0.116	0.736	*Papio-Trachypithecus*	Q	0.915	Slope	0.906	0.350
			Intercept	5.239	0.030				Intercept	4.920	0.035
Papio-Presbytis	Q	0.932	Slope	1.638	0.212	*Papio-Presbytis*	Q	0.943	Slope	1.181	0.287
			Intercept	1.186	0.286				Intercept	3.528	0.072
Macaca-Nasalis	Q	0.956	Slope	0.142	0.708	*Macaca-Nasalis*	Q	0.953	Slope	0.056	0.815
			Intercept	49.018	<0.001				Intercept	50.084	<0.001
Macaca-Colobus	Q	0.896	Slope	10.691	0.002	*Macaca-Colobus*	Q	0.889	Slope	5.786	0.021
			Intercept	0.941	0.337				Intercept	3.224	0.080
Macaca-Trachypithecus	Q	0.881	Slope	0.112	0.739	*Macaca-Trachypithecus*	Q	0.880	Slope	0.372	0.546
			Intercept	6.269	0.017				Intercept	4.074	0.051
Macaca-Presbytis	Q	0.884	Slope	1.932	0.173	*Macaca-Presbytis*	Q	0.880	Slope	0.652	0.425
			Intercept	1.241	0.273				Intercept	2.686	0.110
Nasalis-Colobus	Q	0.833	Slope	8.157	0.009	*Nasalis-Colobus*	Q	0.859	Slope	5.050	0.034
			Intercept	0.553	0.464				Intercept	3.059	0.093
Nasalis-Trachypithecus	Q	0.953	Slope	0.052	0.822	*Nasalis-Trachypithecus*	Q	0.926	Slope	0.444	0.514
			Intercept	7.377	0.015				Intercept	4.181	0.057
Nasalis-Presbytis	Q	0.965	Slope	2.602	0.125	*Nasalis-Presbytis*	Q	0.960	Slope	0.889	0.359
			Intercept	1.643	0.217				Intercept	3.491	0.079
Colobus-Trachypithecus	Q	0.597	Slope	2.184	0.152	*Colobus-Trachypithecus*	Q	0.407	Slope	0.526	0.475
			Intercept	0.053	0.819				Intercept	0.174	0.681
Colobus-Presbytis	Q	0.643	Slope	0.165	0.688	*Colobus-Presbytis*	Q	0.698	Slope	0.232	0.634
			Intercept	0.503	0.484				Intercept	0.056	0.815
Trachypithecus-Presbytis	Q	0.447	Slope	1.452	0.246	*Trachypithecus-Presbytis*	Q	0.588	Slope	0.053	0.820
			Intercept	0.733	0.404				Intercept	0.911	0.354

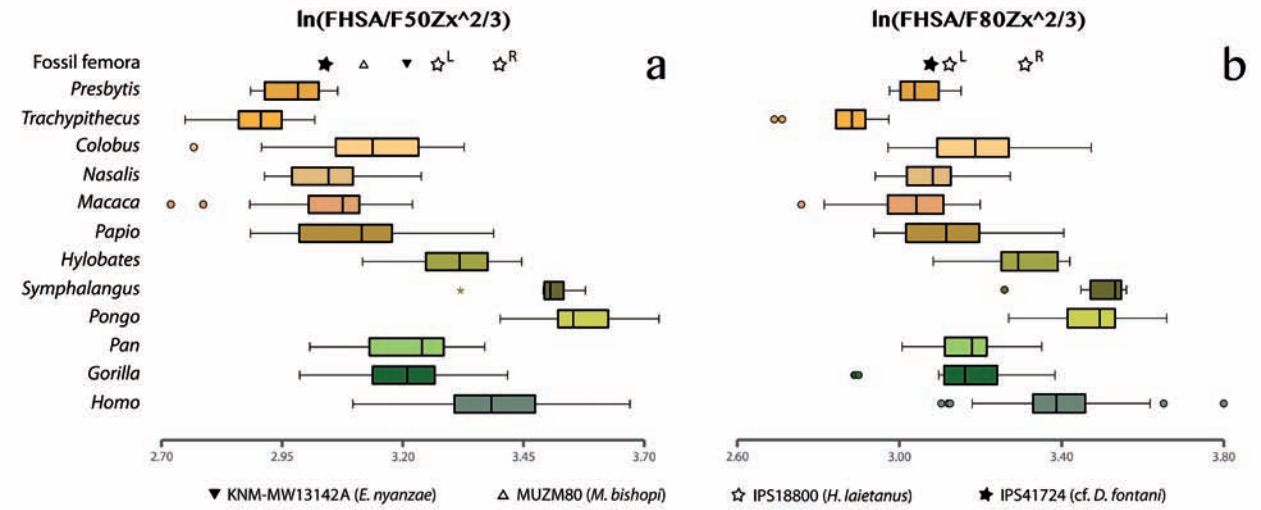

Figure 42 Boxplots showing the relation between femoral head to shaft proportions (femoral head articular surface, FHSA, against anteroposterior section modulus, Zx) at **a**, 50% and **b**, 80% sections. Vertical lines represent the median, boxes the interquartile range (between the 25th and the 75th percentiles), whiskers the extreme values, and circles the outliers. R, right; L, left. Colors represent major taxonomic groups: red, colobines; orange, cercopithecines; green, apes; light blue, humans.

allometric shift between orangutans and hylobatids for the midshaft. Likewise, the baseline of African apes is significantly different regarding the intercept from most of the monkey taxa, and even between them (*Pan-Gorilla*) for both the midshaft and the proximal shaft values (Table 25).

When group mean differences are tested by ANOVAs, statistical differences ($p<0.01$) are found either for the whole extant primate sample or between broad locomotor groups (BBS *vs* Q; see also Table 24). Moreover, although showing some other inter-genera differences, the most relevant differences of Tukey post hoc pairwise comparisons relate to those of suspensory taxa (orangutans and hylobatids), which depart from the rest of extant genera for both midshaft and proximal femur cross-sections (Table 26; Fig. 42). When comparisons are among BBS, gibbons are significantly different of orangutans and siamangs (Table 26). Thus, orangutans and siamangs show the relatively lowest values of anteroposterior diaphyseal strength. Gibbons and humans occupy an intermediate position between orangutans-siamangs and African apes-cercopithecoids. At the midshaft, African apes display relative values of anteroposterior diaphyseal strength slightly lower than cercopithecoids; whereas at the proximal shaft they clearly overlap with papionins and the largest colobines (Fig. 42). Cercopithecoids show the highest relative values of diaphyseal strength at both mid- and proximal shaft (especially *Trachypithecus*; Fig. 42).

Fossil taxa results.- Both cf. *D. fontani* and *H. laietanus* display femoral articular to shaft proportions similar to those of chimpanzees (Fig. 41). However, the former falls within the male chimpanzees values

Table 25 [*previous page*] Scaling differences and allometric grade shifts obtained by means of analyses of covariance (ANCOVA) for pairwise genera of each of the broad locomotor groups (Loc) defined in the text: BBS, below-branch suspensory taxa (orangutans and hylobatids); and Q, "quadrupedal" taxa (cercopithecoids and African apes). *Abbreviations:* FHSA, femoral head articular surface; F50Zx and F80Zx, anteroposterior bending strength at the midsahft (50%) and proximal shaft (80&); r2, squared correlation coerficient; p, significance.

and closer to those of female gorillas at both mid- and proximal shaft. Besides, this taxon shows a value for this ratio slightly downshifted relative to the Q baseline (Fig. 41). Otherwise, *H. laietanus* ratio at midshaft resembles those of female chimpanzees and are upshifted relative to the Q baseline, showing a trend towards the baseline of BBS taxa; Fig. 41a). Although slightly less marked, this tendency is also observed at the proximal shaft (Fig. 41b). Furthermore, some differences are observed between the left and right femora of the *H. laietanus* IPS18800 partial skeleton. In both cases (50% and 80%), the left femur is closer to the Q baseline than the right femur (more similar to BBS taxa; see below). Otherwise, when comparing the articular to midshaft proportions ratio of other Miocene hominoids with those of the Vallès-Penedès great apes, *H. laietanus* is more similar to *M. bishopi* and *E. nyanzae* than cf. *D. fontani*, being the former similar to female chimpanzees (Fig. 41a).

The aforementioned trends for cf. *D. fontani* and *H. laietanus* are also observed at Figure 42. Thus, the relative anteroposterior strength at the mid-point and proximal femoral shaft in cf. *D. fontani* overlaps with the interquartile range of extant cercopithecoids (except *Trachypithecus*), but also the lower ranges of African apes at the midshaft and chimpanzees at the proximal shaft (Fig. 42). On the other hand, *H. laietanus* overlaps with the interquartile ranges of gibbons and humans (and the upper ranges of African apes) for the midshaft, and with these groups and also cercopithecoids for the proximal shaft (Fig. 41b). Specifically, for the relative anteroposterior strength of the proximal shaft, *H. laietanus* displays closer values to cf. *D. fontani* (differences among

POST HOC PAIRWISE COMPARISONS

	Homo	*Gorilla*	*Pan*	*Pongo*	*Symphalangus*	*Hylobates*	*Papio*	*Macaca*	*Nasalis*	*Colobus*	*Trachypithecus*
ln(FHSA/F50Zx^2/3)											
Gorilla	**										
Pan	**	NS									
Pongo	**	**	**								
Symphalangus	NS	**	**	NS							
Hylobates	NS	NS	NS	**	*						
Papio	**	NS	NS	**	**	**					
Macaca	**	**	**	**	**	**	NS				
Nasalis	**	*	**	**	**	**	NS	NS			
Colobus	**	NS	NS	**	**	**	NS	NS	NS		
Trachypithecus	**	**	**	**	**	**	**	**	NS	**	
Presbytis	**	**	**	**	**	**	NS	NS	NS	NS	NS
ln(FHSA/F80Zx^2/3)											
Gorilla	**										
Pan	**	NS									
Pongo	NS	**	**								
Symphalangus	NS	**	**	NS							
Hylobates	NS	NS	NS	**	*						
Papio	**	NS	NS	**	**	*					
Macaca	**	*	**	**	**	**	NS				
Nasalis	**	NS	NS	**	**	**	NS	NS			
Colobus	**	NS	NS	**	**	NS	NS	**	NS		
Trachypithecus	**	**	**	**	**	**	**	**	**	**	
Presbytis	**	NS	NS	**	**	**	NS	NS	NS	NS	*

Table 26 Significance of Tukey post hoc pairwise comparisons among extant primates for the ln ratio between the femoral head surface area (FHSA) relative to the anteroposterior section modulus (Zx) with the denominator corrected for differences in measurements units: ln(FHSA/F50Zx^2/3) and ln(FHSA/F80Zx^2/3). *Abbreviations:* NS, not significant; *, $p<0.05$; **, $p<0.01$.

extant taxa are also less clear than for the midshaft; Fig. 41b). In addition, the left and right femora of *H. laietanus* show a great variability between them, with the left specimen closer to cercopithecoid-values, mainly at the proximal shaft (the ratio value for 80% is also very similar to that of cf. *D. fontani*). Regarding the rest of fossil apes, *M. bishopi* and *E. nyanzae* display an intermediate position between cf. *D. fontani* and *H. laietanus* concerning the midshaft relative anteroposterior strength. Thus, *E. nyanzae* is more similar to *H. laietanus*, whereas *M. bishopi* is closer to cf. *D. fontani* (Fig. 41a).

Ever tried. Ever failed. No matter. Try again.
Fail again. Fail better. Read more.

-- Samuel Beckett --

Section V. THE TIBIA

Chapter 4
External morphology of the tibia

DESCRIPTION

IPS18800.- Left distal tibia

Distal fragment of a left tibia (IPS18800; Fig. 43) from CLL2 that belongs to the partial skeleton of *Hispanopithecus laietanus* described by Moyà-Solà and Köhler (1996). It represents ca. 30% of total bone length (judging on the basis of 23.6 cm of total tibial length, estimated by Moyà-Solà and Köhler 1996 based on femoral length). Although the distal portion of the shaft is partly damaged, the epiphysis is well preserved. The latter is mediolaterally wider than anteroposteriorly thick (see measurements in Table 27). At the proximal (broken) end, the cross-section of the shaft is subcircular in shape and exposed cortical thickness is the following: 2.6 mm anterior, 2.4 mm medial, 2.9 mm lateral and 2.6 mm posterior (the last measure taken more distally than the others, due to the irregular shape of the natural break; Fig. 43b). In lateral view, the *interosseous* crest is well developed, ending at a triangular and well-marked fibular facet. The latter makes a slightly obtuse angle with the articular surface, being about 5.4 mm high proximodistally and 11.7 mm long anteroposteriorly. The *interosseous* crest defines the anterior border of the fibular facet, whereas the posterior border is poorly developed. Distally and medially, a robust medial malleolus is strongly projected. Its posterior side exhibits a deep *tibialis posterior* groove, which

Figure 43 Distal fragment of left tibia of *Hispanopithecus laietanus* (IPS18800) in **a**, medial; **b**, posterior; **c**, lateral; **d**, anterior; **e**, proximal; and **f**, distal views. M, medial; P, posterior.

Table 27 External measurements (in mm) of the distal fragment of left tibia of *Hispanopithecus laietanus*. For measurement abbreviations see Table 6.

IPS18800 LEFT DISTAL TIBIA													
Catalogue no.	**Taxon**	**APM**	**MLM**	**MLE**	**MLMM**	**APSMM**	**SISMM**	**A**	**B**	**C**	**D**	**E**	**F**
IPS18800	*H. laietanus*	21.9	31.6	32.8	11.1	15.3	12.9	24.1	20.2	24.1	19.3	21.4	15.5

displays strong crests on either side. The lateral edge shows a surface for the attachment of the *flexor hallucis longus* muscle. The maximum distal projection of the medial malleolus occurs anteriorly and it has a well-developed intercollicular groove for the posterior tibiotalar ligament. The articular surface on the malleolus faces laterally with a moderate extension onto the anterior surface. In anterior view, the medial malleolus makes a right angle with the articular surface. The latter is quadrangular and conspicuously defined by marked anterior and posterior lips. A rounded and anteroposteriorly concave median keel connects the anterior and posterior surfaces, dividing the articular surface into a large medial section and a smaller lateral section. The lateral portion of the articular surface slopes proximally away from the medial portion, which slightly slopes anteriorly, creating a secondary facet on the articular surface ("bony stop"; see below). The median keel also defines the maximum anteroposterior diameter of the articular surface.

COMPARATIVE SAMPLE, MEASUREMENTS AND STATISTICAL ANALYSIS

The *Hispanopithecus laietanus* tibia (IPS18800) has been compared with a sample of extant and fossil specimens listed in Tables 28 and 29, respectively. Linear measurements taken on every specimen are specified in Table 29 and illustrated in Figure 12b. Moreover, the relative thickness of the medial malleolus and the metaphyseal shape have been calculated by means of the indices MLMM/APMM and MLM/APM, which have been outlined to be functionally meaningful. MLMM/APMM measures the relative thickness of the medial malleolus of the tibia, being apparently indicative of weight transmission in inverted

EXTANT PRIMATE TIBIAE				
Taxon	**Males**	**Females**	**Unknown**	**N**
Gorilla beringei beringei	4	3		**7**
Gorilla beringei graueri	12	7		**19**
Gorilla gorilla gorilla	9	7	1	**17**
Pan paniscus	9	10		**19**
Pan troglodytes schweinfurthii	9	7	4	**20**
Pan troglodytes sspp.	9	5	4	**18**
Pongo pygmaeus	2	5	3	**10**
Hylobates lar	13	13		**26**
Papionins	25	9	10	**44**
Macaca fascicularis	13	13		**26**
Cercopithecus sp.	18	13		**31**
Chlorocebus sp.	3	3	1	**7**
Nasalis larvatus	13	12		**25**
Colobus sp.	22	13	2	**37**
Presbytis sp.	16	15		**31**
Atelids	11	16	9	**36**
Cebus apella	15	12		**27**
			Total N	**400**

Table 28 Tibial comparative sample of extant primates. Papionins include *Papio hamadryas* subspp., *Mandrillus sphinx*, *Mandrillus leucophaeus* and *Lophocebus* sp. Atelids include *Alouatta caraya*, *A. seniculus*, *A. fusca*, *A. palliata*, *A. seniculus*, *Ateles belzebuth*, *At. fusciceps*, *At. geoffroyi*, and *At. paniscus*. N, sample size.

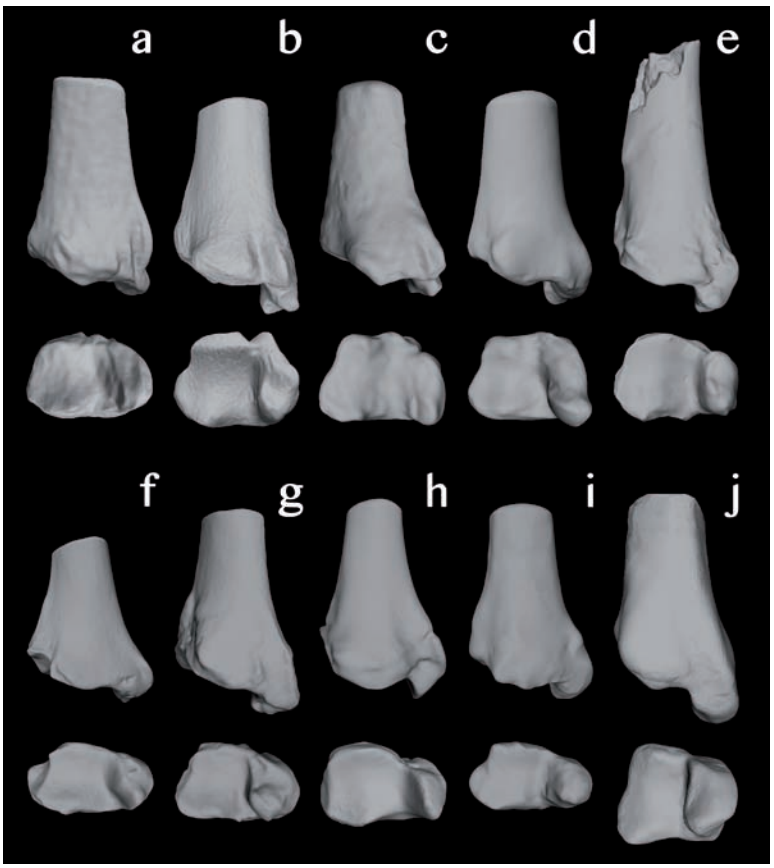

Figure 44 Digital renderings of 3D models of the distal tibia of *Hispanopithecus laietanus* compared with those of a selected extant primate sample: **a**, *Colobus guereza*; **b**, *Nasalis larvatus*; **c**, *Macaca fascicularis*; **d**, *Papio hamadryas*; **e**, *H. laietanus* (IPS18800, left); **f**, *Gorilla gorilla*; **g**, *Pan troglodytes*; **h**, *Pongo pygmaeus*; **i**, *Symphalangus syndactylus*; and **j**, *Hoolock hoolock*. For comparative purposes, all models were scaled to the same mediolateral metaphysis length and shown as if from the left side. For each model, posterior (top) and distal (bottom) views are shown.

positions of the ankle joint (DeSilva *et al.* 2010). Otherwise, MLM/APM relates to the capacity of dorsiflexion of the foot and the range of mobility of the ankle joint (DeSilva *et al.* 2010).

The procedure for statistical comparisons among extant and fossil tibiae follows that explained in the previous section for proximal femora analyses (see Chapter 1). Thereby, values for the two indices are depicted in boxplots and significance of Tukey's post hoc comparisons among extant taxonomic groups are summarized in Table 30.

COMPARISONS

The tibia of *Hispanopithecus laietanus* from CLL2 (IPS18800) resembles those of cercopithecoids (particularly *Macaca* and *Nasalis*) in several aspects (Fig. 44), such as the keeled and symmetrical articular surface, the moderate anterior protrusion of the medial malleolus, and the well-developed *intercollicular* groove for the posterior tibiotalar ligament. However, both the subrectangular shape of the articular surface and the mediolaterally thick medial malleolus of *H. laietanus* more closely resemble the condition of living apes (Fig. 44).

The relative thickness of the medial malleolus.- MLMM/APMM (Fig. 45; Table 30) is related to the loading of the ankle joint in an inverted position (DeSilva *et al.* 2010). Regarding this ratio, *Cebus* and

Table 29 Comparative sample of fossil primates. Table includes the distal tibia measurements (in mm) used in this work. See Table 6 for measurement abbreviations.

FOSSIL PRIMATE TIBIAE						
Catalogue no.	**Taxon**	**MLM**	**APM**	**MLMM**	**APMM**	**Measurements source**
KNM-RU1939	*Ekembo nyanzae*	24.6	21.5	9.3	15.2	This study
NAP I58	*Proconsul major*	43.1	29.9	13.8	22.9	Rafferty *et al.* 1995, Nakatsukasa *et al.* 2012
KNM-LG583	*Dendropithecus* sp. or *Proconsul africanus*	17.1	11.3	5.7	9.8	This study
KNM-RU3589	*Ekembo heseloni*	15.4	14.2	6.0	11.0	This study
YGSP1656	*Sivapithecus indicus*	21.9	15.3	8.7	13.7	DeSilva *et al.* 2010

cercopithecoids show anteroposteriorly thicker medial malleolus than chimpanzees, orangutans and atelids. Nonetheless, anthropoid monkeys also overlap with gibbons and the lowermost range of atelids. On the other hand, gibbons and gorillas display intermediate values for this index (although the latter being more similar to the rest of great apes and atelids). Chimpanzees, orangutans and atelids display the anteroposteriorly narrowest medial malleoli, although the range of the latter (atelids) is broad and also overlap with that of gorillas, gibbons and cercopithecoids (however, they are statistically different; Fig. 45; Table 30). The tibia of *H. laietanus* overlaps with the interquartile range of chimpanzees (*P. troglodytes troglodytes*), orangutans and atelids (Fig. 45). As aforementioned, apes and atelids have a relatively mediolaterally broad medial malleolus than cercopithecoids and *Cebus*. This is also the case of the *H. laietanus* medial malleolus. The rest of fossil tibiae show a relatively thinner medial malleolus thickness (mediolaterally narrow), which is intermediate between the *Cebus*-cercopithecoids group and the atelids-great apes group, mainly overlapping with gibbons (Fig. 45). KNM-RU3589 (*E. heseloni*) shows the most cercopithecoid-like relative medial malleolus thickness (lowest value of the index) among fossil taxa, being the most different to that of *H. laietanus*.

Metaphysis dimensions.- In the case of MLM/APM (Fig. 46; Table 30), differences among extant primates are less clear, since the ranges of variation are highly broad. With the exception of *G. b. graueri* (whose range of variation does not overlap with that of colobines), all the remaining taxa ranges overlap among them. Nonetheless, cercopithecoids are statistically different from the rest of catarrhines, thus displaying a more quadrangular shape of the metaphysis (mediolaterally similar to anteroposteriorly). On the other hand, the rest of taxa show a mediolaterally wider than anteroposteriorly thick metaphysis. This condition is more extreme in gorillas and atelids, which exhibit the highest values for this index. This metaphyseal shape (wider mediolaterally than anteroposteriorly) has been associated with motion of the ankle joint in diverse postures and the capability of hyperdorsiflexion during vertical climbing (DeSilva 2008; DeSilva *et al.* 2010). Thus, cercopithecoids display the opposite pattern, with an anteroposteriorly broader metaphysis related to movements restricted to the parasagittal plane (Fig. 46; Harrison 1989). In the case of fossil tibiae, *H. laietanus* resembles the condition of great apes and atelids, showing an anteroposteriorly flattened metaphysis (Fig. 46). Moreover, the metaphyseal shape of this taxon is very similar to that of *P. major* (NAP I'58) and *S. indicus* (YGSP1656), and clearly differs from those of *Ekembo*

spp., which are more cercopithecoid-like (Fig. 46; although *E. nyanzae* also overlaps with the lower range of gibbons, and bonobos). KNM-LG583 (*Dendropithecus*/*Proconsul africanus*) shows the highest value for this index and, therefore, the most mediolaterally expanded metaphysis among fossil apes, resembling mainly gorillas, orangutans and atelids.

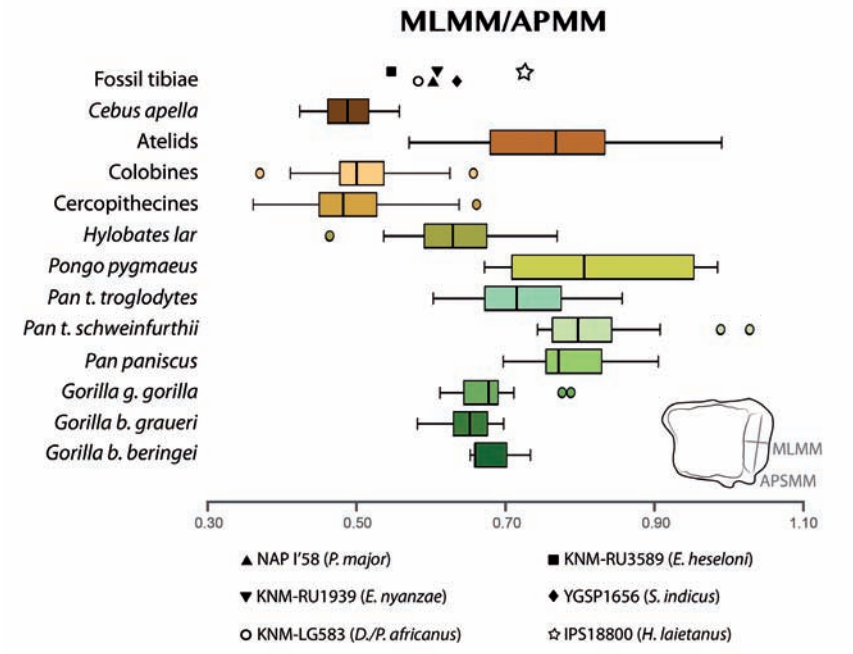

Figure 45 Boxplot showing variation in the relative medial malleolus thickness (MLMM/APSMM) in fossil hominoids compared to a sample of extant primates. Vertical lines represent the median, boxes the interquartile range (between the 25th and the 75th percentiles), whiskers the extreme values, and circles the outliers. Cercopithecines (*Papio*, *Mandrillus*, *Lophocebus*, *Macaca*, *Cercopithecus* and *Chlorocebus*), colobines (*Nasalis*, *Colobus*, and *Presbytis*), and atelids (*Alouatta* and *Ateles*) taxa are shown grouped for easier comparisons since no statistical differences among the taxa of each group have been found.

Groove for the* tibialis posterior *tendon.- The tibia of *H. laietanus* displays a deep groove for the *tibialis posterior* tendon that is similar to those of *Nasalis* or *Pan*, a trait associated with powerful grasping abilities during climbing and arboreal quadrupedalism (Lewis 1980a).

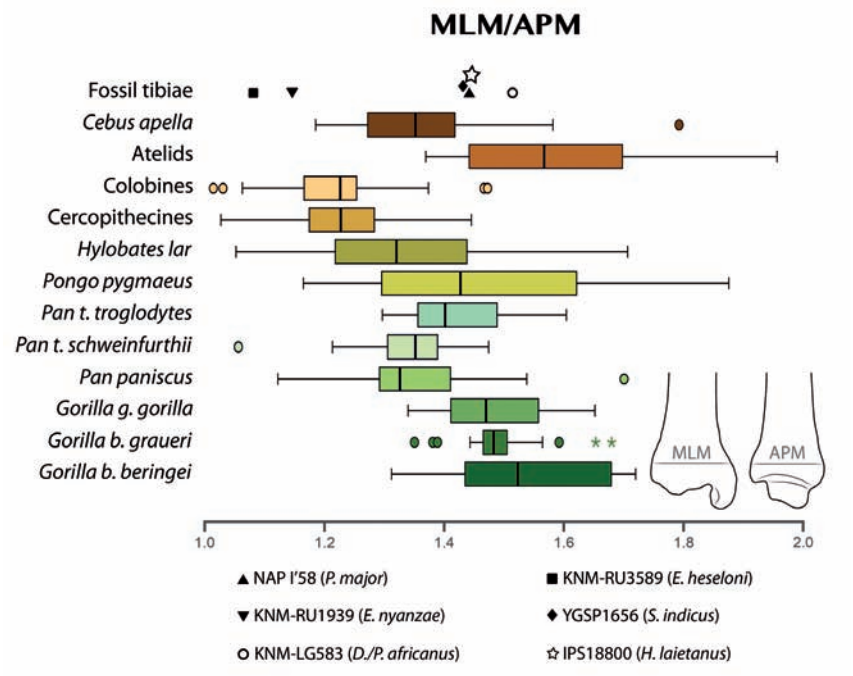

Figure 46 Boxplot showing variation in the metaphysis dimensions (MLM/APM) in fossil hominoids compared to a sample of extant primates. Vertical lines represent the median, boxes the interquartile range (between the 25th and the 75th percentiles), whiskers the extreme values, and circles the outliers. Cercopithecines (*Papio*, *Mandrillus*, *Lophocebus*, *Macaca*, *Cercopithecus* and *Chlorocebus*), colobines (*Nasalis*, *Colobus*, and *Presbytis*), and atelids (*Alouatta* and *Ateles*) taxa are shown grouped for easier comparisons since no statistical differences among the taxa of each group have been found.

The anteroposterior compression of the distal shaft and a large fibular facet of *H. laietanus* more resemble the ape condition. Among apes, the tibia of *H. laietanus* is most similar to that of hylobatids, since it does not display the specialized vertical climbing features observed in great apes (e.g., large fibular facet and mediolaterally expanded articular surface). Compared to other fossil apes, the tibia of *H. laietanus* is similar in the overall shape of the medial malleolus (marked distal projection) and the articular surface (subrectangular and with a median keel) to that of *E. nyanzae* (KNM-RU1939), for which adaptations to above-branch quadrupedalism have been inferred (Rafferty *et al.* 1995; DeSilva 2008). Although similar in some traits (e.g., metaphysis dimensions), the tibia of *H. laietanus* differs from that of *P. major* and *S. indicus*, which show some traits associated with arboreal quadrupedalism (e.g., marked distal projection of the medial malleolus and relatively small fibular facet), but also others related to vertical climbing (e.g., somewhat flat articular surface and an intermediate relative thickness of the medial malleolus; Rafferty *et al.* 1995; DeSilva 2008; DeSilva *et al.* 2010).

Table 30 Significance of post hoc pairwise comparisons (Tukey) for the size of the relative thickness of the tibial medial malleolus (MLMM/APML) and the metaphysis dimensions (MLM/APM) among extant primates.

POST HOC PAIRWISE COMPARISONS											
	G. b. beringei	*G. b. graueri*	*G. g. gorilla*	*P. paniscus*	*P. t. schweinfurthii*	*P. troglodytes*	*Po. pygmaeus*	*H. lar*	Cercopithecines	Colobines	Atelids
MLMM/APMM											
G. b. graueri	NS										
G. g. gorilla	NS	NS									
P. paniscus	**	**	**								
P. t. schweinfurthii	**	**	**	NS							
P. troglodytes	NS	*	NS	NS	**						
Po. pygmaeus	**	**	**	NS	NS	**					
H. lar	NS	NS	NS	**	**	**	**				
Cercopithecines	**	**	**	**	**	**	**	**			
Colobines	**	**	**	**	**	**	**	**	NS		
Atelids	NS	**	**	NS	NS	NS	NS	**	**	**	
C. apella	**	**	**	**	**	**	**	**	NS	NS	**
MLM/APM											
G. b. graueri	NS										
G. g. gorilla	NS	NS									
P. paniscus	**	**	*								
P. t. schweinfurthii	**	**	**	NS							
P. troglodytes	NS	NS	NS	NS	NS						
Po. pygmaeus	NS	NS	NS	NS	*	NS					
H. lar	**	**	**	NS	NS	NS	NS				
Cercopithecines	**	**	**	**	**	**	**	**			
Colobines	**	**	**	**	**	**	**	**	NS		
Atelids	NS	NS	NS	**	**	**	NS	**	**	**	
C. apella	*	**	*	NS	NS	NS	NS	NS	**	**	**

Abbreviations: NS, not significant; *, p<0.05; **, p<0.01.

You see things and you say “Why?”; but I dream
things that never were and and I say “Why not?”.

-- G. Bernard Shaw --

Section VI. THE PATELLA

Chapter 5
External morphology of the patella

DESCRIPTION

IPS21350.37.- Complete left patella

Apart from the diaphyseal fragments and the pedal elements (see Chapter 1 and Almécija *et al.* in prep.b, respectively), the left patella (IPS21350.37) is the only well preserved hindlimb element available for *Pierolapithecus catalaunicus*, and its part of the holotype partial skeleton (Fig. 47; Moyà-Solà *et al.* 2004). This patella displays very minor damage on its proximal and medial portions, and some slight abrasion on the distal end, although its shape and size are well preserved. IPS21350.37 is mediolaterally broader (ML = 24.9 mm) than proximodistally long (PD = 21.9 mm); it is anteroposteriorly thin (AP = 9.7 mm) throughout its length, and it slightly wedges distalward. On the proximal half of its anterior side there is a rough surface for the insertion of the *vastus lateralis*, *medialis*, *intermedius* and *rectus femoris* muscles (i.e., the *quadriceps* muscle group). The articular surface for the femoral patellar groove occupies almost the whole posterior side of the patella (PDAS = 17.1 mm). A medial and a lateral regions can be distinguished in the articular surface. They are asymmetrical, with the lateral aspect larger than the medial. Toward its distal edge, the patella shows a medially oriented rough area for the insertion of the patellar ligament.

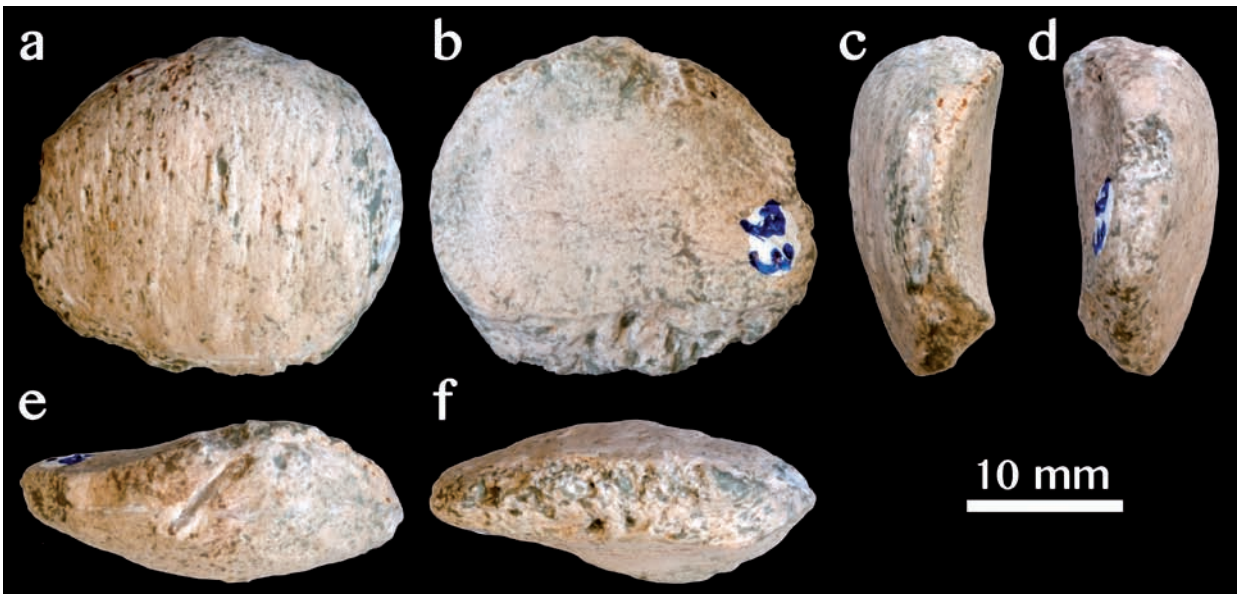

Figure 47 Left patella of *Pierolapithecus catalaunicus* (IPS21350.37, holotype) from ACM/BCV1 in **a**, anterior; **b**, posterior; **c**, lateral; **d**, medial; **e**, proximal; and **f**, distal views.

COMPARATIVE SAMPLE, MEASUREMENTS AND STATISTICAL ANALYSIS

To compare this specimen with the patellae of other (extant and extinct) anthropoids, four variables were measured following Ward *et al.* (1995): total proximodistal height of the patella (PD); proximodistal height of the articular surface (PDAS); anteroposterior thickness (AP); and mediolateral breadth (ML). These variables are intended to capture the overall proportions of the patella while being biomechanically meaningful. Measurements were taken using a digital caliper to the nearest 0.1 mm. The individual values for *P. catalaunicus* were compared with the sample of extant anthropoids used by Ward *et al.* (1995: tables 1 and 2), as well as selected fossil hominoid specimens, for which measurements were taken from the literature (McCrossin 1994a; Ward *et al.* 1995; Nakatsukasa *et al.* 2012). In all cases, only adult specimens for which all measurements were available were included in the analyses. The fossil hominoid sample included: KPS PT3 and KPS PT4 (*Ekembo heseloni*; Ward *et al.* 1995); KNM-RU 17382 (*Ekembo nyanzae*; Ward *et al.* 1995); KNM-BG 15535 (*Nacholapithecus kerioi*, referred to *Kenyapithecus* in Ward *et al.* 1995); BAC 122 (*Oreopithecus bambolii*, measured by Sergio Almécija from a cast: PD = 22.2 mm, PDAS = 19.9 mm, AP = 8.9 mm, ML = 23.0 mm); and KNM-MB 24738 (*Equatorius africanus*; McCrossin 1994a).

For shape comparisons, linear dimension were divided by overall patellar size, which was approximated by the geometric mean (GM) of the four original lengths. Size-adjusting the patellar linear dimensions by the GM produces dimensionless Mosimann shape ratios characterizing each individual irrespective of the remaining individuals in the sample (unlike residuals derived from regressions; Mosimann 1970; Jungers *et al.* 1995). Comparisons of patellar size (GM) and shape (Mosimann variables) were depicted by means of boxplots for descriptive purposes. Further, major patterns of patellar shape variation between extant anthropoids and fossil hominoids were summarized by means of a principal components analysis (PCA) performed on the covariance matrix of the taxa means. Individual PC scores were computed and plotted a posteriori in order to show variation within extant anthropoids. The method, known as between-group PCA (bgPCA), is extensively described elsewhere (Mitteroecker and Bookstein 2011). Shape variables were log-transformed (using natural logarithms) before being introduced into the analysis. Statistical differences between the bgPC scores obtained (bgPC1 and bgPC2 in this case) from the extant sample of primates were inspected by means of analyses of their variance (ANOVA), as well as multivariate analyses of variance (MANOVA; to inspect both principal axes together), and their associated Bonferroni post hoc multiple comparisons. All shape analyses were performed with the statistical packages *SPSS* v 15 and *PAST* v 2.15.

Patellar mediolateral breadth (ML) has been previously found to scale with body mass (BM) in non-human hominoids (Jungers 1990b). Hence, the scaling of ML against BM and GM was inspected in the sample of non-human anthropoid primates by means of phylogenetic generalized least-squares (PGLS) regressions of the log-transformed, sex-specific means. Humans were excluded from the analyses for being clear outliers in the sample regarding ln ML *vs* ln BM. The regression coefficients and the error term

are all computed by means of maximum likelihood (Martins and Hansen 1997), with phylogenetic signal (Pagel 1999; Freckleton *et al.* 2002) incorporated into the error term. The degree of phylogenetic signal is given by l, which varies between values of 0 (no signal) and 1 (strong signal; *ibid*). All PGLS regressions results are based on female species means; the male results were similar and therefore are not shown. PGLS regression statistics were calculated using the 'base' and 'caper' libraries of *R* v 2.9 (R Core Team 2015). The consensus topology and branch lengths for the extant primate sample were taken from the 10k Trees website (v3; Arnold *et al.* 2010).

COMPARISONS

Mosimann shape ratios

The range of variation of the patellar size (GM), as well as the Mosimann shape variables for the different extant genera and fossil individuals, are depicted in Figure 48 by means of boxplots (see Figure 49 for patellar morphological comparisons). Regarding the overall patellar size (GM), African apes and, especially, humans have the largest patellae (Fig. 48a). Orangutans and baboons display an intermediate patellar size between African apes and hylobatids, non-*Papio* cercopithecoids and platyrrhines. Finally, hylobatids (gibbons and siamangs) overlap with anthropoid monkeys and *Cebus*, showing the latter the smallest patellar size. Apart from *E. heseloni* and *N. kerioi*, which are similar to hylobatids and monkeys (platyrrhines and cercopithecoids), the rest of Miocene apes, including *P. catalaunicus*, have patellae of intermediate size between the monkey-hylobatid group (except *Papio*) and African ape-human group, overlapping with the ranges of orangutans and baboons.

Monkeys and hylobatids exhibit proximodistally longer patellae than extant great apes and humans (Fig. 48b). Ranges of PD variation of cercopithecoid and platyrrhine monkeys and gibbons are very similar to one another. The patella of *Symphalangus* is exceptionally proximodistally high, its lower non-interquartile range overlapping only with the upper range of cercopithecoid monkeys, but not with that of *Hylobates*. For extant great apes and humans, only the uppermost range of *Pan* overlaps with that of platyrrhine and cercopithecoid monkeys and *Hylobates*. Great apes and humans overlap among them. *Pierolapithecus catalaunicus* (similarly as *O. bambolii*) falls within the interquartile range of all great apes and humans, while the rest of Miocene apes exhibit slightly proximodistally longer patellae, falling in the range of monkeys and *Hylobates*.

For PDAS, differences between genera are less clear (Fig. 48c). Although most ranges overlap, humans, cercopithecoids and *Cebus* show proximodistally shorter articular surfaces than *Pan, Pongo*, hylobatids and *Ateles*. Gorillas display a wide range, overlapping with the interquartile ranges of the remaining great apes and all monkeys. *Hylobates* shows the highest values of PDAS, closely followed by

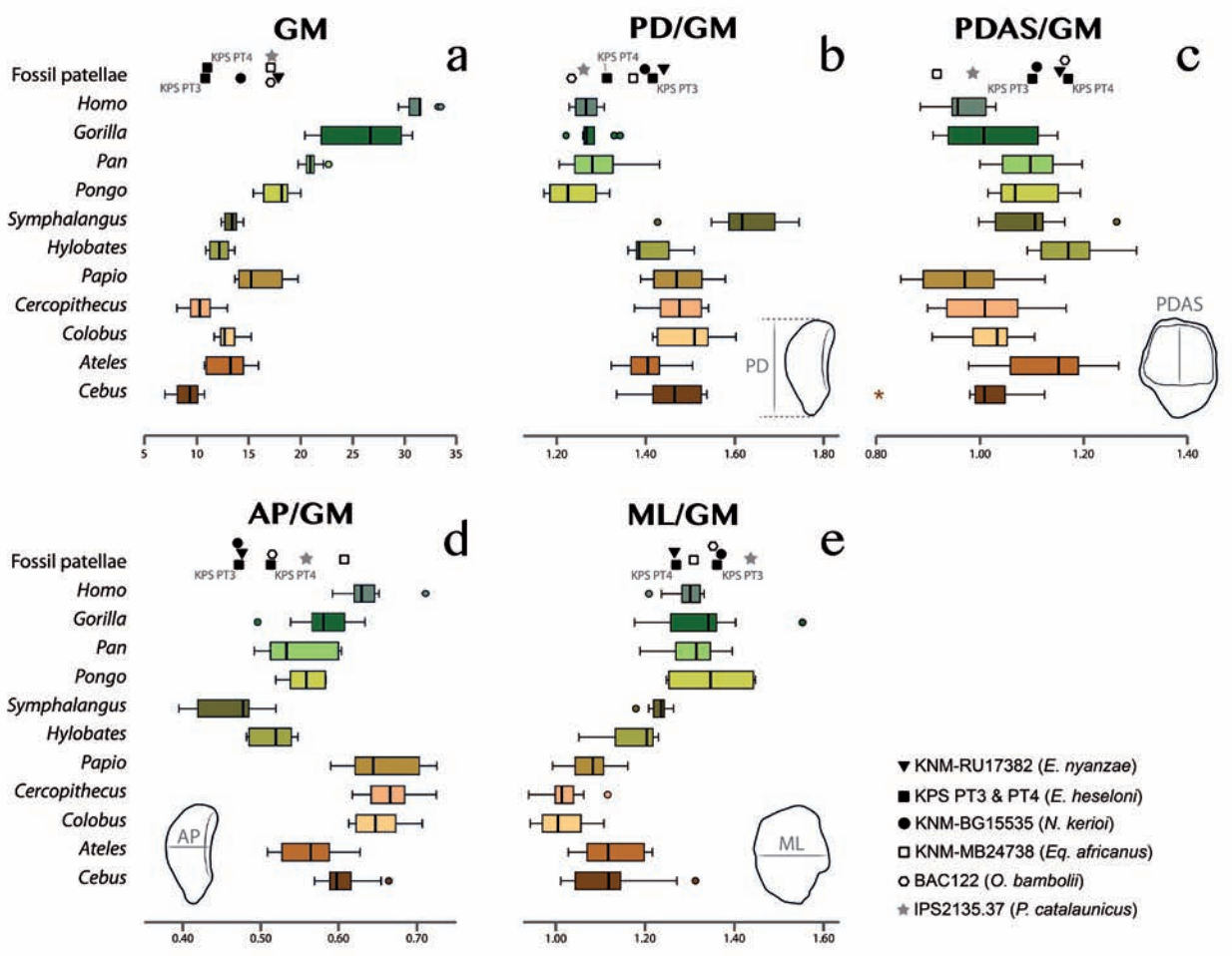

Figure 48 Boxplots representing patellar size (GM) and Mosimann shape variables. **a**, patellar size (GM); **b-f**, shape variables standardized by GM based on the four original variables. Vertical lines represent the median, boxes the interquartile range (between the 25th and the 75th percentiles), whiskers the extreme values, circles the outliers and asterisks the extreme outliers. Measurements abbreviations in Table 6.

Ateles. Nonetheless, in both cases, their ranges overlap with those of the rest of taxa (except for *Hylobates* which not overlaps with humans). The PDAS value of *P. catalaunicus* overlaps with humans, gorillas and monkeys (although only slightly with the lowermost range of *Ateles*). *Equatorius africanus* shows the lowest value of this index and overlaps with humans, gorillas, cercopithecoids and *Cebus*. The rest of Miocene apes ratios overlap with those of apes and *Ateles*, displaying *N. kerioi* and *E. heseloni* (KPS PT3) a shorter PDAS than *E. nyanzae*, *E. heseloni* (KPS PT4), and *O. bambolii*.

In contrast, marked differences are observed concerning anteroposterior thickness (Fig. 48d). Hylobatids display the thinnest patellae and overlap (mainly gibbons) with the lower ranges of chimpanzees, orangutans and *Ateles*. Cercopithecoids and humans show the opposite condition (thickest patellae), thus overlapping with the uppermost ranges of gorillas and platyrrhines. Great apes and *Ateles* have intermediate values for this index. This is also the case of *P. catalaunicus*. *Oreopithecus bambolii*, *N. kerioi* and *Ekembo* spp. show slightly thinner patellae than great apes, overlapping with the lowest range of *Pan*, *Ateles* and hylobatids. *Equatorius africanus* is more similar to humans and cercopithecoids, although it also falls in the range of gorillas and *Cebus*. Finally, cercopithecoids display the narrowest patellae (Fig.

48f), followed by platyrrhines, hylobatids, and great apes and humans. The latter two groups overlap one each other, and also with siamangs. Gibbons overlap with the lower ranges of humans and African apes, as well as cercopithecoid and platyrrhine monkeys. Miocene apes mainly overlap with the ranges of humans and great apes, showing one specimen of *E. heseloni* (KPS PT 4) and *E. nyanzae* the lowest values of ML among fossils. *Equatorius africanus*, *O. bambolii*, the other individual of *P. heseloni* (KPS PT 3) and *N. kerioi* show intermediate values for fossils, being *P. catalaunicus* the specimen with the broadest mediolateral length of the patella.

Size scaling of patellar mediolateral breadth

Allometric regression results are given in Figure 50 and Table 31. For both the ML *vs* BM and ML *vs* GM, the results are near expectations based on isometric dimensional scaling. Mediolateral patellar breadth exhibits a strong correlation with BM, and scales with a slope of 0.376±0.025. Because $\lambda = 0.000$ (no phylogenetic signal), the 95% confidence intervals (CI) was calculated using a t distribution for small samples (DF = 8, t = 2.306, $\alpha = 0.05$), yielding a slope CI of 0.318–0.433, which overlaps the isometric expectation of 0.333. ML also exhibits a strong correlation with GM, and scales with a slope of 1.190. The $\lambda = 1.000$ (strong phylogenetic signal) complicates use of standard statistical tables in this instance. However, it is likely that this scaling pattern has a significantly positive allometry by a small margin (est. 95% CI 1.020–1.360), based on an isometric expectation of 1.000. Therefore, the above-explained differences between hominids and the hylobatid-monkey group in the Mosimann ratio ML/GM (Fig. 48f) may be due to scaling effects.

Between-group principal components analysis

Most of the patellar shape variation (91.6%) among extant and fossil taxa is explained by the two first between-group principal components (bgPCs; Fig. 51; Table 32). bgPC1 (61.4% of variance) is highly correlated with positive values of mediolateral patellar breadth (ML) and especially negative values of anteroposterior patellar thickness (AP). This axis completely separates apes from cercopithecoids.

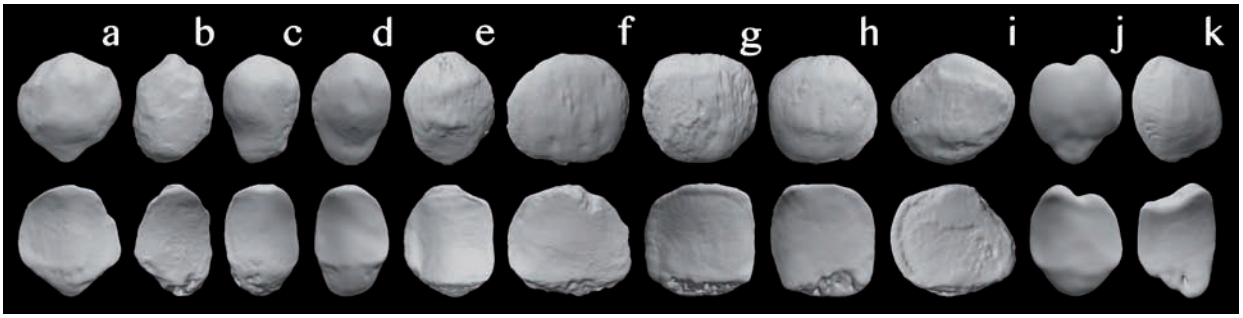

Figure 49 Digital renderings of 3D models of the patella of *Pierolapithecus catalaunicus* compared with those of a selected extant primate sample: **a**, *Cebus albifrons*; **b**, *Ateles belzebuth*; **c**, *Colobus angolensis*; **d**, *Cercopithecus mitis*; **e**, *Papio cynocephalus;* **f**, *Pierolapithecus catalaunicus* (IPS31250.37); **g**, *Gorilla gorilla*; **h**, *Pan troglodytes*; **i**, *Pongo pygmaeus*; **j**, *Symphalangus syndactylus*; and **k**, *Hylobates agilis*. For comparative purposes, all models are scaled to the same proximodistal height and show as if from the left side. For each model, anterior (top) and posterior (bottom) views are shown.

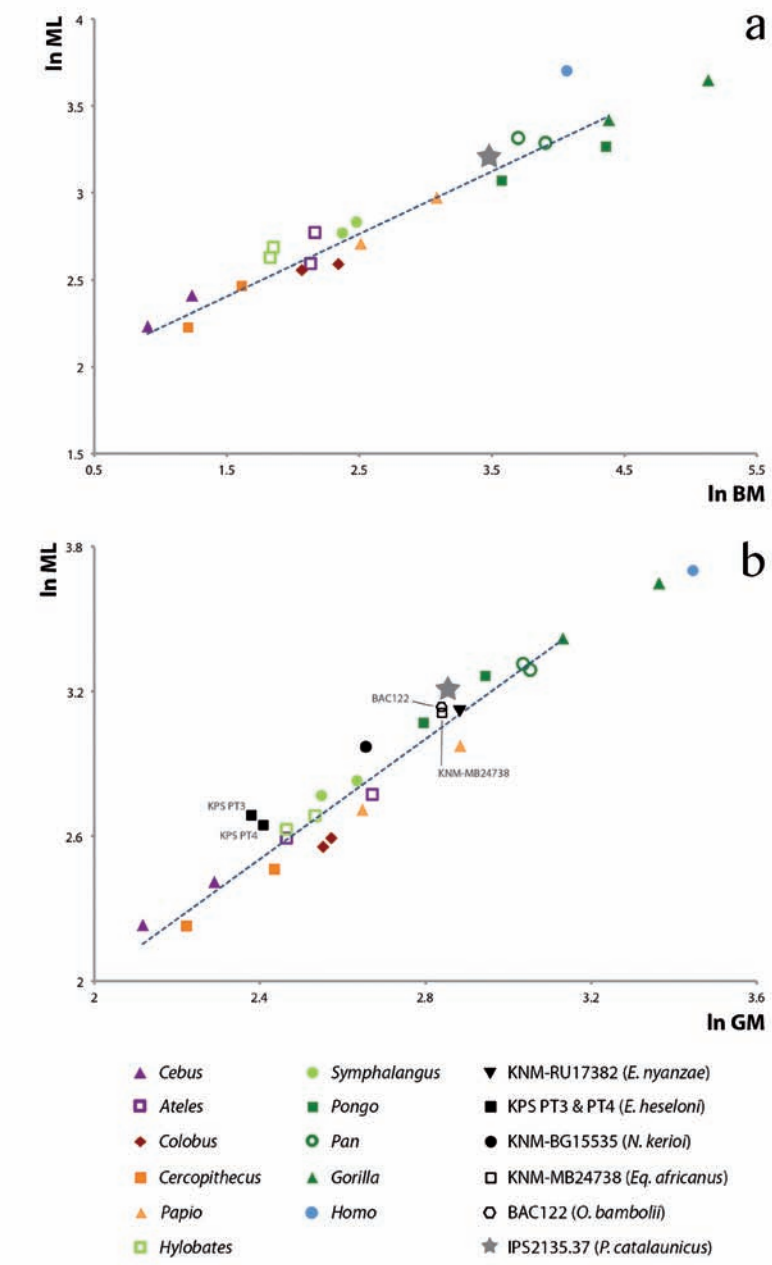

Figure 50 Allometric bivariate plots. **a**, mediolateral breadth (ML) *vs* body mass (BM); **b**, ML *vs* patellar size (GM). The OLS and PGLS allometric regression equations are reported in Table 31; dashed dark blue lines denotes female means of non-humans primates OLS regression (see text for further explanation). Because of the isometric relationship between ML and BM, the former can be used as a surrogate of BM (see text).

However, platyrrhines and humans overlap on this axis and occupy an intermediate position between cercopithecoids and apes (overlapping with both). Differences in bgPC1 scores between taxa are statistically significant ($F = 50.378$, $p < 0.001$; see Table 33 for specific differences). These results highlight the fact that monkeys and, especially, cercopithecoids have anteroposteriorly thicker and mediolaterally narrower patellae than extant great apes (see also Fig. 49). *Symphalangus* exhibits the extreme condition for hominoids, being statistically different from the remaining taxa except for *Hylobates* ($p = 1.000$; Table 33). Conversely, modern humans, although in the range of platyrrhines, show significant differences with all cercopithecoids and extant ape genera ($p < 0.05$; Table 32). bgPC2 (30.3% of variance) is highly correlated with positive values of proximodistal patellar length (PD) and negative values of mediolateral breadth (ML). bgPC scores for this axis also show statistical differences among genera ($F = 14.882$, $p < 0.001$). Cercopithecoids, platyrrhines and hylobatids display overall significant differences from extant great apes and humans ($p < 0.05$; Table 33). Thus, although there is overlapping in the bgPC2 ranges of

Table 31 Ordinary least squares (OLS) and phylogenetic generalized least-squares (PGLS) allometric regressions for mediolateral breadth of the patella (ML) relative to body mass (BM) and patellar size (GM). Regressions were derived in the extant non-human anthropoids sample (8 species: 5 monkeys, 3 great apes) using female individuals data set (sex-pooled humans were not included in the analyses; see text for further explanation).

ALLOMETRIC REGRESSIONS EQUATIONS										
OLS	**Intercept**	**s.e.**	**Slope**	**s.e.**	**95% CI**	**F**	**p-value**	**Adj R**		
ML *vs* BM	1.864	0.064	0.360	0.024	0.305-0.414	229.875	<0.001	0.962		
ML *vs* GM	-0.478	0.222	1.243	0.085	1.047-1.439	214.469	<0.001	0.960		
PGLS	**Intercept**	**s.e.**	**Slope**	**s.e.**	**95% CI**	**t -value**	**p-value**	**Adj R**	**λ**	**DF**
ML *vs* BM	1.815	0.067	0.376	0.025	0.318-0.433	15.037	<0.001	0.960	0.000	8
ML *vs* GM	-0.348	0.192	1.190	0.075	1.020-1.360	15.930	<0.001	0.970	1.000	8

Abbreviations: ML, mediolateral breadth of the patella; BM, body mass; GM, geometic mean based on the four lengths measured on the patella; s.e., standard deviation; CI, confidence interval; Adj, adjusted; DF, degrees of freedom. α, $p < 0.05$, based on t-statistic for the coefficient.

all great apes with those of hylobatids and monkeys, the two latter groups show relatively longer and narrower patellae than great apes and humans (see also Fig. 49). Again, *Symphalangus* shows the extreme positive values along bgPC2, by having the highest relative patellar proximodistal length and lowest anteroposterior thickness. The MANOVA results reveal that, when the two first bgPC axes are considered

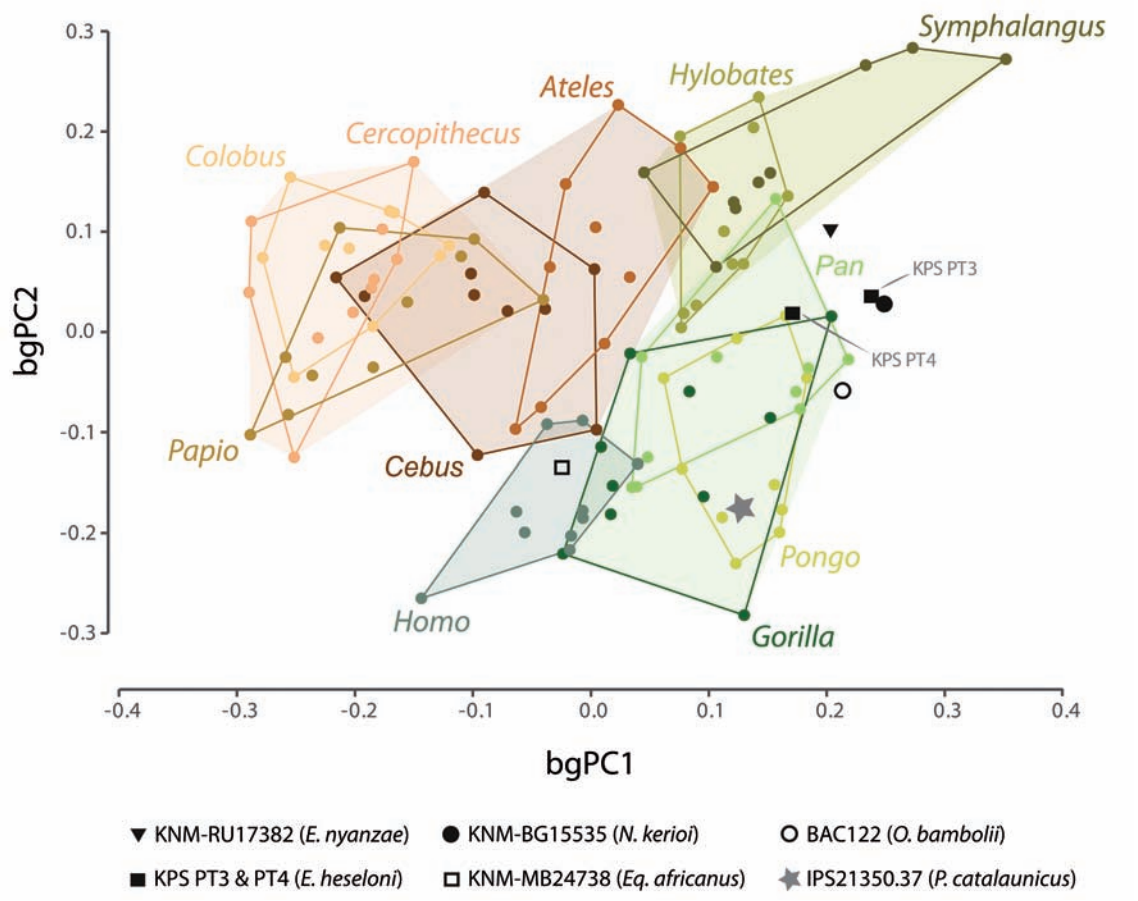

Figure 51 Between groups principal components analysis (bgPCA) performed on extant taxa and individual fossil patellae. The first two axes explain up to 91.6% of the total variance (bgPC1, 61.4%; bgPC2, 30.3%). Major taxonomic groups are indicated by colours as follows: orange, cercopithecoids; brown, platyrrhines; pistachio, hylobatids; light green, great apes; dark green, humans.

bgPCA		
	bgPC1	bgPC2
% variance	61.371	30.285
Variable loadings [a]		
PD	-0.18	**0.61**
PDAS	0.34	0.38
AP	**-0.73**	-0.41
ML	**0.57**	**-0.57**

Table 32 Results of the Between Groups Principal Components Analysis (bgPCA) based on patellar measurements. *Abbreviations:* bgPC, between-group principal component; PD, total proximodistal height of the patella; PDAS, proximodistal height of the articular surface; AP, anteroposterior thickness; ML, mediolateral breadth. **a**, Each original variable was size-adjusted by the geometric mean (GM) of the four variables and log-transformed (using natural logarithms) prior incorporation into the analysis. The variables with absolute loadings of 0.5 or more are marked in bold. Only the two first bgPC axes provided meaningful discrimination and are therefore shown.

together, statistical differences are also detected. Specifically, all cercopithecoid taxa are statistically different from the ape taxa, and *Symphalangus* shows differences with the remaining primate genera to the exception of *Hylobates* ($p < 0.001$). Modern humans display differences with apes and cercopithecoids ($p < 0.05$), but not with platyrrhines ($p = 1.000$; Table 32). Thus, to some degree, patellar shape differences (as identified by the bgPCA) relate to phylogeny. Great apes are more similar among them than to hylobatids, cercopithecoid taxa are more similar to each other than to great apes, and this is also the case of platyrrhine taxa. However, concerning bgPC1 (the axis that explains the highest amount of variance), cercopithecoids are more distinct from hominoids than are platyrrhines (intermediate between both).

Most fossil apes (the two species of *Ekembo*, *N. kerioi* and *O. bambolii*) fall close in the bgPC1-bgPC2 morphospace, highly overlapping with *Symphalangus* and great apes (mainly the specimens KPS PT4, BAC122 and KNM-RU17382) for bgPC1. These fossil apes occupy a central position along bgPC2, overlapping with extant apes and monkeys. BAC122 (*O. bambolii*) shows the lowest values among the above-mentioned Miocene apes, and KNM-RU 17382 (*E. nyanzae*) the highest. Overall, the patella of these Miocene apes is relatively thin anteroposteriorly and wide mediolaterally, in the uppermost range or just above the extant great ape range (bgPC1), and in the upper range of great apes for bgPC2 (by discounting one *Pan* outlier), but fully within the monkey range for the latter axis. Two fossil ape patellae depart from the others: KNM-MB24738 (*Eq. africanus*) and IPS21350.37 (*P. catalaunicus*). They show both lower bgPC1 (especially *E. africanus*) and bgPC2 values than the remaining Miocene apes. When both bgPC axes are inspected together, to the exception of KPS PT4 (*E. heseloni*, which overlaps with *Pan* and is also close to *Pongo*), the other *Ekembo* spp., *N. kerioi* and *O. bambolii* specimens fall in a unique region of the morphospace. *Equatorius africanus* shows its closest affinities with modern humans, and *P. catalaunicus* overlaps with *Pongo* and *Gorilla*.

POST HOC PAIRWISE COMPARISONS

	Cebus	*Ateles*	*Colobus*	*Cercopithecus*	*Papio*	*Hylobates*	*Symphalangus*	*Pongo*	*Pan*	*Gorilla*
bgPC1										
Ateles	*									
Colobus	*	**								
Cercopithecus	**	**	NS							
Papio	NS	**	NS	NS						
Hylobates	**	*	**	**	**					
Symphalangus	**	**	**	**	**	NS				
Pongo	**	**	**	**	**	NS	NS			
Pan	**	*	**	**	**	NS	NS	NS		
Gorilla	**	NS	**	**	**	NS	*	NS	NS	
Homo	NS	NS	**	**	**	**	**	**	**	*
bgPC2										
Ateles	NS									
Colobus	NS	NS								
Cercopithecus	NS	NS	NS							
Papio	NS	NS	NS	NS						
Hylobates	NS	NS	NS	NS	NS					
Symphalangus	**	NS	NS	*	**	NS				
Pongo	*	**	**	**	NS	**	**			
Pan	NS	*	*	NS	NS	**	**	NS		
Gorilla	**	**	**	**	*	**	**	NS	NS	
Homo	**	**	**	**	**	**	**	NS	NS	NS
MANOVA (bgPC1 and bgPC2)										
Ateles	*									
Colobus	*	**								
Cercopithecus	**	**	NS							
Papio	NS	**	NS	NS						
Hylobates	**	*	**	**	**					
Symphalangus	**	**	**	**	**	NS				
Pongo	**	**	**	**	**	NS	NS			
Pan	**	*	**	**	**	NS	NS	NS		
Gorilla	**	NS	**	**	**	NS	*	NS	NS	
Homo	NS	NS	**	**	**	**	**	**	**	*

Table 33 Significance for the ANOVA and MANOVA multiple post hoc comparisons (Bonferroni method) for scores of bgPC 1 and 2 according to extant primates genera. *Abbreviations:* bgPC, between-group principal component; NS, not significant; *, $p<0.05$; **, $p<0.01$.

Chapter 6
Patellar biomechanics during knee flexion

The knee is considered to be as one of the most complex joints of the mammalian body and is crucial for locomotion and weight bearing (e.g., Masourus *et al.* 2010). Thus, it has been extensively and deeply studied in humans, mainly through orthopaedic and clinical approaches (see some recent examples such as Garth 2001; Li *et al.* 2004; Masourus *et al.* 2010; Schindler and Scott 2011; Fitzpatrick *et al.* 2011, 2013, 2016; Adouni *et al.* 2012; Stephen *et al.* 2013; Zabala *et al.* 2013; and Smoger *et al.* 2015). Despite all the information generated from extensive study, the kinetic behaviour of the human knee joint still remains not fully understood (Engel *et al.* 2011). In particular, very little attention has been paid to the study of the non-human primate (NHP) knee biomechanics, and most of the (still little) research is largely focused on mere anatomical descriptions (e.g., Diogo *et al.* 2012, 2013; Ingham *et al.* 2015), bone shape and functional morphology (e.g. Kumakura 1989; Lovejoy 2007), or more theoretical approximations (e.g., Preuschoft 1970; Badoux 1974; Preuschoft and Tardieu 1996). Nonetheless, the last years have seen the emergence of a number of *in vivo* and experimental studies of primate locomotion that have also yielded interesting data on this joint (such as muscle architecture, moment arms, joint angles, or forces acting about the knee; Larson *et al.* 2001; Larney and Larson 2004; Schmidt 2005; Wunderlich and Shaum 2007; Polk *et al.* 2009; Channon *et al.* 2010a; Demes 2011; Sellers *et al.* 2013; among others).

Although the patella has an important role in knee biomechanics (as observed in humans), its analysis has been frequently neglected as compared to the preferential study of the distal femur and/or the proximal tibia. Moreover, and importantly, few works focus on fossil patellar remains beyond the description of the bone. There are some recent analyses that have outlined patellar shape differences among living primates, and between these and fossil taxa, as well as the relation of the patella to the knee joint function in NHP primates (see Chapter 5; Ward *et al.* 1995; DeSilva *et al.* 2013). Because the acquisition of bipedalism involves a number of anatomical changes, including several within the knee (e.g., increasing of the femoral bicondylar angle; Lovejoy 2007), the study of that joint in living NHP, especially fossil apes, is essential to better comprehend the evolutionary context of modern human bipedalism and its anatomical specialization.

The increasing application of innovative techniques in palaeontology, mostly derived from the engineering fields, allows for a more precise and accurate study of the structure, function and interactions of biologically important structures (e.g., bones, teeth, tendons) than traditional techniques (e.g., linear morphometric analysis). These new techniques provide the opportunity to virtually work with the

structures through the modification of their digital models, thus opening the possibility of testing the effect of specific morphological and evolutionary changes. Finite element analysis (FEA) is a mathematical modelling technique that has emerged as a useful tool in vertebrate palaeontology to study the mechanical role of biological structures, such as skulls (Fortuny *et al.* 2015), jaws (Serrano-Fochs *et al.* 2015), postcranial bones (Bishop *et al.* 2015), teeth (DeMiguel *et al.* 2006, 2015), claws (Lautenschlager 2014), and many others. The generation of FE models could help us to understand the behaviour of the different knee joint components under dynamic loading, as evidenced by applied work to the human knee to analyse the performance of the patella (Engel *et al.* 2011; Fitzpatrick *et al.* 2011; Fitzpatrick and Rullkoetter 2012). As far as it is known, this is the first work in where NHP patellae are analysed through FEA.

The first aim of this work is therefore to test the mechanical role of some specific patellar traits (i.e., anteroposterior thickness and proximodistal height), as well as the behaviour of the patellar apex (that is, the distal peak of the bone). Secondly, this specific study also focus on tracking the evolutionary scenario of the apex and the mechanical role of the patella in the origin and evolution of orthograde positional behaviours (e.g., vertical climbing and below-branch suspension) within the Hominoidea. To do so, the patellae of two Miocene taxa were included for analysis, the putative stem catarrhine *Epipliopithecus vindobonensis* (Zapfe 1958, 1960) and the great ape *Pierolapithecus catalaunicus* (Moyà-Solà *et al.* 2004). Hence, to address these points, the following three aims are inspected using finite element methods:

Table 34 Number of nodes and elements of the three-dimensional (3D) models of the primate patellae. Nature of the models refers to living (extant) or extinct (fossil) primates, and patellar 3D models that have been digitally transformed in this study (modified). See text for further explanation on abbreviations of modified patellae.

MESHES GEOMETRY					
Patellar model	**Species**	**Catalogue no.**	**Nature**	**Nodes**	**Elements**
Cebus	*Cebus olivaceus*	AMNH42873	Extant	394,422	265,287
Ateles	*Ateles belzebuth*	AMNH259	Extant	331,604	221,888
Cercopithecus	*Cercopithecus mitis*	AMNH52402	Extant	270,139	181,383
Mandrillus	*Mandrillus sphinx*	AMNH89358	Extant	427,434	285,657
Colobus	*Colobus guereza*	AMNH52241	Extant	446,929	300,227
Hylobates	*Hylobates lar*	MCZ41412	Extant	403,089	268,374
Symphalangus	*Symphalangus syndactylus*	AMNH106581	Extant	439,722	295,965
Pongo	*Pongo pygmaeus*	AMNH62586	Extant	368,020	247,551
Pan	*Pan troglodytes*	MCZ23164	Extant	383,969	256,695
Gorilla	*Gorilla gorilla*	AMNH9029	Extant	363,359	246,392
Homo	*Homo sapiens*	SBU collection	Extant	356,758	240,169
Cercopithecus-ThinAP	-	-	Modified	260,199	173,600
Symphalangus-ThickAP	-	-	Modified	376,202	248,887
Gorilla-HighPD	-	-	Modified	436,513	296,334
Cercopithecus-NoApex	-	-	Modified	272,467	182,826
Gorilla-WApex	-	-	Modified	428,921	289,836
Pongo-WApex	-	-	Modified	327,870	218,663
Epipliopithecus	*Epipliopithecus vindobonensis*	NHMW1970/1397/0024	Fossil	374,517	249,422
Pierolapithecus	*Pierolapithecus catalaunicus*	IPS21350.37	Fossil	337,482	224,277

(1) Because both African and Asian great apes mainly rely on orthograde behaviours (vertical climbing and below-branch suspension, among others; Isler 2005; Crompton *et al.* 2010; Fleagle 2013) and they are the only primates that lack the patellar apex, here it is tested whether the apex (which is characteristic of pronograde quadruped primates, hylobatids, and modern humans) might have a mechanical role primarily related to specific requirements of quadrupedalism.

(2) The presence of an apex in humans and hylobatids (gibbons and siamangs), which is absent in both great apes and the stem hominid *P. catalaunicus*, raises the interesting question as to why modern humans have this structure in their patella (retained or reversed). Thus, it is also explored whether the mechanical and/or structural role of the patellar apex in humans is similar (or not) to that of quadrupeds.

(3) Several functions have been attributed to the human patella (Heegaard *et al.* 1995; Sarin *et al.* 1999): (*i*) improve the efficiency of the extensor forces during knee flexion (which entails a biomechanical advantage); (*ii*) centralize the forces of the different components of the *quadriceps* muscle complex; (*iii*) provide a smooth sliding mechanism for the *quadriceps* muscle (protection of the tendons); and (*iv*) indirectly contribute to the global stability of the knee. Considering that, apart from these functions, variation of some morphological parameters in NHP (e.g., anteroposterior thickness, AP, and proximodistal height, PD) might be apparently associated with increasing the torque of the joint during knee extension by lengthening the moment arm of the involved muscles and thus optimizing the extension of the knee, the last hypothesis to test is whether the variation of AP and PD influence the patellar stress distribution.

The goal of these aims is to deepen our knowledge of the structure, function and biomechanical meaning of the patella (and its apex) and its response to knee flexion through an innovative FEA, as well as to inspect the functional role of the apex and the patellar shape of primates from an evolutionary viewpoint, especially within the Hominoidea.

COMPARATIVE SAMPLE

The material studied consists of 11 different patellar three-dimensional (3D) models of living primate species (Fig. 52; Table 34). The sample comprises all major taxonomic groups of primates and includes platyrrhines (*Cebus* and *Ateles*), cercopithecines (*Cercopithecus* and *Mandrillus*), colobines (*Colobus*), lesser apes (*Hylobates* and *Symphalangus*), Asian (*Pongo*) and African (*Pan* and *Gorilla*) great apes, and modern humans (*Homo*). Moreover, two of the best-known Miocene taxa were added to the sample, *Epipliopithecus vindobonensis* and *Pierolapithecus catalaunicus*, which allow us to inspect the biomechanical evolutionary scenario of the patellar shape and its apex. *Epipliopithecus vindobonensis* is a stem catarrhine (early middle Miocene), which preserves abundant postcranial remains that belong to several individuals (including two patellae that show a distal apex; Zapfe 1960). *Pierolpithecus catalaunicus* is a stem hominid (late middle Miocene) that is considered the first unambiguous evidence of an orthograde great ape and is therefore

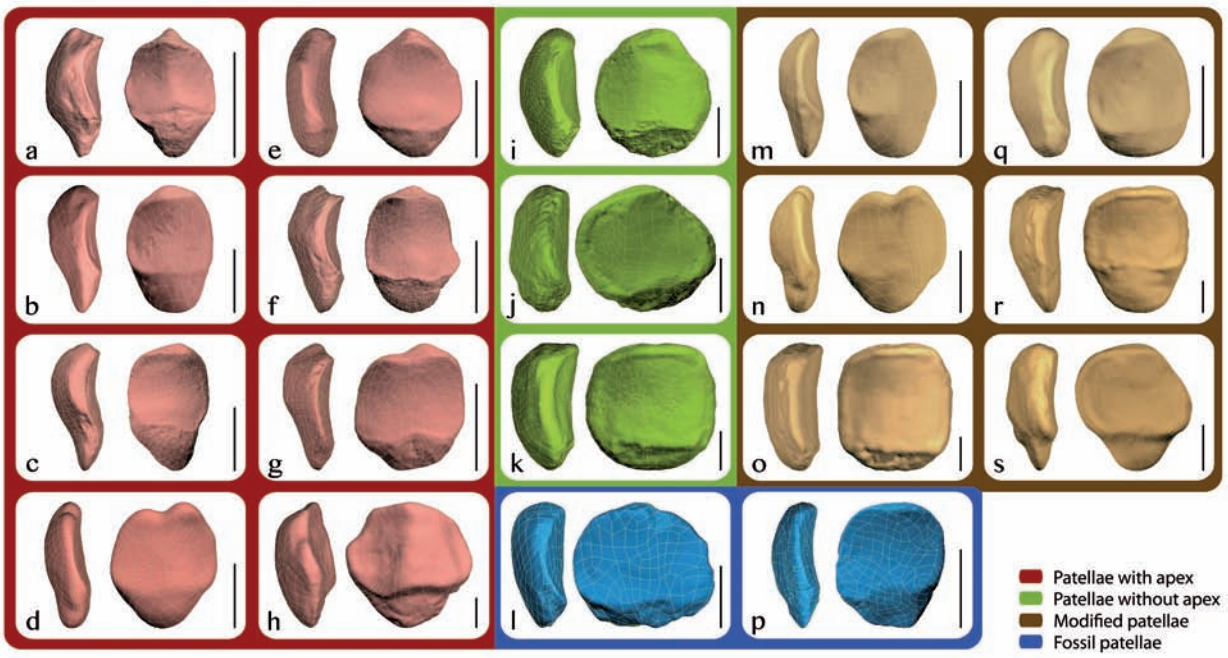

Figure 52 Snapshots of CAD (computer-aided design) models of the patellae included in this work in lateral (left) and posterior (right) views. **a**, *Cebus olivaceus*; **b**, *Cercopithecus mitis*; **c**, *Colobus guereza*; **d**, *Symphalangus syndactylus*; **e**, *Ateles belzebuth*; **f**, *Mandrillus sphinx*; **g**, *Hylobates lar*; **h**, *Homo sapiens*; **i**, *Pan troglodytes*; **j**, *Pongo pygmaeus*; **k**, *Gorilla gorilla*; **l**, *Pierolapithecus catalaunicus*; **m**, *Cercopithecus*-ThinAP; **n**, *Symphalangus*-ThickAP; **o**, *Gorilla*-HighPD; **p**, *Epipliopithecus vindobonensis*; **q**, *Cercopithecus*-NoApex; **r**, *Gorilla*-WApex; **s**, *Pongo*-WApex. Scale bar = 10 mm.

key for understanding the origins of orthogrady within the Hominidae (Moyà-Solà *et al.* 2004; Alba 2012). Among more than 80 fossil remains recovered for *P. catalaunicus*, the only complete (non-pedal) hindlimb remain is that of a left patella (without distal apex; Moyà-Solà *et al.* 2004).

THE FE METHOD

The FE method (Zienkiewicz 1971; Zienkiewicz *et al.* 2005) was used to inspect the patellar response to knee flexion in a group of living and fossil primates, and assess the effects of morphological change in several virtually modified models.

Knee modelling

In order to accurately analyse the primate knee biomechanical behaviour, a brief summary of the most relevant anatomical and mechanic traits related to the patella and its relation with the other knee elements are provided below. Given that the NHP knee kinematics is still largely unknown, as noted above, the human knee is taken as reference to construct the model. Thus, the human patella is embedded within the ligaments and muscles of the *quadriceps* complex and the synovial capsule of the joint (Platzer 2008). During motion, the contact area between the articular surface of the posterior side of the patella and that

on the anterior side of the femur (patellar groove) varies depending on the degree of flexion of the knee, moving proximally in both the distal femur and the patella when the knee flexes (Nisell 1985; Masouros *et al.* 2010; Schindler and Scott 2011). Furthermore, there exists a lateral movement of the patella during knee flexion, quantified as the Q angle and defined as the angle between the line of action of the patellar ligament, and the resultant line of the action of the *quadriceps* muscle. This angle ranges between 12-18º in humans with the knee extended, and decreases during flexion (Masouros *et al.* 2010). Moreover, the existence of the Q angle implies that the contact area between the articular surface of the femur and the patella changes, moving to the lateral side of the patellar articular surface and becoming more discontinuous proximally (when the knee is completely flexed; Masouros *et al.* 2010; Schindler and Scott 2011).

From a kinematic viewpoint, forces in the patello-femoral joint are a function of the *quadriceps* muscle force, and the angle of flexion of the knee (Schindler and Scott 2011). The most superficial parts of the patella are in tension due to the action of two opposite forces, that of the *quadriceps* muscle and that of the patellar ligament (Oxnard 1971; see Nisell 1985: Fig. 1 for a diagram of forces acting in a semi-flexed knee, as well as further explanation of the knee kinematic model used in this work; see below). The compression of the femur against the patella during knee flexion generates a patellar reaction force (PRF) that increases progressively (Nisell 1985; Lovejoy 2007; Masouros *et al.* 2010).

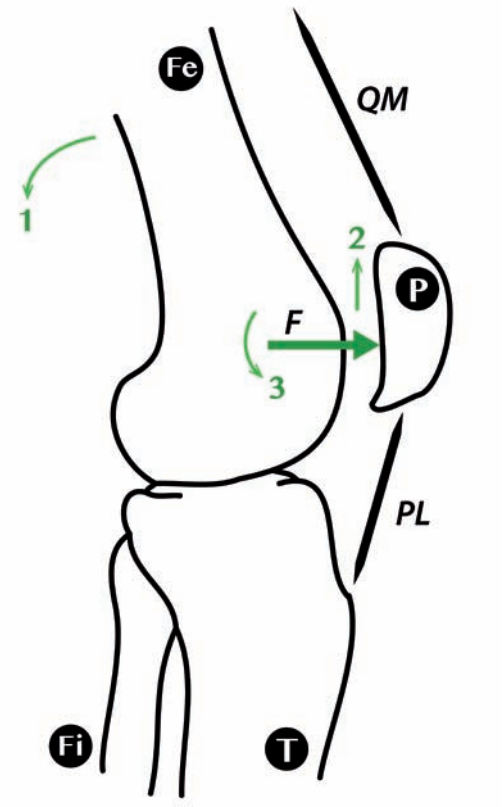

Figure 53 Schematic representation of the knee kinematic model used to perform the finite element analyses (see text for a more extended explanation of the model). The patella (P) is constrained by the quadriceps muscle (QM) and patellar ligament (PL) areas of attachment. Contact between the femur (Fe) and the patella generates a force (F). This force acts in the distal part of the articular surface of the patella when the knee is extended. When the joint flexes (**1**), the force (contact) moves proximally (**2**) and its angle of actions changes (**3**). T, tibia; Fi, fibula.

The most important issue for generating a rigorous knee model relates to the inherent complexity of this joint, the number of elements that compounds it, and the six degrees of freedom between the femur and the tibia (Heegaard *et al.* 1995; Masouros *et al.* 2010). In order to create an easy-to-analyse, yet realistic and comparable model, the human knee joint was simplified in the modelling approach implemented here. Specifically, only the solid elements (bones) and basic forces acting in the knee during its flexion (Fig. 53) were modelled. The kinematic model results in two forces that stretch the patella in opposite directions due to the action of the *quadriceps* muscle (QM) and the patellar ligament (PL), and a third reaction force (PRF) resulted from the contact between the patellar and femoral articular surfaces (Fig.

53). The direction of PRF also changes with the flexion of the knee, from been almost perpendicular to the main axis of the patella to acute (related to the horizontal line) in a flexed position (Fig. 53). Lateral movement of the patella during flexion (Q angle) has not been included in this work in order reduce the potential incorporation of error into the model and because no angle data are available for the selected NHP sample at this point in time.

Model construction

The first requirement for successful FE analyses is to generate a sufficiently accurate geometric model of the structure of interest. Thus, 3D models of patellae were obtained from both superficial laser scanning or extracting the surface from computed tomography scans. Models were imported to the software *Geomagic Studio* 2012 to repair and refine the surface meshes. The polygonal models were converted to CAD models using engineering techniques (Marcé-Nogué *et al*. 2011), which converts the hollow polygonal models intro solid objects. Irregularities in the new CAD models were repaired again with refinement and smoothing tools from the softwares *Geomagic Studio* 2012 and *Rhinoceros* 5.0. Final FE models were meshed with an adaptive mesh of 10-noded tetrahedral elements (Marcé-Nogué *et al.* 2015). Thus, a mesh of level of accuracy and density was created in order to capture the stress and displacement patterns and variations, and assure the stability of the results (Dumont *et al*. 2009; Tseng and Flynn 2014). Final geometry properties of the 19 patellae models are listed in Table 34.

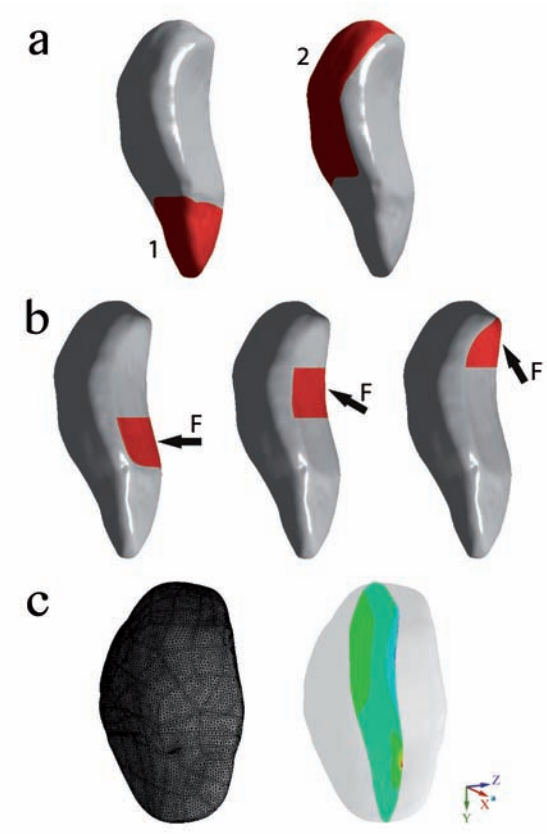

Figure 54 3D models of primate patellae were transformed to CAD objects to implement the model depicted in Figure 53 and extensively explained in the text. **a**,In every CAD model boundary conditions were applied: 1, patellar ligament attachment area; and 2, quadriceps muscle attachment area. **b**, Likewise, the force (F) was applied in different areas and with different directions (black arrows) that represent three steps of knee flexion (joint extended, left; semi-flexed knee, centre; full-flexed knee, right). **c**, Finally, a sagittal image in the mediolateral midpoint (right) of each patellar model (left) was selected for comparison.

Material properties

The second step in a successful FEA is a realistic estimate of the material properties of the structure being modelled. Isotropic, homogeneous and linear elastic properties have been assumed for the models. Mechanical properties of human patellae cortical bone were applied following Heegaard *et al.* (1995): Young's modulus E = 150 GPa, and Poisson ratio ν = 0.3. It must be stressed, however, that these values are not crucial for this study due to its comparative

nature, since the equations of the elasticity used in FEA for linear isotropic and homogeneous materials do not affect stress patterns (DeMiguel *et al.* 2015; Gil *et al.* 2015).

Constraints and loading conditions

The third requirement for successful FE modelling is to apply realistic forces to the models. Thus, in order to virtually implement the knee kinematic model, the areas of attachment of the *quadriceps* muscle and the patellar ligament were selected as constrained regions (Fig. 54a). The articular surface of the patella was divided in three strips to simulate the proximal displacement of the patellofemoral contact (Fig. 54b), from extended (distal strip), to semi-flexed (central strip), and fully-flexed joint (proximal strip). In each of the steps of flexion (i.e., every strip), a pressure (F) was applied with an increased angle related to the anteroposterior horizontal line: 0º (extended knee), 30º (semi-flexed knee), and 60º (full-flexed knee; Fig. 54b).

Forces scaling

A mandatory requirement for a realistic comparison of the models being studied when they differ in size is force scaling. Patellae 3D models included in this study are very diverse in size, ranging from the smallest *Cebus olivaceus* patella (mean body weight of the species ~3 kg; Smith and Jungers 1997) to that of *Gorilla gorilla* (mean body weight of the species ~121 kg, although males can weigh more than 170 kg; Smith and Jungers 1997), with that of the latter being more than 40 times larger in volume than that of *Cebus*. Therefore, the forces applied to the different patellae were scaled (as originally proposed by Dumont *et al.* 2009) to avoid size effects on the results and focus exclusively on the patellar shape role during knee flexion. Scaled forces were calculated by adapting the formulations proposed by Marcé-Nogué *et al.* (2013) to 3D models and following Fortuny *et al.* (2015) to make the patellar models comparable among them. Equation 1 and 2 show the formulation used to calculate the scaled forces applied to the models for von Mises stress (equation 1) and displacement (equation 2) responses.

Equation 1

$$F_A = \left(\sqrt[3]{\frac{V_A}{V_B}}\right)^2 F_B$$

Equation 2

$$F_A = \left(\sqrt[3]{\frac{V_A}{V_B}}\right) F_B$$

Cercopithecus patella was taken as reference model with an arbitrary force value of 1 N. Thereby, F_B and V_B are the force and volume of the reference model, respectively; and F_A and V_A the force and volume of the scaled model. Scaled values for the 19 patellae models are listed in Tables 35 (stress) and 36 (displacements).

Table 35 Scaled forces (in Newtons) based on patellae volume (in mm³) and calculated following *Equation 1* to stress comparisons among patellar models in each of the three steps of knee flexion: extended knee (0º), semi-flexed knee (30º), and full-flexed knee (60º).

SCALED FORCES VON MISSES STRESS								
			F extended knee		F semi-flexed knee		F full-flexed knee	
Patellar model	**Volume**	**Applied F**	**X**	**Y**	**X**	**Y**	**X**	**Y**
Cebus	312.44	0.599	0.599	0.000	0.519	0.299	0.299	0.519
Ateles	880.48	1.195	1.195	0.000	1.035	0.597	0.597	1.035
Cercopithecus	674.12	1.000	1.000	0.000	0.866	0.500	0.500	0.866
Mandrillus	1,019.80	1.318	1.318	0.000	1.141	0.659	0.659	1.141
Colobus	1,118.50	1.402	1.402	0.000	1.214	0.701	0.701	1.214
Hylobates	556.05	0.880	0.880	0.000	0.762	0.440	0.440	0.762
Symphalangus	1,258.80	1.516	1.516	0.000	1.313	0.758	0.758	1.313
Pongo	4,240.00	3.407	3.407	0.000	2.951	1.704	1.704	2.951
Pan	4,353.40	3.468	3.468	0.000	3.003	1.734	1.734	3.003
Gorilla	12,892.00	7.151	7.151	0.000	6.193	3.576	3.576	6.193
Homo	12,719.00	7.087	7.087	0.000	6.138	3.544	3.544	6.138
Cercopithecus-ThinAP	529.16	0.851	0.851	0.000	0.737	0.425	0.425	0.737
Symphalangus-ThickAP	1,323.50	1.568	1.568	0.000	1.358	0.784	0.784	1.358
Gorilla-HighPD	15,532.00	8.097	8.097	0.000	7.012	4.049	4.049	7.012
Cercopithecus-NoApex	623.70	0.949	0.949	0.000	0.822	0.475	0.475	0.822
Gorilla-WApex	14,590.00	7.766	7.766	0.000	6.726	3.883	3.883	6.726
Pongo-WApex	4,419.50	3.503	3.503	0.000	3.034	1.751	1.751	3.034
Epipliopithecus	774.55	1.097	1.097	0.000	0.950	0.549	0.549	0.950
Pierolapithecus	2,405.10	2.335	2.335	0.000	2.022	1.167	1.167	2.022

Abbreviations: F, force; X, force applied in X direction; Y, force applied in Y direction. See text for further explanation on abbreviations of modified patellae.

FE analyses and results.- The final step in the process was to obtain and analyse the results. Thus, a structural static analysis was performed for the 19 patellae models using *ANSYS* 15.0 FE package. In order to compare the models, von Mises stress and displacement distribution maps were obtained. Von Mises stress was selected since it directly measures how the state of stress at any point distort the material and consequently it is an adequate criterion for predicting the yield of ductile materials when isotropic material properties are used in the organic bone (Doblaré *et al.* 2004; Dumont *et al*. 2009). To aid visualization and comparison of results, a sagittal slice at the mediolateral midpoint of the 19 patellae was selected for each model (Fig. 54c).

EXPERIMENTAL FE ANALYSES

In order to inspect the biomechanical role of the patellar shape during dynamic knee flexion and explore the three aims mentioned above, the following changes were virtually applied to some models. Firstly, the patellar apex was digitally removed or added: it was removed in the pronograde quadruped *Cercopithecus* (*Cercopithecus*-NoApex)—thus allowing to check the biomechanical response of a patella

Table 36 Scaled forces (in Newtons) based on patellae volume (in mm^3) and calculated following *Equation 2* to displacements comparisons among patellar models in each of the three steps of knee flexion: extended knee (0º), semi-flexed knee (30º), and full-flexed knee (60º).

SCALED FORCES DISPLACEMENT								
			F extended knee		F semi-flexed knee		F full-flexed knee	
Patellar model	**Volume**	**Applied F**	**X**	**Y**	**X**	**Y**	**X**	**Y**
Cebus	312.44	0.774	0.774	0.000	0.670	0.387	0.387	0.670
Ateles	880.48	1.093	1.093	0.000	0.947	0.547	0.547	0.947
Cercopithecus	674.12	1.000	1.000	0.000	0.866	0.500	0.500	0.866
Mandrillus	1,019.80	1.148	1.148	0.000	0.994	0.574	0.574	0.994
Colobus	1,118.50	1.184	1.184	0.000	1.025	0.592	0.592	1.025
Hylobates	556.05	0.938	0.938	0.000	0.812	0.469	0.469	0.812
Symphalangus	1,258.80	1.231	1.231	0.000	1.066	0.616	0.616	1.066
Pongo	4,240.00	1.846	1.846	0.000	1.599	0.923	0.923	1.599
Pan	4,353.40	1.862	1.862	0.000	1.613	0.931	0.931	1.613
Gorilla	12,892.00	2.674	2.674	0.000	2.316	1.337	1.337	2.316
Homo	12,719.00	2.662	2.662	0.000	2.306	1.331	1.331	2.306
Cercopithecus-ThinAP	529.16	0.922	0.922	0.000	0.799	0.461	0.461	0.799
Symphalangus-ThickAP	1,323.50	1.252	1.252	0.000	1.084	0.626	0.626	1.084
Gorilla-HighPD	15,532.00	2.846	2.846	0.000	2.464	1.423	1.423	2.464
Cercopithecus-NoApex	623.70	0.974	0.974	0.000	0.844	0.487	0.487	0.844
Gorilla-WApex	14,590.00	2.787	2.787	0.000	2.413	1.393	1.393	2.413
Pongo-WApex	4,419.50	1.872	1.872	0.000	1.621	0.936	0.936	1.621
Epipliopithecus	774.55	1.047	1.047	0.000	0.907	0.524	0.524	0.907
Pierolapithecus	2,405.10	1.528	1.528	0.000	1.323	0.764	0.764	1.323

Abbreviations: F, force; X, force applied in X direction; Y, force applied in Y direction. See text for further explanation on abbreviations of modified patellae.

without apex in a taxon with preferential movements of the hindlimb in the parasagittal plane and emphasis on flexion-extension of the knee joint; and, otherwise, virtually added in the orthograde great apes *Gorilla* (*Gorilla*-WApex) and *Pongo* (*Pongo*-WApex)—in order to inspect whether the apex modifies biomechanical response of the patella during dynamic loading of the joint in two taxa that show a wider range of knee motion, but differential locomotor affinities (gorillas are orthograde quadrupeds that preferentially engage in knuckle-walking, whereas orangutans are specialized orthograde suspensors and clambers).

Secondly, previous authors (Ward *et al.* 1995; see also Chapter 5) have stressed the differential patellar shape of major taxonomic primate groups and its functional relation to locomotor types. Among the most relevant patellar parameters, anteroposterior thickness (AP) and proximodistal height (PD) have been related to the effectiveness of knee extension (Nisell 1985; Harrison 1986; Ward *et al.* 1995). Thus, AP would influence the length of the patellar tendon moment arm, whereas PD would participate in the lever arm length associated with the *quadriceps* muscle complex (Badoux 1974; Nisell 1985; Ward *et al.* 1995). To inspect how these parameters (patellar shape changes) affect the biomechanical patellar response to knee flexion, the *Cercopithecus* patella was anteroposteriorly tightened (*Cercopithecus*-ThinAP) while that of *Symphalangus* was anteroposteriorly swollen (*Symphalangus*-ThickAP). Moreover, the patella of *Gorilla* was proximodistally lengthened (*Gorilla*-HighPD).

RESULTS

Results for living primate patellae are depicted in Figures 55 (von Misses stress) and 56 (displacements), which show the mid-sagittal section of the bone. Likewise, results of fossil *Ep. vindobonensis* and *P. catalaunicus* are shown in Figures 57 and 58; and those for modified patellae are presented in Figures 59 and 60.

Von Mises stress

The obtained results show that there is not a great difference in the biomechanical response of patellae according to locomotor modes. However, some significant differences on von Mises stress distribution are observed in relation to types of body plan. Overall, von Mises stress values increase in all instances from an extended posture of the knee (i.e., forces with 0º) to complete flexion (force tilted 60º; Fig. 55).

All the models with an apex (Fig. 55a-h) show a similar pattern of stress distribution in the proximal half of the patella. Stress in this area is almost absent in the extended joint, and increases with flexion,

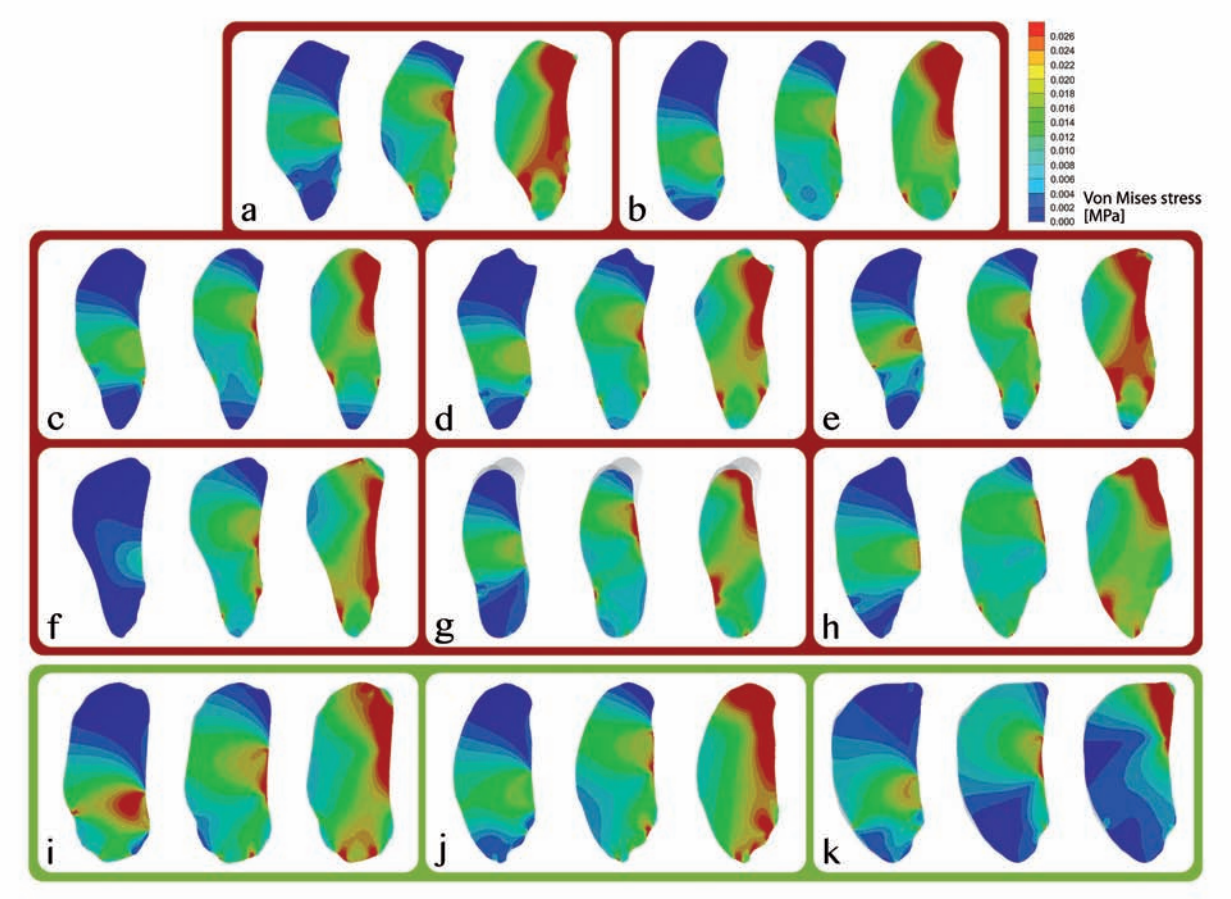

Figure 55 Von Mises stress (in MPa) results in the mid-sagittal section of the patella of extant primates (top, superior; left, anterior) during extended knee (left), semi-flexed knee (middle), and full-flexed knee (right). **a**, *Cebus*; **b**, *Ateles*; **c**, *Cercopithecus*; **d**, *Mandrillus*; **e**, *Colobus*; **f**, *Hylobates*; **g**, *Symphalangus*; **h**, *Homo*; **i**, *Pongo*; **j**, *Pan*; and **k**, *Gorilla*. Colours group patellae with apex (red): anthropoid monkeys (platyrrhines and cercopithecoids), hylobatids (gibbons and siamangs) and humans; and without apex (green): African and Asian great apes. Results were homogenized according to the same stress scale (minimum = 0 MPa; maximum = 0.026 MPa).

especially in the anterior side of the bone. It must be noted that stress distribution within the section follows the direction of the applied force, that is, the highest stress values are more tilted relatively to the horizontal when the knee is fully flexed. However, more significant differences are found in the stress results in the distal half of the bone for this group. In pronograde taxa (*Cebus*, *Ateles*, *Cercopithecus*, *Mandrillus*, and *Colobus*), the highest stress values are found in the posterior side of the patellae, from the proximal end to part of the distal half, in semi- and full-flexed positions of the knee. Furthermore, the most distal region of the apex supports low stress during the three phases of flexion, which is particularly evident in *Cercopithecus* and *Colobus* (Fig. 55c,e). Contrarily, high stress values extend more broadly (mainly anteroposteriorly) through the whole bone in orthograde taxa with apex (*Hylobates*, *Symphalangus* and *Homo*), although they are especially concentrated in the posterodistal side of the distal half and in the anteroproximal corner of the proximal half. In addition, the apex of these taxa show more stressed apices (Fig. 55f-h). Surprisingly, *Hylobates* patella is almost free of stress during its extended knee phase, while approximates in somehow to the pattern of pronograde taxa in a fully flexed position (posterior side of the bone with high stress values also distributed along the distal half; Fig. 55f).

With regard to models without apex (*Pongo*, *Pan*, and *Gorilla*; Fig. 55i-k), *Gorilla* is mechanically very

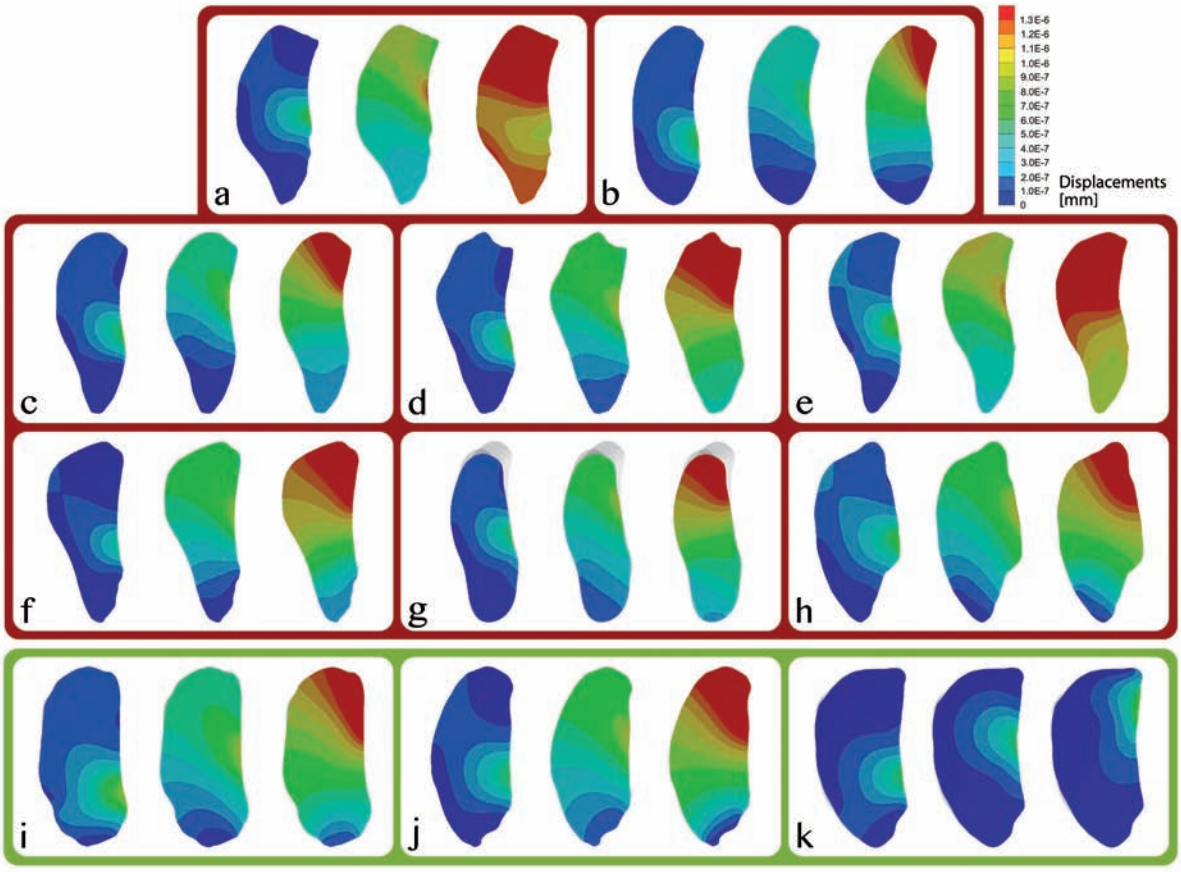

Figure 56 Displacement (in mm) results in the mid-sagittal section of the patella of extant primates (top, superior; left, anterior) during extended knee (left), semi-flexed knee (middle), and full-flexed knee (right). **a**, *Cebus*; **b**, *Ateles*; **c**, *Cercopithecus*; **d**, *Mandrillus*; **e**, *Colobus*; **f**, *Hylobates*; **g**, *Symphalangus*; **h**, *Homo*; **i**, *Pongo*; **j**, *Pan*; and **k**, *Gorilla*. Colours group patellae with apex (red): anthropoid monkeys (platyrrhines and cercopithecoids), hylobatids (gibbons and siamangs) and humans; and without apex (green): African and Asian great apes. Results were homogenized according to the same displacement scale (minimum = 0 mm; maximum = 1.3×10^{-6} mm).

different from the remaining taxa. In all the phases of knee flexion, high stress values are concentrated in those regions where forces are applied, showing broad areas that are absent of stress (Fig. 55k). Otherwise, the overall stress distribution in *Pongo* and *Pan* is more similar to that of *Homo*, with a broad

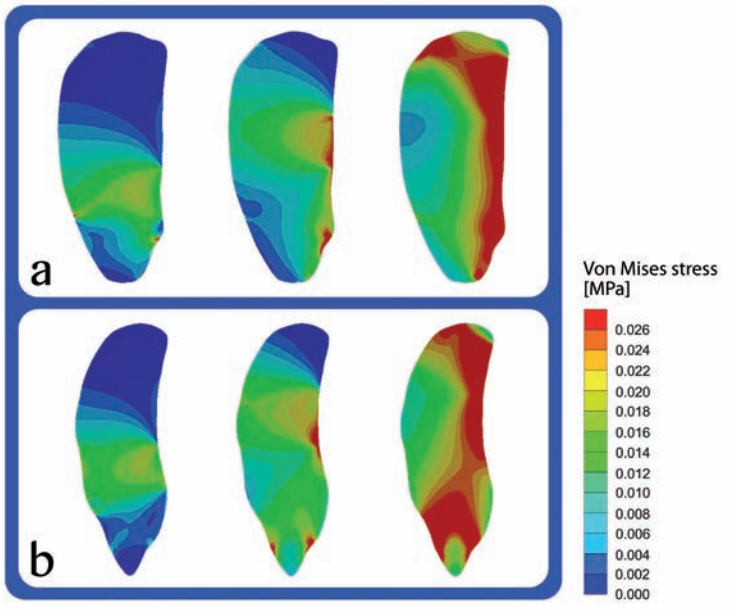

Figure 57 Von Mises stress (in MPa) results for the **a**, *Pierolapithecus catalaunicus* and **b**, *Epipliopithecus vindobonensis* patellae during extended knee (left), semi-flexed knee (middle), and full-flexed knee (right). Mid-sagittal section (top, superior; left, anterior). Stress scale is homogenized accordingly with that of Figure 55.

anteroposterior distribution of high stress, highest values concentrated in the posterior side and the distal areas of the patellae (besides, stress increases with a progressive flexion of the knee; Fig. 55i,j). Moreover, the distribution of the highest stress values in *Pongo* and *Pan* in the first two phases of knee flexion is almost horizontal and only changes the direction in the full-flexed knee simulation (in the patellae with apex this distribution more clearly follows the direction of the applied force).

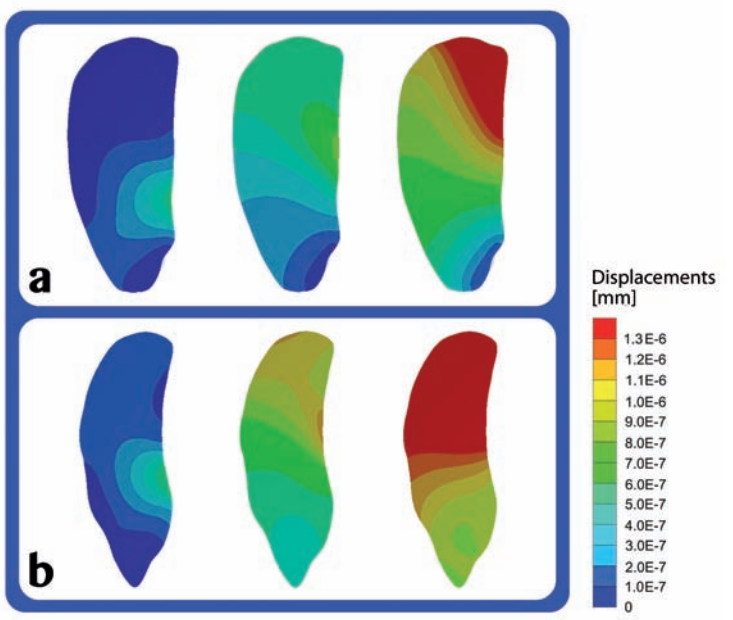

Figure 58 Displacement (in mm) results for the **a**, *Pierolapithecus catalaunicus* and **b**, *Epipliopithecus vindobonensis* patellae during extended knee (left), semi-flexed knee (middle), and full-flexed knee (right). Mid-sagittal section (top, superior; left, anterior). Displacement scale is homogenized accordingly with that of Figure 56.

Stress results for fossil primates.- The stress pattern for *P. catalaunicus* (Fig. 57a) is found to be similar to that of extant *Pongo* and *Pan*, thus showing high stress values distributed across the proximal and distal

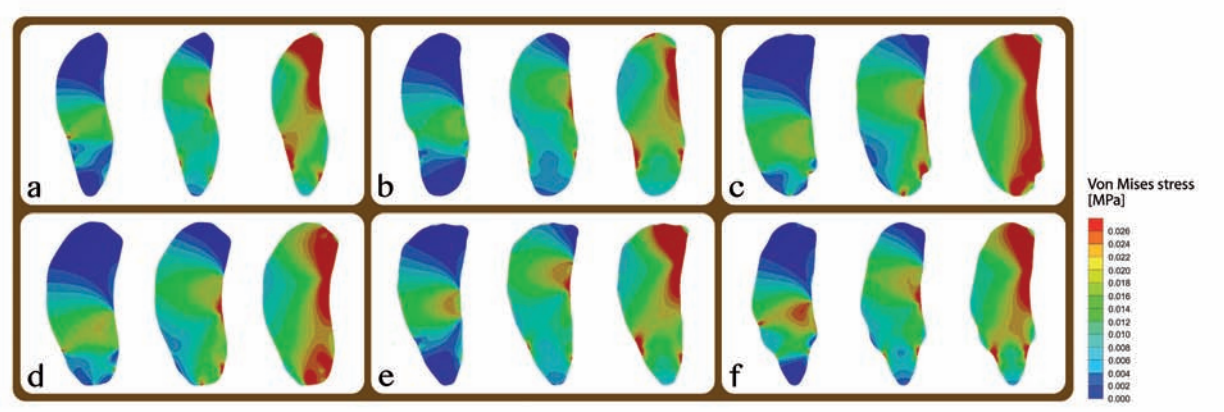

Figure 59. Von Mises stress (in MPa) results in the mid-sagittal section of the modified patella (top, superior; left, anterior) during extended knee (left), semi-flexed knee (middle), and full-flexed knee (right). **a**, *Cercopithecus*-ThinAP; **b**, *Symphalangus*-ThickAP; **c**, *Gorilla*-HighPD; **d**, *Cercopithecus*-NoApex; **e**, *Gorilla*-WApex; and **f**, *Pongo*-WApex. See text for further explanation on modified patellae abbreviations. Stress scale is homogenized accordingly with that of Figure 55.

half of the bone (mainly during full flexion) and concentrated in the posterior side. The *Ep. vindobonensis* patella exhibits instead a stress patter distribution, which is more similar to that of extant taxa with apex (Fig. 57b). More specifically, it is similar to pronograde taxa with apex in the distribution of the stress in

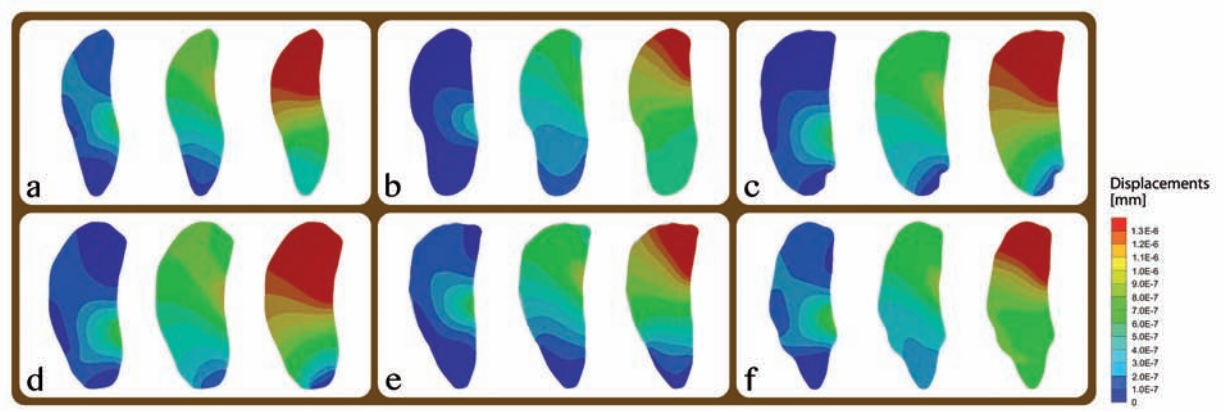

Figure 60 Displacement (in mm) results in the mid-sagittal section of the modified patella (top, superior; left, anterior) during extended knee (left), semi-flexed knee (middle), and full-flexed knee (right). **a**, *Cercopithecus*-ThinAP; **b**, *Symphalangus*-ThickAP; **c**, *Gorilla*-HighPD; **d**, *Cercopithecus*-NoApex; **e**, *Gorilla*-WApex; and **f**, *Pongo*-WApex. See text for further explanation on modified patellae abbreviations. Displacement scale is homogenized accordingly with that of Figure 56.

the proximal half, although the apex exhibits high stress values as observed in the case of orthograde species. Furthermore, the stress distribution in the posterior edge of the *Ep. vindobonensis* patella is closer related to *Colobus* or *Hylobates*, with extension of the high values onto the distal half of the bone.

Experimental FE models results.- When some of the original patellar parameters are modified, it is observed a change in the stress distribution patterns (Fig. 59). First, when the anteroposterior thickness is altered, *Cercopithecus*-ThinAP is found to exhibit a more similar stress pattern to that of *Symphalangus*, mainly regarding the higher values found in the distal apex and the extended distribution of the stress in the patellar body related to the original model (Fig. 59a). On the other hand, *Symphalangus*-ThickAP shows less stress in the most distal part of the apex than in the original model, thus being more similar to

that of *Ateles* (Fig. 59b). Likewise, *Gorilla*-HighPD is different from the original from a mechanical point of view (Fig. 59c). The new simulation shows notable affinities with those stress distribution patterns of the other orthograde taxa that have no apex (*Pongo* and *Pan*), with a broad stress distribution specially concentrated along the posterior side of the bone.

The effect of adding (*Gorilla* and *Pongo*) or removing (*Cercopithecus*) the patellar apex in the original models induces changes in the von Mises stress results obtained at first. That is, the stress distribution of *Cercopithecus*-NoApex is more similar to that of *Pongo* or *Pan* (an even *Homo*) because it concentrates notably higher values of stress in the distal part of the bone (Fig. 59d). On the other hand, results observed in the patellae of *Gorilla*-WApex and *Pongo*-WApex are more similar to those of pronograde taxa with apex in the patella (e.g., *Cercopithecus* or *Mandrillus*; Fig. 59e,f).

Displacement

The pattern of displacement is very similar among all the extant patellae during knee flexion, which does not account for differences according to the presence or absence of the apex, locomotor mode, and/or body plan (except for *Gorilla*, whose results do not resemble any other, and the last phase of flexion in *Cebus*; Fig. 56). Overall, the displacement is concentrated in the area of application of the force when the knee is extended. When flexion occurs, the proximal half displaces strongly, especially when the joint is fully flexed. Moreover, in all the orthograde taxa and *Ateles*, the most distal part of their patellae shows very low (such as in *Hylobates* and *Symphalangus*) or even absent displacements. In *Cebus* (and in *Colobus* in a lesser extent), the highest displacements in full-flexed knee positions are spread widely across the whole bone and reach maximum values in the proximal and distal ends (Fig. 56a). In the case of *Gorilla*, displacements are notably lower than in the remaining models in all the three phases of knee flexion. In sum, it seems that the displacements are highly restricted to those areas where loading occurs, also following the direction of the force (Fig. 56k).

Displacement results for fossil primates.- Regarding fossil species, *P. catalaunicus* shows a pattern of displacement that is similar to that of the remaining models, especially to those of *Pongo* and *Pan* (Fig. 58a). Thus, the most displaced area is the proximal half, which shows increasing values from an extended to a flexed knee. Likewise, the most distal region of the *P. catalaunicus* patella is not displaced in any of the three phases of knee flexion. Otherwise, the patella of *Ep. vindobonensis* shows a pattern of displacements more similar to that of cercopithecoids, especially to *Colobus* (Fig. 58b). In this case, the strongest displacements are observed in the proximal half of the bone, but also spread to the distal half including the apex.

Experimental FE models results.- All of the modified patellae also show the general pattern described for extant primates, with the major displacements in the proximal half of the bone, increasing with knee flexion. Accordingly, there is no discernible change when compared to the original models (Fig. 60).

Results of displacements for the studied sample of patellae do not show identifiable differences among locomotor groups, functional patterns and/or body plan types. Therefore, the absence of differences in the displacements does not allow for functional or locomotor inferences. According to this, only von Mises stress results will be largely discussed in the following section.

Walk a single path, becoming neither cocky with victory nor broken with the defeat, without forgetting caution when all is quiet or becoming frightened when danger threatens.

-- Jigoro Kano --

Section VII. DISCUSSION

FUNCTIONAL INFERENCES

Femur

Inferences on the basis of the external morphology

The external morphology of the femora found in the Vallès-Penedès Basin, IPS41724 (cf. *Dryopithecus fontani*) and IPS18800 (*Hispanopithecus laietanus*, both sides) is distinct. Although qualitative shape differences between these two femora are evident, both taxa could fall within the intraspecific variation displayed by extant species for the measurements inspected in this work (e.g., see Fig. 27). Nonetheless, it is important take into account that linear measurements alone do not always capture clear differences observed in gross morphology.

The femora of these two taxa share some similarities (Table 14): an almost spherical femoral head, whose articular surface slightly extends posteriorly onto the femoral neck and also laterally in the anterior aspect of the neck in cf. *D. fontani* (Fig. 21e, 24e, and 25); and a well-marked and superiorly placed *fovea capitis*. However, femora of cf. *D. fontani* and *H. laietanus* display some differences at the SIH/SIN (Fig. 27a), the NSangle (Fig. 27b), the BMNL (Fig. 28), the proximal femur relative robusticity (Fig. 27c,d), greater trochanter lateral flare and proximal projection (Fig. 25; see also Table 14).

The possession of a spherical femoral head covered by articular surface and a high SIH/SIN index has been related to a wide range of joint excursion and a high capability of abduction and external rotation of the femur at the hip (Ruff 1988; Ward *et al.* 1993; Harmon 2007; Hammond 2014). The more homogeneous distribution of the femoral head articular surface (sphere-shaped) maximizes the hip joint articular surface contact area between the femur and the acetabulum during movement (Ward *et al.* 1993; MacLatchy 1996; MacLatchy and Bossert 1996). Moreover, hominoids articular surface extends posteriorly onto the neck, a morphological pattern that favours abduction and lateral rotation of the hindlimb, and that is also consequence of the laterally facing acetabulum (Jenkins 1972; MacLatchy and Bossert 1996). Additionally, an increasing in femoral head size relative to the neck also participates in broadening the range of motion of the hip joint by increasing the articular surface area relative to the acetabulum (Ruff 1988; Ward *et al.* 1993). Thus, the morphology of the femoral head and neck of *H. laietanus* fits well with the possession of enhanced capabilities of abduction at the hip joint. In contrast, the possession of an almost spherical in cf. *D. fontani* is to some extent contradictory in functional terms with the presence in this taxon of a relatively

large superoinferior diameter of the neck (showing the lowest SIH/SIN value among Miocene apes; Fig. 27a). The femoral head morphology of cf. *D. fontani* might be thus related to a wide range of movements at the hip joint, but its relative neck size would hinder such mobility to some extent, overall suggesting lesser capabilities of hip abduction and lateral rotation than in *H. laietanus*.

Both femora from the Vallès-Penedès display a well-developed *fovea capitis* (although it is deeper in *H. laietanus*). This structure is the attachment for the *teres* ligament, which provides stability at the hip joint by maintaining the *fovea* within the acetabular notch (Aiello and Dean 1990; Ward *et al.* 1993; Harmon 2007). In this regard, orangutans, which are able of strongly abduct the hindlimb, lack the *fovea capitis*, but display a well-developed *teres* ligament attached at the inferior base of their femoral head. This configuration prevents from femur dislocation on extreme positions of the joint (e.g., during abduction; Crelin 1988; Demange *et al.* 2007; Hammond 2014). Moreover, the orangutan-case evidences that the potential occurrence of a well-developed *teres* ligament does not necessary imply the presence of a strongly stabilize joint. Nonetheless, the location of the *fovea capitis* on the head has been traditionally associated with the hip range of motion, since a superior position reduces potential for impinging on the ligament during habitual abducted positions of the hindlimb (Jenkins and Camazine 1977; Ward *et al.* 1993). The superior position of the *fovea capitis* in the femoral head in both cf. *D. fontani* and *H. laietanus* reflects then habitual femoral abduction in these taxa (Ward *et al.* 1993).

The femur of cf. *D. fontani* further displays a smaller head relative to the proximal shaft and a greater proximal robusticity at the proximal femur related to the femoral neck than that of *H. laietanus* (Fig. 27c,d; Table 10). These features are generally related to body size and, in particular, to the proportion of body weight that is loaded by the hindlimbs (Aiello and Dean 1990; Ruff 1988, 2002, 2003). Therefore, such differences might be whether related to the larger body mass inferred for IPS41724 compared to IPS18800 (44.4 kg and 38.6 kg, respectively; Moyà-Solà *et al.* 2009a) and/or the different degree of orthograde behaviours (mainly below-branch suspension) inferred for their locomotor repertoires (probably much more frequent in *H. laietanus*). In the case of cf. *D. fontani*, below-branch suspension cannot be completely ruled out from its positional behaviour on the basis of current evidence (see below), but *H. laietanus* already shows clear adaptations for this locomotor mode in the femur and other anatomical regions (Moyà-Solà and Köhler 1996; Almécija *et al.* 2007; Alba *et al.* 2012a).

The biomechanical neck length (BMNL) has been classically related to gait differences among hominins, since this variable affects the abductor lever arm of the anterior gluteal muscles (*gluteus medius* and *gluteus minimus*) and the efficiency of hip lateral stabilization during the support phase and movement in bipedal locomotion (Lovejoy *et al.* 1973, 2002; McHenry and Corruccini 1976; Lovejoy 1988; Stern and Susman 1991; Pickford *et al.* 2002). The relative BMNL of cf. *D. fontani* is longer than that of *H. laietanus* (Figs. 25 and 26), thus showing, like humans, a more monkey-like morphology (Fig. 28). In contrast, the relative BMNL of *H. laietanus* is close to that of hylobatids and great apes, which habitually perform suspensory and vertical climbing behaviours (Aiello and Dean 1990; Ward *et al.* 1993; Richmond and

Jungers 2008). The presence of a relatively short BMNL in *H. laietanus* is also related to a high neck-shaft angle (NSangle; Fig. 27b). Traditionally, the BMNL, the NSangle, both the greater trochanter proximal projection and lateral flare, and the femoral neck internal structure (cortical bone distribution) have been considered a morphological complex that varies on the basis of (mainly) abductor capabilities of the hip joint (Lovejoy *et al.* 1973, 2002). More specifically, a high NSangle is frequently associated with short BMNL among living apes (mainly great apes), allowing wider ranges of motion (including abduction and lateral rotation) at the hip joint (Aiello and Dean 1990; MacLatchy and Bosset 1996; Lovejoy *et al.* 2002; Hammond 2014). In contrast, a relatively longer BMNL is shown by quadruped monkeys (and modern humans; Fig. 28), being commonly associated with lower neck-shaft angle values and the presence of a marked lateral flare of the greater trochanter (which, in turn, probably reflects a different organization of the glutei muscles complex at the hip joint; Lovejoy *et al.* 1973; Aiello and Dean 1990; Richmond and Jungers 2008). Apart from its biomechanical contribution, the lateral flare and the proximal projection of the greater trochanter also contribute to determine the capability of hip abduction by physically reducing the range of hindlimb motion (Sigmon 1974; Aiello and Dean 1990; Nakatsukasa *et al.* 2004b). Recently, Hammond *et al.* (2016) stressed the difficulties for accurately predict the passive range of abduction from fragmentary fossils and, therefore, inferences associated with this trait should be taken with caution. Thus, the femur of *H. laietanus* displays a more marked lateral flare of the greater trochanter than that of cf. *D. fontani*, although both taxa display a lesser flare than quadrupedal monkeys and other Miocene apes (e.g., *E. nyanzae*). Thereby, both taxa (mainly cf. *D. fontani*) more closely approach the reduced lateral flare of the greater trochanter displayed by living apes.

In addition, the greater trochanter of cf. *D. fontani* is more projected proximally than those of *H. laietanus* (especially than that of the left femur), although not as much as in living cercopithecoids. This morphology might physically reduce mediolateral movements of the hindlimb, but also provide a greater leverage for the action of the *gluteus medius* as an extensor of the hip, thus favouring movements in the parasagittal plane (McHenry and Corruccini 1976; Stern and Susman 1981; Lovejoy *et al.* 2002; Harmon 2007). The presence of a well-developed area on the greater trochanter for the insertion of the *gluteus medius* muscle also supports the aforementioned inferences derived from the cf. *D. fontani* femur (Fig. 21c,d). In contrast, the greater trochanter of *H. laietanus* is more clearly situated below the femoral head (especially in the left femur), which coupled with its higher neck-shaft angle (Figs. 23, 24, 26 and 27b) would have probably favoured greater abduction capabilities in this taxon (Aiello and Dean 1990; Harmon 2007). In a biomechanical regard, this configuration reduces the efficiency of the *gluteus medius* in hindlimb extension (and medial rotation during climbing), but amplifies the functional range of motion of the joint by increasing the collinearity of the femoral neck and shaft (McHenry and Corruccini 1976; Stern and Susman 1981; MacLatchy 1996; Lovejoy *et al.* 2002; Harmon 2007; Hammond 2014).

Overall, the femur of cf. *D. fontani* displays several features related to enhanced joint motion (e.g., round femoral head whose articular surface comprises a very complete portion of an sphere, the superior

position of the *fovea capitis*, and not-pronounced lateral flare of the greater trochanter), which contrast with other features associated with the stabilization of the hip joint and hindlimb movements to a large extent restricted to the parasagittal plane (e.g., small femoral head relative to the neck, and a similar proximal projection of the head relative to the greater trochanter associated with lower NSangle than in *H. laietanus*). The latter features would have hindered a wide range of movement (particularly abduction and lateral rotation) of the hindlimb at the hip joint, thus being indicative of quadrupedalism. However, the existence of some incipiently developed, more derived (i.e., modern ape-like) features in the femur suggests that this taxon probably engaged to some extent in some orthograde behaviours that required more extended hindlimb joints, such as vertical climbing. In contrast, the femur of *H. laietanus* more clearly shows ape-like features that are derived for enhanced hip abduction, that are interpreted as adaptations for orthograde behaviours, including below-branch suspension (e.g., large femoral head relative to the neck, high NSangle, short BMNL, and relative position of the head relative to the greater trochanter). Nevertheless, the femur of *H. laietanus* still retains some more primitive features associated with quadrupedalism (e.g., presence of a deep *fovea capitis*, and marked lateral flare of the greater trochanter).

Inferences on the loading patterns of fossil apes

Hitherto, the analysis of the femoral neck cortical bone (FNCB) distribution has been mainly focused on humans and early hominins. These bipedal taxa display a superior cortex thinner than the inferior one (Ohman *et al.* 1997; Demes *et al.* 2000; Lovejoy *et al.* 2002), thus contrasting with the more homogeneous cortical thickness of extant apes, which possess thicker inferior and especially superior cortices relative to bipeds, resulting in a uniform supero-inferior ratio closer to 1 along the neck (Ohman *et al.* 1997). However, when a more comprehensive primate sample is considered, it emerges that humans largely overlap with most other locomotor groups, with the exception of knuckle-walkers (which also rely on vertical climbing and suspensory behaviours in some extent; see below) and specialized suspensory taxa when index and intrinsic proportions are taken into account (Rafferty 1998; Demes *et al.* 2000; Matsumura *et al.* 2010b). According to the results of the present work, two different patterns of distribution of FNCB thickness can be distinguished among extant primates, which are functionally attributable to differences in the direction of weight transfer through the femur and, consequently, to different loading stresses experienced by this bone depending on the type of locomotion (Scherf 2008).

Both generalized quadrupedal and bipedal taxa display a superior cortex thinner than the inferior one. This configuration indicates a predominantly unidirectional (verticalized) pattern of weight transmission at the hip joint, resulting in the concentration of loading stresses on the inferior side of the femoral neck. This stereotyped pattern can be functionally related to the predominance of adducted positions of the femur in these taxa, in which the hindlimbs move habitually along the parasagittal plane. In contrast, both knuckle-walkers (which are also vertical climbers—from around 0.2% of its locomotion in *Gorilla beringei* to around 49% in *Pan troglodytes*—and suspensors in some degree—ranging from 0% to 8.7%

of their locomotion; Tuttle and Watts 1985; Hunt 1991a, 2004, 2016) and suspensory taxa (Asian apes, which primarily rely on this behaviour, around 10%-80% of their locomotor activity; and atelids, with around 20.8%-38.6% of suspensory behaviours; Chivers 1972; Mittermeier 1978; Fleagle and Mittermeier 1980; Cant 1987; Cant *et al.* 2001; Hunt 2016) display a thicker superior cortex, resulting in a more homogeneous distribution of cortical bone in the femoral neck. That is, the results of this study reveal that extant anthropoid primates exhibiting a significant amount of orthograde behaviours (suspension and/or vertical-climbing) display non-specific loading distribution patterns at the femoral neck. This homogeneous pattern occurs irrespective of whether they are specialized suspensory taxa (such as hylobatids and orangutans) or combine arboreal climbing and/or suspension with knuckle-walking (African apes). Rafferty (1998) suggested that the more homogeneous distribution of cortical bone in the femoral neck of non-human hominoids and suspensory atelids may be associated with their less stereotyped locomotor behaviours, including the frequent use of very abducted hindlimb postures, which would imply more varied distributions of stresses through the femoral neck, depending on posture. On the basis of this trait, knuckle-walking taxa cannot be discerned from those suspensory taxa that are not knuckle-walkers, due to the fact that the former are also suspensors and vertical climbers in some extent (mainly during their feeding activity). Even though the functional demands of knuckle-walking surely differ from those of suspensory behaviours during travelling (hindlimbs used in compression with more stereotyped loadings at the hip joint rather than in tension in African apes; Stern 1975; Scherf 2008), it should be taken into account that both groups of taxa display much more varied (i.e., less stereotyped) locomotor repertoires than other primates because suspension and other orthograde-related behaviours (e.g., vertical climbing and/or clambering) take also an important part of their locomotor repertoire (Isler 2005; Crompton *et al.* 2008, 2010). Hence, these functional inferences suggest that knuckle-walking was probably a secondary adaptation in African apes.

Paleobiological inferences

The homogeneous cortical bone distribution found at the femoral neck of *H. laietanus* resembles that of extant apes (similar superior and inferior thicknesses), thus assuming comparable functional requirements than in these living primates. Therefore, *H. laietanus* represents the oldest evidence of a homogeneous cortical bone distribution in the hominoid fossil record. Consequently, a weight transmission pattern most closely resembling taxa with orthograde behaviours (vertical climbing and/or suspension) can be inferred from the relatively thicker superior cortical thickness of *H. laietanus* compared to non-hominoid primates (with the exception of some atelids; Rafferty 1998). Together with the evidences provided by the more derived (ape-like) adaptations observed in its postcranium (Chapter 1; Moyà-Solà and Köhler 1996; Köhler *et al.* 2002; Almécija *et al.* 2007; Alba *et al.* 2010c, 2012a), the obtained results for the FNCB of *H. laietanus* would imply a higher range of movements at the hip joint than in generalized quadrupedal taxa, being indicative of a varied arboreal locomotor repertoire with a significant orthograde component including

suspensory behaviours. Overall, the distribution of the cortical bone in the femoral neck of *H. laietanus* is in agreement with its external morphology and proportions (e.g., size of the femoral head relative to the neck, or the high femoral neck-shaft angle), previously associated with suspensory adaptations (Moyà-Solà and Köhler 1996; Köhler *et al.* 2002; see also Chapter 1). The internal structure of the femur of *H. laietanus* is thus in further agreement with the external morphology of other anatomical regions, which similarly indicate the presence of an orthograde body plan with adaptations for suspensory behaviours (e.g., at the hand; Moyà-Solà and Köhler 1996; Almécija *et al.* 2007; Alba *et al.* 2010c, 2012a; Susanna *et al.* 2014). Although results for the distribution of FNCB do not allow for discerning knuckle-walking behaviours, the latter can be clearly discounted for *H. laietanus* based on hand anatomy (Almécija *et al.* 2007; Alba *et al.* 2010c). Whereas the obtained results for FNCB thickness confirm the possession of orthograde behaviours in this taxon, the retention of specific quadrupedal behaviours cannot be either confirmed (or discounted) on this basis. This is illustrated by the impossibility to discern among semi-terrestrial knuckle-walkers, the more suspensory hylobatids and orangutans, and even the South-American atelids (which combine suspension with arboreal quadrupedalism) based on the femoral neck internal structure.

Results obtained for the FNCB distribution in the neck of cf. *Dryopithecus* reveal that this taxon has a more asymmetric distribution of the cortical bone, implying that it suffered more stereotyped loadings in the femoral neck than *H. laietanus*. An asymmetrical pattern is typical of modern humans, but also of quadruped monkeys (Rafferty 1998; Lovejoy *et al.* 2002). Thus, this stereotyped loading pattern (typical of quadruped and biped taxa) fits well with the generalized "Miocene ape-like" quadrupedal behaviour inferred for cf. *D. fontani* on the basis of other postcranial remains (most of which are tentatively assigned to this taxon as explained elsewhere; Pilbeam and Simons 1971; Alba *et al.* 2011a; Almécija *et al.* 2012; see also Section I). However, fossil remains attributed to *Dryopithecus*, including (tentatively) the IPS41724 partial femur, also display some traits related to orthograde-like behaviours and enhancement of joint mobility (see Chapter 1 for the external morphology of the femur). However, these adaptations are not reflected in the FNCB distribution, suggesting that this taxon might preferentially engage in locomotor patterns involving stereotyped loading of the hip joint. Assuming that *Dryopithecus* was an unlikely biped, the stereotyped loading pattern of this taxon would probably relate to some type of currently unknown quadrupedalism.

Interestingly, the aforementioned results for cf. *D. fontani* FNCB distribution have relevant evolutionary implications. Previous works accounted for a plesiomorphic condition of the symmetrical FNCB distribution in great apes, being the asymmetric pattern derived for humans and, hence, a diagnostic trait for inferring bipedal behaviours (e.g., Ohman *et al.* 1997; Lovejoy *et al.* 2002; Galik *et al.* 2004). Similarities in the asymmetric pattern at the midneck and base-of-neck section shared by the fossil great ape represented by the femur IPS41724 (cf. *D. fontani*), early hominins and modern humans suggest that an asymmetric patter might be the plesiomorphic condition for the great ape and human clade (i.e., the Hominidae). These results raise the interesting question as to whether early hominins are derived or

just largely plesiomorphic for this feature. Therefore, further analyses in a larger sample (including not only more fossil apes but also anthropoid monkeys), as well as a formal evolutionary modelling using phylogenetic informative methods, are needed to shed light on this question.

Mechanical inferences on the basis of the femoral diaphysis

The Vallès-Penedès great apes cf. *D. fontani* and *H. laietanus* display clear differences in their cross-sectional mechanical properties, both at the mid- and proximal femoral shaft. The IPS41724 proximal femur (cf. *D. fontani*) displays a conjunct of cross-sectional geometric properties related to higher axial (e.g., %CA), bending (e.g., I and Z), and torsional (e.g., J) strength and rigidity (in absolute values) than in the case of the IPS18800 proximal femora (*H. laietanus*). Apart from %CA (related to compressive loading), the rest of mechanical properties (I, Z and J) reflect either the distribution of bone about the cross-section centroid and the stress directionality preferences. It seems therefore that the results obtained for cf. *D. fontani* indicate higher anteroposterior mechanical loads than in *H. laietanus*. More specifically, when comparing the relative anteroposterior strength of the diaphysis at the mid-point and the proximal shaft with a sample of extant catarrhines, cf. *D. fontani* shows clear affinities with "quadrupedal" (Q) taxa (pronograde cercopithecoids and African apes), whereas *H. laietanus* most resembles gibbons at the midshaft, and gibbons and African apes at the proximal shaft. In addition, the left and right femora of the same *H. laietanus* individual display a slightly different mechanical signal. Due to the large range of variability observed in some of the extant primates (e.g., *Colobus* or *Papio*; Fig. 42), such differences between both sides may be due to whether intraspecific variability and/or asymmetry between the left-right sides within the same individual. In this case, the suspensory trend observed in *H. laietanus* would be less marked (indices values of the left femur clearly overlap with some of the Q taxa; Fig. 42). On the other hand, if the left femur was somewhat distorted due to some taphonomic process (especially reflected at its larger femoral head; Table 10; see also Chapter 1), this might clearly influence the final results, since FHSA is derived from femoral head measurements. Then, a larger femoral head would explain that the left femur shown relatively higher anteroposterior strength at both the mid- and proximal shaft sections, being more similar to Q taxa (especially at 80%). As occurs for the external morphology, further analyses are needed to discern whether intraspecific variability, intra-individual side asymmetry, or a possible taphonomic distortion is the most feasible cause of the dissimilarities found between the left and right femora of *H. laietanus*. Therefore, as argued for the external morphology, results for the right femur are here considered more representative. Hence and despite this, results on diaphyseal strength obtained for *H. laietanus* fit well with its inferred locomotor repertoire combining above-branch quadrupedalism and orthograde behaviours, specifically vertical climbing and below-branch suspension (e.g., Moyà-Solà and Köhler 1996; Almécija *et al.* 2007; Tallman *et al.* 2013). The suspensory adaptations (hindlimbs used preferentially in tension and low stereotyped movements) shown in the *H. laietanus* postcranium are reflected in the trend towards suspensory taxa observed at the relative anteroposterior section modulus

(Zx) results (Figs. 41 and 42). The lower relative anteroposterior strength and %CA than cf. *D. fontani*, and an Ix/Iy index close to 1 (biomechanical "shape" close to circularity; Ruff *et al.* 1999), probably relate to lower compressive and a more homogeneous (i.e., less stereotyped) loading along the *H. laietanus* femoral shaft. Moreover, the use of its limbs in tension is also associated with habitual extended and diverse positions of the joints, such as in orangutans (Ruff 1988, 2002; Jungers *et al.* 1998; Carlson 2005; Crompton *et al.* 2008, 2010). Due to their habitual suspensory and clambering behaviours, orangutans use their hindlimbs for propulsive purposes less than other primates (e.g., quadrupeds and leapers), thus reducing the loads experienced by the posterior extremities (Schaffler *et al.* 1985; Ruff 1988). In this regard, *H. laietanus* is the earliest and the only hominoid exhibiting the above-mentioned features more clearly related to suspensory adaptations in the hindlimb. These probably reflect novel mechanical requirements in its femoral shaft. In summary, *H. laietanus* displays some cross-sectional geometric properties more similar to orangutans (trend to lower values of relative anteroposterior strength and relatively low %CA), but still maintains some plesiomorphic properties functionally related to above-branch quadrupedalism (lower values of Imax at the midshaft respect to the proximal shaft; see below). These results match those of the femoral neck cortical bone distribution obtained for the right femur (see Chapter 2), since *H. laietanus* displays clear similarities with African apes at both regions, the femoral neck and the femoral shaft (Fig. 42). African apes rely mainly on knuckle-walking behaviours (a type of quadrupedalism performed on the ground where hindlimbs are used in compression), but also include in their locomotor repertoire a suite of arboreal orthograde behaviours, mainly vertical climbing and suspension (Tuttle 1970; Hunt 1991a; Isler 2005; Tocheri *et al.* 2011). Therefore, load patterns and mechanical traits of the *H. laietanus* femoral shaft are compatible with a positional repertoire combining behaviours where the hindlimbs are used in compression, such as generalized quadrupedalism, with others more related to orthogrady, like suspension and/or vertical climbing as occurs in African apes, mainly chimpanzees. However, knuckle-walking adaptations can be discarded in this taxon based on hand morphology (Moyà-Solà and Köhler 1996; Almécija *et al.* 2007). In general, the results found in this study support previous hypotheses based on other anatomical regions (Moyà-Solà and Köhler 1996; Almécija *et al.* 2007; Alba 2012; Tallman *et al.* 2013).

On the other hand, cf. *D. fontani* display higher robusticity and relative anteroposterior bending strength along its femoral shaft (Table 23; Figs. 41 and 42). Furthermore, the cross-section shape in this fossil ape is elliptical and its biomechanical "shape" clearly deviates from circularity (showing a mediolateral expansion of the shaft; Table 23; Figs. 38 and 39). The results of cf. *D. fontani* results also show that %CA decreases from proximal to midshaft, whereas bending strength and rigidity increase. All these traits correspond with the quadruped biomechanical pattern observed in extant primates (Burr *et al.* 1981; Jungers *et al.* 1998; Ruff 2002), as well as in the results for the relative anteroposterior strength (in which cf. *D. fontani* is clearly similar to cercopithecoids, and African apes to some extent; Figs. 41 and 42). Cercopithecoids (and African apes when they are involved in knuckle-walking) commonly use their

lower extremities for active propulsion in limited parasagittal planes and with more flexed postures of the limbs, thus suffering higher axial compressive and mediolateral loads than stricter suspensory taxa, such as hylobatids (Burr *et al.* 1981; Ruff and Runestad 1992; Jungers *et al.* 1998; Carlson 2005). However, cf. *D. fontani* displays higher bending stiffness (Imax) at the midshaft than macaques (and presumably other typical quadrupeds like these; Burr *et al.* 1981). This feature has been related to enhancement flexibility of the bone during galloping and leaping (a fact that is also recurrent among modern humans; *ibid*). Thus, results presented here show that cf. *D. fontani* displays similar bending stiffness at both proximal and midshaft, a combination that is not present in living macaques, which might be associated with the "Miocene ape-like" quadrupedalism described for some fossil apes (Rose 1983, 1994). It could be therefore hypothesized that joints of fossil hominoids that engaged in this "Miocene ape-like" quadrupedalism might have wider range of motion and less stereotyped loadings than those of living quadrupeds, and probably incorporated some movements (e.g., hip abduction and thigh lateral rotation) that are less frequently used in living quadrupeds (Rose 1983, 1994; Ward *et al.* 1993; Fleagle 2013; Ward 2015). If true, these two facts would explain the slight mechanical differences between extant quadrupeds (cercopithecoids in this case) and Miocene apes.

In addition, several works focused on the mechanical evolution of the human femur proposed that the mediolateral buttressing of the proximal shaft could be related to an elongation of the femoral neck, which would imply higher mediolateral bending at this region of the bone (e.g., Ruff 1989, 1995; Ruff *et al.* 1999, 2015). The femur of cf. *D. fontani* exhibits a longer femoral biomechanical length than African apes, cercopithecoids, and also *H. laietanus* (Fig. 28; see also Almécija *et al.* 2013). This morphology iswell in accordance with the geometric structural properties obtained for the proximal shaft of cf. *D. fontani* (high resistance to torsional loads; see J in Table 23). A longer femoral neck laterally displaces the diaphysis of the bone from the hip joint, probably increasing mediolateral-bending moments in the shaft (higher proximally than distally) that are somewhat counteracted by enhancing strength and rigidity of the bone diaphysis (Lovejoy *et al.* 1973; Burr *et al.* 1981; Ruff *et al.* 1999). Moreover, Lovejoy *et al.* (1973, 2002) described the tight relationship between proximal femur variations in neck-shaft angle, greater trochanter morphology, biomechanical neck length, and also internal distribution of cortical bone at the femoral neck. In general, and as explained in Chapter 2, the cortical bone distribution in cf. *D. fontani* reveals the presence of stereotyped loads along its femoral neck (asymmetric distribution of the cortical bone), such as the case of quadrupeds, modern humans and early hominins (e.g., Rafferty 1998; Ruff and Higgins 2013). In fact, modern humans, early hominins and cf. *D. fontani* have also in common a long biomechanical femoral length, and therefore they probably shared similar biomechanical requirements at the hip joint (as it is also evidenced by the mediolateral reinforcement of the proximal shaft in this Miocene ape; Burr *et al.* 1981; Ruff *et al.* 2015). These results point out that the morphological and mechanical complex observed in cf. *D. fontani* (long biomechanical neck length, high neck-shaft angle, asymmetric distribution of the femoral neck cortical bone, and mediolateral reinforcement of the proximal shaft) could

be the plesiomorphic condition for hominids. It that were the case, it would imply that living apes would be secondarily derived (homoplastically for hylobatids and hominids) for these traits (as in the case of the femoral neck cortical bone distribution; Chapter 2).

Irrespective of the evolutionary scenario, from a functional viewpoint, the results obtained for the cf. *D. fontani* proximal femur might corroborate the more relevant quadrupedal component hypothesized for this taxon respect to *H. laietanus* (Moyà-Solà *et al.* 2009a; Alba *et al.* 2011a; Almécija *et al.* 2012), since the overall mechanical demands of the former more resemble those of Q taxa.

Tibia

Inferences on the basis of the external morphology

The distal tibia of *H. laietanus* shows a unique combination of monkey-like and ape-like morphological traits. Among the monkey-like features, the medial malleolus markedly projects distally and have a convex (bulbous) articular surface in those primates that mainly rely on quadrupedalism (Harrison 1989; Davis 1996). Consequently, the talus normally displays a deep cup-shaped depression where the medial malleolus is accommodated (Lewis 1980a,b; Conroy and Rose 1983). These two complementary regions result in a close-packed posture when the joint is in a dorsiflexed position, thus transversally stabilizing the ankle and facilitating parasagittal movement of the talo-crural joint in quadrupeds (Lewis 1980a; Harrison 1989; Davis 1996). In addition, quadrupeds tend to have strong ligaments (e.g., tibiotalar ligaments that originate at the intercollicular groove) that further participate in stabilization of the talo-crual joint by resisting torsional forces (Davis 1996; DeSilva *et al.* 2010). In general, apes (especially orangutans) display a less projected medial malleolus and less developed ligaments (ligament attachment areas are even absent sometimes in orangutans), which outcomes in less restricted movements at the ankle joint (Lewis 1980a; DeSilva 2008, 2009; Tallman *et al.* 2013). Otherwise, cercopithecoids show a quadrangular tibial articular surface and anteroposteriorly broad tibial metaphysis (unlike great apes that display a rectangular-shaped articular surface and mediolaterally expanded metaphysis; DeSilva *et al.* 2010; Tallman *et al.* 2013). These features are associated with a homogeneous distribution of loading through the ankle and lower capabilities of dorsiflexion of the foot (Harrison 1989; DeSilva 2009; DeSilva *et al.* 2010). Furthermore, a squared-shaped articular surface is usually combined with the presence of a strongly marked median keel in cercopithecoids, which runs in the sagittal plane and clearly separates the medial and lateral articular depressions (Harrison 1989). The median keel also favours transverse stabilization of the ankle joint during parasagittal movements (Harrison 1989; DeSilva *et al.* 2010). Instead, the great ape-like morphology (i.e., rectangular-shaped and relatively flat articular surface, and mediolaterally broad metaphysis) enhances the possible range of feet dorsiflexion and implies mediolateral loading of the ankle joint. Hence, this morphology is associated with wide ranges of motion of the talo-crural joint that is loaded in a variety of postures and allows the foot to achieve extremely dorsiflexed or inverted positions during vertical climbing (DeSilva 2008, 2009; DeSilva *et al.* 2010).

Therefore, altogether, the strong distal projection of the medial malleolus and its articular surface, the deep intercollicular groove, the quadrangular articular surface, and the presence of a median keel observed in the *H. laietanus* tibia suggest a relatively stable ankle joint and a restricted dorsiflexion capability of the foot (Lewis 1980a; Harrison 1989; DeSilva 2008; Tallman *et al.* 2013). In contrast, the tibia of *H. laietanus* shows some traits more related to wider mobility of the ankle joint. Among them, it exhibits an anteroposteriorly compressed diaphysis and a broad fibular facet that facilitate a broad range of movements. The latter is a triangular area in the lateral side of the tibia that relates to the weight-bearing role of the fibula and the capacity of inversion-eversion of the foot. This facet is small in cercopithecoids, but relatively large in great apes (*H. laietanus* resembles the great ape-like condition; Lewis 1980a; DeSilva *et al.* 2010; Tallman *et al.* 2013). Likewise, the tibia of *H. laietanus* displays a small articular surface on the anterior margin of the distal articular surface identified as a "bony stop" during hyperdorsiflexion of the foot in vertical climbing behaviours in apes. This small facet has its complementary on the talus (the "tibial stop") and their contact when the tibia progresses on the talus during foot dorsiflexion contributes to the stabilization of the ankle joint (Conroy and Rose 1983; Harrison 1989; Davis 1996). Although the presence of this facet in the anterior margin of the articular surface of the tibia is variable within living primate species (Tallman *et al.* 2013), its occurrence in *H. laietanus* is already significant. In addition, the relative medial malleolus thickness in *H. laietanus* is closer to that of great apes than to that of cercopithecoids. Great apes load the foot in a high variety of postures, including inversion, during vertical climbing. In an inverted foot position, the weight is primarily directed through the medial malleolus favouring an anteroposteriorly broad medial malleolus thickness (Lewis 1980a; DeSilva 2008, 2009; DeSilva *et al.* 2010). Furthermore, the tibia of *H. laietanus* displays a deep groove for the *tibialis posterior* tendon. The groove, situated at the posterior side of the tibia (on the medial malleolus in apes) facilitates that the tendon runs from its origin at the posterior side of the proximal tibia and fibula to the tarsals, acting as a plantar flexor (Lewis 1980; White and Folkens 1991). The *tibialis posterior* tendon is present in all primates and attaches at the navicular tuberosity and the cuneiforms. However, in catarrhines and especially in hominoids, the *tibialis posterior* tendon enters in the sole and also attaches at the metatarsals II, III and IV (Lewis 1964). Thus, the prolongation of the tendon into the sole has been related to a more notable development of the tendon and the enhancement of the grasping abilities by flexing the digits against the hallux during climbing and arboreal quadrupedalism (Lewis 1964, 1980a).

Hence, the shape of the distal tibial of *H. laietanus* resembles in some degree extant cercopithecoids (being indicative of restricted mobility of the ankle) whereas in others is closer to apes morphology (suggesting a wider range of motion of the joint), also showing some adaptations related to grasping capabilities (see Tallman *et al.* 2013). Thereby, the unique combination of features found at the *H. laietanus* tibia indicates that this taxon was probably adapted for both above-branch pronograde quadrupedalism and orthograde vertical climbing behaviours.

Patella

Inferences on the basis of the external morphology

Differences in patellar morphology between monkeys and hominoids (especially great apes) have been previously noted on the basis of the external dimensions used herein (PD, PDAS, AP, and ML): monkeys exhibit proximodistally taller, anteroposteriorly thicker and mediolaterally narrower patellae than great apes (Figs. 49 and 51; Harrison 1986; Ward *et al.* 1995; Nakatsukasa *et al.* 2012). These external dimensions have been used to make functional inferences for Miocene apes (Ward *et al.* 1995). In particular, Ward and colleagues (1995) concluded that differences in external proportions of the patella between monkeys and apes indicate biomechanical differences in their knee function, related to bone stresses. However, it should be noted that only few mechanical models of the non-human primate knee joint have considered the coronal plane (Preuschoft 1970, 1971; O'Neill *et al.* 2013), and this is not the case of the above-mentioned study on Miocene apes. Taking that into account, the following biomechanical comments that follow are only meant to discuss patellar shape differences between monkeys and apes in the light of available mechanical models of the knee—restricted to the sagittal plane—that have been previously used to infer hindlimb function in Miocene apes.

The results agree with a previous study (Jungers 1990b) according to which, in non-human hominoids, the mediolateral breadth of the patella (and also other articular variables of their postcranium) scales with geometric isometry to body mass (BM). Jungers (1990b) further indicates that this assertion holds not only for apes, but for monkeys as well. This isometric relationship could be related to the Alexander's model as to how joint forces and articular stresses should scale with BM (Alexander 1980, 1981; Jungers 1990b). This model is based on either the proportional relationship between maximum joint forces and BM, and the general geometric scaling of skeletal dimensions (Alexander 1980, 1981). In contrast, humans are clear outliers in the ML *vs* BM regression (notably mediolaterally wide patella relative to BM), a feature probably related to their bipedal locomotor behaviour (Fig. 50a; Jungers 1990b). Since no significant grade shifts between monkeys and apes (only hylobatids are slightly upshifted) have been found (see also Fig. 50a; Jungers 1990b; Ward *et al.* 1995), it has been hypothesized that mediolateral patellar breadth is relatively unaffected by the type of locomotion (Ward *et al.* 1995), further providing a good surrogate of BM irrespective of phylogenetic constraints.

However, PD and AP seem to display a strong functional signal (Harrison 1986; Ward *et al.* 1995). In agreement with previous work (Ward *et al.* 1995), these results show that anteroposterior thickness of the patella is relatively higher in cercopithecoids than in platyrrhines and apes, respectively (Fig. 48d); whereas PD is higher in monkeys and hylobatids (displaying *Symphalangus* the proximodistally highest patella) than in great apes (Fig. 48b). This latter fact might be related to the presence of a large non-articular surface, the apex, in the patellae of monkeys and hylobatids (Fig. 49). Therefore, PD and AP mainly differentiate monkeys and great apes (hylobatids show a high PD as in monkeys, but a thin AP

as in great apes). Both parameters have been previously associated with the increase of the moment arm of the *quadriceps* tendon-ligamentum patellae about the knee joint (Badoux 1974; Ward *et al.* 1995). In the case of AP, a thicker patella mainly separates the ligamentum patellae from the centre of rotation of the knee in the sagittal plane, changing the angle of action of the *quadriceps* muscle mainly during flexed knee positions as well as increasing the moment arm of the muscle. Regarding PD, the greater length of the patella (including the apex) increases the lever arm of the *quadriceps* muscle from a flexed posture of the knee, thus enhancing the torque or rotational force of the joint (Nisell 1985; Ward *et al.* 1995). Therefore, the higher moment arms generated by a large proximodistal and thick anteroposterior patellae about the knee joint probably favour the forceful extension of that joint from fully-flexed positions (Badoux 1974; Ward *et al.* 1995; Channon *et al.* 2010a,b). Although not mentioned in previous studies, a higher moment arm also implies a lower angular velocity (Stern 1974), hindering a quick extension of the knee mainly during leaping. In this regard, further work is needed to solve this dichotomy and better determine the biomechanics of the primate knee and its relationship with patellar morphology. Thus, when AP and PD are assessed within a positional context, it can be observed that primates which rely on leaping and galloping (with predominant excursions of the joint from a full-flexed knee to extended positions) display higher values of these two parameters (Figs. 48 and 51; Harrison 1986; Ward *et al.* 1995). This morphology enhances the torque at the knee joint, thus aiding in the effective and powerful extension of the knee (Badoux 1974; Ward *et al.* 1995). Contrarily, the proximodistally short and anteroposteriorly thin patellae of great apes have been associated with a more versatile knee, with a wider range of positions and no habitual full flexion of the knee (Harrison 1986; Ward *et al.* 1995). The locomotor repertoire of these taxa (probably related to their large body mass) does not include frequent leaping or galloping. Instead they practice more frequently orthograde behaviours, such as vertical climbing, below-branch suspension, clambering and bridging (e.g., Ward *et al.* 1995; Gebo 1996; Rose *et al.* 1996). Since great apes show fully-flexed knee positions in a notably lower frequency than monkeys (only orangutans clearly full-extend the knee during arboreal bipedalism; Ward *et al.* 1995; Rose *et al.* 1996; Isler 2003, 2005; Crompton *et al.* 2010), their thinner anteroposteriorly and shorter proximodistally patellae might reflect these different biomechanical demands relative to non-hominid anthropoids (i.e., lower moment arms in the knee since, *a priori*, they do not habitually need to powerfully extend the knee from full-flexed position; Harrison 1986; Ward *et al.* 1995; Isler 2005; Crompton *et al.* 2010).

Furthermore, African apes and orangutans differ in type of locomotion and frequency of arboreal behaviours (Hunt 1991a; Doran 1996; Hunt *et al.* 1996; Crompton *et al.* 2010). The former are characterized by the practice of knuckle-walking, which implies an assemblage of specific adaptations (Tuttle 1967; Jenkins and Fleagle 1975; Gebo 1996). In contrast, orangutans are more arboreal, and mostly rely on below-branch suspension and clambering for traveling horizontally (Isler 2003, 2005; Thorpe and Crompton 2006; Zhilman *et al.* 2011). Apart from a certain degree of suspension, vertical climbing seems to be the common locomotor behaviour among all extant apes (Fleagle 1976; Isler 2003). Hylobatids, and especially

Symphalangus (which employ vertical climbing even more often than great apes; Fleagle 1976), employ less abducted hindlimb positions than the latter during vertical climbing (Fleagle 1976; Isler 2005). It is noteworthy that African apes and orangutans practice vertical climbing in different frequencies, and that there are also some differences in the hindlimb use, since in orangutans the knee is less flexed and more extended, and the hip is more flexed and abducted, than in African apes (Isler 2003, 2005; Thorpe and Crompton 2006). Likewise, orangutans have a larger mass of knee flexor muscles relative to the extensors, thus favouring the rotation and flexion of the knee as well as a wider variety of postures at this joint (Zihlman *et al.* 2011). However, these differences are not reflected in the overall proportions of the patella as captured by the analyses presented here (Figs. 48 and 51). Nonetheless, African apes display a trapezoidal patellar surface in the distal epiphysis of the femur (Fig. 49), which might reflect a decreased mobility of the knee joint compared to orangutans (Nakatsukasa *et al.* 2012). Thus, the African ape configuration seems to be slightly derived among extant great apes, being potentially related to an increase in knee stability during knuckle-walking (terrestrial quadrupedalism). In fact, orangutans show a greater capability of knee rotation, as well as a higher range of motion of their joints, when compared to African apes (Isler 2003; Zihlman *et al.* 2011).

Inferences on knee function based on the patellar shape and the evolution of* Pierolapithecus *and other Miocene apes

As above-mentioned, the patella of *Pierolapithecus catalaunicus* is essentially similar to that of great apes (especially orangutans and gorillas; Figs. 48, 49 and 51). The comparable patellar morphology of *P. catalaunicus* and great apes points out a similar biomechanical loading regime (and associated joint positions), with no habitual and stereotyped flexion-extension of the knee joint. This positional hypothesis is compatible with the orthograde body plan inferred for *P. catalaunicus* on the basis of its thorax morphology (Moyà-Solà *et al.* 2004). In this taxon, the lack of extant ape-like specific adaptations to below-branch suspensory behaviours (e.g., moderate hand length and phalangeal curvature), combined with its orthograde body plan and loss of ulnocarpal contact, led these authors to suggest that enhanced vertical climbing capabilities (compared to older pronograde apes, and not specifically below-branch suspension) was the main target of natural selection shaping the orthograde body plan of *P. catalaunicus* (Moyà-Solà *et al.* 2004, 2005a; Almécija *et al.* 2009; Ward 2015). Previous inferences of above-branch palmigrady for *P. catalaunicus*, based on overall plesiomorphic hand morphology (e.g., dorsally oriented metacarpo-phalangeal joints, and moderate phalangeal length and curvature; Moyà-Solà *et al.* 2004; Almécija *et al.* 2009; Alba *et al.* 2010c), are *a priori* less consistent not only with orthogrady, but also with the great ape-like patellar morphology observed for this taxon in the analyses. However, the above-branch quadrupedalism displayed by *P. catalaunicus* probably had no modern analogue, as previously stressed (Rose 1994; Moyà-Solà *et al.* 2004; Almécija *et al.* 2009, 2014; Alba *et al.* 2010c). The partial remains of the *P. catalaunicus* pelvis suggest that this bony element was similar to that of *Ekembo,* but with a slightly more marked lateral

flaring of the ilia (Hammond *et al.* 2013). Unfortunately, no femoral remains are available for this taxon, although those preserved for other Miocene hominoids have shown to share a similar proximal shape to each other (Almécija *et al.* 2013). This fact may suggest similar and unique hip biomechanics for most of the Miocene apes, which would display (like in *Ekembo* and others) a mosaic postcranial morphology, perhaps combining in the case of *P. catalaunicus* an orthograde body plan with above-branch palmigrady, great ape-like knee function and hip joint with increased ape-like mobility (e.g., Ward *et al.* 1993; Almécija *et al.* 2009; Hammond *et al.* 2013; Ward 2015).

In evolutionary terms, these results shown that cercopithecoids might display, concerning the anteroposterior dimension, the most derived patella among anthropoids (Figs. 48 and 51). However, great apes show somewhat anteroposteriorly thinner patellae than monkeys, although thicker than those of other fossil hominoids (Fig. 51; Table 32). Ward *et al.* (1995) proposed that the patellar morphology of stem hominoids such as *Ekembo* spp. and *N. kerioi* would be representative of the plesiomorphic hominoid (or even catarrhine) condition—i.e., proximodistally higher, anteroposteriorly thinner and mediolaterally narrower patellae compared with those of extant great apes. Therefore, the *quadriceps* muscle mechanical advantage may have increased in the course of hominoid evolution, but never attaining the extreme values of cercopithecoids (highly specialized for stereotyped behaviours). This fact might be related to the more varied locomotor repertoire of great apes than that of monkeys, being *P. catalaunicus* similar to the former group in this regard. The external morphology of the patella of *Eq. africanus*, in turn, is closer to that of African apes, and even to that of modern humans (Figs. 48, 49 and 51). This might be explained by the pronograde, semi terrestrial behaviours inferred for this taxon (McCrossin 1994b; Ward *et al.* 1999; Patel *et al.* 2009). This type of locomotion might be similar in functional requirements (hindlimbs used mainly in compression and loading stereotyped stresses) to the quadrupedal terrestrial knuckle-walking of African apes. Nonetheless, African apes also rely on other orthograde-related behaviours, which require a highly versatile knee joint to combine them with quadrupedalism in both arboreal and terrestrial substrates. Therefore, despite that no orthograde-like traits have been found in *Eq. africanus*, a combination of several locomotor modes performed on different substrates could explain the similarities found between the pronograde semi-terrestrial ape *Eq. africanus* and the orthograde knuckle-walkers (African apes) patellae. In addition to the specimen KPS PT 4 (*E. heseloni*), the patellae of *P. catalaunicus* and *O. bambolii*—the only widely accepted orthograde taxa among the analysed fossil apes (Hürzeler 1968; Moyà-Solà *et al.* 1999, 2004; Susanna *et al.* 2010a,b)—are those that most closely resemble great-ape patellae (Figs. 48, 49 and 51), probably exhibiting a versatile knee joint (in the case of *E. heseloni*, despite its pronograde body plan, authors have outlined enhanced mobility of other anatomical regions, thus also showing a more derived ape-like condition in some cases, e.g., at the hip joint; Walker 1997; Ward 1997, 1998, 2015).

Given that the evolution of the locomotor apparatus in apes during the Miocene apparently proceeded in a mosaic fashion (e.g., Moyà-Solà *et al.* 1999; Alba *et al.* 2010c; Alba 2012; Ward 2015), and the current decimated diversity of extant hominoids, it should not be surprising that there the lack of

extant locomotor analogues for these extinct taxa (Rose 1983, 1994; Moyà-Solà *et al.* 1999, 2004; Alba 2012; Hammond *et al.* 2013). The above-branch quadrupedal component and the lack of specific below-branch suspensory adaptations inferred for *P. catalaunicus* suggest that its great ape-like patellar morphology might be simply attributable to the higher range of knee motion required by orthograde vertical climbing, which would have been probably most similar to that performed by extant great apes (with extended hip joints and flexed knees, and more abducted hindlimb positions than in lesser apes; Isler 2003, 2005; Moyà-Solà *et al.* 2004; Almécija *et al.* 2009; Alba *et al.* 2010c; Susanna *et al.* 2010a,b). All extant hominoids share a similar orthograde body plan, suitable for both vertical climbing and below-branch suspensory behaviours (and bipedalism in hominins; Isler 2003, 2005; Thorpe and Crompton 2006). However, the evidence provided by *P. catalaunicus* (Moyà-Solà *et al.* 2004, 2005a; Almécija *et al.* 2009; Alba *et al.* 2010c; Hammond *et al.* 2013) suggests that the acquisition of suspensory adaptations might have been decoupled from that of vertical climbing (contra Begun and Ward 2005; Deane and Begun 2008, 2010)—with clear suspensory adaptations not being displayed until the late Miocene by *Hispanopithecus*/*Rudapithecus* (see discussion in Alba *et al.* 2012a, but also Moyà-Solà and Köhler 1996; Almécija *et al.* 2007, 2012, 2013; Deane and Begun 2008, 2010; Alba *et al.* 2010c; Begun *et al.* 2012). Concerning *Hispanopithecus*/*Rudapithecus*, the below-branch suspensory adaptations observed on their femora (Moyà-Solà and Köhler 1996; Köhler *et al.* 2002; Begun *et al.* 2012; Almécija *et al.* 2013; see also Chapters 1-3 for *H. laietanus*) and other postcranial remains (Moyà-Solà and Köhler 1996; Almécija *et al.* 2007, 2012; Deane and Begun 2008, 2010; Alba *et al.* 2010c; Begun *et al.* 2012) lead us to predict, based on the analyses above, that the patella of *Hispanopithecus* (if ever found) would probably resemble those of modern great apes, like in *P. catalaunicus* and *O. bambolii*.

Inferences on the basis of the biomechanical response to knee flexion

The functional role of the patellar apex (aim 1).- The presence or absence of a distal apex allows for distinguishing between living great apes (patellae without apex) and the rest of primate species—that is, monkeys (including platyrrhines and cercopithecoids), hylobatids (gibbons and siamangs), and humans (patellae with apex; Fig. 52). In order to interpret the function of this morphology, it was inspected whether the presence of a patellar apex can be related to a functional role, and how it might work from a biomechanical viewpoint. The patella is embedded within the ligaments and muscles of the *quadriceps* muscle complex, and the patellar ligament attaches on the apex (at the distal edge in patellae without this structure; Sarin *et al.* 1999; Platzer 2008). Moreover, the presence of an apex enlarges the proximodistal length of the whole patellae and, consequently, the length of the *quadriceps* muscle-patellar tendon complex. Thus, the effective length of the *quadriceps* muscle action is also lengthened during knee extension (Haxton 1944; Badoux 1974; Ward *et al.* 1995). It is easy to assume that primates with no patellar apex could have different biomechanical requirements than those that display this structure, but this examination of von Mises stress on living primates does not find differences between patellae with and without apex. However, significant differences are observed between pronograde and

orthograde taxa irrespective of the presence/absence of this structure. Although varying in frequency, pronograde primates preferentially use quadrupedal locomotion (Arms *et al.* 2002; Fleagle 2013). In all of the pronograde quadrupedal taxa, the apex seems to participate in some way in stress dissipation through the patella, as the most distal region remains with no (or very low) stress (Fig. 55). This biomechanical role is confirmed by the results obtained for the modified models (Fig. 59). When the apex is removed in *Cercopithecus* (*Cercopithecus*-NoApex), the stress is entirely focused in the posterior side and the distal region of the modified bone; contrarily, the virtual inclusion of an apex in *Pongo* (*Pongo*-WApex) clearly dissipates the original stress concentration at its most distal area (this can be also seen in *Gorilla*, although its original stress pattern distribution is very different and does not show a distal concentration of high stress values; see below).

Given that stress pattern differences are not related to locomotor modes but instead to body plan types, these variations could thus be associated with differential traits that characterize pronogrady-orthogrady, such as habitual knee postures, preferential direction of hindlimbs movement and/or body weight (BW) transmission through the limbs. Thus, pronograde quadrupeds share habitual movements of the hindlimb in the parasagittal plane, with frequent semi-flexed postures of the knee joint, and with only 40% of their body weight (BW) being transmitted through the hindlimbs (Badoux 1974; Martin 1990; Fleagle 2013). In turn, orthograde primates have more versatile positional behaviours, which mainly include vertical climbing, clambering, below-branch suspension, and bipedalism (Hunt 1991a, 2004). A special case is that of humans, which most frequently show a completely extended position of the knee, and transmit their whole BW through their posterior extremities due to obligate terrestrial bipedalism (Martin 1990; Masouros *et al.* 2010; Crompton 2016). Great apes also load the whole BW through the legs when vertical climb or clamber, and the range of flexion of the knee is more varied than during bipedalism, from flexed (climbing) to extended (clambering; Crompton 2016). Thus, hindlimbs in modern humans and great apes (especially in *Pongo*, as it frequently relies on clambering) support the whole BW and the knee joint is used preferentially in extended positions (Isler 2005; Crompton *et al.* 2010). Haxton (1944) proposed that the patella was most functionally important in extended positions of the knee joint based on comparative results in patellar mediolateral breadth. Hence, as previously stated (Crompton *et al.* 2008, 2010; Crompton 2016), here is suggested that due to similarities in preferential knee postures and BW loading, hindlimbs of modern humans and great apes (mainly during clambering) probably require similar biomechanical demands at the knee joint. Nonetheless, results of the two orthograde taxa *Gorilla* and hylobatids depart from the rest. African apes are orthograde primates that primarily rely on quadrupedal knuckle-walking, thus using the hindlimb habitually in compression (Stern 1975; Doran 1996; Hunt 2004). The quadrupedal nature of this locomotor mode is apparently not discerned in the results between chimpanzees and orangutans, as the patella of the former has a biomechanical performance similar to that of *Pongo* (Fig. 55). However, results for the patella of *Gorilla* are clearly different from those of all the remaining taxa, including the other knuckle-walker of the sample (*Pan*). A suitable explanation for these results remains difficult and

further work is needed to explain the singularity of gorilla's results from a biomechanical viewpoint. On the other hand, hylobatids have a more plastic and versatile locomotor repertoire and, though they preferentially engage in brachiation (in where the hindlimbs are free of locomotor tasks; Fleagle 1976; Gittins 1983), they also rely on other locomotor modes (including leaping and bipedalism; Fleagle 1976; Gittins 1983; Vereecke *et al.* 2006; Channon *et al.* 2012) where the legs take an important role. In the case of leaping, the knee is completely flexed in the moment of take off, whereas in bipedal locomotion, this joint is semi-flexed or completely extended (Haxton 1944; Prost 1967; Vereecke *et al.* 2006; Channon *et al.* 2012). Although no data are available for knee posture during travelling by means of brachiation, the knee probably remains less flexed than during leaping and/or bipedal behaviours (Vereecke *et al.* 2006). Results for the hylobatids patellae show a very low stress pattern for an extended knee phase, which could point to the non-intervention of the hindlimbs during brachiation; whereas similarities with modern humans and quadrupeds would be reflected in these results for semi-flexion and full-flexion of the joint (Fig. 55).

Evolutionary scenario for the patellar apex within the Hominoidea (aim 2).- All the hominids except humans lack the apex, and so the presence/absence of the apex might prove useful for interpreting evolutionary scenarios in fossils (Fig. 61). *Epipliopithecus vindobonensis* is a putative stem catarrhine for which several authors have inferred a generalized above-branch quadrupedalism behaviour (or even terrestrial), combined in some extent with climbing, leaping and suspension (Zapfe 1958; Rose 1993; Harrison 2013). This taxon has a patellar shape similar to that of hylobatids (Rose 1993), with a distal apex and a stress pattern distribution similar to that of *Hylobates* (Fig. 57b). The results seem then to reflect the versatile locomotor repertoire inferred for this taxon (e.g., as explained above for living hylobatids; Fleagle 1976; Gittins 1983). Among hominoids, *Ekembo* (formerly *Proconsul*) patellae are the oldest known records for this bone element. They well fit within the patellar morphology proposed for the last common ancestor of apes and humans by Ward and colleagues (1995): proximodistally short and anteroposteriorly thin. Furthermore, these patellae show a distal apex (Ward *et al.* 1995). Following *Ekembo*, other fossil taxa that show patellae with apex include *Equatorius* and *Nacholapithecus* (McCrossin 1994a; Rose *et al.* 1996; Nakatsukasa *et al.* 2012). Contrary to these, the stem great ape *P. catalaunicus* lacks the apex and the results reveal for this taxon a stress pattern similar to that of orangutans and chimpanzees (Fig. 57a), probably reflecting knee postural preferences and BW loading similar to that of great apes (see Chapter 5). Therefore, the apex would probably be a plesiomorphic structure within catarrhine primates, which was apparently lost at some point of the hominid evolutionary history. However, modern humans and early members of its lineage (e.g., *H. floresiensis* and *H. neanderthalensis*; Trinkaus 1983; Jungers *et al.* 2009) have patellar apex. Interestingly, this structure is not displayed by the early hominin *Australopithecus sediba* (Fig. 61; DeSilva *et al.* 2013). Hence, the presence of apex would be primitive for hominoids, including humans, and the lack of this structure in hominids would be a derived trait for this group.

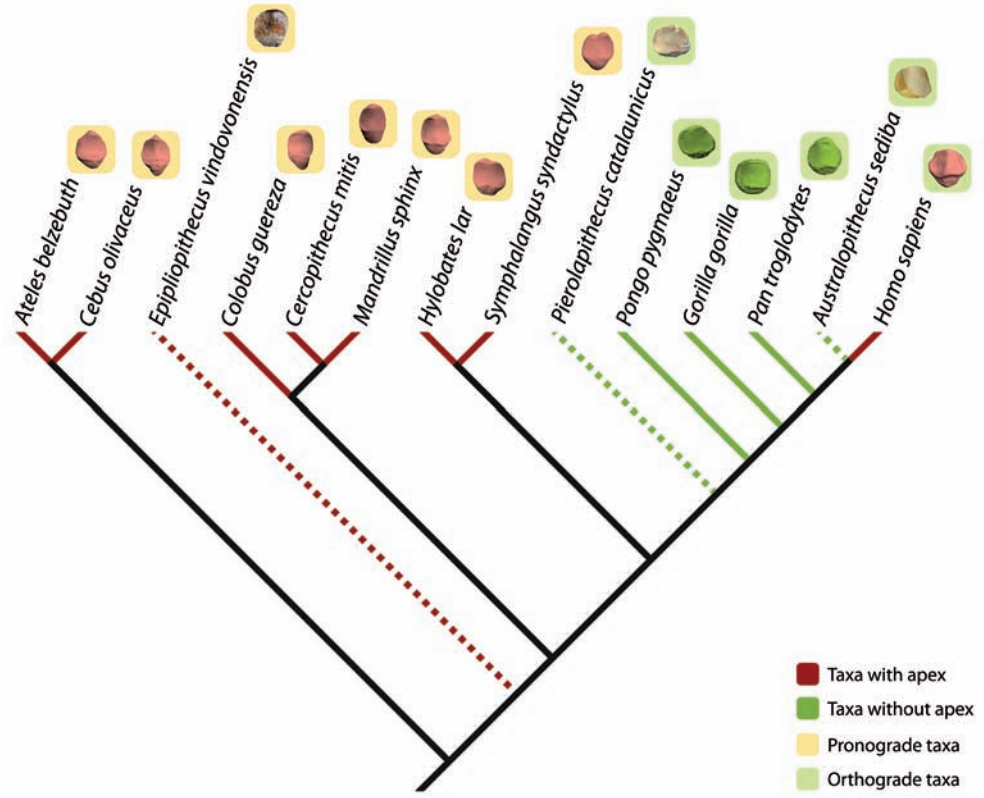

Figure 61 Tree illustrating the presence (red) or absence (green) of patellar apex in the living taxa included in this work (continuous lines). Fossil specimens (dashed lines) comprise *Epipliopithecus vindobonensis* (NHMW1970/1397/0024; reversed), *Pierolapithecus catalaunicus* (IPS21350.37), and *Australopithecus sediba* (MH2-*UW88-79&100*; image from DeSilva *et al.* 2013). The tree does not trace the evolutionary history of this patellar character, but only schematizes the presence/absence of the patellar apex in the primate sample to better visualize its framework combined with the body plan display for every taxa.

Stabilization role of patellar shape (aims 1 and 2).- **The apex:** taking into account the evolutionary scenario of the patellar apex proposed above (being the lack of apex a derived trait for hominids), the presence of apex within the human lineage should represent a response to some kind of extrinsic epigenetic stimulus, since the phylogenetic signal on this bone has been ruled out in previous works (Haxton 1944; Sarin *et al.* 1999; see also Chapter 5). Then, it is hypothesized that the reversion of this character within the genus *Homo* might be related to some mechanical similarities between bipedalism and quadrupedalism. As aforementioned, the von Mises stress results do not reflect locomotor types, but instead the type of body plan. However, as seen above, knee posture during bipedal and quadrupedal travelling is completely different (full-extended *vs* semi-flexed), as well as is the BW loading by the hindlimbs (40% *vs* 100%). Nonetheless, some similarities are found. In both cases, hindlimbs move in the parasagittal plane, the knee posture is continued (virtually all the time extended in bipeds and around semi-flexion in quadrupeds), and the joint needs of a high stabilization in order to avoid luxations of the knee elements during motion (Ward *et al.* 1995; Masouros *et al.* 2010; DeSilva *et al.* 2013; Fleagle 2013). Then, the apex might additionally participate in stabilization of the knee joint, by closing the patella to the tibial tuberosity and shortening the patellar ligament length. This would not interfere with its probable

principal role of lengthening the relative moment arm of the *quadriceps* muscle in quadrupeds and leapers for powerful extension of the knee (a function that is *a priori* less necessary in humans because their continuously extended knee position; Ward *et al.* 1995; Crompton 2016).

The articular surface geometry: apart from the apex, the geometry of the patellar articular surface (together with other ligaments and muscles of the knee joint; Holt and Hamill 1995; Masouros *et al.* 2010; DeSilva *et al.* 2013) is also important in preventing knee joint luxation (Lovejoy 2007). Both bipeds (modern humans) and quadrupeds (cercopithecoids and platyrrhines) display a clear distinction between the medial and lateral sides of the articular surface that are usually separated by a well-marked keel (Fig. 52). Moreover, the patellae of modern humans even show other well-distinguished small facets (see Lovejoy 2007 for further description). Conversely, the patellar articular surface of apes (especially great apes) is completely flat, and does not show any distinction between lateral and medial regions (Fig. 52; Lovejoy 2007). This morphology is reflected in the trochlear surface of the femur, irrespective of its compartmentalized (humans and quadrupeds) or flat (apes) geometry. In humans and quadrupeds, the femoral trochlear surface is deep and besides, in the former, the lateral lip is clearly more projected anteriorly than the medial lip in order to avoid the lateral dislocation of the patella (also observed in monkeys in a lesser degree; Lovejoy 2007; Masouros *et al.* 2010; DeSilva *et al.* 2013). For apes, the femoral trochlear surface is shallow and lateral and medial lips are barely developed. This morphology has been associated with a wider range of motion of the knee joint (Ward *et al.* 1995; Madar *et al.* 2002; Lovejoy 2007). Likewise, Lovejoy (2007) proposed that better congruity between patellar and femoral articular surfaces in apes knee joint would be related to less stress concentration in the patellae (see also Ward *et al.* 1995). FE results in this work do not reflect these differences, even showing a greater similarity between *Homo* and *Pongo-Pan* patellae than *Homo* and monkeys' patellae. The absence of such differences when comparing patellae with more complex articular surfaces and those with flat articular surfaces could be related to the simplified model of the primate knee used. For example, this work does not include the lateral deviation of the patella during knee flexion (Heegaard *et al.* 1995; Masouros *et al.* 2010). However, patellar lateral dislocation is a frequent disease among modern humans (Holt and Hamill 1995), hence the joint displays important mechanisms of stabilization (e.g., femoral trochlear surface morphology and action of muscles and ligaments at the patellofemoral joint) that probably provide with an additional amount of stress not considered in this work (e.g., tension in different directions; Heegaard *et al.* 1995; Ward *et al.* 1995). However, a knee with a wider range of movements in apes would not need as strict structural and dynamic stabilization of the joint as in the case of humans and monkeys, which preferably use the knee in the parasagittal plane (Haxton 1944; Ward *et al.* 1995; Madar *et al.* 2002). Therefore, the inclusion of a lateral movement in the model could incorporate a meaningful increased of stress.

Functional role of patellar AP and PD (aim 3).- The knee is considered to be a hinge joint whose centre of rotation is situated at the femoral condyles (although sometimes there also exists an anteriorly sliding component; Lovejoy 2007; Schindler and Scott 2011). The distance between the centre of rotation and the patella is the effective arm length for the action of the *quadriceps* muscle, whereas the patellar tendon moment arm is the perpendicular length from this tendon to the femur-tibia contact point (Nisell 1985; Schindler and Scott 2011). Several authors (Preuschoft 1970; Badoux 1974; Ward *et al.* 1995) outlined that variation in both patellar AP and PD would favour the lengthening of the moment arms of the *quadriceps* muscle complex and would generate a more powerful extension of the knee joint (e.g., after a patellectomy the *quadriceps* muscle moment strength can decrease up to 15% in a 30º-flexed human knee; Badoux 1974; Nisell 1985). That is, primates that need a powerful extension of the knee for locomotion (i.e., mainly leapers, but also quadrupeds) tend to show thicker AP and higher PD patellae (Ward *et al.* 1995; see Chapter 5).

Results regarding von Mises stress distribution reflect this morphological trend, since the anteroposteriorly thinner *Cercopithecus*-ThinAP patella resembles that of *Symphalangus*, and the anteroposteriorly thicker *Symphalangus*-ThickAP patella pattern is more similar to that of *Ateles* (Fig. 59). Hence, in the case of *Cercopithecus*-ThinAP, the original stress pattern changes from that of a specialized pronograde quadruped (thick AP thickness) to that of a more versatile primate (thin AP thickness), where flexed positions and powerful extension of the knee joint are less relevant within its locomotor repertoire (Ward *et al.* 1995; McGraw 1996; Fleagle 2013; see also Chapter 5). In the case of *Symphalangus*-ThickAP patella, the new obtained stress pattern (similar to that of *Ateles*) could be explained by the lesser frequency of below-branch suspension and a higher frequency of quadrupedalism in spider monkeys than in siamangs, although the locomotor repertoire of *Ateles* is also notably varied (Fleagle 1976; Cant *et al.* 2001, 2003; Youlatos 2002). However, the biomechanical influence of changes in PD length is less clear, and there is a twofold explanation for this phenomenon: the singularity of the stress pattern in the original patella of *Gorilla* that is not possible to currently relate to any functional/locomotor pattern (see above); and the new pattern obtained in the modified patella (*Gorilla*-HighPD), which resembles those of (the other orthograde primates) *Pongo* and *Pan* (irrespective of their preferential locomotor mode, that is, suspension-clambering *vs* knuckle-walking, respectively). In any case, PD elongation of the patella lengthens the moment arm of the *quadriceps* muscle (as occurs with AP) and the contact with the femoral patellar groove is larger, involving an increase of patellar stress that is probably what is observed in the results (Fig. 59c; Ward *et al.* 1995).

Therefore, from a biomechanical point of view, FE obtained results in models with modified AP thickness and PD height would reflect the previously stressed relation between patellar morphology and knee function, as well as the enhanced ability of the *quadriceps* muscle complex for effective and powerful extension of the knee joint in quadrupedal primates with thick AP and high PD patellae.

THE POSITIONAL BEHAVIOUR OF THE FOSSIL GREAT APES FROM THE VALLÈS-PENEDÈS

The hindlimb remains of Vallès-Penedès great apes described in this work, even considering that more than a single taxon is represented, generally reinforce previous inferences that Miocene apes displayed a combination of positional behaviours that does not have any close extant analogue (i.e., each extinct genus shows a unique combination of monkey-like and ape-like postcranial traits, unknown among extant apes; e.g., Rose 1983, 1993; Moyà-Solà and Köhler 1996; Moyà-Solà *et al.* 2004; Almécija *et al.* 2007; Alba 2012; Senut 2015; Ward 2015). The hindlimb morphology of the Vallès-Penedès great apes and its available internal structure is not only distinctive from that of other Miocene hominoids, but also from one another (Moyà-Solà and Köhler 1996; Köhler *et al.* 2001; Moyà-Solà *et al.* 2004; Almécija *et al.* 2007, 2009; Alba 2012; Alba *et al.* 2012a; Hammond *et al.* 2013; Tallman *et al.* 2013; Susanna *et al.* 2014). Thus, the morphological adaptations and internal organization patterns related to above-branch palmigrady and orthograde behaviours (e.g., vertical climbing and below-branch suspension) found in these taxa suggest that they probably incorporated these locomotor modes within their positional behaviour, but in different frequencies. Nonetheless, identifying the functional role of a specific trait is sometimes very difficult. In addition, although the function related to a specific trait was well established, the animal could still retain the ability to perform other locomotor types not directly associated with this functional relationship. This difficulty is more evident regarding plesiomorphic traits, since it is difficult to test whether these features could be already functionally active (participating and maintaining the ancestral behaviour) or just a retention without functional role that not compromise the new acquired (derived) behaviour (Stern and Susman 1981; Latimer 1991; Lauder 1996; Ward 2002). Taking into account both the aforementioned premises and the absence of conclusive results to elucidate the functional role of the primitive characters, here the relevance of plesiomorphic traits will be considered in the same degree than adaptations to infer positional behaviour of the taxa included in this work.

The positional behaviour of cf. **Dryopithecus fontani**

Regarding the postcranium of *Dryopithecus*, besides the Vallès-Penedès femur tentatively assigned to *Dryopithecus fontani* analysed in this work (ca. 11.9 Ma), only a humerus from the type locality (Saint Gaudens, France) and a distal fragment of humeral shaft from Castell de Barberà (Vallès-Penedès Basin, Spain) have been attributed to this taxon (in the latter case only tentatively; Depéret 1887; Pilbeam and Simons 1971; Begun 1992b; Alba *et al.* 2011a; Almécija *et al.* in prep.a). Moreover, two phalanges also found in Castell de Barberà might belong to the same taxon (Almécija *et al.* 2012, in prep.b). Despite the generally hominoid-like appearance of the humerus (Alba *et al.* 2011a) and the lack of similarities with living apes on the thumb remains from Castell de Barberà (Almécija *et al.* 2012), the positional behaviour of this taxon is still unclear. The general Miocene ape-like morphology of the phalanges and some of the

humeral traits (e.g., rounded cross-section and deep olecranon and coronoid fossae) suggest that above-branch quadrupedalism might have taken part of the *Dryopithecus* locomotor repertoire (assuming that phalangeal remains belong to this taxon; Begun 1992b; Alba *et al.* 2011a; Almécija *et al.* 2012). Moreover, below-branch suspension cannot be completely ruled out on the basis of humeral morphology (Alba *et al.* 2011a). The shape of the proximal femur tentatively attributed to the same taxon displays features functionally related to generalized arboreal quadrupedalism and others associated with enhancement of hindlimb abduction; whereas the internal structure of the neck and the diaphyseal structural properties are more clearly related to quadrupedal behaviours (see above and Chapter 1). This combination of traits reinforces the view that *Dryopithecus* might represent, like many other Miocene apes, a locomotor stage intermediate between early Miocene stem hominoids and the suspensory extant (and some late Miocene) apes (Alba *et al.* 2011a). This femur alone further suggests that this taxon lacks specific adaptations for below-branch suspensory behaviours, such as the larger femoral head relative to the neck that is displayed by *Hispanopithecus*. However, considering the whole postcranial evidence that probably belong to *Dryopithecus*, and given the mosaic evolution of the hominoid postcranium evidenced by this and other Miocene apes, suspensory behaviours cannot be completely discounted for this taxon (Alba *et al.* 2011a). Furthermore, it is also important to take into account the body weight estimated for *Dryopithecus*, between 40-50 kg on the basis of the femoral head (Moyà-Solà *et al.* 2009a). This body weight is situated slightly above the 40 kg proposed as the maximum value for efficient arboreal quadrupedalism (Cartmill 1985; Demes *et al.* 1994; Larson 1998b). Then, *Dryopithecus* might have adopted two possible solutions to this biomechanical constrain. On the one hand, to engage in more orthograde-like behaviours such as the vertical climbing or below-branch suspension that allowed it to better negotiate with an arboreal milieu (Cartmill 1985). This evidenced by the presence of some traits associated with wider range of hip joint motion and related to vertical climbing (mainly on the studied femur; see above). Otherwise, another possible explanation is that *Dryopithecus* could eventually go down to the ground, thus relying on terrestrial quadrupedalism in some degree. However, no specific evidence of terrestriality is found within the fossil femur.

Overall, above-branch quadrupedalism with powerful grasping capabilities and some degree of vertical climbing (without completely discounted below-branch suspension and some degree of terrestriality) seems the most likely locomotor repertoire for *Dryopithecus* based on the information provided by the IPS41724 femur and the other few postcranial remains assigned to this genus.

The positional behaviour of **Pierolapithecus catalaunicus**

The strong curvature of the ribs, a large clavicle, and the lumbar vertebral morphology (e.g., lack of ventral keel and transverse processes inserted in the pedicle-body junction) suggest that *Pierolapithecus* (ca. 11.9 Ma) would have an orthograde body plan with a relatively broad and shallow thorax, being the first unambiguous evidence of this body plan in the fossil record (Moyà-Solà *et al.* 2004; Susanna *et al.*

2010a). In addition, this taxon shows other hominoid-like postcranial features related to this type of body plan, whether incipient (e.g., somewhat iliac flaring; Hammond *et al.* 2013) or clearly related to orthogrady (e.g., lack of ulnocarpal contact; Moyà-Solà *et al.* 2004). In contrast, more primitive traits are observed in the pelvic remains (e.g., concave gluteal surface; Hammond *et al.* 2013) and fingers of *Pierolapithecus* (moderate length of metacarpals and phalanges; Moyà-Solà *et al.* 2004, 2005a). Moreover, the phalanges show a series of traits related to powerful-grasping palmigrady with assistance of the pollex, such as a proximodorsally tilted proximal articular facet that is besides wide and flat, and a large and widely separated plantar tubercles surrounding a deep central depression (Moyà-Solà *et al.* 2004; Almécija *et al.* 2009). Furthermore, the phalanges are not as long and markedly curved as in suspensory primates (Moyà-Solà *et al.* 2004, 2005a; Alba *et al.* 2010c; contrary, Deane and Begun 2008, 2010) suggesting that *Pierolapithecus* could integrate an important component of below-branch suspension based on phalangeal curvature. Besides the foot elements, the only complete hindlimb bone of *Pierolapithecus* is the left patella (Moyà-Solà *et al.* 2004). Ward *et al.* (1995) already highlighted the relevance of the functional signal provided by this bone by means of a morphometric study of its external dimensions. The patella of *Pierolapithecus* displays an overall great ape-like morphology, thus being functionally related to the performance of relatively versatile movements of the knee as well as a low emphasis on fully-flexed positions at this joint (Harrison 1986; Ward *et al.* 1995). In accordance, the biomechanical response of this bone to knee flexion is also similar to that observed in great apes (especially chimpanzees and orangutans), which has been associated with habitual extended positions of the knee and low stereotyped movements of the hindlimb (see above). Therefore, the external morphology and biomechanics of the patella are compatible with *Pierolapithecus* displaying orthograde adaptations for vertical climbing, although are less compatible with the previously inferred above-branch palmigrade quadrupedalism for this taxon (Moyà-Solà *et al.* 2004; Almécija *et al.* 2009; Alba *et al.* 2010c; Hammond *et al.* 2013). Despite these apparent incompatibilities, as occurs in other fossil apes, the locomotor repertoire inferred for *Pierolapithecus* is probably not observable among living primates, again highlighting the mosaic-nature of the hominoids postcranium during the Miocene.

The positional behaviour of **Hispanopithecus laietanus**

The younger *Hispanopithecus laietanus* (ca. 9.6 Ma) femora and tibia are indicative of a locomotor repertoire combining orthograde behaviours (below-branch suspension and vertical climbing, as derived from its femoral neck-shaft angle, relative width of the tibial medial malleolus, the homogeneous distribution of the femoral neck cortical bone, and the diaphyseal structural properties of the femur, among other features) with above-branch palmigrade quadrupedalism (as suggested among others by the shape of the tibial articular surface). These results are in accordance with the previously proposed positional behaviour for this taxon on the basis of other anatomical regions, as well as those also focused on the hindlimb bones (Moyà-Solà and Köhler 1996; Köhler *et al.* 2001, 2002; Almécija *et al.* 2007, 2009;

Alba *et al.* 2010c, 2012a; Tallman *et al.* 2013). As in the case of *Pierolapithecus*, vertebrae morphology of *Hispanopithecus* (e.g., no ventral keel and transverse processes originating from a the pedicle in lumbar vertebrae) indicates the presence of a hominoid-like wide and shallow thorax with a somewhat short and stiff lumbar region (Moyà-Solà and Köhler 1996; Köhler *et al.* 2001; Susanna *et al.* 2014). In this regard, the morphology of the scapula (acromion process longer and more compressed than in monkeys), and first rib (e.g., craniocaudally compression) from the partial skeleton of the fossil site of Can Feu also support these inferences (Alba *et al.* 2012a). Evidences from the *Hispanopithecus* forelimb also point out the orthograde-related component within its locomotor profile, by displaying features associated with broad movements (including forelimb abduction), pronation-supination, and stabilization of the elbow during flexion-extension (e.g., slightly convex deltoid plane, a markedly curved radius, and reduced olecranon process in the ulna; Moyà-Solà and Köhler 1996; Alba *et al.* 2012a). Nonetheless, other ulnar features are more related to quadrupedal behaviours, such as the posteromedially tilted olecranon process (Alba *et al.* 2012a). Manual phalanges of *Hispanopithecus* are long and highly curved, thereby highlighting the use of the hand in suspensory behaviours. Contrarily, some other traits in the proximal phalanges (i.e., dorsal extension of the articular surface) and metacarpal proportions and morphology (short length and stoutness) are more closely related to above-branch palmigrade quadrupedalism (Moyà-Solà and Köhler 1996; Almécija *et al.* 2007; Deane and Begun 2008; Alba *et al.* 2010c; see Begun *et al.* 2012 for a different interpretation). Moreover, powerful grasping capabilities are inferred from the marked insertions for the flexors on the phalangeal shafts and the large pits for the collateral ligaments (Almécija *et al.* 2007).

Altogether (and even with every fossil remain alone), the *Hispanopithecus* postcranial morphological evidence suggests that this taxon would retain some degree of above-branch palmigrady combined with orthograde behaviours, showing clear adaptations for below-branch suspension (although it might also relied on vertical climbing in some extent).

Evolutionary scenario of orthogrady

The unambiguous appearance of the isolated anatomical traits that characterize living hominoids started with the taxa recognized as stem hominoids from the early Miocene of Africa, although in a very incipient fashion: *Morotopithecus*, *Ekembo*, *Proconsul*, *Equatorius*, and *Nacholapithecus*. Apart from *Morotopithecus*, which displays some putative orthograde-related adaptations at the vertebrae and its body plan remains unclear (Walker and Rose 1968; Gebo *et al.* 1997; MacLatchy 2004; Nakatsukasa 2008), the remaining of stem Miocene apes still preserved a pronograde-like body plan, with narrow and deep thoraxes, mainly associated with quadrupedal behaviours (e.g., Ward 1993; Ward *et al.* 1999; Nakatsukasa 2004; Nakatsukasa and Kunimatsu 2009). In spite of their primitive organisation, these stem hominoid already show more derived (incipient ape-like) features, such as the lack of an external tail, powerful-grasping abilities, and enhanced joints mobility (e.g., Ward *et al.* 1993; McCrossin 1994a, 1997; Rafferty *et al.* 1995; MacLatchy *et al.* 2000; Gommery *et al.* 2002; Nakatsukasa *et al.* 2012; Senut 2015; see also a review

in Ward 2015). The most accepted ongoing hypothesis is that early Miocene taxa were habitual above-branch pronograde quadrupeds that already displayed some incipient (more derived) orthograde-related traits. More recent apes from the middle Miocene of Europe, including those of the Vallès-Penedès Basin, follow the trend observed in the African fossil taxa: they probably still preserved a significant component of arboreal quadrupedalism within their locomotor repertoires (Begun 1992b, 2013; Alba 2012); however, the first unambiguous evidences of orthogrady (*Pierolapithecus*, ca. 11.9 Ma) and below-branch suspensory behaviours (*Rudapithecus* and *Hispanopithecus*, ca. 9.6-10 Ma) are found at the Miocene of Europe (e.g., Begun 1992b, 1993; Moyà-Solà and Köhler 1996; Moyà-Solà *et al.* 2004; Almécija *et al.* 2007; Alba 2012; Begun *et al.* 2012).

Thus, early to late Miocene hominoid postcranial remains evidence the high diversity (and associated locomotor profiles) among these taxa, as well as the mosaic nature evolution of the orthograde behaviours (Rose 1983; Rae 1999; Moyà-Solà *et al.* 2004; Almécija *et al.* 2007; Ward 2007, 2015; Alba *et al.* 2012a; among others). In this regard, the femora, tibia and patella of the Vallès-Penedès great apes described and analysed in this work further underpin the previously inferred diversity within their postcranial morphology and, at the same time, point out the morphological uniqueness of Miocene hominoids postcranium and locomotor repertoires compared to their closest extant relatives. Nonetheless, further research is still needed concerning the internal structure and biomechanical properties of the Miocene apes postcranial elements in order to better understand them (but also the relation of the internal structure-biomechanical properties to positional behaviours performed by living hominoids). Nonetheless, the external shape, the internal organization, and the structural features of the hindlimb remains of the Vallès-Penedès great apes corroborate the mosaic evolution of the locomotor apparatus in the Hominoidea during the Miocene (e.g., Rose 1983; Rae 1999; Moyà-Solà *et al.* 2004; Almécija *et al.* 2007; Ward 2007, 2015; Alba *et al.* 2012a).

Interestingly, the middle Miocene great ape *Pierolapithecus* is characterized by a modern orthograde design that suggests an important vertical climbing component within its locomotor repertoire but, contrary to *Hispanopithecus* (late Miocene), lacks adaptations to below-branch suspension (Chapter 5; Moyà-Solà *et al.* 2004; Almécija *et al.* 2009; Alba *et al.* 2010c). This fact suggests that enhanced vertical climbing capabilities (instead of suspension) was the main target of natural selection in terms of the acquisition of an orthograde body plan. Thus, if this orthograde body plan was originally related to vertical climbing in functional regards, then suspensory behaviours might evolve independently in several hominoid lineages (hylobatids and hominins; Moyà-Solà *et al.* 2004, 2005a; Almécija *et al.* 2009, 2013, 2015; Ward 2015; among others). Moreover, this homoplastic evolution would be also evidenced by the presence of suspensory adaptations in the further-phylogenetic related atelids (Erikson 1963; Youlatos 1993, 2002; Larson 1998a; Hunt 2016). Therefore, the great apes of the Vallès-Penedès are key to elucidate the still controversial positional behaviour of the crown hominoid / hominid last common ancestor (LCA). At this respect, functional adaptations found in the Iberian Miocene great apes outline that the hominid LCA might not display the whole set of locomotor synapomorphies characteristic of living apes (it actually

would lack extant analogues). The current evidence suggests that the LCA possessed an orthograde body plan associated with vertical climbing but not specifically suspensory adaptations.

The combination of traits found at the IPS41724 femur (cf. *Dryopithecus fontani*), especially those of its internal structure, are also especially interesting in evolutionary regards. External shape adaptations observed at this femur suggest that *Dryopithecus* might be less specialized for enhancing hip abduction than *Hispanopithecus* and modern apes and, given its older age, it could represent a good model for the plesiomorphic hominid (great ape and human clade) femur. However, the femur of cf. *Dryopithecus* shows interesting similarities with *Australopithecus* and modern humans in terms of FCNB and mechanical properties of the shaft (Chapters 2 and 3). These results further support previous works that highlighted closer anatomical affinities (that are functionally-related) between early hominins and Miocene apes than between the former and modern apes (e.g., Lovejoy *et al.* 2009; Almécija *et al.* 2013). Therefore, the similarities of these traits in Miocene apes might indicate either that hominin bipedalism evolved from some type of Miocene ape-like quadrupedalism, or that the mechanical demands of hominin bipedalism and Miocene ape-like quadrupedalism are convergent.

The study of the Miocene great apes found in the Vallès-Penedès Basin, as also evidenced in this thesis, is yielding highly relevant results that are of potential interest for unravelling and better understanding not only the origin of orthogrady and the ape-like specialized behaviours such as vertical climbing and below-branch suspension, but also the largely controversial origin of bipedal adaptations (and its particular loading regimes) in the hominin clade (taking into account that this is "the postcranial autopomorphy" of the group).

It wasn't until late in life that I discovered
how easy it is to say "I don't know".

-- W. Somerset Maugham --

Section VIII. SUMMARY AND CONCLUSIONS

The main contributions and conclusions derived from this thesis are summarized below:

1.- The hindlimb external morphology of the Vallès-Penedès taxa display a combination of primitive (monkey-like) and derived (ape-like) features. The former are mostly related to pronograde quadrupedalism by enhancing stabilization of the hindlimb joints; whereas the latter (derived traits) are associated with orthograde behaviours such as vertical climbing (cf. *Dryopithecus fontani* and *Pierolapithecus catalaunicus*) and below-branch suspension (*Hispanopithecus laietanus*). The observed derived features in the Vallès-Penedès great apes are mainly related to the enhancement of hip abduction and knee wide mobility, being more similar to those of living apes, whose hindlimb joints display broad ranges of motion.

2.- The distribution of the cortical bone around the femoral neck (FNCB) in extant primates is functionally related to their positional behaviour. Thus it can be employed to reliably infer key aspects of the locomotor repertoire of fossil primates. Although the FNCB distribution has been traditionally used to infer bipedalism (asymmetric pattern), results presented in this work outline that the FNCB only enables distinguishing two loading patterns: stereotyped (quadruped anthropoids and bipeds) and non-stereotyped (taxa that rely on suspensory behaviours to some extent, that is, apes and atelids). Thus, primates that load the hindlimb in non-stereotyped positions display a homogeneous (superoinferiorly similar) distribution of the FNCB (apes and atelids); whereas those primates with marked stereotyped load patterns show an asymmetric (superiorly thinner) distribution of the FNCB (anthropoid quadrupeds and humans).

3.- The Vallès-Penedès hominoids are the only fossil apes where FNCB distribution has been explored. *Hispanopithecus laietanus* displays the oldest evidence across the fossil record of a homogeneous, extant ape-like pattern of FNCB distribution in the fossil record, consistent with higher mobility (specifically abduction) at the hip joint than in generalized quadrupedal taxa. On the other hand, cf. *D. fontani* shows an asymmetric distribution of the FNCB. This pattern is related to stereotyped loadings at the hip joint, such as in generalized quadrupeds and also modern humans. In evolutionary terms, assuming that the IPS41724 femur belongs to the great ape *Dryopithecus*, it follows that its asymmetric pattern (more similar to hominins than to living apes) could represent the plesiomorphic condition for the great ape and human clade (i.e., Hominidae), instead of the symmetric pattern of extant hominoids, as previously proposed. However, formal testing is still required to ascertain whether the condition of hominins is plesiomorphic or derived.

4.- The Vallès-Penedès great apes cf. *D. fontani* and *H. laietanus* show different cross-section mechanical properties at the femoral shaft that probably relate to distinct functional demands. IPS41724 (cf. *D. fontani*) has some clear similarities to cercopithecoids and African apes (to some extent). On the other hand, IPS18800 (*H. laietanus*) displays some variability between the left and right femora. Anteroposterior strength results for the right femora show a shift towards suspensory primates (especially gibbons), whereas results for the left specimen resemble those of African apes and even those of cercopithecoids at the proximal shaft. Overall, IPS41724 proximal femur shows higher femoral shaft robusticity, rigidity and strength than both femora of the IPS18800 partial skeleton. These results suggest that cf. *D. fontani* might retain an important component of plesiomorphic above-branch quadrupedalism within its positional behaviour. The suspensory trend observed in the results for *H. laietanus* might be associated with similar biomechanical demands that those taxa that perform orthograde-like behaviours, such as below-branch suspension, in which the femoral shaft displays less anteroposterior strength. Nonetheless, *H. laietanus* also shows some affinities with quadrupedal primates. Since the morphologies inspected here have been previously associated with specific functional differences related to locomotion, mechanical results on the *H. laietanus* femora support the hypothesis that this taxon combined both plesiomorphic (quadrupedalism) and derived (orthograde-related) locomotor behaviours. Therefore, the study of the structural properties of the Iberian Miocene great apes allows sheds light into the biomechanical requirements of the unique (i.e., they have no extant analogues) locomotor behaviours of these fossil taxa.

5.- When the biomechanical response of the patella during knee flexion is examined through finite element analysis, similar results are obtained from the sample of extant and extinct anthropoids, and few significant differences are found regarding body plan types. The most relevant difference is the low-stress nature of the most distal region of the patellar apex in pronograde primates. Contrarily, orthograde taxa show a distal area with higher values of stress, independently of whether or not their patellae have an apex (hylobatids and humans) or do not (great apes). These results have been associated with a possible role of stress dissipation of the apex in pronograde quadrupeds, as well as to the habitual semi-flexed postures of the knee and the loading of only 40% of body weight through the hindlimbs that characterized pronogrady. Besides, patellar shape could also have an important role in knee stabilization, by shortening the patellar ligament (apex presence) and by avoiding lateral luxation (compartmentalized articular surface geometry). Otherwise, results presented in this work corroborate that both anteroposterior patellar thickness and proximodistal height are likely associated with variations on the moment and lever arm of the *quadriceps* muscle complex and its ability for effective and powerful extension of the knee joint.

6.- In evolutionary terms, the presence of the patellar apex to be a hominoid plesiomorphic condition (found in the stem putative catarrhine *Epipliopithecus vindobonensis* and the stem hominoid *Ekembo* spp. The lack of a patellar apex in the stem great ape *P. catalaunicus* and the early hominin *Australopithecus sediba*, and its presence in fossil *Homo* species reveals that this would be a derived trait for hominids (great

apes and humans), posteriorly reversed in the *Homo* lineage. Given that human bipedalism shares with pronograde quadrupedalism the preferential movements of the hindlimb in the parasagittal plane and, hence, the necessity of joint stabilization, the presence of patellar apex in humans could probably respond to these structural demands (therefore reinforcing its functional meaning).

7.- Results obtained for the hindlimb remains of the Vallès-Penedès great apes underpin the previously inferred positional behaviours for cf. *D. fontani*, *P. catalaunicus* and *H. laietanus*. All these taxa probably had an above-branch quadrupedal component within their locomotor repertoire, which would be especially relevant in cf. *D. fontani* and *P. catalaunicus*. In addition, both taxa might have relied on vertical climbing behaviours to some extent. On the other hand, *H. laietanus* is the first fossil ape with unambiguous below-branch suspensory adaptations, adaptations that have been also found in the hindlimb remains. Nonetheless, this taxon might have also engaged in other orthograde-like behaviours such as vertical climbing and clambering. Likewise, *H. laietanus* probably relied on above-branch quadrupedalism to some degree.

8.- The femora, tibia and patella of the Vallès-Penedès great apes highlight the diversity in postcranial morphology (and associated locomotor behaviours) among these taxa and, at the same time, point out the uniqueness of the morphological and mechanical complexity observed in the Miocene hominoids fossil remains compared to their closest extant relatives. Likewise, the hindlimb remains of these fossil taxa corroborate the mosaic evolution of the locomotor apparatus in the Hominoidea during the middle to late Miocene. Additionally, these remains play a key role in better comprehending the origin and evolutionary scenario of the orthograde behaviours observed in living hominoids, including modern human bipedalismv.

There's nothing new under the sun, but
there are lots of old things we don't know.

-- Ambrose Bierce --

Section IX. REFERENCES

Adams DC, Rohlf FJ & Slice DE. 2004. Geometric morphometrics: ten years of progress following the 'revolution'. *Italian Journal of Zoology,* **71**: 5–16.

Adams DC, Rohlf FJ & Slice DE. 2013. A field comes of age: geometric morphometrics in the 21st century. *Hystrix, the Italian Journal of Mammalogy,* **24**: 7–14.

Adouni M, Shirazi-Adl A & Shirazi R. 2012. Computational biodynamics of human knee joint in gait: From muscle forces to cartilage stresses. *Journal of Biomechanics,* **45**: 2149–2156.

Ager DV. 1965. Serial grinding techniques. *In:* B Kummel & D Raup (eds). *Handbook of Palaeontological Techniques*. San Fransisco: H. Freeman and Company. pp 212–224.

Agustí J, Cabrera L & Garcés M. 2001. Chronology and zoogeography of the Miocene hominoid record in Europe. *In:* L de Bonis, GD Koufos & P Andrews (eds). *Hominoid Evolution and Climatic Change in Europe. Volume 2, Phylogeny of the Neogene Hominoid Primates of Eurasia.* Cambridge: Cambridge University Press. pp 2–18.

Aiello LC. 1992. Allometry and the analysis of size and shape in human evolution. *Journal of Human Evolution,* **22**: 127–147.

Aiello LC & Dean C. 1990. The hominoid femur. *In:* LC Aiello & C Dean (eds). *An Introduction to Human Evolutionary Anatomy.* London: Academic Press. pp 457–482.

Alba DM. 2012. Fossil apes from the Vallès-Penedès basin. *Evolutionary Anthropology,* **21**: 254–269.

Alba DM & Moyà-Solà S. 2012. A new pliopithecid genus (Primates: Pliopithecoidea) from Castell de Barberà (Vallès-Penedès Basin, Catalonia, Spain). *American Journal of Physical Anthropology,* **147**: 88–112.

Alba DM, Robles JM, Rotgers C, Casanovas-Vilar I, Galindo J, Moyà-Solà S, Garcés M, Cabrera L, Furió M, Carmona R & Bertó Mengual JV. 2009. Middle Miocene vertebrate localities from Abocador de Can Mata (els Hostalets de Pierola, Vallès-Penedès Basin, Catalonia, Spain): an update after the 2006-2008 field campaigns. *Paleolusitana,* **1**: 59–73.

Alba DM, Moyà-Solà S, Malgosa A, Casanovas-Vilar I, Robles JM, Almécija S, Galindo J, Rotgers C & Mengual JVB. 2010a. A new species of *Pliopithecus* Gervais, 1849 (Primates: Pliopithecidae) from the Middle Miocene (MN8) of Abocador de Can Mata (els Hostalets de Pierola, Catalonia, Spain). *American Journal of Physical Anthropology,* **141**: 52–75.

Alba DM, Fortuny J & Moyà-Solà S. 2010b. Enamel thickness in the Middle Miocene great apes *Anoiapithecus*, *Pierolapithecus* and *Dryopithecus*. *Proceedings of the Royal Society B,* **277**: 2237–2245.

Alba DM, Almécija S & Moyà-Solà S. 2010c. Locomotor inferences in *Pierolapithecus* and *Hispanopithecus*: Reply to Deane and Begun (2008). *Journal of Human Evolution,* **59**: 143–149.

Alba DM, Moyà-Solà S & Almécija S. 2011a. A partial hominoid humerus from the Middle Miocene of Castell de Barberà (Vallès-Penedès Basin, Catalonia, Spain). *American Journal of Physical Anthropology,* **144**: 365–381.

Alba DM, Moyà-Solà S, Robles JM, Casanovas-Vilar I, Rotgers C, Carmona R & Galindo J. 2011b. Middle Miocene tragulid remains from Abocador de Can Mata: The earliest record of *Dorcatherium naui* from Western Europe. *Geobios,* **44**: 135–150.

Alba DM, Almécija S, Casanovas-Vilar I, Méndez JM & Moyà-Solà S. 2012a. A partial skeleton of the fossil great ape *Hispanopithecus laietanus* from Can Feu and the mosaic evolution of crown-hominoid positional behaviors. *PLoS ONE,* **7**: e39617.

Alba DM, Casanovas-Vilar I, Almécija S, Robles JM, Arias-Martorell J & Moyà-Solà S. 2012b. New dental remains of *Hispanopithecus laietanus* (Primates: Hominidae) from Can Llobateres 1 and the taxonomy of Late Miocene hominoids from the Vallès-Penedès Basin (NE Iberian Peninsula). *Journal of Human Evolution,* **63**: 231–246.

Alba DM, Almécija S, DeMiguel D, Fortuny J, de los Ríos MP, Pina M, Robles JM & Moyà-Solà S. 2015. Miocene small-bodied ape from Eurasia sheds light on hominoid evolution. *Science,* **350**: aab2625.

Alba DM, Pérez de los Ríos M & Moyà-Solà S. in prep. Dentognatic remains. *In:* DM Alba, S Moyà-Solà & S.Almécija (eds). *Fossil Hominoid Primates from the Vallès-Penedès Basin. Volume 1: taxonomy*. Dordrecht: Springer.

Alexander RMcN. 1980. Forces in animal joints. *Engineering in Medicine,* **9**: 93–97.

Alexander RMcN. 1981. Analysis of force platform data to obtain joint forces. *In:* D Dowson & V Wright (eds). *An Introduction to the Biomechanics of Joints and Joint Replacements.* London: Mechanical Engineering Publishers. pp 30–35.

Alexander RMcN. 1984. Walking and running: Legs and leg movements are subtly adapted to minimize the energy costs of locomotion. *American Scientist,* **72**: 348–354.

Alexander RMcN. 1991 Characteristics and advantages of human bipedalism. *In:* JMV Rayner & RJ Wooton (eds). *Biomechanics in Evolution.* Cambridge: Cambridge University Press. pp 225–266.

Almécija S, Alba DM, Moyà-Solà S, and Köhler M. 2007. Orang-like manual adaptations in the fossil hominoid *Hispanopithecus laietanus*: first steps towards great ape suspensory behaviours. *Proceedings of the Royal Society B,* **274**: 2375–2384.

Almécija S, Alba DM & Moyà-Solà S. 2009. *Pierolapithecus* and the functional morphology of Miocene ape hand phalanges: paleobiological and evolutionary implications. *Journal of Human Evolution,* **57**: 284–297.

Almécija S, Moyà-Solà S & Alba DM. 2010. Early origin for human-like precision grasping: A comparative study of pollical distal phalanges in fossil hominins. *PLoS ONE,* **5**: e11727.

Almécija S, Alba DM, and Moyà-Solà S. 2012. The thumb of Miocene apes: New insights from Castell de Barberà (Catalonia, Spain). *American Journal of Physical Anthropology,* **148**: 436–450.

Almécija S, Tallman M, Alba DM, Pina M, Moyà-Solà S & Jungers WL. 2013. The femur of *Orrorin tugenensis* exhibits morphometric affinities with both Miocene apes and later hominins. *Nature Communications,* **4**: 2888.

Almécija S, Shrewsbury M, Rook L & Moyà-Solà S. 2014. The morphology of *Oreopithecus bambolii* pollical distal phalanx. *American Journal of Physical Anthropology,* **153**: 582–597.

Almécija S, Smaers JB & Jungers WL. 2015a. The evolution of human and ape hand proportions. *Nature Communications,* **6**: 7717.

Almécija S, Wallace IJ, Judex S, Alba DM & Moyà-Solà S. 2015b. Comment on "Human-like hand use in *Australopithecus africanus*". *Science,* **348**: 1101.

Almécija S, Nakatsukasa M, Kivell T, Alba DM & Moyà-Solà S. in prep,a. Hand remains. *In:* DM Alba, S Moyà-Solà & S.Almécija (eds). *Fossil Hominoid Primates from the Vallès-Penedès Basin. Volume 1: taxonomy*. Dordrecht: Springer.

Almécija S, Alba DM & Moyà-Solà S. in prep,b. Foot remains. *In:* DM Alba, S Moyà-Solà & S.Almécija (eds). *Fossil Hominoid Primates from the Vallès-Penedès Basin. Volume 1: taxonomy*. Dordrecht: Springer.

Andrews P, Harrison T, Martin L & Pickford M. 1981. Hominoid primates from a new Miocene locality named Meswa Bridge in Kenya. *Journal of Human Evolution,* **10**: 123–128.

Andrews P, Harrison T, Delson E, Bernor L & Martin L. 1996. Distribution and biochronology of European and southwest Asian Miocene catarrhines. *In:* RL Bernor, V Fahlbusch & H-W Mittmann (eds). *The Evolution of Western Eurasian Neogene Mammal Faunas.* New York: Columbia University Press. pp 168–206.

Anemone RL. 1993. The functional anatomy of the hip and thigh in primates. *In:* DL Gebo (ed). *Postcranial Adaptation in Nonhuman Primates.* Dekalb: Northern Illinois University Press. pp 150–174.

Arias-Martorell J, Alba DM, Potau JM, Bello-Hellegouarch G & Pérez-Pérez A. 2015. Morphological affinities of the proximal humerus of *Epipliopithecus vindobonensis* and *Pliopithecus antiquus*: Suspensory inferences based on a 3D geometric morphometrics approach. *Journal of Human Evolution,* **80**: 83–95.

Arms A, Voges D, Fischer MS & Preuschoft H. 2002. Arboreal locomotion in small New-World monkeys. *Zeitschrift für Morphologie und Anthropologie,* **83**: 243–263.

Arnold C, Matthews LJ & Nunn CL. 2010. The 10kTrees website: A new online resource for primate phylogeny. *Evolutionary Anthropology,* **19**: 114–118.

Azzaroli A, Boccaletti M, Delson E, Moratti G & Torre D. 1986. Chronological and paleogeographical background to the study of *Oreopithecus bambolii*. *Journal of Human Evolution,* **15**: 533–540.

Badoux DM. 1974. An introduction to biomechanical principles in primate locomotion and structure. *In:* FA Jenkins (ed). *Primate Locomotion.* New York: Academic Press. pp 1–43.

Bacon A-M. 2001. *La locomotion des Primates du Miocène d'Afrique et d'Europe. Cahiers de paléoanthropologie.* Paris: CNRS Éditions.

Barry JC, Morgan ME, Flynn LJ, Pilbeam D, Behrensmeyer AK, Raza SM, Khan IA, Badgley C, Hicks J & Kelley J. 2002. Faunal and environemental change in the Late Miocene Siwaliks of Northern Pakistan. *Paleobiology Memoirs 3,* **28**: 1–72.

Beard KC, Teaford MF & Walker A. 1986. New wrist bones of *Proconsul africanus* and *P. nyanzae* from Rusinga Island, Kenya. *Folia Primatologica,* **47**: 97–118.

Begun DR. 1989. New species of *Dryopithecus* from the Vallesian of Can Ponsic (Northeastern Spain). *American Journal of Physical Anthropology,* **78**: 191.

Begun DR. 1992a. *Dryopithecus crusafonti* sp. nov., a new Miocene hominoid species from Can Ponsic (Northeastern Spain). *American Journal of Physical Anthropology,* **87**: 291–309.

Begun DR. 1992b. Phyletic diversity and locomotion in primitive European hominids. *American Journal of Physical Anthropology,* **87**: 311–340.

Begun DR. 1993. New catarrhine phalanges from Rudabanya (Northeastern Hungary) and the problem of parallelism and convergence in hominoid postcranial morphology. *Journal of Human Evolution,* **24**: 373–402.

Begun DR. 1994. Relationships among the great apes and humans: new interpretations based on the fossil great ape *Dryopithecus*. *Yearbook of Physical Anthropology,* **37**: 11–63.

Begun DR. 2002. European hominoids. *In:* C Hartwig (ed). *The Primate Fossil Record.* Cambridge: Cambridge University Press. pp 339–368.

Begun DR. 2009. Dryopithecins, Darwin, de Bonis, and the European origin of the African apes and human clade. *Geodiversitas,* **31**: 789–816.

Begun DR. 2013. The Miocene hominoid radiations. *In:* DR Begun (ed). *A Companion to Paleoanthropology.* Chichester: Blackwell Publishing. pp 398–416.

Begun DR. 2015. Fossil record of Miocene Hominoids. *In:* W Henke & I Tattersall (eds). *Handbook of Paleoanthropology.* Berlin Heidelberg: Springer-Verlag. pp 1261–1332.

Begun DR & Güleç E. 1998. Restoration of the type and palate of *Ankarapithecus meteai*: Taxonomic and phylogenetic implications. *American Journal of Physical Anthropology,* **105**: 279–314.

Begun DR & Kivell TL. 2011 Knuckle-walking in *Sivapithecus:* The combined effects of homology and homoplasy and implications for the origin of human bipedalism. *Journal of Human Evolution,* **60**: 158–170.

Begun DR & Ward CV. 2005. Comment on "*Pierolapithecus catalaunicus*, a new Middle Miocene great ape from Spain". *Science,* **208**: 203c.

Begun DR, Moyà-Solà S & Köhler M. 1990. New Miocene hominoid specimens from Can Llobateres (Vallès Penedès, Spain) and their geological and paleoecological context. *Journal of Human Evolution,* **19**): 255–268.

Begun DR, Teaford MF & Walker A. 1993. Comparative and functional anatomy of *Proconsul* phalanges from the Kaswanga Primate Site, Rusinga Island, Kenya. *Journal of Human Evolution,* **26**: 89–165.

Begun DR, Ward CV & Rose MD. 1997. Events in hominoid evolution. *In:* DR Begun, CV Ward & MD Rose (eds). *Function, Phylogeny, and Fossils: Miocene Hominoid Evolution and Adaptations*. New York: Plenum Press. pp 389–415.

Begun DR, Nargolwalla MC & Kordos L. 2012. European Miocene hominids and the origin of the African ape and human clade. *Evolutionary Anthropology,* **21**: 10–23.

Benefit BR & McCrossin ML. 1993. New *Kenyapithecus* postcrania and other primate fossils from Maboko Island, Kenya. *American Journal of Physical Anthropology,* **36(S16)**: 55–56.

Bertram JEA. 2004. New perspectives on brachiation mechanics. *Yearbook of Physical Anthropology,* **47**: 100–117.

Bishop PJ, Walmsley CW, Phillips MJ, Quayle MR, Boisvert CA & McHenry CR. 2015. Oldest pathology in a tetrapod bone illuminates the origin of terrestrial vertebrates. *PLoS ONE,* **10**: e0125723.

Bleuze M. 2012. Proximal femoral diaphyseal cross-section geometry in *Orrorin tugenensis*. *HOMO–Journal of Comparative Human Biology,* **63**: 153–166.

Bock WJ & von Wahlert G. 1965. Adaptation and the form-function complex. *Evolution,* **19**: 269–299.

Bookstein FL. 1991. *Morphometric Tools for Landmark Data. Geometry and biology*. Cambridge: Cambridge University Press.

Bookstein FL. 1997. Landmark methods for forms without landmarks: localizing group differences in outline shape. *Medical Image Analysis,* **1**: 225–243.

Brandon-Jones D, Eudey AA, Geissmann T, Groves CP, Melnick DJ, Morales JC, Shekelle M & Stewart C-B. 2004. Asian primate classification. *International Journal of Primatology,* **25**: 97–164.

Bruijn SM, Meijer OG, van Dieën JH, Kingma I & Lamoth CJC. 2008. Coordination of leg swing, thorax rotations, and pelvis rotations during gait: the organisation of total body angular momentum. *Gait Posture,* **27:** 455–462.

Brunet M, Guy F, Pilbeam D, Mackaye HT, Likius A, Ahounta D, Beauvilain A, Blondel C, Bocherens H, Boisserie J-R, De Bonis L, Coppens Y, Dejax J, Denys C, Duringer P, Eisenmann V, Fanone G, Fronty P, Geraads D, Lehmann T, Lihoreau F, Louchart A, Mahamat A, Merceron G, Mouchelin G, Otero O, Pelaez Campomanes P, Ponce de Leon M, Rage J-C, Sapanet M, Schuster M, Sudre J, Tassy P, Valentin X, Vignaud P, Viriot L, Zazzo A & Zollikofer C. 2002. A new hominid from the Upper Miocene of Chad, Central Africa. *Nature,* **418**: 145–151.

Bumpus HC. 1898. The elimination of the unfit as illustrated by the introduced sparrow *Passer domesticus*. *Biological lectures delivered at the Marine Biological Laboratory of Wood's Holl,* **11**: 209–226.

Burr DB, Piotrowski G & Miller GJ. 1981. Structural strength of the macaque femur. *American Journal of Physical Anthropology,* **54**: 305–319.

Caldecott J & Miles L. 2005. *World Atlas of Great Apes and their Conservation*. Berkeley: UNEP-WCMC, University of California Press.

Campbell BG. 1966. *Human Evolution*. London: Heinemann Ed. Books, Ltd.

Cant JGH. 1987. Positional behavior of female Bornean orangutans (*Pongo pygmaeus*). *American Journal of Primatology,* **46**: 1–14.

Cant JGH. 1992. Positional behavior and body size of arboreal primates: A theoretical framework for field studies and an illustration of its application. *American Journal of Physical Anthropology,* **88**: 273–283.

Cant JGH, Youlatos D & Rose MD. 2001. Locomotor behavior of *Lagothrix lagothricha* and *Ateles belzebuth* in Yasuní National Park, Ecuador: general patterns and non-suspensory modes. *Journal of Human Evolution,* **41**: 141–166.

Cant JGH, Youlatos D & Rose MD. 2003. Suspensory locomotion of *Lagothrix lagothrica* and *Ateles belzebuth* in Yasuní National Park, Ecuador. *Journal of Human Evolution,* **44**: 685–700.

Carlson KJ. 2005. Investigating the form-function interface in African Apes: Relationships between principal moments of area and positional behaviors in femoral and humeral diaphyses. *American Journal of Physical Anthropology,* **127**: 312–334.

Cartmill M. 1972. Arboreal adaptations and the origin of the order primates. *In:* R Tuttle R (ed). *The Functional and Evolutionary Biology of Primates.* Chicago: Aldine. pp 97–122.

Cartmill M. 1985. Climbing. *In:* M Hildebrand, D Bramble, K Liem & D Wake (eds). *Functional Vertebrate Morphology*. Cambridge: Belknap Press. pp 73–88.

Cartmill M & Milton K. 1977. The lorisiform wrist joint and the evolution of "brachiating" adaptations in the Hominoidea. *American Journal of Physical Anthropology,* **47**: 249–272.

Casanovas-Vilar I & Agustí J. 2007. Ecogeographical stability and climate forcing in the Late Miocene (Vallesian) rodent record of Spain. *Palaeogeography, Palaeoclimatology, Palaeoecology,* **248**: 169–189.

Casanovas-Vilar I, Alba DM, Moyà-Solà S, Galindo J, Furió M, Robles JM, Köhler M & Angelone C. 2008a. Biochronological, taphonomical, and paleoenvironmental background of the fossil great ape *Pierolapithecus catalaunicus* (Primates, Hominidae). *Journal of Human Evolution*, **55**: 589–603.

Casanovas-Vilar I, Alba DM, Almécija S, Robles JM, Galindo J & Moyà-Solà S. 2008b. Taxonomy and paleobiology of the genus *Chalicomys* Kaup, 1832 (Rodentia, Castoridae), with the descrisption of a new species from Abocador de Can Mata (Vallès-Penedès Basin, Catalonia, Spain). *Journal of Vertebrate Paleontology*, **28**: 851–862.

Casanovas-Vilar I, Alba DM, Garcés M, Robles JM & Moyà-Solà S. 2011. Updated chronology of the Miocene hominoid radiation in Western Eurasia. *Proceedings of the National Academy of Sciencies USA,* **108**: 5554–5559.

Casanovas-Vilar I, Madern A, Alba DM, Cabrera L, García-Paredes I, van den Hoek Ostende LW, DeMiguel D, Robles JM, Furió M, van Dam J, Garcés M, Angelone C & Moyà-Solà S. 2015, in press. The Miocene mammal record of the Vallès-Penedès Basin (Catalonia). *Comptes Rendus Palevol,* doi:10.1016/j.crpv.2015.07.004.

Chan LK. 2008. The range of passive arm circumduction in primates: Do hominoids really have more mobile shoulders? *American Journal of Physical Anthropology,* **136**: 265–277.

Channon AJ, Crompton RH, Günther MM & Vereecke EE. 2010a. Muscle moment arms of the gibbon hind limb: implications for the hylobatid locomotion. *Journal of Anatomy,* **216**: 446–462.

Channon AJ, Crompton RH, Günther MM, D'Août K & Vereecke EE. 2010b. The biomechanics of leaping in gibbons. *American Journal of Physical Anthropology,* **143**: 403–416.

Channon AJ, Usherwood JR, Crompton RH, Günther MM & Vereecke EE. 2012. The extraordinary athletic performance of leaping gibbons. *Biology Letters,* **8**: 46–49.

Chatterjee HJ, Ho SYW, Barnes I & Groves C. 2009. Estimating the phylogeny and divergence times of primates using a supermatrix approach. *BMC Evolutionary Biology,* **9**: 259.

Chivers DJ. 1972. The siamang and the gibbon in the Malay peninsula. *In:* DM Rumbaugh (ed). *The Gibbon and the Siamang, Volume 1.* Basel: Karger. pp 103–135.

Cierniak R. 2011. *X-Ray Computed Tomography in Biomedical Engineering.* London: Springer-Verlag.

Claussen C & Lochner B. 1985. *Dynamic Computer Tomography. Basic Principles and Clinical Applications.* Berlin Heidelberg: Springer-Verlag.

Claxton A. 2015. A preliminary look into the ontogeny of femoral neck cortical bone distribution using u-CT [Abstract]. **156(S60)**: 106–107.

Clough RW. 1960. The finite element method in plane stress analysis. *Proceedings of American Society of Civil Engineers,* **23**: 345–37.

Clough RW. 2004. Early history of the finite element method from the view point of a pioneer. *International Journal for Numerical Methods in Engineering,* **60**: 283–287.

Coleman MN & Colbert MW. 2007. Technical Note: CT thresholding protocols for taking measurements on three-dimensional models. *American Journal of Physical Anthropology,* **133**: 723–725.

Conroy GC & Rose MD. 1983. The evolution of the primate foot from the earliest primates to the Miocene hominoids. *Foot & Ankle International,* **3**: 342–364.

Crelin ES. 1988. Ligament of the head of the femur in the orangutan and Indian elephant. *The Yale Journal of Biology and Medicine,* **61**: 383–388.

Crompton RH. 2016. The hominins: a very conservative tribe? Last common ancestors, plasticity and ecomorphology in Hominidae. Or, What's in a name? *Journal of Anatomy,* **228**: 686–699.

Crompton RH, Vereecke EE & Thorpe SKS. 2008. Locomotion and posture from the common hominoid ancestor to fully modern hominins, with special reference to the last common panin/hominin ancestor. *Journal of Anatomy,* **212**: 501–543.

Crompton RH, Sellers WI & Thorpe SKS. 2010. Arboreality, terrestriality and bipedalism. *Philosophical Transactions of the Royal Society B,* **365**: 3301–3314.

Crusafont Pairó M & Hürzeler J. 1969. Catálogo comentado de los póngidos fósiles de España. *Acta Geológica Hispánica,* **4**: 44–48.

Crusafont-Pairó M & Golpe-Posse JM. 1973. New pongids from the Miocene of Vallès Penedès Basin (Catalonia, Spain). *Journal of Human Evolution,* **2**: 17–23.

Dabnichki P & Avital E. 2006. Influence of the postion of crew members on aerodynamics performance of two-man bobsleigh. *Journal of Biomechanics,* **39**: 2733–2742.

Daegling DJ. 2002. Estimation of torsional rigidity in primate long bones. *Journal of Human Evolution,* **43**: 229–239.

Davis LC. 1996. Functional and phylogenetic implications of ankle morphology in Goeldi's monkey. *In:* MA Norconk, AL Rosenberger & PA Garber (eds). *Adaptive Radiations of Neotropical Primates.* New York: Plenum Press. pp 133–156.

de Bonis L & Koufos G. 1997. The phylogenetic and functional implications of *Ouranopithecus macedoniensis*. *In:* DR Begun, CV Ward & MD Rose (eds). *Function, Phylogeny and Fossils: Miocene Hominoid Evolution and Adaptation.* New York: Plenum Press. pp 317–326.

Deane AS & Begun DR. 2008. Broken fingers: retesting locomotor hypotheses for fossil hominoids using fragmentary proximal phalanges and high-resolution polynomial curve fitting (HR-PCF). *Journal of Human Evolution,* **55**: 691–701.

Deane AS & Begun DR. 2010. *Pierolapithecus* locomotor adaptations: a reply to Alba et al.'s comment on Deane and Begun (2008). *Journal of Human Evolution,* **59**: 150–154.

Demange MK, Kakuda CMS, Pereira CAM, Sakaki MH & Albuquerque RF. 2007. Influence of the femoral head ligament on hip mechanical function. *Acta Ortopédica Brasileira,* **15**: 187–190.

Demes B. 2011.Three-dimensional kinematics of capuchin monkey bipedalism. *American Journal of Physical Anthropology,* **145**: 147–155.

Demes B, Jungers WL & Selpien K. 1991. Body size, locomotion, and long bone cross-sectional geometry in indriid primates. *American Journal of Physical Anthropology,* **86**: 537–547.

Demes B, Larson SG, Stern JT Jr, Jungers WL, Biknevicius AR & Schmitt D. 1994. The kinetics of primate quadrupedalism: "hindlimb drive" reconsidered. *Journal of Human Evolution,* **26**: 353–374.

Demes B, Jungers WL & Walker C. 2000. Cortical bone distribution in the femoral neck of strepsirhine primates. *Journal of Human Evolution,* **39**: 367–379.

Demes B, Qin Y-X, Stern JT, Larson SG & Rubin CT. 2001. Patterns of strain in the macaque tibia during functional activity. *American Journal of Physical Anthropology,* **116**: 257–265.

DeMiguel D, Cegoñino J, Azanza B, Ruíz I & Morales J. 2006. Aplicación del análisis 3D de elementos finitos en el estudio biomecánico de la dentición de mamíferos. Análisis preliminar en *Procervulus ginsburgi* (Cervidae,

Artiodactyla). *Estudios Geológicos,* **62**: 115–122.

DeMiguel D, Azanza B & Morales J. 2011. Paleoenvironments and paleoclimate of the Middle Miocene of central Spain: A reconstruction from dental wear of ruminants. *Palaeogeography, Palaeoclimatology, Palaeoecology*, **302**: 452-463.

DeMiguel D, Alba DM & Moyà-Solà S. 2014. Dietary specialization during the evolution of Western Eurasian hominoids and the extinction of European great apes. *PLoS ONE,* **9**: e97442.

DeMiguel D, Azanza B, Cegoñino J, Ruíz I & Morales J. 2015. The interplay between increased tooth crown-height and chewing efficiency, and implications for Cervidae evolution. *Lethaia,* **49**: 117–129.

Depéret C. 1887. Sur la faune vertebres miocène de La Grive Saint Alban (Isère). *Archives du Muséum d'Histoire Naturelle de Lyon,* **5**: 3–27.

DeSilva JM. 2008. *Vertical climbing adaptations in the anthropoid ankle and midfoot: Implications for locomotion in Miocene catarrhines and Plio-Pleistocene hominins.* PhD dissertation. University of Michigan.

DeSilva JM. 2009. Functional morphology of the ankle and the likelihood of climbing in early hominins. *Proceedings of the National Academy of Sciences USA,* **106**: 6567–6572.

DeSilva JM, Morgan ME, Barry JC & Pilbeam D. 2010. A hominoid distal tibia from the Miocene of Pakistan. *Journal of Human Evolution,* **58**: 147–154.

DeSilva JM, Holt KG, Churchill SE, Carlson KJ, Walker CS, Zipfel B & Berger LR. 2013. The lower limb and mechanics of walking in *Australopithecus sediba*. *Science,* **340**: 1232999-1–1232999-5.

Diogo R, Potau JM, Pastor JF, de Paz FJ, Ferrero EM, Bello G, Barbosa M, Aziz MA, Burrows AM, Arias-Martorell J & Wood BA. 2012. *Photographic and Descriptive Musculoskeletal Atlas of Gibbons and Siamangs* (Hylobates*). With Notes on the Attachments, Variations, Innervation, Function and Synonymy and Weight of the Muscles.* St. Helier: CRC Press.

Diogo R, Potau JM, Pastor JF, de Paz FJ, Ferrero EM, Bello G, Barbosa M, Aziz MA, Burrows AM, Arias-Martorell J & Wood BA. 2013. *Photographic and Descriptive Musculoskeletal Atlas of Chimpanzees. With Notes on the Attachments, Variations, Innervation, Function and Synonymy and Weight of the Muscles.* St. Helier: CRC Press.

Doblaré M, García JM & Gómez MJ. 2004. Modelling bone tissue fracture and healing: a review. *Engineering Fracture Mechanics*, **71**: 1809–1840.

Doran DM. 1992. The ontogeny of chimpanzee and pygmy chimpanzee locomotor behavior: a case study of paedomorphism and its behavioral correlates. *Journal of Human Evolution,* **23**: 139–157.

Doran DM. 1993. The comparative locomotor behavior of chimpanzees and bonobos: the influence of morphology on locomotion. *American Journal of Physical Anthropology,* **91**: 83–98.

Doran DM. 1996. Comparative positional behavior of the African apes. *In:* WC McGrew, LF Marchant & T Nishida (eds). *Great Ape Societies*. Cambridge: Cambridge University Press. pp 213–224.

Doran DM. 1997. Ontogeny of locomotion in mountain gorillas and chimpanzees. *Journal of Human Evolution,* **32**: 323–344.

Doube M, Kłosowski MM, Arganda-Carreras I, Cordeliéres F, Dougherty RP, Jackson J, Schmid B, Hutchinson JR & Shefelbine SJ. 2010. BoneJ: free and extensible bone image analysis in ImageJ. *Bone,* **47**: 1076–1079.

Dryden IL & Mardia KV. 1998. *Statistical Shape Analysis*. New York: Wiley.

Dumont ER, Grosse IR & Slater GJ. 2009. Requirements for comparing the performance of finite element models of biological structures. *Journal of Theoretical Biology*, **256**: 96–103.

Dumont ER, Grosse IR & Slater GJ. 2009. Requirements for comparing the performance of finite element models of biological structures. *Journal of Theoretical Biology,* **256**: 96–103.

Eng JJ & Winter DA. 1995. Kinetic analysis of the lower limbs during walking: What information can be gained

from a three-dimensional model? *Journal of Biomechanics,* **28**: 753–758.

Engel K, Herpers R & Hartmann U. 2011. Biomechanical computer models. *In:* V Klika (ed). *Theoretical Biomechanics.* Rijeka: InTech. pp 93–112.

Erikson GE. 1963. Brachiation in New World monkeys and in anthropoid apes. *Symposia of the Zoological Society of London,* **10**: 135–164.

Finarelli JA & Clyde WC. 2004. Reassessing hominoid phylogeny: evaluating congruence in the morphological and temporal data. *Paleobiology,* **30**: 614–651.

Fitzpatrick CK & Rullkoetter PJ. 2012. Influence of patellofemoral articular geometry and material on mechanics of the unresurfaced patella. *Journal of Biomechanics*, **45**: 1909–1915.

Fitzpatrick CK, Baldwin MA, Ali AA, Laz PJ & Rullkoetter PJ. 2011. Comparison of patellar bone strain in the natural and implanted knee during simulated deep flexion. *Journal of Orthopaedic Research,* **29**: 232–239.

Fitzpatrick CK, Kim RH, Ali AA, Smoger LM & Rullkoetter PJ. 2013. Effects of resection thickness on mechanics of resurfaced patellae. *Journal of Biomechanics,* **46**: 1568–1575.

Fitzpatrick CK, Steensen RN, Tumuluri A, Trinh T, Bentley J & Rullkoetter PJ. 2016. Computational analysis of factors contributing to patellar dislocation. *Journal of Orthopaedic Research,* **34**: 444–453.

Fleagle JG. 1976. Locomotion and posture of the Malayan siamang and implications for hominoid evolution. *Folia primatologica,* **26**: 245–269.

Fleagle JG. 1978. Locomotion, posture, and habitat utilization in two sympatric, Malaysian leaf-monkeys (*Presbytis obscura* and *Presbytis melalophos*). *In:* GE Montgomery (ed). *The Ecology of Arboreal Folivores.* Washington DC: Smithsonian Press. pp 243–251.

Fleagle JG. 1980. Locomotion and posture. *In:* DJ Chivers (ed). *Malayan Forest Primates: Ten Year's Study in Tropical Rain Forest.* New York: Plenum Press. pp 191–207.

Fleagle JG. 1983. Locomotor adaptations of Oligocene and Miocene hominoids and their phyletic implications. *In:* RL Ciochon & RS Corruccini (eds). *New Interpretations of Ape and Human Ancestry.* New York: Plenum Press. pp 301–324.

Fleagle JG. 2013. *Primate Adaptation and Evolution*. San Diego: Academic Press.

Fleagle JG & Mittermeier RA. 1980. Locomotor behavior, body size, and comparative ecology of seven Surinam monkeys. *American Journal of Physical Anthropology,* **52**: 301–314.

Fleagle JG, Stern JT Jr, Jungers WL, Susman RL, Vangor AK & Wells JA. 1981. Climbing: a biomechanical link with brachiation and with bipedalism. *Symposia of the Zoological Society of London,* **48**: 359–375.

Fontaine R. 1990. Positional behavior in *Saimiri boliviensis* and *Ateles geoffroyi*. *American Journal of Physical Anthropology,* **82**: 485–508.

Fortuny J, Marcé-Nogué J, Heiss E, Sanchez M, Gil L & Galobart À. 2015. 3D bite modeling and feeding mechanics of the largest living amphibian, the Chinese giant salamander *Andrias davidianus* (Amphibia: Urodela). *PLoS ONE,* **10**: e0121885.

Frankel VH. 1960. *The Femoral Neck.* Uppsala: Almqvist and Wiksells Boktryckeri AB.

Freckleton RP, Harvey PH & Pagel M. 2002. Phyogenetic analysis and comparative data: A test and review of evidence. *The American Naturalist,* **160**: 712–726.

Furió M, Casanovas-Vilar I, Moyà-Solà S, Köhler M, Galindo J & Alba DM. 2011. Insectivores (Eulipotyphla; Mammalia) from the Middle Miocene of Barranc de Can Vila 1 (Vallès-Penedès Basin, Catalonia, Spain). *Geobios,* **44**: 199–213.

Furió M, Prieto J & van den Hoek Ostende LW. 2015. Three million years of "Terror-Shrew" (Dinosorex, Eulipotyphla, Mammalia) in the Miocene of the Vallès-Penedès Basin (Barcelona, Spain). *Comptes Rendus Palevol,* **14**: 111–124.

Galik K, Senut B, Pickford M, Gommery D, Treil J, Kuperavage AJ & Eckhardt RB. 2004. External and

internal morphology of the BAR 1002´00 *Orrorin tugenensis* femur. *Science,* **305**: 1450–1453.

Garber PA, Blomquist GE & Anzenberger G. 2005. Kinematic analysis of trunk-to-trunk leaping in *Callimico goeldii*. *International Journal of Primatology,* **26**: 223–240.

Garth WPJ. 2001. Clinical biomechanics of the patellofemoral joint. *Operative Techniques in Sports Medicine,* **9**: 122–128.

Gebo DL. 1996. Climbing, brachiation, and terrestrial quadrupedalism: Historical precursors of hominid bipedalism. *American Journal of Physical Anthropology,* **101**: 55–92.

Gebo DL. 2011. Vertical clinging and leaping revisited: Vertical support use as the ancestral condition of Strepsirrhine primates. *American Journal of Physical Anthropology,* **146**: 323–335.

Gebo DL & Chapman CA. 1995. Positional behavior in five sympatric Old World monkeys. *American Journal of Physical Anthropology,* **97**: 49–76.

Gebo DL, MacLatchy L, Kityo R, Deino A, Kingston J & Pilbeam D. 1997. A hominoid genus from the early Miocene of Uganda. *Science,* **276**: 401–404.

Gervais P. 1872. Sur un singe fossile, d'une espèce non encore décrite, qui a été découverte au monte Bamboli. *Comtpes Comptes Rendus de l'Acadèmie des Sciences,* **74**: 1217–1223.

Gil L, Marcé-Nogué J & Sánchez M. 2015. Insights into the controversy over materials data for the comparison of biomechanical performance in vertebrates. *Palaeontologia Electronica*, **18.1.12A**: 1–24.

Gittins SP. 1983. Use of the forest canopy by the agile gibbon. *Folia Primatologica,* **40**: 134–144.

Golpe Posse JM. 1993. Los Hispanopitecos (Primates, Pongidae) de los yacimientos del Vallès-Penedès (Cataluña, España). II: Descripción del material existente en el Instituto de Paleontología de Sabadell. *Paleontologia i Evolució,* **26-27**: 151–224.

Gommery D & Senut B. 2006. The terminal thumb phalanx of *Orrorin tugenensis* (Upper Miocene of Kenya). *Geobios,* **39**: 372–384.

Gommery D, Senut B & Pickford M. 1998. Nouveaux restes postcrâniens d'Hominoidea du Miocène inférieur de Napak, Ouganda. *Annales de Paléontologie,* **84**: 287–306.

Gommery D, Senut B, Pickford M & Musiime E. 2002. Les nouveaux restes du squelette d'*Ugandapithecus major* (Miocène inférieur de Napak, Ouganda). *Annales de Paléontologie,* **88**: 167–186.

Gorganovic-Kramberger D. 1906. *Der Diluviale Mensch von Krapina in Kroatien: ein Beitrag zur Paläoanthropologie*. Wiesbaden: Kreidel.

Gould SJ. 1966. Allometry and size in ontogeny and phylogeny. *Biological Reviews,* **41**: 587–640.

Grand TI. 1972. A mechanical interpretation of terminal branch feeding. *Journal of Mammalogy,* **53**: 198–201.

Gröning F, Fagan M & O'Higgins P. 2013. Comparing the distribution of strains with the distribution of bone tissue in a human mandible: A Finite Element study. *The Anatomical Record,* **296**: 9–18.

Groves C. 2001. *Primate Taxonomy.* Washington and London: Smithsonian Institution Press.

Hammond AS. 2014. *In vivo* baseline measurements of hip joint range of motion in suspensory and nonsuspensory anthropoids. *American Journal of Physical Anthropology,* **153**: 417–434.

Hammond AS, Alba DM, Almécija S & Moyà-Solà S. 2013. Middle Miocene *Pierolapithecus* provides a first glimpse into early hominid pelvic morphology. *Journal of Human Evolution,* **64**: 658–666.

Hammond AS, Plavcan JM & Ward CV. 2016, in press. A validated method for modeling anthropoid hip abduction *in silico*. *American Journal of Physical Anthropology*. doi: 10.1002/ajpa.22990

Hara T, Tanck E, Homminga J, Huiskes R. 2002. The influence of microcomputed tomography threshold variations on the assessment of structural and mechanical trabecular bone properties. *Bone,* **31**: 107–109.

Harmon EH. 2007. The shape of the hominoid proximal femur: a geometric morphometric analysis. *Journal of Anatomy,* **210**: 170–185.

Harrison T. 1982. *Small-bodied apes from the Miocene of East Africa.* PhD dissertation. University College London.

Harrison T. 1986. A Reassessment of the phylogenetic relationships of *Oreopithecus bambolii* Gervais. *Journal of Human Evolution*, **15**: 541–583.

Harrison T. 1987. The phylogenetic relationships of the early catarrhine primates: a review of the current evidence. *Journal of Human Evolution*, **16**: 41–80.

Harrison T. 1989. New postcranial remains of *Victoriapithecus* from the middle Miocene of Kenya. *Journal of Human Evolution*, **18**: 3–54.

Harrison T. 1991a. The implications of *Oreopithecus bambolii* for the origins of bipedalism. *In:* Y Coppens & B Senut (eds). *Origin(s) de la Bipédie chez les Hominidés.* Paris: Cahiers de Paleoanthropologie, CNRS. pp 235–244.

Harrison T. 1991b. Some observations on the Miocene hominoids from Spain. *Journal of Human Evolution*, **19**: 515–520.

Harrison T. 2002. Late Oligocene to middle Miocene catarrhines from Afro-Arabia. *In:* WC Hartwig (ed). *The Primate Fossil Record.* Cambridge: Cambridge University Press. pp 311–338.

Harrison T. 2010a. Dendropithecoidea, Proconsuloidea, and Hominoidea. *In:* L Werdelin & WJ Sanders (eds). *Cenozoic Mammals of Africa.* Berkeley: University of California Press. pp 429–469.

Harrison T. 2010b. Apes among the tangled branches of human origins. *Science*, **327**: 532–534.

Harrison T. 2013. Catarrhine origins. *In:* DR Begun (ed). *A Companion to Paleoanthropology.* Chichester: Blackwell Publishing. pp 377–396.

Harrison T & Rook L. 1997. Enigmatic anthropoid or misunderstood ape? The phylogenetic status of *Oreopithecus bambolii* reconsidered. *In:* DR Begun, CV Ward & MD Rose (eds). *Function, Phylogeny and Fossils: Miocene Hominoid Evolution and Adaptation.* New York: Plenum Press. pp 327–362.

Haxton H. 1944. The patellar index in mammals. *Journal of Anatomy*, **78**: 106–107.

Heegaard J, Leyvraz PF, Curnier A, Rakotomanana L & Huiskes R. 1995. The biomechanics of the human patella during passive knee flexion. *Journal of Biomechanics*, **28**: 1265–1279.

Heinrich RE & Biknevicius AR. 1998. Skeletal allometry and interlimb scaling patterns in mustelid carnivorans. *Journal of Morphology*, **235**: 121–134.

Henke W & Tattersall I. 2015. *Handbook of Paleoanthropology.* Berlin Heidelberg: Springer-Verlag.

Herr H & Popovic M. 2008. Angular momentum in human walking. *Journal of Experimental Biology*, **211**: 467–481.

Hildebrand M. 1967. Symmetrical gaits of primates. *American Journal of Physical Anthropology*, **26**: 119–130.

Hill A & Ward S. 1988 Origin of the Hominidae: The record of African large hominoid evolution between 14 My and 4 My. *Yearbook of Physical Anthropology*, **31**: 48–83.

Hill EC & Durband AC. 2014. Mobility and subsistence at the Willandra Lakes: A comparative analysis of femoral cross-sectional properties in the Lake Mungo 3 skeleton. *Journal of Human Evolution*, **73**: 103–106.

Hill A, Leakey M, Kingston JD & Ward S. 2002. New cercopithecoids and a hominoid from 12.5 Ma in the Tugen Hills succession, Kenya. *Journal of Human Evolution*, **42**: 75–93.

Hirasaki E, Kumakura H & Matano S. 2000. Biomechanical analysis of vertical climbing in the spider monkey and the Japanese macaque. *American Journal of Physical Anthropology*, **113**: 455–472.

Hofman MA. 1988. Allometric scaling in palaeontology: A critical survey. *Human Evolution*, **3**: 177–188.

Holt KG & Hamill J. 1995. Running injuries and treatment: A dynamic approach. *In:* GJ Sammarco (ed). *Rehabilitation of the Foot and Ankle.* St. Louis: Mosby. pp 241–258.

Hounsfield GN. 1973. Computerized transverse axial scanning (tomography). Part I. Description of system. *The British Journal of Radiology*, **46**:1016–1022.

Hounsfield GN. 1976. Historical notes on computerized axial tomography. *Journal of the Canadian Association of Radiologists*, **27**: 135–142.

Hrenikoff A. 1941. Solution of problems in elasticity by the framework method. *Journal of Applied Mechanics, ASME DC*, **A8**: 169–175.

Hsieh J. 2009. *Computed Tomography: Principles, Design, Artifacts, and Recent Advances.* Bellingham: Wiley Inter-Science & Spie Press.

Hunt KD. 1991a. Positional behavior in the Hominoidea. *International Journal of Primatology,* **12**: 95–118.

Hunt KD. 1991b. Mechanical implications of chimpanzee positional behavior. *American Journal of Physical Anthropology,* **86**: 521–536.

Hunt KD. 1992. Positional behavior of *Pan troglodytes* in the Mahale mountains and Gombe Stream National Parks, Tanzania. *American Journal of Physical Anthropology,* **87**: 83–105.

Hunt KD. 2004. The special demands of great ape locomotion and posture. *In:* AE Russon & DR Begun (eds). *The Evolution of Though Evolutionary Origins of Great Ape Intelligence.* New York: Cambridge University Press. pp 172–189.

Hunt KD. 2016. Why are there apes? Evidence for the co-evolution of ape and monkey ecomorphology. *Journal of Anatomy,* **228**: 630–685.

Hunt KD, Cant JGH, Gebo DL, Rose MD, Walker SE & Youlatos D. 1996. Standardized descriptions of primate locomotor and postural modes. *Primates,* **37**: 363–387.

Hürzeler J. 1968. *Oreopithecus bambolii* Gervais. A preliminary report. *Verhandlungen Naturforchenden Gesellschaft Basel,* **69**: 1–48.

Ingham S, de Carvalho R, Martins CQ, Lertwanich P, Abdalla R, Smolinski P, Lovejoy CO & Fu F. 2015, published online. Anterolateral ligament anatomy: a comparative anatomical study. *Knee Surgery, Sports Traumatology, Arthroscopy.* pp 1–7. doi 10.1007/s00167-015-3956-2

Ishida H & Pickford M. 1997. A new Late Miocene hominoid from Kenya: *Samburupithecus kiptalami* gen. et sp. nov. *Comptes Rendus de l'Academie des Sciences Series D,* **325**: 823–829.

Ishida H, Kunimatsu Y, Nakatsukasa M & Nakano Y. 1999. New hominoid genus from the middle Miocene of Nachola, Kenya. *Anthropological Science,* **107**: 189–191.

Ishida H, Kuminatsu Y, Takano T, Nakano Y & Nakatsukasa M. 2004. *Nacholapithecus* skeleton from the Middle Miocene of Kenya. *Journal of Human Evolution,* **46**: 69–103.

Isler K. 2003. *3D-kinematics of vertical climbing in hominoids.* PhD dissertation. Universität Zürich.

Isler K. 2005. 3D-kinematics of vertical climbing in hominoids. *American Journal of Physical Anthropology,* **126**: 66–81.

Jenkins FA. 1972. Chimpanzee bipedalism: a cineradiographic analysis and implications for the evolution of gait. *Science,* **178**: 877–879.

Jenkins FA & Fleagle JG. 1975. Knuckle-walking and the functional anatomy of the wrists in living apes. *In:* RH Tuttle (ed). *Primate Functional Morphology and Evolution.* The Hague: Mouton. pp 213–227.

Jenkins FA & Camazine SM. 1977. Hip structure and locomotion in ambulatory and cursorial carnivores. *Journal of Zoology,* **181**: 351–370.

Johnson SE & Shapiro LJ. 1998. Positional behavior and vertebral morphology in atelines and cebines. *American Journal of Physical Anthropology,* **105**: 333–354.

Johnson GD, Opdyke ND, Tandon SK & Nanda AC. 1983. The magnetic polarity stratigraphy of the Siwalik Group at Haritalyangar (India) and a last appearance datum for *Ramapithecus* and *Sivapithecus*. *Paleogeography, Paleoclimatology, and Paleoecology,* **44**: 223–249.

Jungers WL. 1976. Hindlimb and pelvic adaptations to vertical climbing and clinging in *Megaladapis*, a giant subfossil prosimian from Madagascar. *Yearbook of Physical Anthropology,* **20**: 508–524.

Jungers WL. 1984a. Aspects of size and scaling in primate biology with special reference to the locomotor skeleton. *American Journal of Physical Anthropology,* **27**: 73–97.

Jungers WL. 1984b. Scaling of the hominoid locomotor skeleton with special reference to lesser apes. *In:* H Preuschoft, DJ Chivers, WY Brockelmann & N Creel (eds). *The Lesser Apes.* Edinburgh: Edinburgh University Press. pp 146–169.

Jungers WL. 1985. Body size and scaling of limb proportions in primates. *In:* WL Jungers (ed). *Size and Scaling in Primate Biology.* New York: Plenum Press. pp 345–381.

Jungers WL. 1987. Body size and morphometric affinities of the appendicular skeleton in *Oreopithecus bambolii* (IGF 11778). *Journal of Human Evolution,* **16**: 445–456.

Jungers WL. 1990a. Problems and methods in reconstructing body size in fossil primates. *In:* J Damuth & BJ MacFadden (eds). *Body Size in Mammalian Paleobiology Estimation and Biological Implications.* Cambridge: Cambridge University Press. pp 107–118.

Jungers WL. 1990b. Scaling of postcranial joint size in hominoid primates. *In:* FK Jouffroy, MH Stack & C Niemitz (eds). *Gravity, Posture and Locomotion in Primates.* Firenze: Editrice "Il Sedicesimo". pp 87–95.

Jungers WL, Falsetti AB & Wall CE. 1995. Shape, relative size, and size-adjustments in morphometrics. *Yearbook of Physical Anthropology,* **38**: 137–161.

Jungers WL, Burr DR & Cole MS. 1998. Body size and scaling of long bone geometry, bone strength, and positional behavior in cercopithecoid primates. *In:* E Strasser, J Fleagle, A Rosenberger & H McHenry (eds). *Primate Locomotion Recent Advances*. New York: Plenum Press. pp 309–330.

Jungers WL, Larson SG, Harcourt-Smith W, Morwood MJ, Sutikna T, Due Awe R & Djubiantono T. 2009. Descriptions of the lower limb skeleton of *Homo floresiensis*. *Journal of Human Evolution,* **57**: 538–554.

Kak AC & Slaney M. 1988. *Principles of Computerized Tomographic Imaging*. New York: IEEE Press.

Kappelman J, Kelly J, Pilbeam D, Sheikh KA, Anwar MA, Barry JC, Brown B, Hak P, Johnson NM, Raza SM &. Shah SMI. 1991. The earliest occurrence of *Sivapithecus* from the middle Miocene Chinji Formation of Pakistan. *Journal of Human Evolution,* **21**: 61–73.

Katoh S, Beyene Y, Itaya T, Hyodo H, Hyodo M, Yagi K, Gouzu C, WoldeGabriel G, Hart WK, Ambrose SH, Nakaya H, Bernor RL, Boisserie J-R, Bibi F, Saegusa H, Sasaki T, Sano K, Asfaw B & Suwa G. 2016. New geological and palaeontological age constraint for the gorilla–human lineage split. *Nature,* **530**: 215–218.

Kay RF, Ross C & Williams BA. 1997. Anthropoid origins. *Science,* **275**: 797–804.

Kelley J. 1988. A new large species of *Sivapithecus* from the Siwaliks of Pakistan. *Journal of Human Evolution,* **17**: 305–324.

Kelley J. 1997. Paleobiological and phylogenetic significance of life history in Miocene hominoids. *In:* DR Begun, CV Ward & Rose MD (eds). *Function, Phylogeny, and Fossils: Miocene Hominoid Evolution and Adaptations.* New York: Plenum Press. pp 173–208.

Kelley J. 2002. The hominoid radiation in Asia. *In:* W Hartwig (ed). *The Primate Fossil Record.* Cambridge: Cambridge University Press. pp 369–384.

Kelley J. 2005. Twenty-five years contemplating *Sivapithecus* taxonomy. *In:* DE Lieberman, RH Smith & J Kelley (eds). *Interpreting the Past: Essays on Human, Primate, and Mammal Evolution in Honor of David Pilbeam.* Boston: Brill Academic Publishers. pp 123–143.

Kelley J & Pilbeam D. 1986. The dryopithecines: taxonomy, comparative anatomy, and phylogeny of Miocene large hominoids. *In:* DR Swindler & J Irwin (eds). *Comparative Primate Biology. Volume 1. Systematics, Evolution, and Anatomy.* New York: Liss. pp 361–411.

Kelley J, Ward S, Brown B, Hill A & Duren DL. 2002. Dental remains of *Equatorius africanus* from Kipsaramon, Tugen Hills, Baringo District, Kenya. *Journal of Human Evolution,* **42**: 39–62.

Kelley J, Andrews P & Alpagut B. 2008. A new hominoid species from the middle Miocene site of Paşalar, Turkey. *Journal of Human Evolution,* **54**: 455–479.

Kendall DG. 1984. Shape-manifolds, Procrustean metrics and complex projective spaces. *Bulletin of the London Mathematical Society,* **16**: 81–121.

Kendall DG. 1985. Exact distributions for shapes of random triangles in convex sets. *Advances in Applied Probability,* **17**: 308–329.

Kikuchi Y, Nakatsukasa M, Nakano Y, Kunimatsu Y, Shimizu D, Ogihara N, Tsujikawa H, Takano T & Ishida H. 2015. Morphology of the thoracolumbar spine of the middle Miocene hominoid *Nacholapithecus kerioi* from northern Kenya. *Journal of Human Evolution,* **88**: 25–42.

Kimura T, Okada M & Ishida H. 1979. Kinesiological characteristics of primate walking: Its significance in human walking. *In:* ME Morbeck, H Preuschoft & N Gomberg (eds). *Environment, Behavior and Morphology: Dynamic Interactions in Primates.* New York: Gustav Fischer. pp 297–311.

Kivell TL, Schmitt DD & Walker A. 2009. Independent evolution of knuckle-walking in African apes shows that humans did not evolve from a knuckle-walking ancestor. *Proceedings of the National Academy of Sciences USA,* **106**: 14241–14246.

Klingenberg CP. 1998. Heterochrony and allometry: the analysis of evolutionary change in ontogeny. *Biological Reviews,* **73**: 79–123.

Köhler M & Moyà-Solà S. 1997. Ape-like or hominid-like? The positional behavior of *Oreopithecus bambolii* reconsidered. *Proceedings of the National Academy of Sciences USA,* **94**: 11747–11750.

Köhler M, Moyà-Solà S & Alba DM. 2001. Eurasian hominoid evolution in the light of recent *Dryopithecus* findings. In: L de Bonis, GD Koufos & P Andrews (eds). *Hominoid Evolution and Climatic Change in Europe, Vol 2 Phylogeny of the Neogene Hominoid Primates of Eurasia.* Cambridge: Cambridge University Press. pp 192–212.

Köhler M, Alba DM, Moyà-Solà S & MacLatchy L. 2002. Taxonomic affinities of the Eppelsheim Femur. *American Journal of Physical Anthropology,* **119**: 297–304.

Korhonen RK & Saarakkala S. 2011. Biomechanics and modeling of skeletal soft tissues. *In:* V Klika (ed). *Theoretical Biomechanics.* Rijeka: InTech. pp 113–132.

Kraft TS, Venkataraman VV & Dominy NJ. 2014. A natural history of human tree climbing. *Journal of Human Evolution,* **71**: 105–118.

Kramer CY. 1956. Extension of multiple range test to group means with unequal numbers of replications. *Biometrics,* **12**: 307–310.

Kumakura H. 1989. Functional analysis of the biceps femoris muscle during locomotor behavior in some primates. *American Journal of Physical Anthropology,* **79**: 379–391.

Kunimatsu Y, Nakatsukasa M, Sawada Y, Sakai T, Hyodo M, Hyodo H, Itaya T, Nakaya H, Saegusa H, Mazurier A, Saneyoshi M, Tsujikawa H, Yamamoto A & Mbua E. 2007. A new Late Miocene great ape from Kenya and its implications for the origins of African great apes and humans. *Proceedings of the National Academy of Sciences USA,* **104**: 19220–19225.

Kuperavage AJ, Sommer HJ & Eckhardt RB. 2010. Moment coefficients of skewness in the femoral neck cortical bone distribution of BAR 1002'00. *HOMO-Journal of Comparative Human Biology,* **61**: 244–252.

Kupczik K. 2008. Virtual biomechanics: basic concepts and technical aspects of finite element analysis in vertebrate morphology. *Journal of Anthropological Sciences,* **86**: 193–198.

Larney E & Larson SG. 2004. Compliant walking in primates: Elbow and knee yield in primates compared to other mammals. *American Journal of Physical Anthropology,* **125**: 42–50.

Larson SG. 1988. Subscapularis function in gibbons and chimpanzees: implications for interpretation of humeral head torsion in hominoids. *American Journal of Physical Anthropology,* **76**: 449–462.

Larson SG. 1996. Estimating humeral torsion on incomplete fossil anthropoid humeri. *Journal of Human Evolution,* **31**: 239–257.

Larson SG. 1998a. Parallel evolution in the hominoid trunk and forelimb. *Evolutionary Anthropology,* **6**: 87–99.

Larson SG. 1998b. Unique aspects of quadrupedal locomotion in nonhuman primates. *In:* E Strasser, J Fleagle, A Rosenberger & H McHenry (eds). *Primate Locomotion. Recent Advances.* New York: Plenum Press. pp 157–173.

Larson SG. 2015. Rotator cuff muscle size and the interpretation of scapular shape in primates. *Journal of Human Evolution,* **80**: 96–106.

Larson SG, Stern JT Jr & Jungers WL. 1991. EMG of *serratus anterior* and *trapezius* in the chimpanzee: scapular rotators revisited. *American Journal of Physical Anthropology,* **85**: 71–84.

Larson SG, Schmitt D, Lemelin P & Hamrick M. 2001. Limb excursion during quadrupedal walking: how do primates compare to other mammals? *Journal of Zoology,* **255**: 353–365.

Lartet É. 1856. Note sur un grand singe fossile qui se rettache au grouppe des singes supérieurs. *Comptes Rendus de l'Acad*émie des *Sciences Paris,* **43**: 219–223.

Latimer B. 1991. Locomotor adaptations in *Australopithecus afarensis*: the issue of arboreality. *In:* B Senut & Y Coppens (eds). *Origin(s) de la Bipédie chez les Hominidés.* Paris: Cahiers de Paleoanthropologie, CNRS. pp 169–176.

Lauder GV. 1996. The argument from design. *In:* MR Rose & GV Lauder (eds). *Adaptation*. San Diego: Academic Press. pp 55–92.

Lautenschlager S. 2014. Morphological and functional diversity in therizinosaur claws and the implications for theropod claw evolution. *Proceedings of the Royal Society B: Biological Sciences*, **281**: 20140497. http://dx.doi.org/10.1098/rspb.2014.0497

Lawing AM & Polly PD. 2010. Geometric morphometrics: recent applications to the study of evolution and development. *Journal of Zoology,* **280**: 1–7.

Le Gros Clark WE & Leakey LSB. 1951. The Miocene Hominoidea of East Africa. *Fossil Mammals of Africa,* **1**: 1–117.

Leakey MG, Ungar PS & Walker A. 1995. A new genus of large primate from the Late Oligocene of Lothidok, Turkana District, Kenya. *Journal of Human Evolution,* **28**: 519–531.

Lewis OJ. 1964. The tibialis posterior tendon in the primate foot. *Journal of Anatomy,* **98**: 209–218.

Lewis OJ. 1969. The hominoid wrist joint. *American Journal of Physical Anthropology,* **30**: 251–268.

Lewis OJ. 1980a. The joints of the evolving foot. Part I. The ankle joint. *Journal of Anatomy,* **130**: 527–543.

Lewis OJ. 1980b. The joints of the evolving foot. Part II. The intrinsic joints. *Journal of Anatomy,* **130**: 833–857.

Lewis OJ. 1989. *Functional Morphology of the Evolving Hand and Foot.* Oxford: Oxford University Press.

Li G, DeFrate LE, Sun H & Gill TJ. 2004. *In vivo* elongation of the anterior cruciate ligament and posterior cruciate ligament during knee flexion. *The American Journal of Sports Medicine,* **32**: 1415–1420.

Lovejoy CO. 1988. Evolution of human walking. *Scientific American,* **259**: 118–125.

Lovejoy CO. 2005. The natural history of human gait and posture. Part 2. Hip and thigh. *Gait & Posture,* **21**: 113–124.

Lovejoy CO. 2007. The natural history of human gait and posture: Part 3. The knee. *Gait & Posture,* **25**: 325–341.

Lovejoy CO, Heiple KG & Burnstein AH. 1973. The gait of *Australopithecus*. *American Journal of Physical Anthropology,* **38**: 757–780.

Lovejoy CO, Burstein AH & Heiple KG. 1976. The biomechanical analysis of bone strength: A method and its application to platycnemia. *American Journal of Physical Anthropology,* **44**: 489–505.

Lovejoy CO, Meindl RS, Ohman JC, Heiple KG & White TD. 2002. The Maka femur and its bearing on the antiquity of human walking: Applying contemporary concepts of morphogenesis to the human fossil record. *American Journal of Physical Anthropology,* **119**: 97–133.

Lovejoy CO, Latimer B, Suwa G, Asfaw B & White TD. 2009. Combining prehension and propulsion: the foot of *Ardipithecus ramidus*. *Science,* **326**: 72e1–72e8.

MacLatchy LM. 1996. Another look at the australopithecine hip. *Journal of Human Evolution,* **31**: 455–476.

MacLatchy LM. 2004. The oldest ape. *Evolutionary Anthropology,* **13**: 90–103.

MacLatchy LM & Bossert WH. 1996. An analysis of the articular surface distribution of the femoral head and

acetabulum in anthropoids, with implications for hip function in Miocene hominoids. *Journal of Human Evolution,* **31**: 425–453.

MacLatchy LM & DeSilva J. 2009. The postcranial anatomy of *Proconsul major*. *Journal of Vertebrate Paleontology,* **29(sp1)**: 139A.

MacLatchy LM, Gebo D, Kityo R & Pilbeam D. 2000. Postcranial functional morphology of *Morotopithecus bishopi*, with implications for the evolution of modern ape locomotion. *Journal of Human Evolution,* **39**: 159–183.

MacLatchy LM, Köhler M & Moyà-Solà S. 2001. The femora of *Dryopithecus laietanus*. *American Journal of Physical Anthropology,* **114(S32)**: 100.

MacLatchy LM, Rossie JB & Kingston JD. 2015. The ecological niche of the *Morotopithecus*, with implications for hominoid evolution. *American Journal of Physical Anthropology,* **156(S60)**: 210.

Madar SI, Rose MD, Kelley J, Maclatchy L & Pilbeam D. 2002. New *Sivapithecus* postcranial specimens from the Siwaliks of Pakistan. *Journal of Human Evolution,* **42**: 705–752.

Mafart B, Guipert G, de Lumley M-A & Subsol G. 2004. Three-dimensional computer imaging of hominid fossils: a new step in human evolution studies. *Journal of the Canadian Association of Radiologists,* **55**: 264–270.

Mallison H, Hohloch, A & Pfretzschner, H-U. 2009. Mechanical digitizing for paleontology–New and improved techniques. *Palaeontologia Electronica,* **12**: 4T.

Marcé-Nogué J, Fortuny J, Gil L & Galobart A. 2011. Using reverse engineering to reconstruct tetrapod skulls and analyse its feeding behaviour. *In:* BHV Topping & Y Tsompanakis (eds). *Proceedings of the Thirteenth International Conference on Civil, Structural and Environmental Engineering Computing*. Stirlingshire: Civil-Comp Press. Paper 237. doi:10.4203/ccp.96.237

Marcé-Nogué J, DeMiguel D, De Esteban-Trivigno S, Fortuny J & Gil L. 2013. Quasi-homothetic transformation for comparing the mechanical performance of planar models in biological research. *Palaeontologia Electronica*, **16**: 6T, 15 p.

Marcé-Nogué J, Fortuny J, Gil L & Sánchez M. 2015. Improving mesh generation in Finite Element Analysis for functional morphology approaches. *Spanish Journal of Palaeontology*, **30**: 117–132.

Marchi D. 2007. Relative strength of the tibia and fibula and locomotor behavior in hominoids. *Journal of Human Evolution,* **53**: 647–655.

Marigó J, Susanna I, Minwer-Barakat R, Madurell-Malapeira J, Moyà-Solà S, Casanovas-Vilar I, Robles JM & Alba DM. 2014. The primate fossil record in the Iberian Peninsula. *Journal of Iberian Geology,* **40**: 179–211.

Marmi J, Casanovas-Vilar I, Robles JM, Moyà-Solà S, & Alba DM. 2012. The paleoenvironment of *Hispanopithecus laietanus* as revealed by paleobotanical evidence from the Late Miocene of Can Llobateres 1 (Catalonia, Spain). *Journal of Human Evolution,* **62**: 412–423.

Martin RD. 1990. *Primate Origins and Evolution. A Phylogenetic Reconstruction*. Princeton: Princeton University Press.

Martin RD & Barbour AD. 1989. Aspects of line-fitting in bivariate allometric analyses. *Folia Primatologica,* **53**: 65–81.

Martins EP & Hansen TF. 1997. Phylogenies and the comparative method: a general approach to incorporating phylogenetic information in to the analysis of interspecific data. *The American Naturalist,* **149**: 646–667.

Masouros SD, Bull AMJ & Amis AA. 2010. (i) Biomechanics of the knee joint. *Orthopaedics and Trauma,* **24**: 84–91.

Matsumura A, Nakamura T, Gunji H, Takahashi Y, Nishida T & Okada M. 2010a. Regional differences in cortical thickness of the femoral neck in chimpanzees [Abstract]. *Primate Research,* **Suppl. 26**: 148. http://primate-society.com/ips/public/ips_program/IPS10-293.pdf

Matsumura A, Gunji H, Takahashi Y, Nishida T & Okada M. 2010b. Cross-sectional morphology of the femoral neck of wild chimpanzees. *International Journal of Primatology,* **31**: 219–238.

McCrossin ML. 1994a. *The phylogenetic relationship, adaptations, and ecology of* Kenyapithecus. PhD dissertation. University of California.

McCrossin ML. 1994b. Semi-terrestrial adaptations of *Kenyapithecus* [Abstract]. *American Journal of Physical Anthropology,* **37(S18)**: 142–143.

McCrossin ML. 1997. New postcranial remains of *Kenyapithecus* and their implications for understanding the origins of hominoid terrestriality [Abstract]. *American Journal of Physical Anthropology,* **104(S24)**: 164.

McCrossin ML & Benefit BR. 1997. On the relationships and adaptations of *Kenyapithecus*, a large-bodied hominoid from the Middle Miocene of Eastern Africa. *In:* DR Begun, CV Ward & MD Rose (eds). *Function, Phylogeny and Fossils: Miocene Hominoid Evolution and Adaptation.* New York: Plenum Press. pp 241–267.

McCrossin ML, Benefit BR, Gitau SN, Palmer AK & Blue KT. 1998. Fossil evidence for the origins of terrestriality among Old World higher primates. *In:* E Strasser, J Fleagle, A Rosenberger, & H McHenry (eds). *Primate Locomotion: Recent Advances.* New York: Plenum Press. pp 353–396.

McDonald JH. 2008. *Handbook of Biological Statistics.* Baltimore: Sparky House Publishing.

McGraw WS. 1996. Cercopithecid locomotion, support use, and support availability in the Tai Forest, Ivory Coast. *American Journal of Physical Anthropology,* **100**: 507–522.

McGraw WS. 1998. Posture and support use of old world monkeys (Cercopithecidae): The influence of foraging strategies, activity patterns, and the spatial distribution of preferred food items. *American Journal of Primatology,* **46**: 229–250.

McHenry D. 1943. A lattice analogy for the solution of plane stress problems. *Journal of Institution of Civil Engineers,* **21**: 59–82.

McHenry HM & Corruccini RS. 1976. Fossil hominid femora and the evolution of walking. *Nature,* **259**: 657–658.

McNulty KP, Begun DR, Kelley J, Manthi FK & Mbua EN. 2015. A systematic revision of *Proconsul* with the description of a new genus of early Miocene hominoid. *Journal of Human Evolution,* **84**: 42–61.

Mittermeier RA. 1978. Locomotion and posture in *Ateles geoffroyi* and *Ateles paniscus*. *Folia primatologica,* **30**: 161–193.

Mitteroecker P & Bookstein F. 2011. Linear discrimination, ordination, and visualization of selection gradients in modern morphometrics. *Evolutionary Biology,* **38**: 100–114.

Mongle CS, Wallace IJ & Grine FE. 2015. Cross-sectional structural variation relative to midshaft along hominine diaphyses. II. The hind limb. *American Journal of Physical Anthropology,* **158**: 386–397.

Morgan EF & Bouxsein ML. 2005. Use of finite element analysis to assess bone strength. *IBMS BoneKEy,* **2**: 8–19.

Morgan MlE, Lewton KL, Kelley J, Otárola-Castillo E, Barry JC, Flynn LJ & Pilbeam D. 2015. A partial hominoid innominate from the Miocene of Pakistan: Description and preliminary analyses. *Proceedings of the National Academy of Sciences USA,* **112**: 82–87.

Morton DJ. 1926. Evolution of man's erect posture. Preliminary report. *Journal of Morphology,* **43**: 147–149.

Mosimann JE. 1970. Sixe allometry: Size and shape variables with characterizations of the lognormal and generalized gamma distributions. *Journal of the American Statistical Association,* **65**: 930–945.

Moyà-Solà S & Köhler M. 1993. Recent discoveries of *Dryopithecus* shed new light on evolution of great apes. *Nature,* **365**: 543–545.

Moyà-Solà S & Köhler M. 1995. New partial cranium of *Dryopithecus* Lartet, 1863 (Hominoidea, Primates) from the upper Miocene of Can Llobateres, Barcelona, Spain. *Journal of Human Evolution,* **29**: 101–139.

Moyà-Solà S & Köhler M. 1996. A *Dryopithecus* skeleton and the origin of great-ape locomotion. *Nature,* **379**: 156–159.

Moyà-Solà S, Pons Moyà J & Köhler M. 1990. Primates catarrinos (Mammalia) del Neógeno de la península Ibérica. *Paleontologia i Evolució,* **23**: 41–45.

Moyà-Solà S, Köhler M & Rook L. 1999. Evidence of hominid-like precision grip capability in the hand of the Miocene ape *Oreopithecus*. *Proceeding of the National Academy of Sciences USA,* **96**: 313–317.

Moyà-Solà S, Köhler M & Alba DM. 2001. *Egarapithecus narcisoi*, a new genus of Pliopithecidae (Primates, Catarrhini) from the Late Miocene of Spain. *American Journal of Physical Anthropology,* **114**: 312–324.

Moyà-Solà S, Köhler M, Alba DM, Casanovas-Vilar I & Galindo J. 2004. *Pierolapithecus catalaunicus* a new Middle Miocene great ape from Spain. *Science,* **306**: 1339–1344.

Moyà-Solà S, Köhler M, Alba DM, Casanovas-Vilar I & Galindo J. 2005a. Response to comment on "*Pierolapithecus catalaunicus*, a new Middle Miocene great ape from Spain". *Science,* **308**: 203d.

Moyà-Solà S, Köhler M & Rook L. 2005b. The *Oreopithecus* thumb: a strange case in hominoid evolution. *Journal of Human Evolution,* **49**: 395–404.

Moyà-Solà S, Köhler M, Alba DM, Casanovas-Vilar I, Galindo J, Robles JM, Cabrera L, Garcés M, Almécija S & Beamud E. 2009a. First partial face and upper dentition of the Middle Miocene hominoid *Dryopithecus fontani* from Abocador de Can Mata (Vallès-Penedès Basin. Catalonia. NE Spain): taxonomic and phylogenetic implications. *American Journal of Physical Anthropology,* **139**: 126–145.

Moyà-Solà S, Alba DM, Almécija S, Casanovas-Vilar I, Köhler M, de Esteban-Trivigno S, Robles J, Galindo J & Fortuny J. 2009b. A unique Middle Miocene European hominoid and the origins of the great ape and human clade. *Proceedings of the National Academy of Science USA,* **106**: 9601–9606.

Muir-Wood HM. 1934. On the internal structure of some Mesozoic Brachiopoa. *Philosophical Transactions of the Royal Society B,* **505**: 511–567.

Nakano Y, Ogihara N, Makishima H, Shimizu D, Kagaya M, Kunimatsu Y & Ishida H. 2004. The locomotor adaptation in the pelvic morphology of *Nacholapithecus*. *Anthropological Sciences,* **112**: 301.

Nakatsukasa M. 2004. Acquisition of bipedalism: the Miocene hominoid record and modern analogues for bipedal protohominids. *Journal of Anatomy,* **204**: 385–402.

Nakatsukasa M. 2008. Comparative study of Moroto vertebral specimens. *Journal of Human Evolution,* **55**: 581–588.

Nakatsukasa M & Kunimatsu Y. 2009. *Nacholapithecus* and its importance for understanding hominoid evolution. *Evolutionary Anthropology,* **18**: 103–119.

Nakatsukasa M, Yamanaka A, Kunimatsa Y, Shimizu D & Ishida H. 1998. A newly discovered *Kenyapithecus* skeleton and its implications for the evolution of postural behavior in Miocene East African hominoids. *Journal of Human Evolution,* **34**: 657–664.

Nakatsukasa M, Tsujikawa H, Shimizu D, Takano T, Kunimatsu Y, Nakano Y & Ishida H. 2003a. Definitive evidence for tail loss in *Nacholapithecus*, an East African Miocene hominoid. *Journal of Human Evolution,* **45**: 179–186.

Nakatsukasa M, Kuminatsu Y, Nakano Y, Takano T & Ishida H. 2003b. Comparative and functional anatomy of phalanges in *Nacholapithecus kerioi*, a Middle Miocene hominoid from northern Kenya. *Primates,* **44**: 371–412.

Nakatsukasa M, Ward CV, Walker A, Teaford MF, Kunimatsu Y & Ogihara N. 2004a. Tail loss in *Proconsul heseloni*. *Journal of Human Evolution,* **46**: 777–784.

Nakatsukasa M, Yamanaka A, Yutaka K, Shimizu D & Ishida J. 2004b. A newly discovered *Kenyapithecus* skeleton and its implications for the evolution of positional behavior in Miocene East African hominoids. *Journal of Human Evolution,* **34**: 657–664.

Nakatsukasa M, Kunimatsu Y, Nakano Y & Ishida H. 2007a. Vertebral morphology of *Nacholapithecus kerioi* based on KNM-BG 35250. *Journal of Human Evolution,* **52**: 347–369.

Nakatsukasa M, Kunimatsu Y, Nakano Y, Egi N & Ishida H. 2007b. Postcranial bones of infant *Nacholapithecus*: ontogeny and positional behavioral adaptation. *Anthropological Sciences,* **115**: 201–213.

Nakatsukasa M, Pickford M, Egi N & Senut B. 2007c. Femur length, body mass, and stature estimates of *Orrorin tugenensis*, a 6 Ma hominid from Kenya. *Primates,* **48**: 171–178.

Nakatsukasa M, Kunimatsu Y, Shimizu D, Nakano Y, Kikuchi Y & Ishida H. 2012. Hind limb of the *Nacholapithecus kerioi* holotype and implications for its positional behavior. *Anthropological Science,* **120**: 235–250.

Napier JR. 1964. The evolution of bipedal walking in the hominids. *Archives de Biologie,* **75**: 637–708.

Napier JR & Davis PR. 1959. The fore-limb skeleton and associated remains of *Proconsul africanus*. *Fossil Mammals of Africa,* **16**: 1–69.

Napier JR & Walker AC. 1967. Vertical clinging and leaping–a newly recognized category of locomotor behavior of Primates. *Folia Primatologica,* **6**: 204–219.

Nisell R. 1985. Mechanics of the knee. A study of joint and muscle load with clinical applications. *Acta Orthopaedica Scandinava,* **Suppl. 216**: 1–42.

Ogihara N, Almécija S, Nakatsukasa M, Nakano Y, Kikuchi Y, Kunimatsu Y, Makishima H, Shimizu D, Takano T, Tsujikawa H, Kagaya M & Ishida H. 2016, in press. Carpal bones of *Nacholapithecus kerioi*, a Middle Miocene Hominoid From Northern Kenya. *American Journal of Physical Anthropology*. doi: 10.1002/ajpa.22984.

Ohman JC, Krochta TJ, Lovejoy CO, Mensforth RP & Latimer B. 1997. Cortical bone distribution in the femoral neck of hominoids: Implications for the locomotion of *Australopithecus afarensis*. *American Journal of Physical Anthropology,* **104**: 117–131.

O'Neill MC, Lee L-F, Larson SG, Demes B, Stern JT Jr & Umberger BR. 2013. A three-dimensional musculoskeletal model of the chimpanzee (*Pan troglodytes*) pelvis and hind limb. *Journal of Experimental Biology,* **216**: 3709–3723.

Oxnard CE. 1963. Locomotor adaptations in the primate forelimb. *Symposia of the Zoological Society of London,* **10**: 165–182.

Oxnard CE. 1971. Tensile forces in skeletal structures. *Journal of Morphology,* **134**: 425–436.

Pagel M. 1999. Inferring the historial patterns of biological evolution. *Nature,* **401**: 877–884.

Patel BA, Susman RL, Rossie JB & Hill A. 2009. Terrestrial adaptations in the hands of *Equatorius africanus* revisited. *Journal of Human Evolution,* **57**: 763–772.

Patel BA. 2010. The interplay between speed, kinetics and hand postures during primate terrestrial locomotion. *American Journal of Physical Anthropology,* **141**: 222–234.

Pérez de los Ríos M, Moyà-Solà S & Alba DM. 2012. The nasal and paranasal architecture of the Middle Miocene ape *Pierolapithecus catalaunicus* (primates: Hominidae): Phylogenetic implications. *Journal of Human Evolution,* **63**: 497–506.

Pickford M & Andrews P. 1981. The Tinderet Miocene sequence in Kenya. *Journal of Human Evolution,* **10**: 11–33.

Pickford M, Senut B & Gommery D. 1999. Sexual dimorphism in *Morotopithecus bishopi,* an early Middle Miocene hominoid from Uganda and a reassessment of its geological and biological contexts. *In:* P Andrews & P Banham P (eds). *Late Cenozoic Environments and Hominid Evolution: A Tribute to Bill Bishop.* London: The Royal Geological Society. pp 27–38.

Pickford M, Senut B, Gommery D & Treil J. 2002. Bipedalism in *Orrorin tugenensis* revealed by its femora. *Comptes Rendus Palevol,* **1**: 191–203.

Pilbeam DR & Simons EL. 1971. Humerus of *Dryopithecus* from Saint Gaudens, France. *Nature,* **229**: 406–407.

Pilbeam DR & Young DL. 2001. *Sivapithecus* and hominoid evolution: some brief comments. *In:* L de Bonis, GD Koufos & P Andrews (eds). *Hominoid Evolution and Climatic Change in Europe. Volume 2, Phylogeny of the Neogene Hominoid Primates of Eurasia.* Cambridge: Cambridge University Press. pp 349–364.

Pilbeam DR, Rose MD, Badgley C & Lipschutz B. 1980. Miocene hominoids from Pakistan. *Postilla,* **181**: 1–94.

Pilbeam D, Rose MD, Barry JC & Shah SMI. 1990. New *Sivapithecus* humeri from Pakistan and the relationship of *Sivapithecus* and *Pongo*. *Nature,* **348**: 237–239.

Platzer W. 2008. *Color Atlas of Human Anatomy. Locomotor System.* Stuttgart: Thieme.

Polk JD, Williams SA & Peterson JV. 2009. Body size and joint posture in primates. *American Journal of Physical Anthropology,* **140**: 359–367.

Pontzer H, Holloway JH, Raichlen DA & Lieberman DE. 2009. Control and function of arm swing in human walking and running. *Journal of Experimental Biology,* **212**: 523–534.

Povinelli DJ & Cant JGH. 1995. Arboreal clambering and the evolution of self-conception. *Quarterly Review of Biology*, **70**: 393–421.

Preuschoft H. 1970. Functional anatomy of the lower extremity. *In:* G Bourne (ed). *The Chimpanzee*. Basel / München / New York: Karger. pp 221–294.

Preuschoft H. 1971. Body posture and more of locomotion in Early Pleistocene Hominids. *Folia Primatologica*, **14**: 209–240.

Preuschoft H. 2004. Mechanisms for the acquisition of habitual bipedality: are there biomechanical reasons for the acquisition of upright bipedal posture? *Journal of Anatomy*, **204**: 363–384.

Preuschoft H & Demes B. 1984. Biomechanics of brachiation. *In:* H Preuschoft, DJ Chivers, WY Brockelman & N Creel (eds). *The Lesser Apes: Evolutionary and Behavioral Biology*. Edinburgh: Edinburgh University Press. pp 96–118.

Preuschoft H & Tardieu C. 1996. Biomechanical reasons for the divergent morphology of the knee joint and the distal epiphyseal suture in hominoids. *Folia Primatologica*, **66**: 82–92.

Preuschoft H, Godinot M, Beard C, Nieschalk U & Jouffroy KK. 1993. Biomechanical considerations to explain important morphological characters of primate hands. *In:* H Preuschoft & DJ Chivers (eds). *Hands of Primates*. Wien: Springer-Verlag. pp 245–256.

Prost JH. 1965. A definitional system for the classification of primate locomotion. *American Anthropologist*, **67**: 1198–1214.

Prost JH. 1967. Bipedalism of man and gibbons compared using estimates of joint motion. *American Journal of Physical Anthropology*, **26**: 135–148.

Puech P-F, Cianfarani F & Ribot I Trafi F. 1989. Maxillary canine microwear in *Dryopithecus* from Spain. *American Journal of Physical Anthropology*, **80**: 305–312.

Puymerail L, Ruff CB, Bondioli L, Widianto H, Trinkaus E & Macchiarelli R. 2012. Structural analysis of the Kresna 11 *Homo erectus* femoral shaft (Sangiran, Java). *Journal of Human Evolution*, **63**: 741–749.

R Core Team. 2015. R: A language and environment for statistical computing. R Foundation for Statistical Computing, Vienna, Austria. URL http://www.R-project.org/

Rae TC. 1999. Mosaic evolution in the origin of the Hominoidea. *Folia Primatologica*, **70**: 125–135.

Rafferty KL. 1998. Structural design of the femoral neck in primates. *Journal of Human Evolution*, **34**: 361–383.

Rafferty KL, Walker A, Ruff CB, Rose MD & Andrews P. 1995. Postcranial estimates of body weight in *Proconsul*, with a note on a distal tibia of *P. major* from Napak, Uganda. *American Journal of Physical Anthropology*, **97**: 391–402.

Rafferty KL, Herring SW & Marshall CD. 2003. Biomechanics of the rostrum and the role of facial structures. *Journal of Morphology*, **257**: 33–44.

Rayfield EJ. 2007. Finite Element Analysis and understanding the biomechanics and evolution of living and fossil organisms. *Annual Review of Earth and Planetary Sciences*, **35**: 541–576.

Rayfield EJ, Norman DB, Horner CC, Horner JR, Smith PM, Thomason JJ & Upchurch P. 2001. Cranial design and function in a large theropod dinosaur. *Nature*, **409**: 1033–1037.

Raza SM, Barry JC, Pilbeam D, Rose MD, Shah SMI & Ward SC. 1983. New hominoid primates from the Middle Miocene Chinji Formation, Potwar Plateau, Pakistan. *Nature*, **406**: 52–54.

Reed KE, Fleagle JG & Leakey RE. 2013. *The Paleobiology of* Australopithecus. Dordrecht: Springer.

Reilly DT & Burstein AH. 1974. The mechanical properties of cortical bone. *The Journal of Bone and Joint Surgery*, **56-A**: 1001–1022.

Rein TR, Harrison T & Zollikofer CPE. 2011. Skeletal correlates of quadrupedalism and climbing in the anthropoid forelimb: implications for inferring locomotion in Miocene catarrhines. *Journal of Human Evolution*, **61**: 564–574.

Remis MJ. 1995. Effects of body size and social context on the arboreal activities of lowland gorillas in the Central African Republic. *American Journal of Physical Anthropology,* **97**: 413–433.

Ribot F, Gibert J & Harrison T. 1996. A reinterpretation of the taxonomy of *Dryopithecus* from Vallès-Penedès, Catalonia (Spain). *Journal of Human Evolution,* **31**: 129–141.

Richmond BG & Whalen M. 2001. Forelimb function, bone curvature and phylogeny of *Sivapithecus*. *In:* L de Bonis, GD Koufos & P Andrews (eds). *Hominoid Evolution and Climatic Change in Europe. Volume 2, Phylogeny of the Neogene Hominoid Primates of Eurasia.* Cambridge: Cambridge University Press. pp 326–348.

Richmond BG & Jungers WL. 2008. *Orrorin tugenensis* femoral morphology and the evolution of hominin bipedalism. *Science,* **319**: 1662–1665.

Richmond BG, Begun DR & Strait DS. 2001. Origin of human bipedalism: The knuckle-walking hypothesis revisited. *Yearbook of Physical Anthropology,* **44**: 70–105.

Rodman PS. 1979. Individual activity patterns and the solitary nature of orangutans. *In:* DA Hamburg & ER McCown (eds). *The Great Apes*. Menlo Park: Benjamin/Cummings. pp 235–256.

Rohlf FJ & Marcus LF. 1993. A revolution in morphometrics. *Trends in Ecology and Evolution,* **8**: 129–132.

Rook L, Harrison T & Engesser B. 1996. The taxonomic status and biochronological implications of new finds of *Oreopithecus* from Baccinello (Tuscany, Italy). *Journal of Human Evolution,* **30**: 3–27.

Rook L, Bondioli L, Köhler M, Moyà-Solà S & Macchiarelli R. 1999. *Oreopithecus* was a bipedal ape after all: Evidence from the iliac cancellous architecture. *Proceedings of the National Academy of Sciences USA,* **96**: 8795–8799.

Rook L, Renne P, Benvenuti M & Papini M. 2000. Geochronology of *Oreopithecus*-bearing succession at Baccinello (Italy) and the extinction pattern of European Miocene hominoids. *Journal of Human Evolution,* **39**: 577–582.

Rose MD. 1973. Quadrupedalism in primates. *Primates,* **14**: 337–357.

Rose MD. 1978. Feeding and associated positional behavior of black and white colobus monkeys (*Colobus guereza*). *In:* GE Montgomery (ed). *The Ecology of Arboreal Folivores.* Washington DC: Smithsonian Press. pp 253–262.

Rose MD. 1983. Miocene hominoid postcranial morphology: Monkey-like, ape-like, neither, or both? *In:* RL Ciochon & RS Corruccini (eds). *New Interpretations of Ape and Human Ancestry*. New York: Plenum Press. pp 405– 417.

Rose MD. 1986. Further hominoid postcranial specimens from late Miocene Nagri Formation of Pakistan. *Journal of Human Evolution,* **15**: 333–367.

Rose MD. 1988. Another look at the anthropoid elbow. *Journal of Human Evolution,* **17**: 193–224.

Rose MD. 1989. New postcranial specimens of catarrhines from the Middle Miocene Chinji Formation, Pakistan: descriptions and a discussion of proximal humeral functional morphology in anthropoids. *Journal of Human Evolution,* **18**: 131–162.

Rose MD. 1993. Locomotor anatomy of Miocene hominoids. *In:* DL Gebo (ed). *Postcranial Adaptation in Nonhuman Primates.* Dekalb (Illinois): Northern Illinois University Press. pp 252–272.

Rose MD. 1994. Quadrupedalism in some Miocene catarrhines. *Journal of Human Evolution,* **26**: 387–411.

Rose MD, Nakano Y & Ishida H. 1996. *Kenyapithecus* postcranial specimens from Nachola, Kenya. *African Study Monographs,* **Suppl 24**: 3–56.

Rotgers C, Alba DM, Robles JM, Casanovas-Vilar I, Galindo J, Bertó JV & Moyà-Solà S. 2011. A new species of *Anchitherium* (Equidae: Anchitheriinae) from the Middle Miocene of Abocador de Can Mata (Vallès-Penedès Basin, NE Iberian Peninsula). *Comptes Rendus Palevol,* **10**: 567–576.

Ruff CB. 1987. Structural allometry of the femur and tibia in Hominoidea and *Macaca*. *Folia Primatologica,* **48**: 9–49.

Ruff CB. 1988. Hindlimb articular surface allometry in hominoidea and *Macaca*, with comparisons to diaphyseal scaling. *Journal of Human Evolution,* **17**: 687–714.

Ruff CB. 1989. New approaches to structural evolution of limb bones in primates. *Folia Primatologica,* **53**: 142–159.

Ruff CB. 1995. Biomechanics of the hip and birth in early Homo. *American Journal of Physical Anthropology,* **98**: 527–574.

Ruff CB. 1998. Evolution of the hominid hip. *In:* E Strasser, A Rosenberger, H McHenry & J Fleagle J (eds). *Primate Locomotion: Recent Advances.* Davis: Plenum Press. pp 449–469.

Ruff CB. 2002. Long bone articular and diaphyseal structure in Old World Monkeys and apes. I: Locomotor effects. *American Journal of Physical Anthropology,* **119**: 305–342.

Ruff CB. 2003. Long bone articular and diaphyseal structure in Old World monkeys and apes. II: Estimation of body mass. *American Journal of Physical Anthropology,* **120**: 16–37.

Ruff CB & Hayes WC. 1983. Cross-sectional geometry of Pecos Pueblo femora and tibiae—A biomechanical investigation: I. Method and general patterns of variation. *American Journal of Physical Anthropology,* **60**: 359–381.

Ruff CB & Runestad JA. 1992. Primate limb bone structural adaptations. *Annual Review of Anthropology,* **21**: 407–433.

Ruff CB & Higgins R. 2013. Femoral neck structure and function in early hominins. *American Journal of Physical Anthropology,* **150**: 512–525.

Ruff CB, Walker A & Teaford MF. 1989. Body mass, sexual dimorphism and femoral proportions of *Proconsul* from Rusinga and Mfangano Islands, Kenya. *Journal of Human Evolution,* **18**: 515–536.

Ruff CB, McHenry HM & Thackeray FJ. 1999. Cross-sectional morphology of the SK 82 and 97 proximal femora. *American Journal of Physical Anthropology,* **109**: 509–521.

Ruff CB, Puymerail L, Macchiarelli R, Sipla J & Ciochon RL. 2015. Structure and composition of the Trinil femora: Functional and taxonomic implications. *Journal of Human Evolution,* **80**: 147–158.

Russo GA & Shapiro LJ. 2013. Reevaluation of the lumbosacral region of *Oreopithecus bambolii*. *Journal of Human Evolution,* **65**: 253–265.

Sanz de Siria Catalán A. 1993. Datos sobre la paleoclimatología y paleoecología del Neógeno del Vallès-Penedès según las macrofloras halladas en la cuenca y zonas próximas. *Paleontologia i Evolució,* **26–27**: 281–289.

Sanz de Siria Catalán A. 1994. La evolución de las paleofloras en las cuencas cenozoicas catalanas. *Acta Geologica Hispanica,* **29**: 169–189.

Sarin VK, Erickson GM, Giori NJ, Bergmann AG & Carter DR. 1999. Coincident development of sesamoid bones and clues to their evolution. *The Anatomical Record,* **257**: 174–180.

Sarmiento EE. 1987. The phylogenetic position of *Oreopithecus* and its significance in the origin of the Hominoidea. *American Museum Novitates,* **2881**: 1–44.

Sarmiento EE. 1988. Anatomy of the hominoid wrist joint: its evolutionary and functional implications. *International Journal of Primatology,* **9**: 281–345.

Sarmiento EE. 1989. A mechanical model of ape and human climbing and its bearing on body proportions [Abstract]. *American Journal of Physical Anthropology,* **78:** 296.

Schaffler MB, Burr DB, Jungers WL & Ruff CB. 1985. Structural and mechanical indicators of limb specialization in primates. *Folia Primatologica,* **45**: 61–75.

Scherf H. 2008. Locomotion-related femoral trabecular architectures in primates - high resolution computed tomographies and their implications for estimations of locomotor preferences of fossil primates. *In:* H Endo & R Frey (eds). *Anatomical Imaging.* Tokio: Springer. pp 39–59.

Schindler OS & Scott WN. 2011. Basic kinematics and biomechanics of the patello-femoral joint. Part 1: The native patella. *Acta Orthopaedica Belga,* **77**: 421–431.

Schindelin J, Arganda-Carreras I, Frise E, Kaynig V, Longair M, Pietzsch T, Preibisch S, Rueden C, Saafeld S, Schmid B, Tinevez J-Y, White DJ, Hartenstein V, Eliceiri K, Tomancak P & Cardona A. 2012. Fiji: an open-source platform for biological-image analysis. *Nature Methods,* **9**: 676–682.

Schmidt M. 2005. Quadrupedal locomotion in squirrel monkeys (Cebidae: *Saimiri sciureus*): A cineradiographic study of limb kinematics and related substrate reaction forces. *American Journal of Physical Anthropology,* **128**: 359–370.

Schultz AH. 1936. Characters common to higher primates and characters specific to man. *The Quarterly Review of Biology,* **11**: 259–283.

Schultz AH. 1950. The physical distinctions of man. *Proceedings of the American Philosophical Society,* **94**: 428–449.

Schultz AH. 1960. Einige beobachtungen und maße am skelett von *Oreopithecus* in vergleich mit anderen catarrhinen primaten. *Zeitschrift für Morphologie und Anthropologie,* **50**: 136–149.

Schultz AH. 1961. Vertebral column and thorax. *Primatologia,* **4**: l–66.

Schultz AH. 1963. Relations between the lengths of the main parts of the foot skeleton in primates. *Folia Primatologica,* **1**: 150–171.

Sellers WI, Margetts L, Bates KT & Chamberlain AT. 2013. Exploring diagonal gait using a forward dynamic three-dimensional chimpanzee simulation. *Folia Primatologica,* **84**: 180–200.

Senut B. 2015. Morphology and environment in some fossil Hominoids and Pedetids (Mammalia). *Journal of Anatomy,* doi: 10.1111/joa.12427.

Senut B, Pickford M, Gommery D & Kunimatsu Y. 2000. A new genus of Early Miocene hominoid from East Africa: *Ugandapithecus major* (Le Gros Clark & Leakey, 1950). *Comptes Rendus de l'AcadÈmie des Sciences–Series IIA–Earth and Planetary Science,* **331**: 227–233.

Senut B, Pickford M, Gommery D, Mein P, Cheboi K & Coppens Y. 2001. First hominid from the Miocene (Lukeino Formation, Kenya). *Comptes Rendus de l'Acadèmie des Sciences–Series IIA–Earth and Planetary Science,* **332**: 137–144.

Senut B, Nakatsukasa M, Kunimatsu Y, Nakano Y, Takano T, Tsujikawa H, Shimizu D, Kagaya M & Ishida H. 2004. Preliminary analysis of *Nacholapithecus* scapula and clavicle from Nachola, Kenya. *Primates,* **45**: 97–104.

Serrano-Fochs S, De Esteban-Trivigno S, Marcé-Nogué J, Fortuny J & Fariña RA. 2015. Finite Element Analysis of the cingulata jaw: An ecomorphological approach to armadillo's diets. *PLoS ONE,* **10**: e0120653.

Shaw CN & Ryan TM. 2012. Does skeletal anatomy reflect adaptation to locomotor patterns? Cortical and trabecular architecture in human and nonhuman anthropoids. *American Journal of Physical Anthropology,* **147**: 187–200.

Sherwood RJ, Ward RJ, Hill A, Duren DL, Drown B & Downs W. 2002. Preliminary description of the *Equatorius africanus* partial skeleton KNM-TH 28860 from Kipsaramon, Tugen Hills, Baringo District, Kenya. *Journal of Human Evolution,* **42**: 63–73.

Sigmon BA. 1974. A functional analysis of pongid hip and thigh musculature. *Journal of Human Evolution,* **3**: 161–185.

Skinner HB, Kilgus DJ, Keyak J, Shimaoka EE, Kim AS & Tipton JS. 1994. Correlation of computed finite element stresses to bone density after remodeling around cementless femoral implants. *Clinical Orthopaedics and Related Research,* **305**: 178–189.

Skinner MM, Stephens NB, Tsegai ZJ, Foote AC, Nguyen NH, Gross T, Pahr DH, Hublin J-J & Kivell TL. 2015a. Human-like hand use in *Australopithecus africanus*. *Science,* **347**: 395–399.

Skinner MM, Stephens NB, Tsegai ZJ, Foote AC, Nguyen NH, Gross T, Pahr DH, Hublin J-J & Kivell TL. 2015b. Response to Comment on "Human-like hand use in *Australopithecus africanus*". *Science,* **348**: 1101.

Sládek V, Berner M, Galeta P, Friedl L & Kudrnová Š. 2010. Technical note: The effect of midshaft location on the error ranges of femoral and tibial cross-sectional parameters. *American Journal of Physical Anthropology,* **141**: 325–332.

Slice DE. 2007. Geometric morphometrics. *Annual Review of Anthropology,* **36**: 261–281.

Smith RJ. 1994. Regression models for prediction equations. *Journal of Human Evolution,* **26**: 239–244.

Smith RJ. 2009. Use and misuse of the reduced major axis for line-fitting. *American Journal of Physical Anthropology,* **140**: 476–186.

Smith RJ & Jungers WL. 1997. Body mass in comparative primatology. *Journal of Human Evolution,* **32**: 523–559.

Smoger LM, Fitzpatrick CK, Clary CW, Cyr AJ, Maletsky LP, Rullkoetter PJ & Laz PJ. 2015. Statistical modeling to characterize relationships between knee anatomy and kinematics. *Journal of Orthopaedic Research,* **33**: 1620–1630.

Sokal RR & Rohlf FJ. 1995. *Biometry: The Principles and Practice of Statistics in Biological Research.* New York: W.H. Freeman.

Sollas WJ. 1903 A method for the investigation of fossils by serial sections. *Philosophical Transactions of the Royal Society B,* **196**: 259–265.

Sollas IBJ & Sollas WJ. 1913. A study of the skull of a *Dicynodon* by means of serial sections. *Philosophical Transactions of the Royal Society B,* **204**: 201–225.

Southwell RV. 1946. *Relaxation Methods in Theoretical Physics*. Oxford: Clarendon Press.

Spoor CF, Sondaar PY & Hussain ST. 1991. A new hominoid hamate and first metacarpal from the Late Miocene Nagri Formation of Pakistan. *Journal of Human Evolution,* **21**: 413–424.

Spoor CF, Zonneveld FW & Macho GA. 1993. Linear measurements of cortical bone and dental enamel by computed tomography: Applications and problems. *American Journal of Physical Anthropology,* **91**: 469–484.

Spoor F, Jeffery N & Zonneveld F. 2000a. Using diagnostic radiology in human evolutionary studies. *Journal of Anatomy,* **197**: 61–76.

Spoor F, Jeffery N & Zonneveld F. 2000b. Imaging skeletal growth and evolution. *In:* P O'Higgins & MJ Cohn (eds). *Development, Growth, and Evolution: Implications for the Study of the Hominid Skeleton*. San Diego: Academic Press for the Linnean Society of London. pp 123–161.

Sprent P. 1972. The mathematics of size and shape. *Biometrics,* **28**: 23–37.

Springer MS, Meredith RW, Gatesy J, Emerling CA, Park J, Rabosky DL, Stadler T, Steiner C, Ryder OA, Janecka JE, Fisher CA & Murphy WJ. 2012. Macroevolutionary dynamics and historical biogeography of primate diversification inferred from a species supermatrix. *PLoS ONE,* **7**: e49521.

Stensiö EA. 1927. The Downtonian and Devonian vertebrates of Spitzbergen. *Skr Svalbard Nordishavet,* **12**: 1–31.

Stephen JM, Kader D, Lumpaopong P, Deehan DJ & Amis AA. 2013. Sectioning the medial patellofemoral ligament alters patellofemoral joint kinematics and contact mechanics. *Journal of Orthopaedic Research,* **31**: 1423–1429.

Stern JT Jr. 1971. Functional myology of the hip and thigh of cebid monkeys and its implications for the evolution of erect posture. *Bibliotheca Primatologica,* **14**: 1–318.

Stern JT Jr. 1974. Computer modelling of gross muscle dynamics. *Journal of Biomechanics,* **7**: 411–428.

Stern JT Jr. 1975. Before bipedality. *Yearbook of Physical Anthropology.* **19**: 59–68.

Stern JT Jr & Jungers WL. 1985. Body size and proportions of the locomotor skeleton in *Oreopithecus bambolii*. *American Journal of physical Anthropology,* **66**: 233.

Stern JT Jr & Oxnard CE. 1973. Primate locomotion: some links with evolution and morphology. *Primatologia,* **4**: 1–93.

Stern JT Jr & Susman RL. 1981. Electromyography of the gluteal muscles in *Hylobates*, *Pongo*, and *Pan*: Implications for the evolution of hominid bipedality. *American Journal of Physical Anthropology,* **55**: 153–166.

Stern JT Jr & Susman RL. 1991. "Total morphological pattern" versus the "magic trait": conflicting approaches to the study of early hominid bipedalism. *In:* Y Coppens & B Senut (eds). *Origin(s) de la Bipédie chez les Hominidés.* Paris: Cahiers de Paleoanthropologie, CNRS. pp 99–119.

Stern JT Jr, Jungers WL & Susman RL. 1995. Quantifying phalangeal curvature: an empirical comparison of alternative methods. *American Journal of Physical Anthropology,* **97**: 1–10.

Stevens NJ, Seiffert ER, O'Connor PM, Roberts EM, Schmitz MD, Krause C, Gorscak E, Ngasala S, Hieronymus TL & Temu J. 2013. Palaeontological evidence for an Oligocene divergence between Old World monkeys and apes. *Nature,* **497**: 611–614.

Straus WL Jr. 1963. The classification of *Oreopithecus*. *In:* SL Washburn (ed). *Classification and Human Evolution.* Chicago: Aldine. pp 146–177.

Sugardjito J. 1982. Locomotor behaviour of the Sumatran orang-utan *(Pongopygmaeus abelii)* at Ketambe, Gunung Leuser National Park. *Malayan Nature Journal,* **35**: 57–64.

Sugardjito J & van Hooff JA. 1986. Age-sex class differences in the positional behaviour of the Sumatran orang-utan (*Pongo pygmaeus abelii*) in the Gunung Leuser National Park, Indonesia. *Folia Primatologica (Basel),* **47**: 14–25.

Susanna I, Alba DM, Almécija S & Moyà-Solà S. 2010a. The lumbar vertebrae of the Middle Miocene stem great ape ape *Pierolapithecus catalaunicus* (Primates: Hominidae). *Cidaris,* **30**: 311–316.

Susanna I, Alba DM, Almécija S & Moyà-Solà S. 2010b. The lumbar vertebrae of the Middle Miocene stem great ape *Pierolapithecus catalaunicus* (Primates: Hominidae). *American Journal of Physical Anthropology,* **141(S50)**: 227.

Susanna I, Alba DM, Almécija S & Moyà-Solà S. 2014. The vertebral remains of the late Miocene great ape *Hispanopithecus laietanus* from Can Llobateres 2 (Vallès-Penedès Basin, NE Iberian Peninsula). *Journal of Human Evolution,* **73**: 15–34.

Susman RL. 1979 Comparative and functional morphology of hominoid fingers. *American Journal of Physical Anthropology,* **50**: 215–236.

Susman RL. 1984. The locomotor behavior of *Pan paniscus* in the Lomako Forest. *In:* RL Susman (ed). *The Pygmy Chimpanzee: Evolutionary Biology and Behavior.* New York: Plenum. pp 369–393.

Susman RL. 2004. *Oreopithecus bambolii*: an unlikely case of hominidlike grip capability in a Miocene ape. *Journal of Human Evolution,* **46**: 105–117.

Susman RL. 2005. *Oreopithecus*: still apelike after all these years. *Journal of Human Evolution,* **49**: 405–411.

Sutton MD. 2008. Tomographic techniques for the study of exceptionally preserved fossils. *Proceedings of the Royal Society B: Biological Sciences,* **275**: 1587–1593.

Sutton MD, Briggs DEG, Siveter DJ & Siveter DJ. 2001. Methodologies for the visualization and reconstruction of three-dimensional fossils from the Silurian Herefordshire Lagerstätte. *Paleontologica Electronica,* **4**: 2.

Suwa G, Kono RT, Katoh S, Asfaw B & Beyene Y. 2007. A new species of great ape from the late Miocene epoch in Ethiopia. *Nature,* **448**: 921–924.

Tafforeau P, Boistel R, Boller E, Bravin A, Brunet M, Chaimanee Y, Cloetens P, Feist M, Hoszowska J, Jaeger J-J, Kay RF, Lazzari V, Marivaux L, Nel A, Nemoz C, Thibault X, Vignaud P & Zabler S. 2006 Applications of X-ray synchrotron microtomography for non-destructive 3D studies of paleontological specimens. *Applied Physics A,* **83**: 195–202.

Takano T, Nakatsukasa M, Kunimatsu Y, Nakano Y & Ishida H. 2003. Functional morphology of the *Nacholapithecus* forelimb long bones. *American Journal of Physical Anthropology,* **120(S36)**: 205–206.

Tallman M, Almécija S, Rober SL, Alba DM & Moyà-Solà S. 2013. The distal tibia of *Hispanopithecus laietanus*: more evidence for mosaic evolution in Miocene apes. *Journal of Human Evolution,* **64**: 319–327.

Thomason JJ. 1991. Cranial strength in relation to estimated biting forces in some mammals. *Canadian Journal of Zoology,* **69**: 2326–2333.

Thorpe SKS & Crompton RH. 2006. Orangutan positional behavior and the nature of arboreal locomotion in Hominoidea. *American Journal of Physical Anthropology,* **131**: 384–401.

Tocheri MW, Solhan CR, Orr CM, Femiani J, Frohlich B, Groves CP, Harcourt-Smith WE, Richmond BG, Shoelson B & Jungers Wl. 2011. Ecological divergence and medial cuneiform morphology in gorillas. *Journal of Human Evolution,* **60**: 171-184.

Trinkaus E. 1983. *The Shanidar Neandertals.* New York: Academic Press.

Trinkaus E, Churchill SE & Ruff CB. 1994. Postcranial robusticity in *Homo*. II: Humeral bilateral asymmetry and bone plasticity. *American Journal of Physical Anthropology,* **93**: 1–34.

Tseng ZJ & Flynn JJ. 2014. Convergence analysis of a finite element skull model of *Herpestes javanicus* (Carnivora, Mammalia): implications for robust comparative inferences of biomechanical function. *Journal of Theoretical Biology*, **365**: 112–148.

Tuniz C, Bernardini F, Cicuttin A, Crespo ML, Dreossi D, Gianoncelli A, Mancini L, Mendoza Cuevas A, Sodini N, Tromba G, Zanini F & Zanolli C. 2013. The ICTP-Elettra X-ray laboratory for cultural heritage and archaeology. *Nuclear Instruments and Methods in Physics Research A*, **711**: 106–110.

Turnquist JE, Schmitt D, Rose MD & Cant JGH. 1999. Pendular motion in the brachiation of captive *Lagothrix* and *Ateles*. *American Journal of Primatology,* **48**: 263–281.

Tuttle RH. 1967. Knuckle-walking and the evolution of hominoid hands. *American Journal of Physical Anthropology,* **26:** 171–206.

Tuttle RH. 1969. Quantitative and functional studies on the hands of the Anthropoidea. I. the Hominoidea. *Journal of Morphology,* **128**: 309–364.

Tuttle RH. 1970. Postural, propulsive, and prehensile capabilities in the cheiridia of chimpanzees and other great apes. In: GH Bourne (ed). *The Chimpanzee, vol. 2*. Basel, New York: Karger. pp 167–253.

Tuttle RH. 1975. Parallelism, brachiation, and hominoid phylogeny. *In:* WP Luckett & FS Szalay (eds). *Phylogeny of the Primates: A Multidisciplinary Approach.* New York: Plenum Press. pp 447–480.

Tuttle RH & Watts DP. 1985. The positional behavior and adaptive complexes of *Pan gorilla*. *In:* S Kondo (ed). *Primate Morphophysiology, Locomotor Analysis and Human Bipedalism.* Tokyo: Tokyo University Press. pp 261–288.

Vereecke EE, D'Août K & Aerts P. 2006. Locomotor versatility in the white-handed gibbon (*Hylobates lar*): A spatiotemporal analysis of the bipedal, tripedal, and quadrupedal gaits. *Journal of Human Evolution,* **50**: 552–567.

Vidal LM. 1913. Nota sobre la presencia del "Dryopithecus" en el mioceno superior del Pirineo catalán. *Boletín de la Real Sociedad Española de Historia Natural,* **13**: 499–507.

Villalta Comella JF & Crusafont Pairó M. 1944. Dos nuevos antropomorfos del Mioceno español y su situación dentro de la moderna sistemática de los símidos. *Notas y Comunicaciones del Instituto Geológico y Minero de España,* **13**: 1–51.

Walker A. 1973. New *Australopithecus* femora from East Rudolf, Kenya. *Journal of Human Evolution,* **2**: 545–555.

Walker A. 1997. *Proconsul*. Function and phylogeny. *In:* DR Begun, CV Ward & MD Rose (eds). *Function, Phylogeny and Fossils: Miocene Hominoid Evolution and Adaptation.* New York: Plenum Press. pp 209–224.

Walker A & Rose MD. 1968. Fossil hominoid vertebra from the Miocene of Uganda. *Nature,* **217**: 980–981.

Walker AC & Pickford M. 1983. New postcranial fossils of *Proconsul africanus* and *Proconsul nyanzae*. *In:* RL Ciochon & RS Corruccini (eds). *New Interpretations of Ape and Human Ancestry.* New York: Plenum Press. pp 325–351.

Walker A & Teaford MF. 1988. The Kaswanga primate research site; and early Miocene hominoid site on Rusinga Island, Kenya. *Journal of Human Evolution,* **17**: 539–544.

Walker A, Teaford MF & Leakey RE. 1985. New information regarding the R114 *Proconsul* site, Rusinga Island, Kenya. *In:* J Else & P Lee (eds). *Primate Evolution*. Cambridge: Cambridge University Press. pp 143–149.

Walker A, Teaford MF, Martin L & Andrews P. 1993. A new species of *Proconsul* from the early Miocene of Rusinga/ Mfangano Islands, Kenya. *Journal of Human Evolution,* **25**: 43–56.

Ward CV. 1993. Torso morphology and locomotion in *Proconsul nyanzae*. *American Journal of Physical Anthropology,* **92**: 291–328.

Ward CV. 1997. Fuctional anatomy and phyletic implications of the hominoid trunk and hindlimb. *In:* DR Begun, CV Ward & Rose MD (eds). *Function, Phylogeny, and Fossils: Miocene Hominoid Evolution and Adaptations.* New York: Plenum Press. pp 101–130.

Ward CV. 1998. *Afropithecus*, *Proconsul*, and the primitive hominoid skeleton. *In:* E Strasser, J Fleagle, A Rosenberger & H McHenry (eds). *Primate Locomotion Recent Advances.* New York: Plenum Press. pp 337–352.

Ward CV. 2002. Interpreting the posture and locomotion of *Australopithecus afarensis*: Where do we stand? *Yearbook of Physical Anthropology,* **45**: 185–215.

Ward CV. 2015. Postcranial and locomotor adaptations of hominoids. *In:* W Henke & I Tattersall (eds). *Handbook of Paleoanthropology.* Berlin Heidelberg: Springer. pp 1363–1386.

Ward CV, Walker A & Teaford MF. 1991. *Proconsul* did not have a tail. *Journal of Human Evolution,* **21**: 215–220.

Ward CV, Walker A, Teaford MF & Odhiambo I. 1993. Partial skeleton of *Proconsul nyanzae* from Mfangano Island, Kenya. *American Journal of Physical Anthropology,* **90**: 77–111.

Ward CV, Ruff CB, Walker A, Teaford F, Rose MD & Nengo IO. 1995. Functional morphology of *Proconsul* patellas from Rusinga Island, Kenya, with implications for other Miocene-Pliocene catarrhines. *Journal of Human Evolution,* **29**: 1–19.

Ward S, Brown B, Hill A, Kelley J & Downs W. 1999. *Equatorius*: a new hominoid genus from the Miocene of Kenya. *Science,* **285**: 1382–1386.

Warton DI, Wright IJ, Falster DS & Westoby M. 2006. Bivariate line-fitting methods for allometry. *Biological Reviews,* **81**: 259–291.

White TD & Folkens PA. 1991. *Human Osteology.* San Diego (California): Academic Press.

White TD, Suwa G & Asfaw B. 1994. *Australopithecus ramidus*, a new species of early hominid from Aramis, Ethiopia. *Nature,* **371**: 306–312.

White TD, Asfaw B, Beyene Y, Haile-Selassie Y, Lovejoy CO, Suwa G & WoldeGabriel G. 2009. *Ardipithecus ramidus* and the paleobiology of early hominids. *Science,* **326**: 75–86.

Williams SA, Middleton ER, Villamil CI & Shattuck MR. 2016. Vertebral numbers and human evolution. *Yearbook of Physical Anthropology,* **159**: S19-S36.

Woodward AS. 1914. On the lower jaw of an anthropoid ape (*Dryopithecus*) from the Upper Miocene of Lérida (Spain). *The Quarterly Journal of the Geological Society of London,* **70**: 316–320.

Wunderlich RE & Shaum JC. 2007. Kinematics of bipedalism in *Propithecus verreauxi*. *Journal of Zoology,* **272**: 165–175.

Yamanaka A, Gunji H & Ishida H. 2005. Curvature, length, and cross-sectional geometry of the femur and humerus in anthropoid primates. *American Journal of Physical Anthropology,* **127**: 46–57.

Youlatos D. 1993. Passages within a discontinuous canopy: bridging in the red howler monkey (*Alouatta seniculus*). *Folia Primatologica,* **61**: 144–147.

Youlatos D. 2002. Positional behavior of black spider monkeys (*Ateles paniscus*) in French Guiana. *International Journal of Primatology,* **23**: 1071–1093.

Young NM. 2003. A reassessment of living hominioid postcranial variability: implications for ape evolution. *Journal of Human Evolution,* **45**: 441–464.

Young NM & MacLatchy L. 2004. The phylogenetic position of *Morotopithecus*. *Journal of Human Evolution,* **46**: 163–184.

Zabala ME, Favre J, Scanlan SF, Donahue J & Andriacchi TP. 2013. Three-dimensional knee moments of ACL reconstructed and control subjects during gait, stair ascent, and stair descent. *Journal of Biomechanics,* **46**: 515–520.

Zapfe H. 1958. The skeleton of *Pliopithecus* (*Epipliopithecus*) *vindobonensis* Zapfe and Hürzeler. *American Journal of Physical Anthropology,* **16**: 441–457.

Zapfe H. 1960. Die Primatenfunde aus der miozänen Spaltenfüllung von Neudorf an der March (Devinská Nová Ves), Tschechoslowakei. *Schweizerische palaeontologische Abhandlungen / Mémoires Suisses de Paléontologie,* **78**: 1–293.

Zienkiewicz OC. 1971. *The Finite Element Method in Engineering Science.* London: McGraw-Hill.

Zienkiewicz OC. 2004. The birth of the finite element method and of computational mechanics. *International Journal of Numerical Methods in Engineering*, **60**: 3–10.

Zienkiewicz OC, Taylor RL & Zhu JZ. 2005. *The Finite Element Method: Its Basis and Fundamentals*. Oxford: Butterworth-Heinemann.

Zihlman AL, McFarland RK & Underwood CE. 2011. Functional anatomy and adaptation of male gorillas (*Gorilla gorilla gorilla*) with comparison to male orangutans (*Pongo pygmaeus*). *The Anatomical Record,* **294**: 1842–1855.

Zuckerman S, Ashton, EH, Flinn RM, Oxnard CE & Spence TF. 1973. Some locomotor features of the pelvic girdle in primates. *Symposia of the Zoological Society of London,* **33**: 75–165.

To myself I am only a child playing on the beach,
while vast ocean of truth lie undiscovered before me.

-- Isaac Newton --

Section X. APPENDIX A

LOCOMOTOR MODES IN EXTANT PRIMATES

One of the major aspects of animals' ecology and behaviour is related to the way they move and use the environment (i.e., access to resources, type of substrate, or efficiency on travelling, among others; Fleagle 2013). This conjunct of habits and movements has been called *positional behaviour*. When refers to positional behaviour, it includes the total locomotor conduct (animals movements) and postural habits (postures used during feeding, resting and sleeping) performed, in this case, by primates (Prost 1965; Martin 1990). More specifically, *locomotion* was defined by Prost (1965) as "the intra-body activity occurring during the act of moving from place to place", which implies the physical displacement of the primate body mass relatively to its environmental surroundings. When no changes between the primate body mass and its environmental surroundings occur, that is, the summary displacement (ratio between positional change and time) of body mass is less than a threshold value, this alternative is called *posture* (opposite state to locomotion; Prost 1965).

Depending on the type of substrates, supports, and the use of forelimbs/hindlimbs, researchers have tried to establish a series of locomotor and postural categories (see below). However, it remains difficult to classify primates positional behaviour into one single category, since it leads to an over simplification of the total locomotor repertoire diversity observed in living species. These animals usually combine several locomotor modes in different proportions within its positional behaviour set and, consequently, their bone morphology reflects a compromise of the biomechanical requirements of the complete locomotor repertoire (Rose 1983; Madar *et al.* 2002). Nonetheless, most of them tend to rely preferentially on one of these locomotor categories, which have been frequently used to classify the species. Taking this premise into account, primates can be classified (in some cases in a broad sense) within the following locomotor modes:

- ***Quadrupedalism*** (Fig. 3a,b): progression along approximately horizontal supports by using the four limbs that contact the support in a particular sequence (Hunt *et al.* 1996). Contrary to the most of mammal species (lateral support sequence), primates employ a diagonal sequence support (symmetrical gait walk), moving alternatively the left forelimb with the right hindlimb, and the right forelimb with the left hindlimb (Hildebrand 1967; Martin 1990). Within quadrupedalism, the most frequent is that primates walk (slow movement with 2-4 limbs leaning on the substrate at the same time) or gallop (faster travelling that usually implies that only one limb lean on the support with a period of free flight,

and more asymmetrical and irregular gaits; Hunt 1992; Hunt *et al.* 1996; Fleagle 2013). A special type of quadrupedalism is the *slow* or *cautious climbing*, which implies travelling without leaping or galloping, but with sure-grasp movements of one limb at a time (typical mainly of small lorisines; Fig. 3c; Cartmill 1985; Martin 1990; Hunt *et al.* 1996). Moreover, depending on the support, quadrupedalism is divided in *arboreal* (on continuous network of branches and trunks, with or without grasping assistance of hands and feet) and *terrestrial* (on the ground; Rose 1973; Fleagle 2013). Likewise, primates can use the fingers (digitigrady) or the fingers and the whole palm of the hand (palmigrady) during quadrupedalism. The former is more frequent in the ground, whereas palmigrady is more habitual in arboreal supports and is frequently assisted by grasping (Hunt 1992; Hunt *et al.* 1996; Patel 2010).

Quadrupedalism is usually performed by pronograde primates although considering it in a laxer sense, *knuckle-walking* and *fist-walking* of African apes and *Pongo*, respectively, are also included in this category (Fig. 3d). These two groups are orthograde primates that move leaning on the support (usually the ground) the dorsal face of either the second phalanges (African apes) or the lateral margin of the first phalanges (orangutans; Tuttle 1967, 1970; Rose 1973; Martin 1990; Hunt *et al.* 1996). During knuckle-walking the forelimbs move in an adducted position and the elbow is completely extended (Hunt 1992).

- *Leaping* (Fig. 3e): progression through the air with the aid of a propulsive force performed by the hindlimbs in a rapid and single movement of powerful extension of the legs. Forelimbs' role at take-off of the leap is normally symbolic, although in some taxa its movement can aid on increasing the push-off distance with swinging movements (e.g., gibbons; Hunt *et al.* 1996; Channon *et al.* 2010b; 2012). Nonetheless, the number of limbs involved in landing is very diverse, although the most common is that primates land with both fore- and hindlimbs (Fleagle 1978). Accordingly, forelimbs in these primates are usually equal or shorter than the hindlimbs (see below; Gebo 2011; Fleagle 2013). Leaping is usually performed by small to medium-size primates, since it becomes risky for large-bodied species (the weight threshold for frequent leaping performance range between the 8-10 kg of the largest colobines that usually conduct this type of locomotion; Rose 1978; Gebo 2011). Leaping facilitates quick travels between discontinuous supports (e.g., separate trees or branches; Fleagle 2013).

- *Vertical clinging and leaping* (Fig. 3f): progression along predominantly vertical tree trunks with the body very close to the support (clinging) and posterior progression through the air by leaping between the vertical supports (Napier and Walker 1967; Martin 1990). This locomotor pattern was firstly named by Napier and Walker (1967) to characterize the positional behaviour of several strepsirrhine and tarsier primates. Vertical clinging and leaping (VCL) is a hindlimb-dominated behaviour, where legs aid on propulsion and absorption of shock on landing. Indeed, when these primates move along horizontal branches or on the ground, where they use to conduct bipedal hopping instead of quadrupedalism. Gebo (2011) separates three groups of vertical clingers and leapers depending on their anatomy: tarsiers and galagos that have elongated calcanei; callitrichids that use their claw-like nails in the vertical support; and indriids and *Lepilemur* that exhibit a lemur-like anatomy in the hindlimb and nails (lemurs are not

consider vertical clingers and leapers). Anthropoid primates do not generally conduct this locomotor category (with the exception of some callitrichids and some members of the genus *Pithecia*; Davis 1996; Garber *et al.* 2005; Gebo 2011).

- *Below-branch suspension* (Fig. 3g,h): progression through a three-dimensional, discontinuous arboreal setting by means of hanging below supports with varying combinations of fore- and hindlimbs (Hunt *et al.* 1996). Suspension implies the use of only one support at a time, since primates propel by using two limbs (in tension) alternatively (Stern and Ornard 1973; Fontaine 1990; Johnson and Shapiro 1998). This type of locomotion allows larger species to spread their weight among small supports, avoiding the problem of balancing their body above the support (see below; Cartmill 1985; Fleagle 2013). Commonly, the limbs used for suspensory movements are the forelimbs, hand over hand, bearing more of the half of the body weight (*uni-* and *bimanual suspension* or *arm-hanging* and *swinging*; Hunt 1992; Hunt *et al.* 1996). In suspensory prehensile-tailed platyrrhines, suspension is virtually always assisted by the tail (Fig. 3h; Hunt *et al.* 1996; Johnson and Shapiro 1998; Turnquist *et al.* 1999; Youlatos 2002).

However, there also exists the *bipedal suspension* where the feet are those that grasp the substrate in an "inverted" suspension. Likewise, the most common is that the trunk remains vertical or perpendicular to the substrate, although orangutans and spider monkeys (*Ateles*) can also move with the trunk horizontal to the substrate by using both forelimbs and hindlimbs in tension (*quadrumanus suspension*; Cant 1987; Hunt *et al.* 1996).

Below-branch suspension is usually slow and the trunk rotates under the supporting hand. Nevertheless, hylobatids usually practice the named *brachiation* (or ricochetal brachiation; Fig. 3g) that implies a faster pendulous movements (swinging by the two forelimbs) with a phase of free flight between handholds (a brief aerial phase has been also observed in *Ateles*; Hunt 1991a, 1992; Hunt *et al.* 1996; Turnquist *et al.* 1999; Bertram 2004; Fleagle 2013).

- *Clambering* (=*quadrumanous scrambling*; Fig. 3i): horizontal progression (pronograde or orthograde) through a three-dimensional, discontinuous arboreal setting by using multiple supports of varying orientation and diameter that are grasped by hands and/or feet (Cant 1987; Hunt *et al.* 1996). During clambering, the body weight is distributed simultaneously through the four limbs (or even the tail in platyrrhines). The limbs participate in propulsion, provide support and are characterized by being used in tension (Hunt *et al.* 1996; Cant *et al.* 2001). These four (or five) extremities move in virtually all directions to reach and grasp the supports, reducing the impact of substrate instability (Cant 1987). Both pronograde and orthograde taxa rely on clambering, although the latter is characterized by load the limbs in both compression and tension (Hunt *et al.* 1996). Clambering is considered *bridging* when gaps between discontinuous supports are cautiously crossed (Cartmill 1985; Youlatos 1993).

- *Vertical climbing* (Fig. 3j,k): progression along vertical or steeply sloping (more than 45º from the horizontal line) arboreal supports, by employing the propulsive force created by the limbs (Cartmill 1985; Hunt *et al.* 1996; Madar *et al.* 2002). Usually, the arboreal support is held approximately vertical,

with the hands and feet grasping on one or more supports (Cant 1987). Contrary to leaping, forelimbs have the main role during vertical climbing (Hunt *et al.* 1996). Nonetheless, hindlimbs also participate in propulsion, usually by a contralateral sequence (i.e., left forelimb and right hindlimb *vs* right forelimb and left hindlimb; Hunt 1992). In apes and spider monkeys, climbing shows extended-elbow positions; whereas, cercopithecoids use the forelimb in a different way than apes and *Ateles*, by employing flexed-elbow positions (see further details in the following section; Martin 1990; Hunt *et al.* 1996).

- *Bipedalism* (Fig. 3l): progression along a continuous, horizontal or oblique support involving only the hindlimbs (Hunt 1992; Fleagle 2013). Depending on the substrate, bipedalism is divided in arboreal and terrestrial. The former is usually assisted by the forelimbs that participate in the support (one or both arms). Nonetheless, the most common type of bipedalism is performed on the ground. Many primate species are able of conducting the so-called "facultative" bipedalism, that is, they can travel for a short period of time using exclusively the hindlimbs with the hip and knees in a bent (semi-flexed) positions (Hunt 1992; Hunt *et al.* 1996). However, only modern humans rely primarily on this type of locomotion, since they are able to walk on two legs for long distances during a long time (Senut 2015). Thus, humans are "obligate" bipeds, moving on a continuous substrate while freeing the hands from locomotor tasks (hip and knee joints are extended; Hunt *et al.* 1996). As in the case of quadrupedalism, depending on the velocity of the movement, humans can walk (one hindlimb contacts the ground at any moment) or run (there exist moments with no support on the ground of the legs; Hunt *et al.* 1996).